AD-A099 165 CATHOLIC UNIV OF AMERICA WASHINGTON D C DEPT OF MECH--ETC F/G 20/4
RECENT DEVELOPMENT IN FLOW SEPARATION.(U)
MAY 80 P K CHANG AFOSR-78-3636

UNCLASSIFIED AFOSR-TR-81-0451 NL

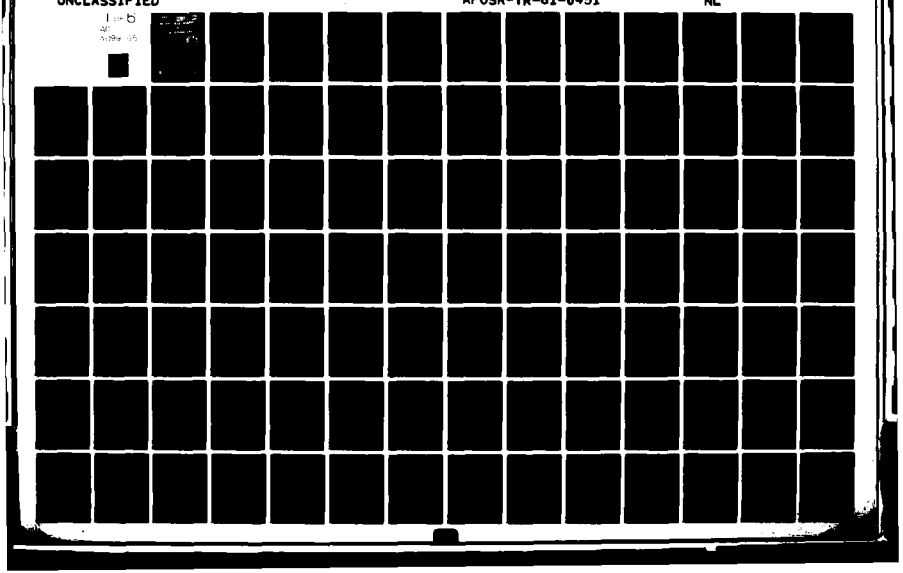

AFOSR-TR-81-0281

LEVEL II

RECENT DEVELOPMENTS IN FLOW SEPARATION

By

PAUL K. CHANG

FINAL
Technical Report for the period of

June 1978 to May 1980

Grant No. AFOSR-78-3388

United States Air Force

Office of Scientific Research

Washington D.C. 20032

May 1980

The Catholic University of America

Department of Mechanical Engineering

Washington D.C. 20064

81 5 20 029

ERRATA

page	line	for	read
26	22	in	is
42	bottom	nsition	Transition
51	9	degress	degrees
59	bottom of Fig.I.28	(add)	$K = p_b/p_{b(\delta=0)}$
68	22	opponent	component
79	4	wakes	near wakes
88	1	definding	defining
88	figure	Fig.I.49	Fig.I.48
89	5	inviscid	of inviscid
100	1	$\frac{dpe}{dx} = \rho_e u_e$	$p = p_{inviscid} + \rho_e u_e^2$
107	10	extalish	establish
113	18	$u_e + c$	$u_e = c$
117	3	trip-	triple-
120	2	tance	tence
123	19	tribial	trivial
133	1	66	67
133	15	w	voticity ω
135	21	1966	1965
136	4	of v_H with $\bar{\delta} = 1$	of v_H. v_H is streamwise velocity of the thick Stoke flow layer upstream edge of a base at the vertical position $\bar{\delta} = 1$.
141	23	tailing	trailing
141	bottom	tailing	trailing critical point p.
160	bottom	160	161
161	"	161	160
169	22	example	example of the
189	bottom	Chartwat	Charwat
201	4	layer	larger
238	6	trucco	Trucco
240	7 and 9	face	force
246	9	layer	result from the expansion of the initial subsonic portion of boundary layer
256 269	8 3	shown that destructive	shown the distentive
275	22	p_w	p_a
275	23	attack. The subscript	attack. p_a is surface pressure just upstream of the corner. In the reference p_a is noted by p_w. The subscript
276	5	number after	number. After
279	9	Tje	The
282	Fig.	(d_{neck}/d)	$(d_{neck}/d) = \delta/d$
285	10	58	58a
287	20	quatient	quotient
290	10	dimin	dimen
314	7	bar	bow
317	11-12	flow angle of bending	flow turning angle
317	19	From IV.11. it	It
317	21	increase	increase of Re_L
326	20	propu	protu
340	bottom	geneous	genous
343	5	Aconst	Acoust

ERRATA

page	line	for	read	page	line	for	read
356	16	transpot	transport	489	16	tric	tion
359	22	place	placed	492	12	number	number J_η
359	25	propot	proport	492	20	S.I.	I_{sp}
365	9	downside	downwind	492	Fig	10^5	J_η 10^5
369	18	and ex-planed	are explained				
391	5	analysis	analyses				
394	21	crossec-tional	cross-sectional				
411	16	VI.a.	VI.11a.				
412	23	VI.b.	VI.11b.				
415	4	aconstic	acoustic				
424	Fig	B	L_Σ				
425	3	L	integrated pressure fluctuation level L_Σ				
428	Fig	ΔA_D	ΔL_o				
428	24	drecal	drical				
433	5	jet,	jet, with				
433	6	is jet	has				
454	11	VII.2b.	VII.1b.				
455	6	Graven	Craven				
471	25	with	width				
478	5	milanty	milarity				
482	20	inveiscid	inviscid				
486	2	decle	decele				
489	14	stagnatric	stagnation				

UNCLASSIFIED

SECURITY CLASSIFICATION OF THIS PAGE *(When Data Entered)*

REPORT DOCUMENTATION PAGE	READ INSTRUCTIONS BEFORE COMPLETING FORM
1. REPORT NUMBER: AFOSR-TR-81-0451 / 2. GOVT ACCESSION NO.: AD-A099165	3. RECIPIENT'S CATALOG NUMBER
4. TITLE *(and Subtitle)*: RECENT DEVELOPMENT IN FLOW SEPARATION	5. TYPE OF REPORT & PERIOD COVERED: FINAL, June 1978 – May 1980
	6. PERFORMING ORG. REPORT NUMBER
7. AUTHOR(s): PAUL K CHANG	8. CONTRACT OR GRANT NUMBER(s): AFOSR-78-3636
9. PERFORMING ORGANIZATION NAME AND ADDRESS: CATHOLIC UNIVERSITY OF AMERICA, DEPARTMENT OF MECHANICAL ENGINEERING, WASHINGTON D C 20064	10. PROGRAM ELEMENT, PROJECT, TASK AREA & WORK UNIT NUMBERS: 2307/A1, 61102F
11. CONTROLLING OFFICE NAME AND ADDRESS: AIR FORCE OFFICE OF SCIENTIFIC RESEARCH/NA, BOLLING AFB DC 20332	12. REPORT DATE: May 1980
	13. NUMBER OF PAGES: 500
14. MONITORING AGENCY NAME & ADDRESS *(if different from Controlling Office)*	15. SECURITY CLASS. *(of this report)*: UNCLASSIFIED
	15a. DECLASSIFICATION/DOWNGRADING SCHEDULE

16. DISTRIBUTION STATEMENT *(of this Report)*

Approved for public release; distribution unlimited

17. DISTRIBUTION STATEMENT *(of the abstract entered in Block 20, if different from Report)*

18. SUPPLEMENTARY NOTES

19. KEY WORDS *(Continue on reverse side if necessary and identify by block number)*

FLOW SEPARATION
INCOMPRESSIBLE
COMPRESSIBLE
WAKES
THERMAL EFFECTS
REATTACHMENT
SEPARATION CONTROL

20. ABSTRACT *(Continue on reverse side if necessary and identify by block number)*

A review and evaluation of recent Russian scientific literature on flow separation has been completed. The principal material reviewed were the papers appearing in NASA TTF 117 as well as two books "Gradient and Separated Flows" (1976) and "Gas Dynamics of Near Wake" (1976). This research activity has been related to separated flow research in the West. A book in 24 chapters has been prepared with the following major sections: Analysis of Flow Separation, Incompressible Flow Separation, Compressible Flow Separation, Base Flow and Wake, Thermal effects on Flow Separation and Reattachment, Separated Flow Affected by Annular Outflow, and Separated Flow Control.

DD FORM 1 JAN 73 1473 EDITION OF 1 NOV 65 IS OBSOLETE

UNCLASSIFIED

SECURITY CLASSIFICATION OF THIS PAGE *(When Data Entered)*

RECENT DEVELOPMENT

IN

FLOW SEPARATION

PAUL K. CHANG

The Catholic University of America

Washington D.C. 20064

Foreword and Acknowledgement

This report for the period June 1978 to May 1980 is submitted to Air Force Office of Scientific Research, Washington, D.C. 20037 in fulfilment of the requirements of the Grant No. AFOSR - 78 - 3636.

Research monitored under the technical supervision of Dr. James D. Wilson AFOSR.

The author wishes to thank AFOSR and Dr. James D. Wilson for the support.

Contents

List of General Symbols

A	wetted area or frontal area
a	velocity of sound
C_L	lift coefficient
C_D	drag coefficient
c_f	skin friction coefficient
C_p	pressure coefficient
c_p	specific heat at constant pressure
D	drag
d	diameter
H	shape factor of boundary layer, $H = \delta^*/\theta$
h	heat transfer coefficient or height
Le	levis number
M	Mach number
Nu	Nusselt number
n	index of power
Pr	Prandtl number
p	pressure
r	radius
q	dynamic pressure
Re	Reynolds number
Sh	Strouhal number
s	distance
T	temperature

t	time
u	streamwise velocity component
v	velocity component in y-direction
w	velocity component in z-direction
x	coordinate, streamwise direction
y	coordinate perpendicular to x-direction
z	coordinate perpendicular to x-and y-direction
α	angle of attack
γ	ratio of specific heats
δ	thickness of boundary layer or shear layer
δ^*	displacement thickness of boundary layer
ε	eddy viscosity
θ	momentum thickness of boundary layer
μ	dynamic viscosity
ν	kinematic viscosity ; Prandtl-Meyer expansion angle
ρ	density of fluid
τ	shear stress
ψ	stream function

Subscripts

b	base
e	conditions at the outer edge of boundary layer
max	maximum
min	minimum

CHAPTER I

SYMBOLS

$a = (\partial u/\partial y)_w \; Re^{-1/2}/u_\infty$

B characteristic length

$B = \frac{Pr-1}{Pr}\left[1 - \frac{\ln \epsilon^{1/4}}{\epsilon}\right]^{1/4}$

c chord length

$c(x) = u/u_{max}$

$C_P = \frac{\zeta\, C_{fs}^{1/2}}{(M_s^2 - 1)^{1/4}}$

F shape parameter

$F' = u/u_e$

$f = \int \frac{u}{u_e}\, d\eta$

G_i injected mass flow rate

$g(\zeta, \eta) = H/H_e$

H height of base section

I enthalpy

i enthalpy

K_θ universal constant

k constant or mixing coefficient

k_c mixing coefficient at reattachment

$m = u_m/u_e$

$m = \begin{cases} 1 & \text{axisymmetric} \\ 0 & \text{two-dimensional} \end{cases}$

$N = \rho\mu/(\rho\mu)_w$

g mass discharge rate into stagnation per unit length

r_o radius of cylinder

T_θ temperature on the wake axis

u_k streamwise velocity component

u_m average velocity or longitudinal velocity at the center of reversed flow

v_M max, normalized vertical velocity component by u_e.

$\hat{x} = (x - L)/ Re_w^{-1/2} \cdot L$

x_c distance to reattachment point or distance to point of deceleration

x_{min} coordinate of minimum pressure

$\tilde{y} = y/Re_w^{-1/2} \cdot L$

$y^+ = y / Re_w^{-3/4} \cdot L$

y_b normal coordinate of constant mass during injection

y_j normal coordinate of separation stream line.

$\alpha = \partial^2 f/\partial\eta^2|_w$

$$\alpha = \frac{F(u_e)}{(u_e)} \frac{d}{d\xi}\left[\frac{u_e}{\varphi(u_e)}\right]$$

$$\beta = \frac{1}{2} \frac{F(u_e)}{\varphi^2(u_e)} \frac{du_e}{d\xi}$$

Δ^* closed contour including displacement thickness round body surface passing through the base section

$$\Delta_k = \int_0^1 \frac{\tau}{\rho_e u_e^2} \left(\frac{u}{u_e}\right)^{k-1} \frac{d}{d\eta}\left(\frac{u}{u_e}\right) d\eta$$

$\overline{\delta^*} = \delta^*/\lambda = \delta^*/Re^{-1/2}$

Θ_c angle between flow velocity vector along external boundary of viscous layer and wall.

$\theta(Ma)$ angle of inviscid flow turning

θ_c reattachment angle

κ turbulent constant

κ_1 coefficient of proportionality

$\mu^+ = \mu/\mu_w$

σ spread factor

τ thickness ratio

$u_b' = u_b/u_a$

$v_b' = v_b/u_a$

$\lambda = Re^{-1/2}$ or $\lambda = (\delta^2/\nu)(du_e/dx)$

χ interaction parameter

ω vortex

ξ see each section

η see each section

<u>superscript</u>

* deceleration (parameter) or conditions along dividing stream line

<u>subscripts</u>

a conditions of primary free stream

b conditions of secondary free stream

c reattachment, joint

CL center line

cr	critical
j	separation stream line
N	neck condition
O	initial
r	reference
T	total
t	total
ϕ	zero line of flow
θ	wake axis

CHAPTER I

Analysis for Flow Separation

Recently the analysis of flow separation at subsonic and supersonic speeds has been further developed. In order to describe this development, the recent investigations on the fundamental aspects of the flow separation phenomena over a cylinder, a blunt-nosed body, downstream of a step and plate, etc., are considered. These findings are referred to the available analysis so that the flow systems of separation may be formulated, and a different analysis based on, the separation stream line, the integral and the use of Navier-Stocke's equations, are presented more distinctively.

1. Flow Systems and Some Recent Investigations

The experimental investigation cited in the reference of Burggraf (1966) for a subsonic cylinder flow which depends upon Reynolds numbers is briefly stated. The aim is to get a better understanding of the structure of a separated flow and to confirm the applicability of the analysis for various phases of complex, separated flow.

As can be seen from Fig.I.1a, at a very low $Re < 1$, stream lines are symmetrical, and form no wake. For this flow regime, the Stokes equations are applicable. With an increase of the Reynolds number up to $Re \ll 1$ (Fig.I.1b), the flow symmetry breaks down due to the stream line divergence, downstream of the cylinder and wake formation. The full Navier-Stokes equations are to be used to solve the problems in this regime.

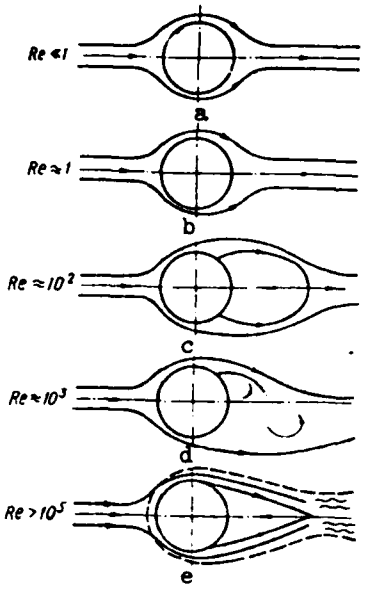

Fig.I.1 Regimes of the flow for a circular cylinder : Burggraf (1966)
a-- established flow, without a wake;
b-- established flow, without a circulating wake;
c-- established, recycled flow;
d-- stable, vortex street;
e-- turbulent wake.

With the further increase of $Re > 5$ (Fig.I.1c), the flow separates, forming a recirculating zone and wake. This phenomena continues until the Reynolds number reaches an order of 10^2.

The oscillation of the downstream wake does not move forward, and thus its effect is not observed in a recirculation vortex. When $Re \simeq 100$, then the Karman vortex street (Fig.I.1d) appears and unsteady Navier-Stokes equations are to be applied. In the region of Re = 100-1,000, vortices alternate, developing into an irregular, unsteady wake; and for $Re > 10^5$ (Fig.I.1e), the flow becomes completely turbulent and quasisteady Reynolds equations are applicable. It is not indicated what analysis is to be used in the regimes $5 < Re < 100$ and $Re \simeq 100 - 10^5$.

For supersonic flow at a much larger $Re > 10^6$, recirculated flow stability is observed, apparently due to strong effects of compressibility.

A supersonic flow field divided into seven regions, and a point downstream of a blunt-nosed body [Sirieix (1967)], is shown in Fig.I.2.

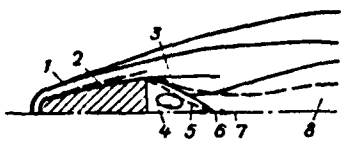

Fig.I.2. Diagram of flow in a wake: Sirieix (1967)
1--vortex layer;
2--boundary layer;
3--mixing layer;
4--reversed flow;
5--near wake;
6--critical point;
7--wake neck;
8--far wake

The upstream flow field around the bow shock wave, and its downstream high-entropy vortex layer 1, can be analyzed by the well-known, available methods. Close to the body surface, a boundary layer forms and interacts with the shock wave and the vortex layer. The region of the separated flow is divided into five areas which are affected by viscosity. The base region 4, close to the symmetry axis, is an area of reverse flow, a part of the near wake 5, bounded by the neck region 7 and followed by an asymptotic, far wake 8. Near wake includes the critical point, upstream of the neck region, which is characterized by a large, streamwise pressure gradient at hypersonic free stream velocity. The main portion of the near wake must be considered as viscous, and its characteristics are to be determined by its mixing through mixing layer 3 and its interaction with the external flow. Far wake 8, with its negligible, streamwise pressure gradient can be studied in terms of the total drag of the body. The flow of the mixing layer, which transfers mass and heat, may be analysed by the boundary layer equations.

Ginevskiy (1969), presented the results of analytical and experimental investigations of turbulent, separated flows with constant and variable density, and he also offered some recent, semi-analytical findings in his monograph. His experimental investigations focus on

the microstructure of various types of flows, including a turbulent wake. His theoretical studies concern the integral, computational, method necessary to solve problems regarding the turbulent boundary layer and supersonic separated flow. Abramovich, et al (1974) presented a monograph on the recent developments regarding a mixing turbulent flow. The authors paid attention, in addition to an analysis for variable density, self-similar solutions, etc., mainly to the analysis required for maximum and minimum mixing. Experimental data for axisymmetric flow, mixing between two flows of different velocities and densities, and profiles of velocity, temperature and concentration, are presented in the form of universal relationships in order to determine the mixing parameters.

Teterin (1964), calculated the turbulent, free-stream of $Pr_T = 1$ by using the combined solutions of the equations of motion and energy, with Tollmien boundary conditions for a range of M = 0 - 10, applying Prandtl's mixing length theory. The ratio of $u_j/u_e = f(M)$ evaluated by Yurchenok (1968), is compared with that of Korst et. al. (1956), who formulated $(u_j/u_e)^2 = 0.348 + 0.018\ M$, and other ratios as seen in Fig.I.3a, indicating the effect of a selected hypothesis in relation to the velocity, on the separation stream line.

In Fig.I.3b, the velocity distribution along the separation stream line, i.e., with respect to $\xi = \nu_e\, s/u_e\theta_o^2$, is also shown, where ν is a kinematic viscosity, s is the distance, $\theta_o = \frac{1}{2}\ \delta_o$ is the initial thickness of the boundary layer.

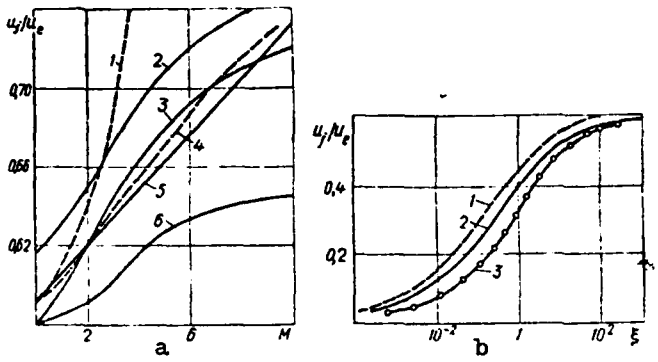

Fig.I.3. Value of velocity on separating stream lines: (Shvets and Shvets (1976))
a--1--v = const (Yurchenok (1968)) ; 2-- (Korst et al (1956)) ; 3--$i_b^* = 1$ (Neyland (1964)) ; 4--$i_b^* = 1$ $Pr_T = 1$ (Yurchenok (1968)) ; 5--(Neyland (1969a)) ; 6--$Pr_T = 0.5$(Teterin (1964)) ; b--1--exponential profiles ($s \to \infty$, $u_0/u_e \to 0.618$); 2--quadratic profile ($s \to \infty$, $u_\phi/u_e \to 0.594$); 3--numerical integration from the Blasius profiles ($s \to \infty$, $u_\phi/u_c \to 0.587$) (Denison and Baum (1963))

During the process of flow expansion, downstream of a body, the initial structure of the boundary layer breaks down and most of its thickness as an inviscid flow. Thus, the effects of the viscosity are significant only in the small area near the wall, i.e., a new sublayer appears, as Weinbaum (1966) as well as Weiss and Weinbaum (1965) found. Experimentally, it is proven that the lateral pressure gradient in the mixing layer is small, justifying the hypothesis of isobaric mixing.

The analysis of inviscid flow can be used in certain cases to determine the pressure in the separated zone. Vagramenko and Puchkova (1973), applied this analysis for an axisymmetric flow in a cylindrical channel of an arbitrarily large area of a cross-section. They were ably to determine the base pressure in the separation zone bounded by

an inviscid, stream line boundary wall of channel and a protuberance at supersonic speed.

1.1 Approximate and Semi-Empirical Methods for Two-Dimensional Separated Flows.

Various approximation methods are classified into two types, first and second, but these refer essentially to the methods of Croco-Lees (1952) based on the mixing theory for a turbulent flow, and Chapman (1951) and Korst (1956), based upon the concept of the dividing stream line.

(i) The first type uses various forms of integral equations and relations obtained from the boundary layer equations, which are extended from the well-known methods for the separation of free layers. For the solution, integration of a system of non-linear, ordinary differential equations is carried out, and thus, the distribution of functions through the boundary layer is not obtainable by this system. Hence, this system is supplemented by the relations connecting the distribution of the boundary layer displacement thickness with the outer flow characteristics, necessitating the proper choice of the family of parameter distribution profiles through the boundary layer thickness. In the USSR, for the analysis of the laminar flow, a single parameter family of power-law velocity and stagnation enthalpy profile in Dorodnitsyn variables, as well as the single parameter of velocity profiles obtained by self-similar boundary layer equations are used. For the analysis of turbulent flow involving separation, integral methods are used, applying the Croco-Lees' theory, because the integral method is better suited for the turbulent flow than the

laminar flow. However, since the basic, closed system of exact equations for the turbulent flows has not yet been obtained, it is not possible to develop a more exact method. Gogish et al (1969), developed the Croco-Lees' integral method for the unified calculation of supersonic laminar and turbulent flow using a minimum number of empirical data. With this data, the turbulent flow solutions for the separated flow regions, for base pressure and for the critical pressure rise, etc. are obtained. Gogish and Stepanov (1966, 1971), published (in 1966), the computed base pressure, near wake and jet flow around bodies and separated flows in channels, and in 1971, the characteristics of the pseudo-shock in the transonic region, from supersonic to subsonic flow in a long channel.

(ii) The second-type, which corresponds to the method of Korst (1956) for turbulent flow and Chapmen (1951) for laminar flow, was found to yield the best results for the separated zone with a constant pressure, not only for a turbulent but also for a laminar flow. This writer (1970), presented the details of this method to determine the base pressure, separation zone length, reattachment, etc., and an analysis leading to the necessary information for various criteria in his book Separation of Flow (Pergamon Press, 1970). In the USSR, Minytov (1961), Tagirov (1961, '63, '66) used this approach and computed the base pressure on a rear facing-step placed in a turbulent flow, and Bondarev (1964), Bondarev and Yudelovich (1965), Yel'kin et al (1963), and Neyland (1963) studied the base pressure for simple-shaped bodies.

Yel'kin et al (1963), indicate that the well-known principle of flow

stabilization as $M_\infty \to \infty$ holds for a separation zone at hypersonic speeds, and established that the base pressure on slender wedges depends on the similarity parameter $M_\infty \cdot \tau$, where τ is the thickness ratio. Yuldel'svich (1965), determined the base pressure on a sphere.

For the solution of the problem of separated flow on the smooth surface, if the separation point is not known as a priori, the Chapman-Korst condition alone, or any modification of this condition, is not sufficient to determine the length of the separation zone and the separation point. Therefore, in order to determine the separation point, it is necessary to use an algebraic relation, the so-called separation criteria, connecting the pressure in the separation zone with the local, boundary layer characteristic, upstream of separation point.

Neyland (1965), presented a generally approximate method for the solution of the separation on a flat plate, upstream of a flap at supersonic speed, and Tagirov (1966), developed a method to estimate the time necessary to established a stationary flow in the turbulent, separated zone, assuming that the slowest process for establishment of the stationary flow in the base region is the turbulent mixing. Murzinov (1970), computed gas temperature in the separated zone, based upon the concept of the isobaric, separated zone.

1.2 Numerical Methods

The numerical methods, developed in the USSR, are to intended to solve Navier-Stokes equations at high Reynolds numbers only, for example, for

the viscous, separated flow over the sharp corner, under the assumptions of Re based upon the asymptotic method and similarity law for laminar and turbulent flows. For steady and unsteady, separated flows, the system of Navier-Stokes equation is approximated by a finite difference system, and by using a computer, solutions with accuracies of the first and second order are obtained.

1.2.1 Steady Separated Flow

Dorodnitsyn and Meller (1968, 1971), obtained only a limited solution of the incompressible diffuser flow of the multiple phases steady two-dimensional cases. Kline (1959), indicates that four, different flow phenomena occur within the diffuser, i.e. a well behaved flow with no separation; a large, transitory stall; steady, fully developed stall and jet-like flow. For the particular geometrical condition of the diffuser (ratio of width of exit to entrance is two) the numerical method is applied to evaluate algebraic equations for each iterating step. The results show that the flow reverses in a short region if Re, based upon the entrance width, reaches 8π and for Re = 32π , a very definite stagnation zone with steady, reverse circulation occurs. But, for Re $> 200\pi$, no solution is obtained, because the iteraction process does not converge and the sequential, approximation oscillates, and approaches no limit.

Myshenkov (1970, 1972a, 1972b), studied the upstream and downstream, separated flows by applying numerical methods for Re amounting

to several hundred, and at Mach numbers 3-5, confirming the concepts of the flow pattern and the influence of the Reynolds number on the geometry of stream lines in the separated flow regions as sketched in Figure I.4, and I.5. Furthermore, Myshenkov (1972b), qualitatively confirmed the existence of a viscous, mixing layer. He calculated the base pressure for the flow, up to Re = 4×10^3, by applying approximated Navier-Stokes equations, obtaining results to second order of accuracy, using an explicit scheme.

In the USSR, the problem of the viscous flow over a cylinder was not solved by a numerical method, due to the difficulties of approximating as nearly as possible to the Navier-Stokes equations and the boundary conditions for an external flow.

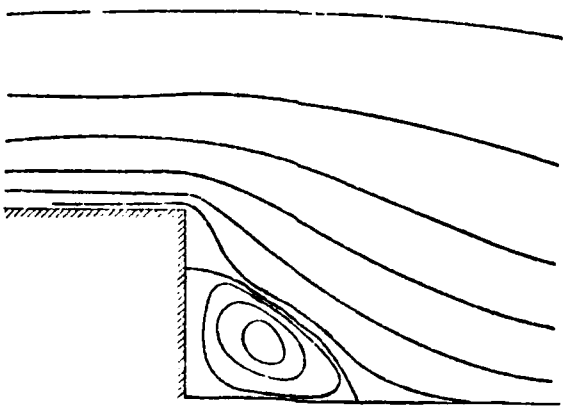

Figure I.4. Example of Separated, base flow calculation. Streamline pattern for M = 5, Re = 800 [Brailovskaya (1971a)].

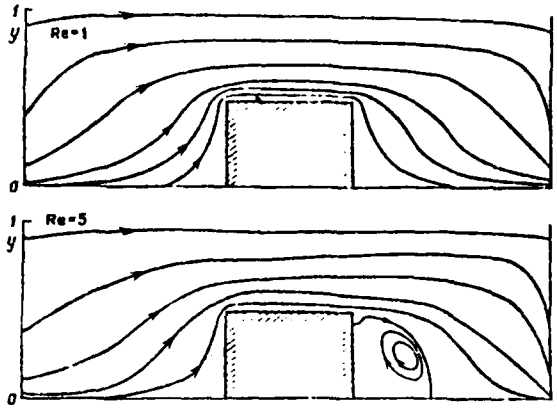

Figure I.5. Exampic of the calculation of a separated flow around a rectangle. Streamline pattern for M = 0.3 and a different Re. [Myshenkov (1972b)] .

For a separated flow with a small Reynolds number, Dumitrescu and Cazacu (1970) in Romania, obtained analytical solutions, for example, the separated flow stream line caused by a flat plate, placed at an angle of attack $\alpha = 45^{\circ}$ and Re = 50, as shown in Fig.I.6. For two-dimensional viscous flow, the equations are :

$$u\frac{\partial u}{\partial x} + v\frac{\partial u}{\partial y} + \frac{1}{\rho}\frac{\partial p}{\partial x} = \nu \left(\frac{\partial^2 u}{\partial x^2} + \frac{\partial^2 u}{\partial y^2} \right)$$

momentum :

$$u\frac{\partial v}{\partial x} + v\frac{\partial v}{\partial y} + \frac{1}{\rho}\frac{\partial p}{\partial y} = \nu \left(\frac{\partial^2 v}{\partial x^2} + \frac{\partial^2 v}{\partial y^2} \right)$$

continuity : $\frac{\partial u}{\partial x} + \frac{\partial v}{\partial y} = 0$

By introducing the stream function ψ given by

$$u = \partial\psi/\partial y \quad , \quad v = -\partial\psi/\partial x$$

these momentum equations are expressed by

$$\nu \Delta \Delta \psi = \frac{\partial \psi}{\partial y}\frac{\partial \Delta \psi}{\partial x} - \frac{\partial \psi}{\partial x}\frac{\partial \Delta \psi}{\partial y}$$

By taking $x^1 = x/B$, $y^1 = y/B$, $\psi^1 = \psi / B \cdot u_m$

$$u^1 = \frac{u}{u_m} = \frac{\partial \psi^1}{\partial y^1} \quad \text{and} \quad v^1 = \frac{v}{u_m} = -\frac{\partial \psi^1}{\partial x^1}$$

where B is characteristic length and u_m is average velocity,

$$\Delta \Delta \psi^1 = \mathrm{Re} \left(\frac{\partial \psi^1}{\partial y^1}\frac{\partial \Delta \psi^1}{\partial x^1} - \frac{\partial \psi^1}{\partial x^1}\frac{\partial \Delta \psi^1}{\partial y^1} \right)$$

is obtained.

The method of Dumitrescu and Cazacu, is to approximate the function ψ^1 and its derivative by the finite Taylor's series and to relax the values at the mesh points at higher Reynolds numbers in order to integrate this differential equation of ψ^1 . Around a point of interest, in the multiple rectangular meshes of the flow field containing up to 20 points, are set up. The terms of Taylor's series of ψ^1 are given by the proper ψ^1 value and the product of derivatives of ψ^1, with respect to coordinates x and y, and the distance between the mesh points. The values of ψ^1 , at points near the surface, are also given in Taylor's series, by considering the singularity.

The stream lines evaluated by the numerical integration of this approximate Navier-Stokes equation (by a computer), in the region of laminar separated flow of a small Reynolds number, are in a good agreement with observation by means of flow visualization using floating paper, as indicated in Fig.I.6.

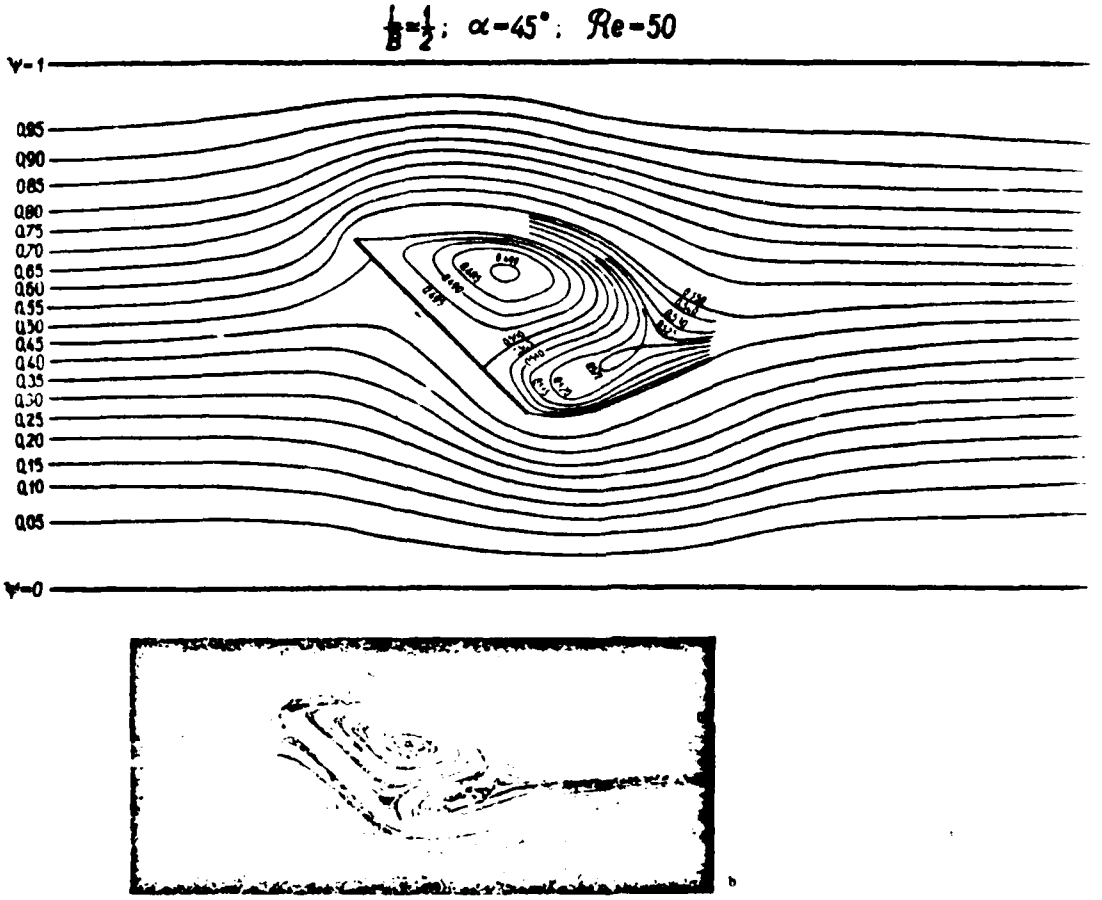

Figure I.6. Flow around plate L/B = ½ in mid-channel at angle of a attack 45°. L is width of the plate and B refers to channel width.

a) computed stream line at Re = 50

b) experimental figure at Re = 45.5

[Dumitrescu and Cazacu, (1970)] .

1.2.2 Unsteady Separated Flow

Il'ichev and Postolovskiy (1972) and Belotserkovskiy and Nisht (1971), attempted to solve the problem involving a separated flow

...er the discontinued tangential surface, by the in[illegible] flow ap-
[illegible] better [illegible], but no complete under-
stand[illegible] has been reached because the point of separation is time
dependent. Il'ichev and Postolovskiy (1972), however, calculated
the flow around a circular cylinder with a given initial flow asym-
metry. The results show that the flow becomes basically periodic, re-
gardless of the form the body is in the order of [illegible] where r_c
the radius of the cylinder and u_∞ is free-stream velocity, as
shown in Fig. I.7. Among the studies done in Western countries con-
[illegible] separated flow, the works of Keller and Takami (1966)
[illegible] Sarratt (1966) have been cited in the USSR. [Chang (1973)].

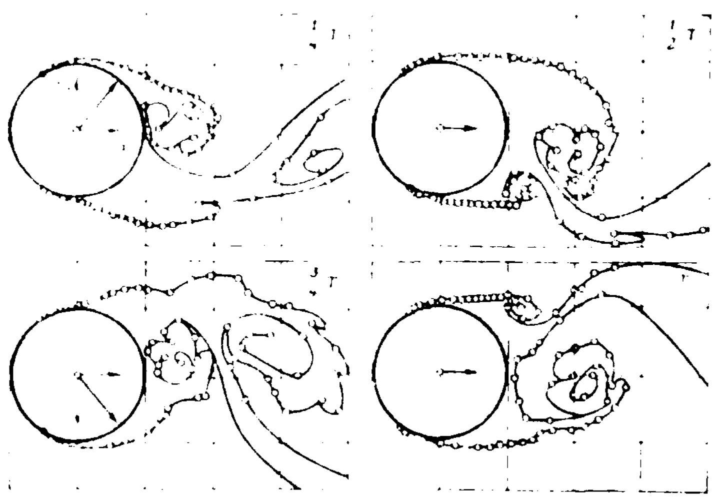

Figure I.7. Example of the calculation of a separated, ideal fluid flow around a cylinder. Vortex sheet at different times during a single period T. [Il'ichev and Postolovskiy, (1972)].

Parametric Method of Solving an Equation for a Two-Dimensional Turbulent Boundary Layer with a Pressure Gradient

An approximate, parametric method for the solution of a turbulent boundary-layer equation not involving semi-empirical integration, has been presented by Vasil'tsev (1971), who uses the parametric presentation of velocity profile as proposed by Loitsianskiy, for laminar boundary layer.

The streamwise velocity profile $f = u/u_e$ expressed by parametric forms,

$$f = f(\xi, a_1, a_2, \text{-------} a_n) \tag{1}$$

where $\xi = y/\delta$, and the symbol a_i refers to the parameter, such as δ, which depend only to streamwise coordinate x.

For the solution of Prandtl's two-dimensional turbulent boundary layer equations $u\,\partial u/\partial x + v\,\partial u/\partial y = (1/\rho)\partial\tau/\partial y + (1/\rho)dp/dx$ and $\partial u/\partial x + \partial v/\partial y = 0$ (2) the following transformations are used.

$$y = \xi \cdot \delta, \quad u = u_e \cdot f, \quad \partial u/\partial y = u_e f' \delta$$

Then

$$\left.\begin{aligned}
\partial u/\partial x &= u_e(\partial f/\partial \xi)(\partial \xi/\partial x) + f\, du_e/dx + u_e(\textstyle\sum \partial f/\partial a_i)(da_i/dx) \\
&= f\cdot u_e - u_e\cdot \xi\, f\delta'/\delta + u_e(\partial f/\partial a_i)\frac{da_i}{dx} \\
v &= v_s - \int_0^y (\partial u/\partial x)dy = v_s - u_e' \int_0^\xi f\, d\xi \\
&\quad - u_e\,\delta' \int_0^\xi f'\xi\, d\xi - \sum \int_0^\xi u_e(\partial f/\partial a_i)\, a_i d\xi
\end{aligned}\right\} \tag{3}$$

The prime over δ , u_e and a_i, indicates the differentiation with respect to x, and the prime over f with respect to ζ .

By substituting eq.(3) into eq.(2), eliminating the derivative δ', using the momentum equation of after double integration,

$$\left.\begin{aligned}
\bar{\tau} &= \tau/(u_e) = C_f \cdot z_1 / 2 + (-\lambda) z_2 + \sum a_i' z_{3i} \\
\text{where} \quad z_1 &= 1 - (\delta/\theta)\left(f\int_0^\zeta f\,d\zeta - \int_0^\zeta f^2 d\zeta\right) \\
z_2 &= \zeta - H\left[f\int_0^\zeta f\,d\zeta - \int_0^\zeta f^2 d\zeta\right] - f\int_0^\zeta f\,d\zeta \\
z_{3i} &= \int_0^\zeta \partial f^2/\partial a_i\, d\zeta - f\int_0^\zeta \partial f/\partial a_i\, d\zeta - (\delta/\theta)\,\partial(\theta/\delta)/\partial a_i \\
&\quad \left[f\int_0^\zeta f\,d\zeta - \int_0^\zeta f^2 d\zeta\right]
\end{aligned}\right\} \quad (4)$$

where $\lambda = \dfrac{\delta^2}{\nu}\dfrac{du_e}{dx}$

This equation (4), can be used to compute shear stress based upon measured data of the velocity profile, parameters c_f , λ , θ/δ , approximate solutions and a turbulence hypothesis.

Rotta (1967) indicates that

$$f = \zeta^n \quad \text{and} \quad f = \zeta^{(H-1)/2}, \quad H = 2^{n+1} \qquad (5)$$

hence, referring to eq.(1), H can be selected as the parameter a_i. Then eq.(4) becomes

$$\bar{\tau} = \tau/\rho u_e^2 = C_f z_1/2 + (-\lambda) z_2 + (dH/dx)\delta/H(H+1) z_3 \qquad (6)$$

where $z_1 = 1 - \xi^H$, $z_2 = \xi - \xi^H$, $z_3 = \xi^H \ln \xi$

Because functions z_2 and z_3 in eq.(6) are similar, by taking

$$z_2 \approx -\sqrt{H}\,(H-1)z_3$$

eq.(6) is reduced to

$$\bar{\tau} = \tau / \rho u_e^2 \approx C_f z_1/2 + (-F) z_2$$

Here the new, gradient shape parameter F is defined by

$$-F = (-\lambda) + (dH/dx)\theta / \left[H(H-1)\sqrt{H} \right] \qquad (7)$$

This parameter F which is also used for separation criterion is more general, when compared to the classic form of parameter λ because λ allows only for the effect of a local, pressure gradient.

Prandtl's hypothesis for the turbulence structure is formulated by

$$df/d\xi = \sqrt{\bar{\tau} / \bar{\tau}_p}\; du_{ep} / d\xi \qquad (8)$$

where the subscript p refers to a flat plate. Using Clauser's (1959) universal concept

$$(1-f_p) / \sqrt{C_{fp}/2} = D_o(\xi) \approx -\frac{1}{\kappa} \left[\ln \xi - 1 + 4\xi^2 - 3\xi^3 \right] \qquad (9)$$

where κ is turbulence constant.

Using eq.(7) and (9), eq.(8) becomes

$$df/d\xi = \left[C_f/2(1-\xi^H)/(1-\xi H_p) + (-F)\xi (1-\xi^{H-1})/(1-\xi H_p) \right]^{0.5} \left[-dD_o/d\xi \right]$$

By integrating the velocity profile, the developed turbulent

boundary layer is given by

$$f = 1 - (1/k)\int_{\zeta}^{1}\left[C_f/2 \cdot (1-\zeta^{H})/(1-\zeta^{Hp}) + (-F)\zeta\,(1-\zeta^{H-1})/\right.$$
$$\left./(1-\zeta^{Hp})\right]^{0.5}(1+8\zeta - 9\zeta^{2})\,d\zeta \qquad (10)$$

Then the critical velocity profile for $C_f = 0$, at flow separation, is given by

$$f_{cr} = 1 - 1/k\int_{\zeta}^{1}\left[(-F_{cr})(1-\zeta^{H-1})/(1-\zeta^{Hp})\right]^{0.5}(1+8\zeta-9\zeta^{2})d\zeta$$

approximating

$$\left[(1-\zeta^{H_{cr}-1})/(1-\zeta^{Hp})\right]^{0.5} \approx 1 + \left\{\left[(H_{cr}-1)/H_p\right]^{0.5}-1\right\}\zeta$$

$$f_{cr} = 1-2(-F_{cr})/k\left\{(1-\sqrt{\zeta}) + 8/5\cdot(1-\zeta^{2}\sqrt{\zeta})-9/7\cdot(1-\zeta^{3}\sqrt{\zeta}) + \right.$$
$$\left.\left[(H_{cr}-1)/Hp-1\right]\left[1/3\cdot(1-\zeta\sqrt{\zeta})+ 8/7\cdot(1-\zeta^{3}\sqrt{\zeta})-(1-\zeta^{4}\sqrt{\zeta})\right]\right\} \qquad (11)$$

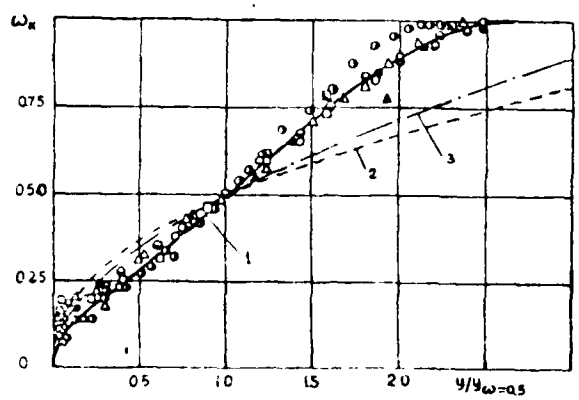

Fig.1.8. Graph of the function $f_{cr} = (y/y_{f=0.5})$.

1 - present theory, Re_0=10000;

2 - theory of [Kutateladze and Leontyev (1962)], $Re_\theta \to \infty$, theory of [Fedyayevskiy et al (1973)], Re_θ = 500;

3 - theory of [Fedyayevskiy et al (1973)], Re = $5\cdot10^5$; data points from experiments in [Bam-Zelikovich (1954)]

This separation velocity profile formulated by eq.(11) is in a good agreement with the experimental data of Bam-Zelikovich (1954) as shown in Figure.I.8.

The shape parameters for separation are given by considering the viscous sublayer as

$$-F^{**}_{cr} = -F_{cr}\,(\theta/\delta)_{cr} = 0.0035 + 0.1\cdot C_{fp}$$

and

$$H_{cr} = 2.33 + (H_p - 1)/2 \qquad (12)$$

For the attached, turbulent boundary-layer, values of θ, Re_θ, H and C_f can be computed by the following skin friction law expressed by ψ^{**} and the differential equation of H.

Defining $\overline{F^{**}} = F^{**}/F^{**}_{cr}$

ψ^{**} is given by $\psi^{**} = (1-\overline{F^{**}})^{0.9}$

Then since

$$(H-1)/(H_p-1) = \left[\,(H_{cr}-1)/(H_p-1)\,\right]^{\overline{F^{**}}} \qquad (13)$$

(S. S. Kutateladze and A. I. Leont'yev)

$$\psi^{**} = \left\{\,1 - \ln\left[(H-1)/(H_p-1)\right] / \ln\left[\,(H_{cr}-1)/(H_p-1)\right]\right\}^{0.9} \qquad (14)$$

This equation correlates well with the experimental data of Proc. AFOSR-JFR of the Stanford Conference (1969), as shown in Figure.I.9.

Another differential equation of H is given by

$$dH/dx = \left\{\,(-\lambda^{**}) - (-F^{**}_{cr})\ln\left[\,(H-1)/(H_p-1)\right] / \ln\left[\,(H_{cr}-1)/(H_p-1)\right]\right\} H\sqrt{H}\,(H^2-1)/\theta$$

where

$$\lambda^{**} = (\theta^2/\nu)(du_e/dx)$$

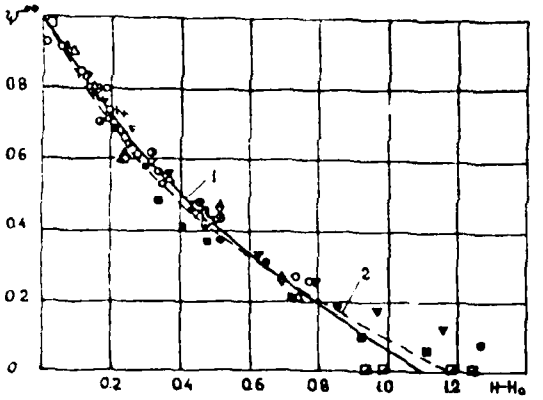

Fig.I.9. Graph of the function $\psi^{**} = f(H - H_o)$, present theory; 1 - $Re_\theta = 10^3$; 2 - $Re_\theta = 10^5$; experimental points from [Proc. AFOSR-JFR, Stanford Conf. vol.2 (1969)]

1.4 Some Recent Analysis of Flow Separation

A theory of flow with free boundaries, where the viscous layers are replaced by lines of velocity discontinuity separating the wake from the external flow and correlating layers of the vortex with a free viscous flow, was presented by Birkhoff (1955) and Roshko (1955). The physical aspects were not clear in this theory, and thus the solution, under a certain hypothesis and in a parameter of the base pressure, was not rigorous. The free boundary flow may be analyzed, based upon potential flow theory, by assuming that the wake is bounded by a free stream line and by idealzing the viscous layer flow involving a velocity disturbance. Such a free stream line concept has been applied for the analytical solutions, using the base pressure as a parameter, by Albernathy (1962), Birkhoff and Zarantonello (1957), and Gurevich (1961).

It is to be noted that in spite of very different theories being used for the shape of free surfaces far from a body, the distribution of pressures along the frontal surface and the shape of the stream line immediately downstream of the flow separation, can be predicted (with good agreement with test data,) provided the experimentally determined point of separation and pressure downstream of the body are referred to. Abramovich (1960), obtained an approximate solution for a turbulent flow in a circulation zone, downstream of a blunt body.
For the solution, the entire circulation zone is divided into two sections. In the first section (the upstream section where the flow rate

in the streamwise and reverse directions becomes equal), the theory of free turbulent stream is applied. In the second section, it is assumed that the flow field can be determined by an ideal fluid theory and the theory of functions of complex variables.

Ginevskiy (1969) obtained a solution for the Vulis (1957) flow model by an integral method. Vulis (1957), not taking into account the external inviscid flow field deformed by separation and low density in the separation zone, obtained a qualitative picture of wake flow. The flow loss of ideal flow momentum by uniform flow over the imaginary distorted body and the discharging turbulent flow is considered equal to the actual loss due to drag.

Khudenko (1961, 1968), by considering, the flow in the base area and wake, simultaneously, determined the potential flow referring to the Efros system. Khudenko proposed that in the first section of the circulation zone, the free stream line, determined by considering reverse flow (based on the experimental value of stagnation zone pressure), should coincide with the lines on which the longitudinal velocity component is equal to the arithmetic mean value of this component on the boundaries of the mixing zone of the external flow.

Kirnasov - Kudryavtsev (1970) flow model for the circulation base zone is as follows:

The static pressure in the base in assumed to be constant and known. The distribution of mean longitudinal velocity in the mixing

zone of streamwise and reverse flow is governed by

$$\frac{u_e-u}{u_e-u_m} = f(\eta), \qquad \eta = \frac{y-y_m}{y_e-y_m}, \qquad u_m < 0$$

where u_m is the longitudinal velocity at the center of reversed flows, y_e and y_m are ordinates of external and internal boundaries of the mixing layer respectively.

The coordinate of ideal flow y_{id} is related to displacement thickness $\Delta^* = y_{id} + \delta_a^*$ where subscript a refers to a trailing edge.

For the base area, $\Delta^* = \int_0^{y_e} (1 - \frac{\rho u}{\rho_e u_e}) dy = (1 + \frac{\rho_m}{\rho_e})y_m + \delta^*$

If $s = \int_0^x \sqrt{1+(y_{id}')^2}\, dx$ then $\delta = ks + \delta_a$ where $k = \text{const}$.

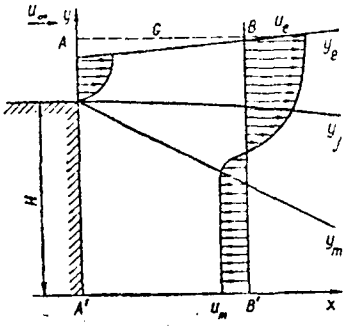

Fig.I.10. Diagram of flow in the circulation zone behind a bluff body.
[Shvets and Shvets (1976)]

The solutions of the conservation equations of mass and momentum in a projection on the x-axis for region A'A BB' lead to the following results:

$$y_e = \delta + \frac{y_{id}+\delta_a^*-\delta^*}{1+\frac{\rho_m}{\rho_e}m}, \quad y_m = \frac{y_{id}+\delta_a^*-\delta}{1+\frac{\rho_m}{\rho_e}m}$$

$$G = \rho_e u_e (H-y_{id});$$

$$\frac{(m+1)\frac{\rho_m}{\rho_e m} y_{id} + (1+\frac{\rho_m}{\rho_e m})\theta_a + (m+1)\frac{\rho_m}{\rho_e m}\delta_a^*}{\frac{m}{e^m}(m+1)H^*(m) + (1+\frac{\rho_m}{\rho_e})H^{**}(m)} = k\int_0^x \sqrt{1+(y_{id})^2}\, dx + \delta_a$$

where $m = -u_m/u_e$, G is the flow rate through AB due to turning of the external inviscid flow caused by base low density. H is step height.

$$\delta = y_e - y_m \qquad \delta^* = \int_{y_m}^{y_e} (1 - \frac{\rho u}{\rho_e u_e}) dy = \delta H^* \quad (m)$$

$$\theta = \int_{h}^{h\delta_a} (1 - \frac{\rho u}{\rho_e u_e}) \, dy = \delta_a \cdot H_a^*$$

$$\theta_a = \int_{h}^{h\delta_a} (1 - \frac{u}{u_e}) \frac{\rho u}{\rho_e u_e} dy = \delta_a H_a^{**}$$

The value of $m(x)$ is determined by these equations. The position of the separating stream line y_j is determined by

$$\int_0^{y_j} \rho u dy = 0$$

By taking the Schlichting's profile $f(\eta) = (1 - \eta^{1.5})^2$ and neglecting the transition section from the boundary layer to the jet stream layers, $\delta_a^* = 0.45 \, \delta_a$, $\theta_a = 0.134 \cdot \delta_a$

The free boundary flow solution obtained from Efros analysis (Kirnasov and Kudryavtsev 1970) was assumed as the boundary of the inviscid flow with the base pressure corresponding to the given boundary layer thickness.

Fig.I.11, shows the computed non-dimensional velocity on the axis of the circulation zone, indicating that the increase of axial velocity gradient is affected by the low density in the base area.

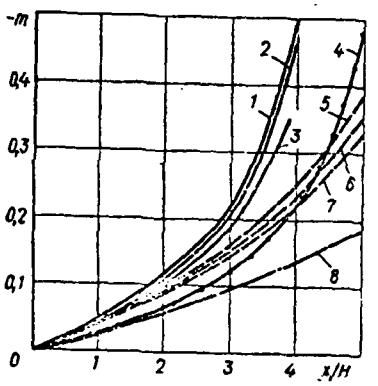

Fig.I.11. Change in dimensionless velocity on the axis of the circulation zone: [Shvets and Shvets(1976)]

1--$\delta_a/H = 0$, $k = 0.3$, $c_{p_b} \neq 0$;

2--$\delta_a/H = 0.15$, $k = 0.3$, $c_{p_b} \neq 0$;

3--$\delta_a/H = 0.5$, $k = 0.3$, $c_{p_b} \neq 0$;

4--$\delta_a/H = 0$, $k = 0.2$, $c_{p_b} = 0$;

5--$\delta_a/H = 0$, $k = 0.3$, $c_{p_b} = 0$;

6--$\delta_a/H = 0.15$, $k = 0.3$, $c_{p_b} = 0$;

7--$\delta_a/H = 0.5$, $k = -.3$, $c_{p_b} = 0$;

8--$\delta_a/H = 0$, $k = 0.2$, $c_{p_b} \neq 0$.

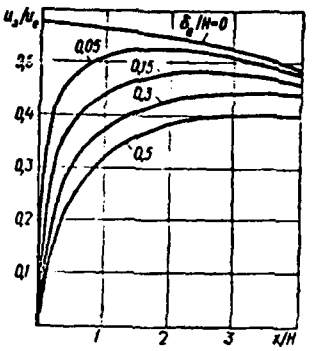

Fig.I.12. The effect of thickness of the initial boundary layer on velocity along the separation lines of flow when k = 0.3. [Shvets and Shvets (1976)]

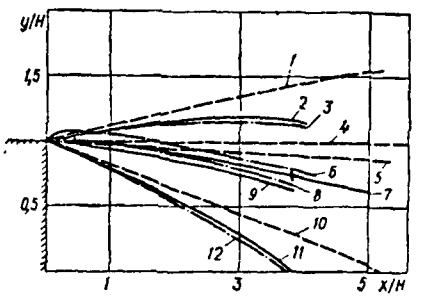

Fig.I.13. The position of characteristics of the boundary of the circulation zone: [Shvets and Shvets(1976)]

Solid lines $c_{p_b} \neq 0$, $\delta_a/H = 0$;

Dashed lines $c_{p_b} = 0$, $\delta_a/H = 0$;

Dashed-dotted lines $c_{p_b} \neq 0$, $\delta_a/H \neq 0$, $k = 0.3$; 3, 6, 12--$\delta_a/H = 0.5$;

8--$\delta_a/H = 0.15$; 1-3--$(y_e-\delta_a)/H$;

4, 7--y_{id}/H; 5, 6, 8, 9--y_j/H;

10-12--y_m/H.

It is also seen that the initial layer thickness causes a decrease in velocity on the axis and it is essential to select a proper constant for linear growth of the boundary layer.

Figure I.12, shows the calculated velocity along the separation stream line for $k = 0.3$

Figure I.13, indicates the effects of various parameters on the positions of characteristic boundaries.

It is noticed that most of the references for the separation zone, downstream of the body, are concerned with the mean motion and do not refer to the base pressure or low density in the base area, even though in the final analysis, the base pressure determines the external inviscid flow. The basic complexity of finding the base pressure at subsonic speed is due to the necessity of simultaneous computation of viscous flow in the separation zone and of external flow. For supersonic flow, however, it is not difficult to determine the external flow and for the cases of suppressed periodic motion (splitter plate) or of absence of periodicity (rearward facing step) in the separated zone. The base pressure can be predicted by the well-known analysis, in good agreement with the experimental data. However if the periodicity is considered, no analytical solution is available.

Nash (1963), presented a semi-empirical analysis to compute the base

pressure downstream of a flat plate using the measured length of the separated region and reattachment pressure. Nash (1964), also established the relation between the potential flow over a flat plate and the viscous flow in the wake. The viscous wake is considered by distributed sources, and their intensities are selected such that pressure in the base area is similar to the measured data. The momentum thickness of a far wake, determined by an integral method of momentum, is used to formulate the drag of an airfoil by

$$C_D = 4 \frac{\rho_e u_e^2 \theta_s}{\rho_\infty u_\infty^2 c} - \oint C_p \, d \frac{\Delta^*}{c}$$

where c is chord length, Δ^* is a closed contour including the displacement thickness round the body surface passing through the base section. The subscripts e and s are external inviscid flow downstream of separation and separation point, respectively. Distribution of C_p is determined based upon the external inviscid flow in a function of base pressure and incompressible flow solution is formulated from the compressible flow snalysis applying the similarity law.

Tanner (1970), obtained an analytical solution for the base pressure downstream of a wedge and a circular cylinder considering the mixing layer between the external flow and base and using experimental data of the drag and circulating fluid quantities.

Tanner (1973), extended this work for an incompressible flow with a zero thickness of the boundary layer to the compressible flow. Kirnasov and Kudryavtsev, computed the base pressure based upon the analytical model

shown in Figure.I.14.

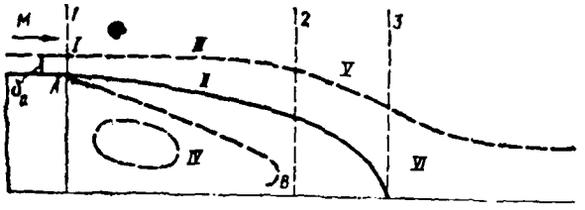

Figure.I.14. Diagram of flow in the wake of a semi-infinite plate: [Shvets and Shvets (1976)]
I--area of separation of the boundary layer; II--area of mixing with constant pressure; III--boundary of inviscid external flow; IV--stagnant zone; V--reattachment area; VI--area of development of the wake; 1, 2, and 3--respectively, the section of separation, beginning of increased pressure and reattachment.

The base section is divided into several characteristic field: In the separation zone, the momentum transfer takes place from the flow in the undisturbed boundary layer to a jet stream. The thickness of this field is an order of the undisturbed boundary layer and thus could be neglected. In Field II, the isobaric layer of mixing develops and the position of the mixing layer relative to the boundary line of the inviscid flow is fixed by the momentum equation.

In the reattachment zone, the pressure rises and the entrained mass is circulated, thus conserving the mass flow rate. Line AB is the separation stream For two-dimensional subsonic flow, the momentum thickness θ_∞ of the far wake, which is a measure of body drag is given by

$$\theta_\infty = \frac{\rho_{e_2} u_{e_2}^2}{\rho_\infty u_\infty^2} \theta_a - \frac{1}{4} \oint C_p \, d\Delta^* \qquad (15)$$

establishing a relationship between the momentum thickness of the far wake and base pressure. If the base pressure is known, the potential flow past a body may be computed based upon free boundaries, obtaining a pressure distribution along the body surface and contour of the stagnation zone close to the base section in satisfactory agreement with experimental data of Birkhoff and Zarantonello (1957), Khudenko (1968) Eppler (1954) and Mimura (1958).

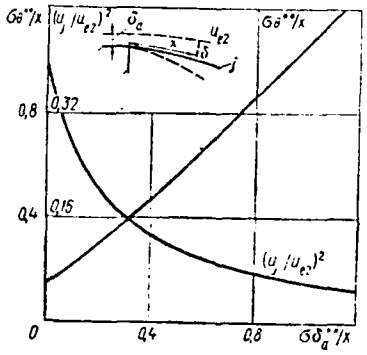

Fig.I.15. Parameters of the turbulent mixing layer (δ =12). [Shvets and Shvets (1976)]

In Figure.I.15, the parameters of the turbulent mixing layer are presented.

The momentum thickness of mixing layer θ^{**} along the separating stream line and the relative flow velocity along the separation stream line $(\bar{u}_j)^2 = (\frac{u_j}{u_{e2}})^2$ are shown in a function of θ_a/x where θ_a and x are the initial thickness of the boundary layer and the distance at which the mixing layer develops, respectively. For the computation, Tollmien's velocity profile of incompressible flow is used. The pressure between sections 2 and 3 is computed by considering the deceleration of flow along a separation stream line.

Denoting the reattachment pressure by p_3,

$$\frac{p_3}{p_2} = (1 - C_{e_2}^2 \bar{u}_j^2)^{\frac{-\gamma}{\gamma-1}} \quad \text{where} \quad C_{e_2} = \frac{\frac{\gamma-1}{2} M_{e_2}^2}{1 + \frac{\gamma-1}{2} M_{e_2}^2} \tag{16}$$

Assuming that the viscosity effect is small in the reattachment zone, the momentum equation of the separation stream line is given by

$$d\theta^{**}/\theta^{**} + (H + 2 - M_e^2)\, du_e/u_e = 0 \tag{17}$$

and the integration between sections 2 and 3 yields

$$\theta_3^{**}/\theta_2^{**} = \left(a_{e_2}/a_{e_3}\right)^{\frac{\gamma+1}{\gamma-1}} \left(M_{e_2}/M_{e_3}\right)^{2+\frac{1}{2}(H_{i2}+H_{i3})} \tag{18}$$

where H_{i2} and H_{i3} are shape factors of incompressible flow in sections 2 and 3 respectively.

The change of momentum thickness at the reattachment point to that at position of $u_e = u_\infty$ may be computed by the Squire and Young formula.

Finally, the momentum thickness far from the body is

$$\theta_\infty^{**}/\theta_2^{**} = \left(a_e/a_\infty\right)^{\frac{\gamma+1}{\gamma-1}} \left(M_{e_2}/M_\infty\right)^{\frac{1}{2}(5+H_{i3})} \left(M_{e_2}/M_{e_3}\right)^{\frac{1}{2}(H_{i2}-1)} \tag{19}$$

and M_{e3} is evaluated by

$$1 + \frac{\gamma-1}{2} M_{e3}^2 = \left(1 + \frac{\gamma-1}{2} M_{e2}^2\right)(1 - C_{e2}^2 \bar{u}_j^2) \tag{20}$$

Since for the separated and reattached flows, $H_{i3} = 2$ by using equa-

tions (20) and (15), the base pressure can be determined because H_{i_2} and θ_2^{**} are to be evaluated from the isobaric mixing layer computation. Another method for computing the incompressible flow base pressure is described here.

For steady flow, Stepanov (1970) and Gaumnes and Mastermat (1966), showed analytically, that the gas in the circulation zone under the dividing stream line is in equilibrium due to the effect of external forces (pressure and friction) on the boundary of the circulation zone. This analytical finding is confirmed by the experimental evidence of Tani, Iuchi and Komoda (1961) which shows that for the turbulent mixing layer, the equivalent force is close to zero. Therefore, by considering the component of resultant external forces in the free stream line direction and that sections 2 and 3 are close to each other, the following approximate equation is formulated;

$$C_{p2} H + 2 \int_A^B (\tau / \rho_\infty u_\infty^2) \, dx_j = 0$$

where H is the half width of base section and x_j is the distance along the separation stream line. Since conservation of momentum along the isobaric mixing layer is given by

$$\int_A^B \tau \cdot dx_j = \rho_{e_2} u_{e_2} (\theta_2^{**} - \theta_a^{**})$$

from these two equations

$$\theta_2^{**} / H = \theta_a^{**}/H - (\rho_\infty u_\infty^2 / \rho_e u_e^2) C_{p2} \qquad (21)$$

where value of θ_2^{**} is computed from the isobaric mixing layer equation. The computed base pressures downstream of a two-dimensional surface are compared with the experimental data in Figure.I.16 and I.17. The external inviscid flow is determined by Kirnasov and Kudryavtsev (1970) using the Efros diagram of reversed flow.

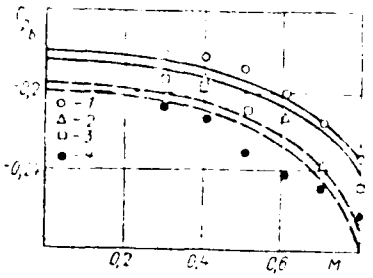

Figure.I.16. Relationship of base pressure behind a two-dimensional surface to the Mach number of free-stream flow (solid curves--calculation according to (21), dashed--according to (15) and (19) [Shvets and Shvets (1976)] :
1--H/θa = 33; 2--H/θa = 38.5;
3--H/θa = 68; 4--H/θa = 100
[Nash et al (1963)] .

In order to evaluate the flow characteristics in a crosssection with an initial pressure increase it is necessary to determine the distance at which the isobaric mixing layer develops. The position of section 2 is determined by the length of constant pressure zone of inviscid flow shown in Figure.I.18.

For convience, the phenomena of unsteady separated flow caused by a blunt body such as a cylinder or a slender body such as a wedge, are briefly presented among the numberous investigations, separately for incompressible and compressible flow.

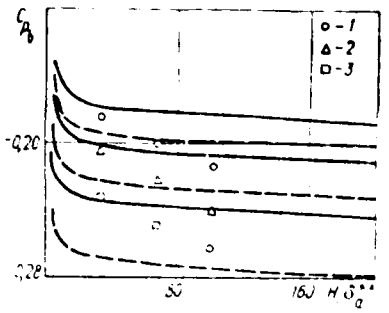

Figure.I.17. The effect of the initial boundary layer on base pressure behind a two-dimensional surface (solid curves--calculation according to (21), dashed--according to (15) and (19) [Nash et al (1963)] : [Shvets and Shvets (1976)]
1--M_∞ = 0.14; 2--M_∞ = 0.6; 3--M_∞ = 0.8.

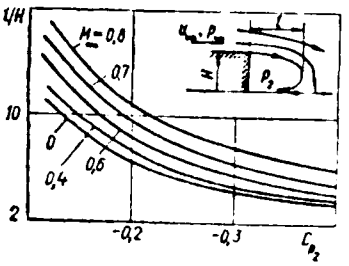

Figure.I.18. The length of zone of constant pressure in an inviscid flow. [Shvets and Shvets(1976)].

1.4.1 Unsteady Incompressible Separated Flow

It is well known that characteristics of the wake flow downstream of a blunt body at subsonic speed depend on the Reynolds number and a free stream turbulence but for the slender body with a fixed separation point the effect of the Reynolds number is less.

A cylinder as a blunt body causes intense action of a wake on external flow and on the body surface; the point of separation shifts. With an increase of the Reynolds number to Re = 30 - 40, the instability of the wake is observed in the Karman vortex street and when Re reaches about 90, one of the vortices breaks off causing asymmetry of flow. As a result, the second vortex separates and causes a state of alternating convergence of vortices. The wake flow is three-dimensional as indicated by Gerrard (1966). When $Re > 10^4$, cylinder flow can be divided into four different regimes; subcri-

tical, critical, supercritical and transcritical.

The subcritical regime is characterized by the plateau of the drag coefficient amounting $C_D = 1.2$ up to $Re \simeq 2 \times 10^5$ as seen in Figure.I.19.

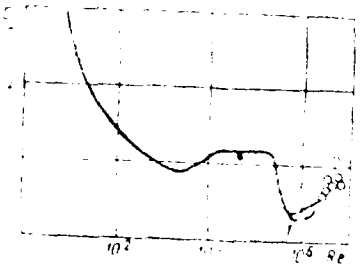

Figure.I.19. Drag coefficient of a cylinder:
[Chvets and Chvets (1976)]
1--[Delaney and Sorensen(1953)];
2--[Roshko(1961)].

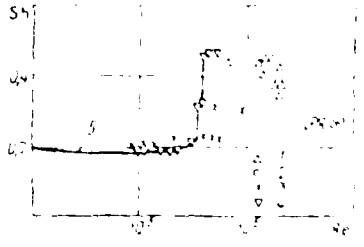

Figure.I.20. Relationship of the Strouhal number of the wake behind a cylinder to the Re number:[Chvets and Chvets(1976)]
1--[Delaney and Simmons(1924)];
2--[Roshko(1961)];
3--[Relf and Simmons(1924)];
4--[Bearman(1969)];
5--[Bittner and Etkin(1958)].

In this regime, the laminar boundary layer separates at a position $\sim 82^o$ measured from the forward stagnation point and a Strouhal number of 0.2.

In the critical regime, C_D decreases to $\simeq 0.3$ but the Strouhal number and the base pressure increase to 0.46 and - 0.2, respectively, as seen in Figure.I.20. Such a sharp decrease of the drag is due to the narrowing of the wake region caused by the shift of the separation point to a downstream position.

When $Re \simeq 3.3 \times 10^5$, the local laminar separation and subsequent reattachment occur, forming a laminar separation bubble and followed by turbulent flow separation at $\simeq 110^o$. Drag drops to $C_D \simeq 0.45$ and base pressure increases to $C_{p_b} = - 0.7$. When $Re \simeq 3.5 \times 10^5$, C_D decreases to 0.3 and C_{p_b} increases to - 0.2.

In the supercritical regime ($5.5 \times 10^5 < Re < 3.5 \times 10^6$) dominant frequency in the wake disappears and the convergence of vortices is irregular. The results of measurement in this regime are ambiguous due to the increased effect of a three-dimensionality caused by the break down of laminar separated bubbles. In the transcritical regime of $Re > 3.5 \times 10^6$, Roshko (1961), found that the definite frequency of the wake differing from the irregular convergence of vortices as usually observed, prevails and the turbulent separation point shifts to an up stream position. Thus, the separated wake region becomes broader and forms another plateau of high drag coefficient as seen in Figure I.19. It is to be noted that the boundaries of the flow regimes described are approximate and depend on the level of turbulence of free stream and on surface roughness. Kalashnikov and Kudin (1969), carried out experimental studies of the vortex, using a polymer solution in order to reduce the friction drag. The intensity of a Karman vortex caused by a wire exposed to a solution of polyoxyethylene, was considerably lower than that of water flow. The random pulsations occurred with small Reynolds numbers.

For the slender body, such as a wedge with a fixed point of separation, the effect of the Reynolds number on the flow characteristics is less than those of a blunt body, but the physical aspects are not as well-known. For the wake flow downstream of a wedge the first instability occurs when the Reynolds number increases up to $\simeq 80$.

The flow measurements after $Re \simeq 80$ up to the subcritical Reynolds number indicate that the characteristics of the wake of a wedge are similar

to those of a cylinder and for a wedge, characteristic points are displaced toward large Reynolds numbers.

1.4.2 Unsteady Compressible Separated Flow

As the free stream Mach number increases, the effect of the Reynolds number to the separated flow is less pronounced.

For $M > 1$, trailing shock occurs, forming a neck region of wake, thus the flow field differs from that of the subsonic flow. The discrete vortices appear downstream of the neck and the effect of periodic motion on the base flow is insignificant as Kuznetsov and Popov (1967, 1968) observed.

1.4.3 Steady Separated Flow

The characteristics of steady separated flow, involving reattachment on a solid two-dimensional surface, such as a step, may be categorized in the following three zones:

a. zone of three-dimensional separation downstream

b. zone of two-dimensional separation where the fluid flows in reverse direction close to the wall and parallel to the direction of free surface

c. zone of periodic changing with time close to the reattachment point.

Roshko and Lau (1965), show that the pressure distribution downstream of different geometrical shapes differ, however, an universal relationship independent of geometrical shapes can be established by correlating

$$\bar{C}_p = (C_p - C_{p_b})/(1 - C_{p_b})$$

with respect to x/x_c where x_c is the distance to the reattachment point as shown in Fig.I.21. This figure also indicates similar differences among maximum pressure and base pressure.

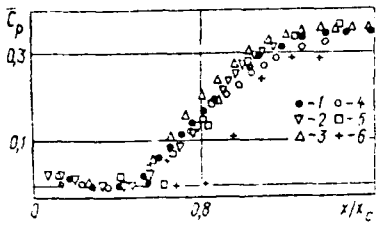

Fig.I.21. Universal distribution of pressure behind a step [Roshko and Lau (1965)]:

$\bar{C}_p = \frac{C_p - C_{p_b}}{1 - C_{p_b}}$, x_c-- is the distance to the reattachment point.

Bespalov and Khudenko (1959), Abramovich et al, (1961), Ukhanova (1966), Akylbayev et al, (1969), Ilizarova (1969) and McErlean and Przirembel (1970) consider that distribution of the mean streamwise and reverse velocities in the mixing zone are governed by the principle of a boundary layer and can be expressed by the universal function of velocity discontinuity. For the axisymmetric flow, the universal pressure distribution along the axis of the wake can be formulated by $\bar{C}_p = (C_p - C_{p_{min}})/(C_{p_{max}} - C_{p_{min}})$ with respect to $\bar{x} = (x - x_{min})/(x_c - x_{min})$ where x_c is distance of the point of deceleration as shown in Figure.I.22. by Calvert (1967).

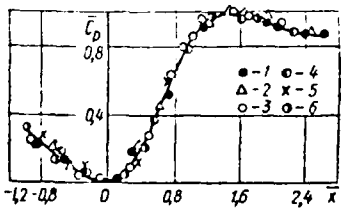

Figure.I.22. Universal distribution of pressure along the axis of the axis of the wake. [Calvert (1967)]
1--$\theta = 0$; 2--$\theta = 20^\circ$;
3--$\theta = 40^\circ$; 4--$\theta = 60^\circ$;
5--$\theta = 90^\circ$; 6--$\theta = 180^\circ$;
cylinder(1), cones(2-5), disk(6)

Sekundov and Yakovlevskiy (1970), measured the temperature downstream of a thin plate and a cylinder and formulated the temperature distribution by

$$T^{o} = (T - T_{\infty})/(T_{o} - T_{\theta}) = \exp(-y^2/Y^2)$$

where T_{∞} and T_{θ} are the temperature of undisturbed flow and on the wake axis respectively, y is the lateral coordinate measured from the wake axis and Y is the characteristic width of the temperature profile.

The magnitude of Y^2 is related to y^2 by

$$y^2 = \int_{0}^{\infty} Y^2 \Delta T^{o}\, dy \;/\; \int_{0}^{\infty} \Delta T^{o}\, dy$$

The magnitude of $Y^2/x.\theta$ (where θ is momentum thickness) is the characteristic intensity of thickening of the wake downstream of the plate and Mair and Maull(1972) found that,

for laminar wake, $Y^2/x.\theta = 7(Pr.Re)^{-1}$

and for turbulent wake, $Y^2/x.\theta = \text{const} \approx 0.1$.

In order to study more details of transonic flow phenomena Shvets (1972), measured the pressure distribution and the reattachment point of the flow past a wedge on a plate in a function of the Mach number as shown in Figure.I.23.

The pressure distribution is qualitatively in agreement with Nash, Quincey and Callinan's (1963) experimental data for a step.

At first, base pressure drops to a minimum at M = 1,02 and increases reaching a local maximum at M = 1.2.

Transition through the speed of sound consists of three phases of

restructuring of the flow: formation of a local supersonic zone in the region of the corners (here the velocity of inviscid fluid inside the mixing layer is subsonic); distribution of the supersonic zone for the entire free viscous layer (velocity of the internal flow after reattachment is subsonic); transition to a completely supersonic flow past a surface with supersonic velocity downstream of the trailing edge.

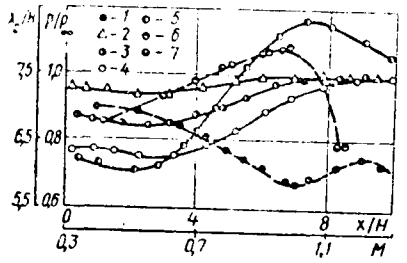

Fig.I.23. Flow behind a wedge on a plate:
[Shvets and Shvets (1976)]
1--base pressure $p/p_\infty = (M)$;
2--5--distribution of pressure on a plate
$p/p_\infty = f(x/H)$(2--M = 0.4; 3--M = 0.6; 4--M = 0.8; 5--M = 1.05); 6,7--reattachment points $x_c/H = f(M)$ according to data of visualization and measurement of pressure.

2. Analysis Based on Inviscid Flow

A presentation is made on the inviscid flow calculations to evaluate the characteristics of the separated flow, which are not usually considered in the contex of the inviscid flow. The separated flow field is viscous and involved with the viscous mixing of the outside inviscid flow with the inside viscous flow. Thus, the analysis based on the inviscid flow is not an easy one due to no clear physical aspects and the results are not exact and limited because of artifice representing dissipative flow by ideal flow. The justification of the inviscid approach is based, among others, on the following phenomena and flow models. Base flow immediately downstream of a wedge exposed to supersonic flow can be studied by an inviscid interaction between a supersonic vortex generated by the boundary layer upstream of the wedge edge and subsonic vortices adjoining in the base region. This problem is similar, to a certain degree, to that of supersonic flow past a blunt body; although the elliptic type of the subsonic flow equation is peculiar and for the solution upstream, perturbation should be considered.

The separation stream line dividing the recirculating flow and the streamwise flow can be considered as a contact surface for an infinite Reynolds number corresponding to the case of inertia force only. Furthemore, this maximum solution at $Re \to \infty$ is essential for asymptotic expansion, because effects of a weak viscous interaction can be studied systematically by referring to $Re \to \infty$. Batchelor (1956) modeled an inviscid incompressible flow by a pair of vortices rotating in opposite directions in the neighborhood of the base section and Weiss' (1967)

model of the inviscid flow expansion of the boundary layer flow is characterized by the transonic vortex flow occurring in a flow past a sharp angle with normal and tangential pressure gradients in the neighborhood of the angle, which are compara le to those equalizing the forces of pure inertia. Experiments of Ohrenberger (1968), indicate that viscous stress in the hypersonic flow expansion is negligible. Erdos and Zakkay's (1971) flow model, indicates that although vortices are created in the base region, viscous stresses and diffusion may not be accounted for.

Amsden and Harlow (1965), applying the numerical method of particles and cells calculated the time dependent development of two-dimensional and cylindrical wake downstream of a flat based projectile flying at supersonic speed, not considering the viscosity effect and real gas properties, although these can be taken into account in the calculations. The governing equations based upon the inviscid approach are the following conservation differential equations of mass, momentum and energy, omitting the viscosity effect and heat conduction.

$$(\partial \rho / \partial t) + (u \nabla) \rho = -\rho \nabla u$$

$$\rho (\partial u / \partial t) + \rho (u \nabla) u = -\nabla p$$

$$\rho (\partial I / \partial t) + \rho (u \nabla) I = -p \nabla u$$

For the calculation, a rectangular grid of fixed Euler cells is used, through which the fluid moves. The fluid is characterized by Lagrangian points of mass and these points are called particles. Each particle carries a constant mass of fluid and the mass of fluid within each cell is equal to the total mass of particles in it. Calculation is carried out at finite time intervals and at each step, new flow para-

meters are determined as follows:

At first, referring to the value of mass, calculations are made for volume, specific internal energy of the cells, and pressure. Then, based on the gradient of pressure, two velocity components are estimated, comparing with their maximum permissible magnitudes. At the second stage, each particle position is changed, referring to the estimated velocity, mass, momentum and energy.

The progress of the solution is recorded at given moments of time in the form of a location diagram of all the particles and other types of graphs and print-outs of the cell parameters. For example, a grid of 35 cells in height and 70 cells in length was used for the computation. When each calculation is completed, more than 36,000 particles have passed through the left boundary of the system.

Weinbaum (1966), investigated the inviscid behavior of a supersonic vortical flow undergoing a rapid expansion by applying the method of rotational characteristics and clarified phenomena of freshly separated flows, e.g., the formation of the separation shock wave and structure of free shear in the base region downstream of a sharp corner. Dynamics of expansion process, except in the immediate vicinity of the wall, are controlled largely by the inviscid pressure mechanics as evidenced by the results of order of magnitude analysis of the Navier-Stokes equations in the vicinity of a corner indicating that viscous terms are smaller than the inviscid terms throughout the boundary except for the highly viscous sublayer adjacent to the wall. Thus, the use of inviscid flow analysis is justified for the supersonic portion of the boundary layer expansion.

Since the entropy gradients normal to stream lines can appear both in the inviscid flow outside the boundary layer and in the viscous conducting layer close to the body surface, due to a free stream non-uniformity and a bow shock wave, the effect of the entropy gradient is considered for the investigation of behavior of a vortical flow in the rapid expansion.

Regardless of whether the shear profiles upstream of the corner expansion is produced by a curved shock wave, by shearing stress in the boundary layer or both, pressure signals emanating at the corner travel along the curved Mach lines and set up a system of reflected Mach waves of the opposite family. Weinbaum (1966), used physically reasonable approximations in order to obtain an inviscid analysis for the supersonic flow downstream of the leading Mach wave. The reflected waves which influence the shape of the dividing stream line and the location of rearward stagnation point, are studied and the variation in strength of the primary Mach wave along its length is determined.

Some of the original reflected waves from the expansion fan are expansion waves that, in turn, must reflect from the free boundary as compression waves. It is the coalescence of these compression wavelets that is responsible for the formation of the separation shock wave.

A numerical rotational characteristic solution for the expansion and separation at Mach number 3 with turbulent boundary layer, indicates that the method of rotational characteristics can be used to provide valuable new insights into freshly separated flow.

Weiss and Weinbaum (1966), carried out the details of a two-dimensional and axisymmetric expansion and separation of a hypersonic boundary layer at the shoulder of a blunt based body assuming the expansion of the body boundary layer is inviscid and obtaining numerical results by rotational characteristic calculation. At a high Mach number, the expansion separation process dominates the entire base flow producing a non-parallel vortical region that extends into the far wake.

Although the method of rotational characteristics is a powerful tool to analyze many aspects of separation process, it provides no infromation about the diffusion of momentum and energy in the vicinity of the dividing stream line. Nevertheless, the method of rotational characteristics well describes the various effects caused by the dominating inviscid pressure.

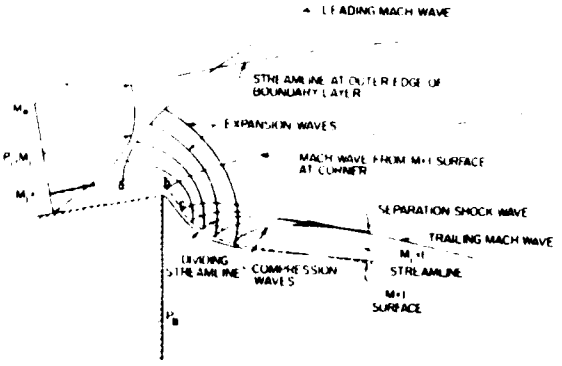

Fig. I.24. Schematic diagram of shoulder expansion region. (Weiss and Weinbaum (1966))

The physically realistic mathematical model used by Weiss and Weinbaum (1966), sketched in Fig. I.24, is the same as that of Weinbaum (1966). For the model, it is assumed that $M_i = 1$ stream between a and c, can be collapsed into a single point and $M_i = 1$ stream line beyond point c is taken to be a constant pressure surface and have the shape of the wall or dividing stream line. Numerical character-

istic computation is carried out based upon this model.

In general, if normal pressure gradients and non-similar boundary layer profiles exist upstream of the corner expansion, the complete specification of initial data would consist of initial profiles for the velocity components and any two state variables. However, if normal pressure gradients are neglected and Crocco's similar enthalpy profiles are assumed, then a complete description of all flow variables at the initial station can be obtained from the velocity profile alone.

The variations of entropy, vorticity and total temperature across the stream line are determined uniquely throughout the expansion once it is described on the initial data curve. To integrate along the characteristic curves the differential expression relating dq (magnitude of velocity) and $d\theta$ (angle the local flow makes with axial coordinate) is given and iteration is performed at each mesh point. Both the slope of the linear segments connecting mesh points and the average values of flow properties along each line are corrected using values obtained from the previous iteration.

Base pressure and behavior of the separated flow downstream of a blunt based wedge and a cone are determined uniquely by just two parameters of the Mach number of external flow, Me prior to expansion and $Re_{\infty s}$ of boundary layer flow at the separation, but at very large $Re_{\infty s}$ where the curvature of the dividing stream line is small, the effect of separation shock wave phenomena is negligible. The separation influences strongly the base region and its characteristic parameter is the ratio of the shoulder boundary layer thickness to the shoulder radius

of curvature δ/r.

Partial cancellation of the reflected waves occurs prior to separation. A significant portion of the reflected expansion waves produced in the primary expansion strikes the sphere of the cylinder surface before the separation point and reflects as expansion waves. The effect of these waves is to cancel the earlier reflected waves.

The iterative method for the solution of the completely coupled base flow problem is proposed by Weiss and Weinbaum (1966) who state as follows:

The characteristic solution provides a first approximation for the shape and length of the dividing stream line. The behavior of the flow in the vicinity of this stream line then can be obtained from a free shear layer solution. This solution yields velocity and temperature distributions and the stagnation pressure and temperature at the rear stagnation point. The velocity and temperature distributions on the dividing stream line can be used to calculate the recirculation region by the use of finite-difference techniques. The resulting pressure distribution in the recirculation region must be consistent everywhere with the pressure distribution in the outer vortical flow. Hence, a new characteristic solution is performed and a new dividing stream line shape determined which satisfies this pressure distribution. A second free shear layer calculation is then performed, taking account of both the corrected shape of the dividing stream line and the adverse pressure gradient in the recompression region. The displacement thickness of the shear layer is calculated and the displacement of the outer

rotational flow is determined for the next iteration on the inviscid flow. The corrected pressure distribution is obtained from a second solution of the recirculation region, based on the corrected values of the velocity and the temperature and the shape of the dividing stream line. In this manner, the inviscid flow, the shear layer, and the recirculation region are corrected systematically in that order. The requirements for a completely matched solution are the continuity of pressure, velocity, shear, temperature, and heat flux across the dividing stream line; the degress of freedom are the location of and velocity and temperature distributions on these stream lines. Such a program is rather ambitious, and it is hoped that a few iterations at most will result in "convergent" and useful solution.

Erdos and Zakkay (1971), analyzed the steady laminar near wake of a slender, two-dimensional flat based body at a hypersonic velocity within the context of an inviscid rotational flow. The upstream boundary layer is considered the source of vorticity convected into the base region but neglecting generation of additional viscous stress, there is heat transfer to the base and diffusion of the vorticity. The overall structure of the base flow pattern is the result of an inviscid interaction between the subsonic recirculating flow and the outer supersonic rotational stream. Numerical solutions are carried out by time-dependent method known as the two-step Lax-Wendroff (1960) technique. The steady-state solution is obtained asymptotically, circumventing the complexities associated with the steady problems.

The near wake flow of a bluff-based body at supersonic flow is

mixed subsonic/supersonic flows involving subsonic recirculating flow. Eros and Nakkay (1971), contributed to the development of a powerful numerical method to solve the general category of the mixed flows. The steady near wake problem in the limit of vanishing viscosity is of the mixed elliptic/hyperbolic type. However, this problem is reduced to purely the hyperbolic type by seeking the steady state solution as the asymptote of a time-dependent problem, subject to steady boundary conditions.

A finite difference technique of Lax is used and since the solutions of hyperbolic equations which contain surfaces of discontinuity are not, in general, unique, uniqueness is a consequence of imposition of additional constraint not implicit in the governing equations. The Lax-Wendroff technique obtains such constraint correctly in the solution through a formulation that allows the differential equations to satisfy the conservation laws, within the accuracy of the difference approximations. The solutions obtained through its use are considered inviscid, because the effects of artificial viscosity are confined to layers of thickness of the order of the small mesh size and the existence of a limit can be demonstrated as the mesh size is progressively diminished.

The conservation equations of Lax are used and for the finite difference formulation the Lax-Wendroff technique, termed the two-step method, is applied.

Comparisons of the predicted values for a 10° wedge at $M_{\infty} = 6$ are in agreement for the following characteristics with the experimental data of Batt and Kudota (1969): base pressure, pressure distribu-

tion normal to the axis, stream line pattern in the near wake, a Reynolds number based on the wedge height as low as 1.4×10^4 and an adiabatic wall condition and static pressure distribution along the wake center on the cold wall condition and wake location.

Erdos and Zakkay (1971), pointed out that their analysis can be easily extended to incorporate the Navier-Stokes equations rather than the Euler equations as governing conservation laws, with minimal change in the numerical details. However, accurate description of the free shear layer along the dividing stream line, of the flow near the rear stagnation point and of the boundary layer on the base in the wake requires a grid size of the corresponding scale and use of an appropriate coordinate transformation or a variable grid size, which is probably essential in this case.

Khoroshko (1969), calculated numerically, by a method of finite difference the characteristics of laminar and turbulent wake flow downstream of blunt bodies exposed to hypersonic speed, evaluating the effect of pressure gradient and chemical reaction on the flow parameters in a rotational external flow. The results also show that the effects of diffusion on the flow parameters are larger, the smaller the Re; indicating that at low free stream pressure or at high altitude, a perturbed flow rapidly encompasses the entire region. For comparison, the change of temperature, density of electron, velocity for laminar and turbulent flow are shown in Fig.I.25 for the same Re.

Krayko and Tagirov (1970), investigated the optium shape of the two-dimensional trailing section which will cause the minimum wave drag

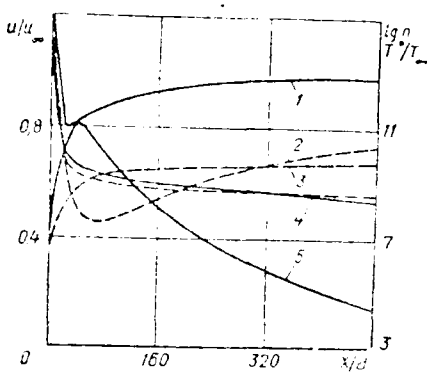

Figure I.25 Change in temperature, density of electrons and velocity in the case of laminar (dashed lines) and turbulent (solid lines) wakes [Khoroshko (1969)] (θ-10°, V_∞=7000 m/s): 1,3--u/u_∞; 2,5--T^*/T_∞; 4--n

for a given lift by taking account of the friction force, assuming that the base pressure is given in a function of M_∞. The optimum shape of the flat trailing section evaluated by a computer when $Re = 10^9$ is close to the contour at $Re \to \infty$, corresponding to that of an ideal flow with no friction.

2.1. Numerical Experiment

Presently, numerical experiments are being progressively expanded for the study of various phenomena described by the equations of mathematical physics.

The method of particles in cells enables the study of the complex phenomena of multicomponent media dynamics particles which "follow" downstream free surfaces and lines of separation involving interaction, etc. The method of "large particles" applicable to gas dynamic problems is described by Belotserkovskiy and Davydov (1971). Using the method of large particles, it is possible for a single algorithm to obtain the flow picture past bodies of various shapes with a broad range of changes of the initial conditions at subsonic, transonic and supersonic speeds.

Applying the method of large particles, Belotserkovskiy and Davydov (1971, 1974), carried out the numerical experiments and reported it in the Nauka Press (1974), edited by Belotserkovskiy, (for separated flow). One of its examples is shown in Fig.I.26, illustrating the stream lines downstream of a sphere generated by incompressible and compressible flows.

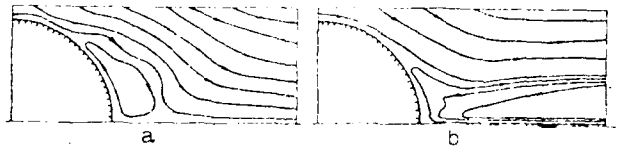

Figure I.26 Stream lines in a base region with flow past a sphere of compressible (a) and incompressible (b) fluid (M = 0.3) [Belotserkovskiy and Davydov (1974)]

For the compressible flow, the separation zone is closed and localized downstream of the body, while for the incompressible flow, the separation zone spreads downstream and flow is unsteady and turbulent.

3. Analysis Based on Separation Stream line and Mixing Layer

In this section, various methods used to evaluate the separated flow characteristics based upon the separation stream lines and mixing layer are reviewed. Since the methods of Chapman-Korst, Nash, Kirk (1959), and Denison and Baum (1963) etc. are described in P. K. Chang's book, Separation of Flow, 1970, Pergamon Press, and elsewhere, no details of these methods are given.

The flow models to be used for analysis based upon the separation stream line with no injection of fluid into the base region and with injection are shown in Fig.I.27a and Fig.I.27b respectively.

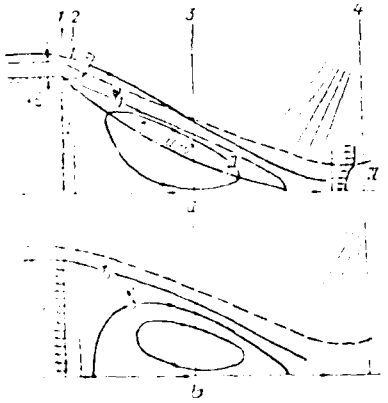

Fig.I.27. A picture of flow in separation method without inflow (a) and with the inflow (b) of a mass (dashed line corresponds to the boundary of an inviscid flow). [Shvets and Shvets (1976)]

The external inviscid supersonic flow region is divided into the following characteristic regions: Undisturbed flow region upstream of section 1, separated flow region in the base with a constant pressure (between sections 2 and 3), a compression region (between sections 3 and 4).

It is assumed that compression takes place isentropically for the laminar flow and through an oblique shock wave for the turbulent flow. In the neglibibly small area I compred to the body height, a transfer of the undisturbed viscous layer to

the isobaric jet stream takes place, compression occurs in area III and the mass is conserved in the base region.

Stream line ψ_b is determined, considering the conservation of the mass as,

$$G_i = \rho_i u_i H = \int_{y_b}^{y_j} \rho u \, dy$$

where G_i is the injected mass flow rate, H is the height of the base section, y_j and y_b are normal coordinates of the separation stream line and the line of constant mass during injection, respectively. When $G_i = 0$, then $\psi_j = \psi_b$. The Chapman-Korst analysis, assuming a zero initial boundary layer thickness, predicts the asymptotic base pressure at large Reynolds numbers, thus for $Re = 10^6 - 10^7$, a good agreement with the experimental data is reached. However, since the initial boundary layer thickness is actually not zero, the finite thickness of the initial boundary layer is considered as a parameter of the mixing layer and reattachment. The velocity profile in the mixing layer is assumed as asymptotic. Such an asymptotic profile can be located by shifting the actual stream, upstream at a distance to be determined from the conditions of equal mass flow and motion of an imaginary inviscid stream corresponding to an actual boundary layer. Sirieix (1960) and Dewey (1965), found experimentally that the compression zone is not so short as the Chapman-Korst model assumes, and that it extends 1-2 body diameters from the trailing critical point. This indicates that there is need for improvement by considering the forces, viscosity and turbulent friction in this zone where the pressure gradient is large.

Bondarev and Yudelovich solution

Bondarev and Yudelovich (1960), approximately evaluated the increase of the base pressure downstream of a wedge at hypersonic speed introducing a certain "effective" surface parallel to the free stream. Effective pressure and a Mach number on this surface were determined by considering the turning of a Prandtl-Meyer flow at an angle β enclosed between the effective surface and the wedge surface. Approximate analysis of the flow past a wedge at hypersonic speed may lead to an interesting phenomena of the base pressure. With an increase of a free stream Mach number, the base pressure decreases at first, then increases rapidly, approaching the free stream pressure. This is due to the fact that at hypersonic Mach numbers, entropy downstream of the oblique shock wave increases, causing the change of the Mach number on the wedge surface. Thus, the pressure on the wedge increases proportionally to the square of a free stream Mach number. The total level of the pressure downstream of the wedge increases and the base pressure exceeds the free stream pressure.

Bondarev (1964), evaluated the base pressure by taking account of the boundary layer effect and compared it to that computed assuming zero thickness of the boundary layer downstream of the base section, as shown in Fig.I.28.

The base pressure increases by $\delta a/H$ and the effect of the boundary layer becomes stronger with an increase of the Mach number. Bondarev (1964), studied the effect of the ratio of specific heats, γ, to the

base pressure assuming a zero initial boundary layer thickness in a parameter of the Mach number as shown in Fig.I.29.

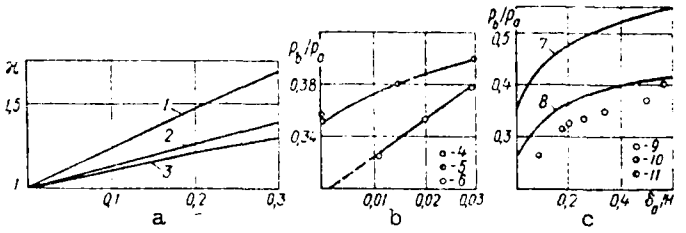

Fig.I.28. Relationship of base pressure to the thickness of the boundary layer in the separation section: [Shvets and Shvets (1976)] a--calculation 1--M = 4 [Bondarev (1964)]; 2--M = 3[Bondarev(1964)]; 3--M = 2[Bondarev(1964)]; b--M = 2.025; Pr_T = g = 1; γ = 1.4; 4--calculation[Tagirov(1961)]; 5--calculation[Korst et al,(1955)]; 6--experiment[Sirieix(1960)]; c--7, 8--closure conditions according to Korst, according to Tagirov[Tagirov(1961)]; 9--experiment, M = 2.025[Sirieix(1960)]; 10--M = 2 (see chapter I Neyland(1969a); 11--M = 2.2[Badrinarayanan(1961)]

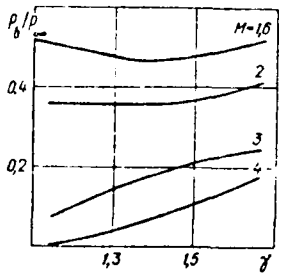

Fig.I.29. The effect of the ratio of specific heats on base pressure [Bondarev (1964)]

Bondarev (1963), computed the time needed to establish to steady parameter conditions of a supersonic separated flow downstream of a two-dimensional surface exposed to sudden changes of an external flow pressure. He assumed that the mixing layer flow is quasi-steady and the change of the base pressure is to be determined by filling (or emptying the base region by the mixing layer fluid.

The Zapirov solution

Zapirov (1964, 63, 66), obtained the simplified analytical solutions for the pressure and the temperature in the base region by considering the initial boundary layer and by dividing the entire flow area into five zones.

The position of the shock wave is determined at the intersection of the zero velocity line and the axis of symmetry. The magnitude of reattachment angle θ_c is evaluated by $\sin \theta_c = k_c$ at the position of the minimum reattaching boundary layer thickness, i.e. at the condition of $d\delta / dx = 0$. The symbol k_c refers to the mixing coefficient at reattachment which is taken, for simplicity, to be equal to k, in the isobaric region.

In the reattachment zone, the interaction of the external inviscid flow with the dissipativ layer is evaluated using the Crocco-Lees theory. The computed base pressure in the absence of heat flow is shown in Fig.I.30 in comparison with the experimental data.

The Korst solution of base pressure is for $\delta_a = 0$ in the mixing zone

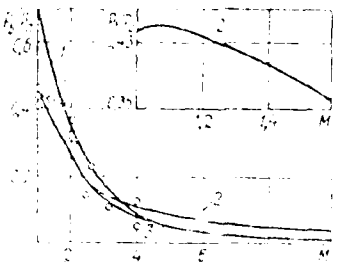

Fig. I.27. Relationship of base pressure to the M number (Pavirov (1966)) :
1--conditions of closure according to the Korst theories;
2--when using the Prandtl-Meyer relationship;
3--method of tangential wedges (marks--experiment).

which is insignificantly affected by the constant empirical parameter of spread rate 6 .

For the computation of the base pressure affected by the initial boundary layer thickness of a turbulent mixing layer, the initial velocity profile after the turning is given by 1/n power law, (n = 7 is used for the calculation). The obtained solution is given in a function of x. Thus, it is not similar, and the effect of δ_a is taken into account through the non-self-similar solution in the turbulent mixing zone. The predicted base pressure is compared with experimental data in Fig.I.28 with a discrepancy of 10% due to the approximation of $k_c = k$. If the Korst analysis is used, predicted values amount to 1.5 times greater than the measured data.

The solution of Neyland and others

Yel'kin and Neyland and Sokolov (1963), using two-dimensional conservation equations of mass, momentum, and energy, attempted to solve the laminar base pressure downstream of a wedge exposed to a high Mach number. By taking account of thermodynamic equilibrium, dissociation of a binary mixture of atoms and molecules, but not of diffusion as well as layer thickness in the laminar mixing zone, a self-similar solution

of ordinary non-linear differential equation has been obtained by using the Dorodnitsyn transformation and a computer.

As shown in Fig.I.31 and I.32, when $M_\infty \to \infty$, then $p_b/p_\infty \to \infty$, and with an increase of wedge thickness, p_b/p_∞ also increases while p_b/p_w, (where p_w is the pressure on the wedge surface) becomes very small.

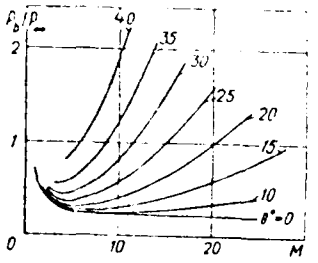

Fig.I.31. Base pressure behind a wedge [Yel'kin et al (1963)]

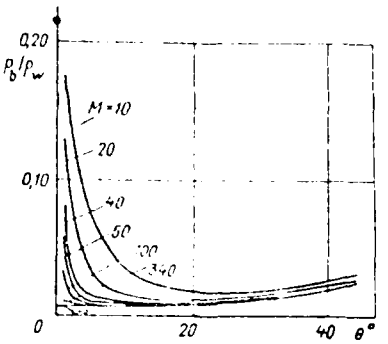

Fig.I.32. Ratio of base pressure to pressure on the wedge [Yel'kin et al (1963)] (the point corresponds to the plate when M = ∞).

The base pressure downstream of a blunt edged plate is given by:

$$\frac{p_b}{p_\infty} = \left[1 + \frac{\gamma-1}{2}\frac{\Sigma-1}{\gamma}\sqrt{\frac{2\gamma}{(\gamma+1)\Sigma + (\gamma-1)}}\right]^{\frac{-2\gamma}{\gamma-1}}$$

where $$\Sigma = \left(\frac{1}{1-\bar{u}^2}\right)^{\frac{\gamma}{\gamma-1}}$$

It is noted that the hypersonic flow principle independent from M_∞ is also applicable for the base flow downstream of an arbitrary body shape. When $M_\infty \to \infty$, the density and velocity of the free stream become constant and the pressure as well as the speed of sound approach to zero. At a large Mach number, the magnitude of flow parameters in

the shock layer affecting the base pressure also become fixed, thus confirming the hypersonic principle.

Neyland and Sokolov (1964), investigated the behavior of the base pressure downstream of a wedge at an angle of attack and supersonic speed and presented the predicted base pressure in Fig.I.33.

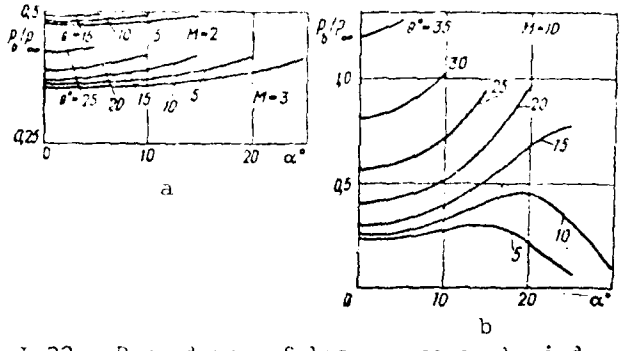

Fig.I.33. Dependence of base pressure behind a wedge on the angle of attack [Neyland and Sokolov (1964)]

If the half-angle is large, depending upon M_∞ , the shock wave on the lower part detaches and the base pressure increases with an increase of the angle of attack. However, if the half-angle is small and the Mach number on the upper part is large, then the base pressure becomes small approaching zero and the shock wave remains attached around the lower surface. The base pressure reaches a maximum value at a certain angle of attack and drops as seen in Fig.I.33.

Neyland (1964), obtained the self-similar solution of the non-linear equation of motion by taking account of compressibility and heat transfer assuming $Pr_T = 1$. For the turbulent mixing zone the following two-dimensional steady flow equations are used.

$$\rho u \frac{\partial u}{\partial x} + \rho v \frac{\partial v}{\partial y} = -\frac{\partial p}{\partial x} + \frac{\partial}{\partial y} \left[(\mu + \epsilon) \frac{\partial u}{\partial y} \right]$$

$$\frac{\partial (\rho u)}{\partial x} + \frac{\partial (\rho v)}{\partial y} = 0$$

$$\rho u \frac{\partial T^*}{\partial x} + \rho v \frac{\partial T^*}{\partial y} = \frac{\partial}{\partial y} \left[(\mu + \epsilon) \frac{\partial T^*}{\partial y} \right]$$

$$+ \left(\frac{1}{Pr} - 1 \right) \frac{\partial}{\partial y} \left(\mu \frac{T}{y} \right) + \left(\frac{1}{Pr} - 1 \right) \frac{\partial}{\partial y} \left(\epsilon \frac{\partial T}{\partial y} \right)$$

where T^* refers to temperature of decelerating flow. For the case of isobaric mixing, since $\frac{\partial p}{\partial x} = 0$.

$$\tau_T = \epsilon \frac{\partial u}{\partial y} \gg \mu \frac{\partial u}{\partial y} \qquad \text{and} \qquad q = \lambda_T \frac{\partial T^*}{\partial y} \gg \lambda \frac{\partial T^*}{\partial y}$$

where λ is conductivity of heat, the governing equations are considerably simplified. For the solution, Prandtl's mixing length theory and Tollmien's boundary conditions are applied.

The McDonald solution

McDonald (1965, 66), studied semi-empirically, a two-dimensional and axisymmetric base pressure with an initial turbulent boundary layer, assuming the isentropic compression of the separation stream line, ignoring the mixing of external flow with a viscous layer as well as the effect of tangential stress. For the external flow passing through the viscous layer in the reattachment zone, the Squire-Young formula is used, assuming that thicknesses of displacement and momentum are the same as those of a flat plate with identical conditions.

The Carriere and Sirieix solution

Carriere and Sirieix, in order to compute the base pressure, consider the angle of reattaching flow θ_c as the criterion for reattachment. The value of θ_c which satisfies the Korst-Chapman condition is smaller than that measured by Carriere (1965) as seen in Fig.I.34.

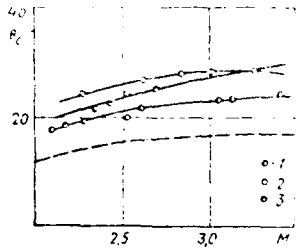

Fig.I.34. Dependence of the reattachment angle of flow on the M number [Carriere (1965)]:
1--two-dimensional flow;
2--reattachment on a cone;
3--reattachment on the internal wall of a cylinder (dashed line--calculation according to the Korst-Chapman formula).

Siriex (1967), proposes that the following equations of θ_c be used after consideration of viscous effects and turning of inviscid flow,

$$\theta_c = \theta(M_a) + c_q \frac{\partial \theta}{\partial cq}$$

$$c_q = \frac{q}{\rho_e u_e L} - \frac{u_k}{\rho_e u_e L} - \frac{\theta}{L}$$

where c_q is the coefficient of injection, $\theta(M_a)$ is the angle of inviscid flow turning, q the mass discharge rate into stagnation per unit of length ($q = \rho_j u_j$), u_k the streamwise velocity component, θ the momentum thickness in the separation zone, L the effective length of mixing field or the length of self-similar layer. This criterion of reattachment at supersonic speed is very useful in practice to evaluate the effect of a mass injection at a low velocity and a small discharge in the stagnation zone. The predicted base pressure using this criterion is in good agreement with experimental data.

A comparison of results obtained by Glotov and Moroz (1970) and Glotov and Lavrukhin (1974), with measured data of $\theta_c = f(M)$ by Carriere (1965), (where θ_c is the angle of reattachment on a channel wall of inviscid stream evaluated by the method of characteristics for measured pressure), indicates that in the self-similar flow, the θ_c value agrees for practical use, although its magnitudeis larger than that obtained by Sirieix, Mirande and Delery (1966) using Korst-Chapman criterion of reattachment.

Attempts to formulate a universal relation of $\theta_c = f(M)$ as well as $x_c = f(M)$ applied, for example, to different shapes of the channel flow downstream of sudden expansion, were not successful. The reattachment criterion based upon the magnitude of maximum increase of relative pressure on the wall did not lead to a universal formulation.

Kessler solution

Kessler (1967), derived a more accurate approximate solution to the turbulent two-stream mixing problem, including initial boundary layer effects. For this solution, only an empirical similarity parameter σ for the turbulent mixing is needed whereas for the complete solution involving initial boundary layer by Korst and Chow's (1966) equivalent bleed concept requires the knowledge of the eddy diffusivity which was not available in 1967.

In order to account for the initial boundary layer effects, Korst and Chow (1966), utilized a lateral displacement of the fully

developed velocity profile, i.e. a profile obtained for a no initial boundary layer. The result shows that the velocity profiles from the equivalent bleed method do not agree until one is much further downstream. Since the origin shift gives better agreement with experimental data for free shear layers, Kessler (1966) extended this technique to the two-stream mixing problem.

Kirk (1959), Nash (1962) and Hill (1966), have proposed to shift the origin of the actual physical jet upstream a distance x_o to an imaginary inviscid jet, i.e. a jet with no initial boundary layer on a free shear layer. The criteria for determining x_o is that the mass flow and momentum of the imaginary jet at $x = x_o$ are respectively equal, to the mass flow and momentum of the actual attached boundary layer.

In Fig.I.35., the actual physical coordinates of the real mixing region with an initial boundary layer by X and Y, while for imaginary two-stream inviscid jet by $P = X + x_o$ and $Q = Y - y_o$. Applying conservation of mass to control volume shown in the Fig.I.35, and introducing the boundary layer displacement thickness δ^*,

$$\rho_a u_a (Y_{Ra} - y_o) + \rho_b u_b (y_o - Y_{Rb}) + \rho_b v_b x_o = \rho_a u_a (Y_{Ra} - \delta_a^*) + \rho_b u_b (-Y_{Rb} - \delta_b^*)$$

where subscripts a and b refer to conditions of the primary free stream and the secondary free stream respectively.

The application of conservation of momentum to the control volume together with the boundary layer momentum displacement thickness δ_m^* at X = 0, leads to

$$\rho_a u_a^2 (Y_{Ra} - y_o) + \rho_b u_b^2 (y_o - Y_{Rb}) + \rho_b v_b x_o u_b = \rho_a u_a^2 (Y_{Ra} - \delta_{ma}^*) + \rho_b u_b^2 (-Y_{Rb} - \delta_{mb}^*)$$

By solving these equations for x_o and y_o and introducing dimensionless velocities $\varphi_b = u_b/u_a$ and $\varphi_b' = v_b/u_a$ and boundary layer momentum thickness θ,

$$y_o = \left[\delta_{ma}^* - \varphi_b \delta_a^* + (\rho_b/\rho_a)\varphi_b^2 \theta_b \right]/(1 - \varphi_b)$$

$$\left[\theta_a - (\rho_b/\rho_a)\varphi_b (\delta_{ma}^* + \delta_b^*) \right] +$$

$$x_o = \frac{(\rho_b/\rho_a)\varphi_b^2(\delta_a^* + \delta_{mb}^*) - (\rho_b/\rho_a)^2 \varphi_b^2 \theta_b}{\left[(\rho_b/\rho_a)\varphi_b'(1 - \varphi_b) \right]}$$

Once the origin shift to the imaginary jet is determined, then the velocity profile of the mixing region can also be determined by using the momentum intergral technique of Korst and Chow (1966) for the "restricted" case (no initial boundary layer). Korst and Chow's (1966) technique uses a linearized solution of the boundary layer equation that gives a velocity distribution

$$\varphi = u/u_a = 0.5 \left[(1 + \varphi_b) + (1 - \varphi_b) \operatorname{erf} \eta \right]$$

where

$$\eta = \sigma y/x \qquad \text{and} \qquad \operatorname{erf} \eta = \left(\frac{2}{\pi^{0.5}} \right) \int_0^{\eta} e^{-B^2} \, dB$$

The velocity profile is considered valid in an instrinsic coordinate system (x,y), which is located relative to the reference coordinate system (P,Q) by means of continuity and momentum integrals.

This origin shift approximation is not restricted to the choice of any particular velocity profile for the mixing region. However, x_o is a function of the selected velocity profile depending explicitly on the vertical opponent of the entrainment velocity v_b.

Hill (1966), showed that the Kessler (1967) approximation agrees with the experimental single stream mixing velocity profile for $X/\theta > 75$,

but for the two-stream mixing velocity profile, with a finite initial boundary layer, no experimental data was available to confirm the applicability of the Kessler (1967) method.

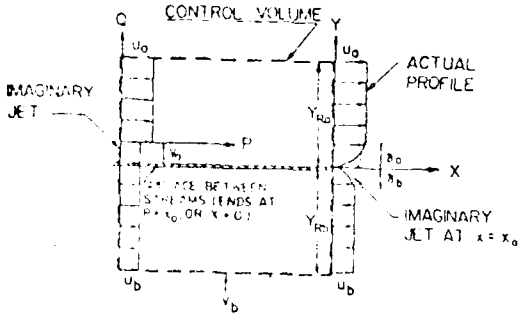

Fig.I.35. Determination of origin displacement. [Kessler (1967)]

The Tarnopol'skiy solution

Tarnopol'skiy and Golikov (1966), calculated the boundary layer thickness using a self-similar mixing layer and shifting a distance x'. The extent of self-similarity is determined by:

$$\left[\int_{y_t}^{y_e} \rho u^2 dy \right]_j = \int_0^{\delta} \rho u^2 dy$$

$$\left[\int_{y_t}^{y_e} \rho u dy \right]_j = \int_0^{\delta} \rho u dy$$

where subscript j and t refer to equivalent self-similar flow and the leading point of a body, respectively. The momentum thickness θ_2 is given by

$$\theta_2 = \int_0^{\delta} \frac{\rho u}{\rho_e u_e} \left(1 - \frac{u}{u_\infty}\right) dy = \left[\int_{y_t}^{y_e} \frac{\rho u}{\rho_e u_e} \left(1 - \frac{u}{u_e}\right) dy \right]_j$$

using $F' = u/u_e$,

$$\int_{y_t}^{y_e} \frac{\rho u}{\rho_e u_e}\left(1 - \frac{u}{u_e}\right) dy = \frac{x_j}{\sigma} \int_{F_1}^{F_2} (1 - F')dF$$

where x_j is the distance of the equivalent flow and x' is then given by

$$x' = \frac{\sigma\, \theta_2}{\left[\int_{F_1}^{F_2} (1-F')\, dF\right]_j}$$

The initial momentum thickness of the boundary layer at the separation point is computed by

$$\frac{\rho_{3e}}{\rho_{1e}} \frac{u_{3e}}{u_{1e}} \frac{\theta_2}{\theta_1} = \frac{M_{1e}^2}{M_{3e}^2}$$

where subscript 3 refers to the downstream of turning. The displacement of the dividing stream line in a function of θ is computed based upon the conservation of the mass between the separation stream line and passing through the lower boundary of the mixing zone of the equivalent system and actual layer i.e.

$$(\psi_j - \psi_t)_{x=0} = (\psi_j - \psi_1)_{x\neq 0}$$

Fig.I.35, shows $\bar{u}_j$ in functions of Crocco number and θ_a/H for Tollmien flow in comparison to predicted and measured data.

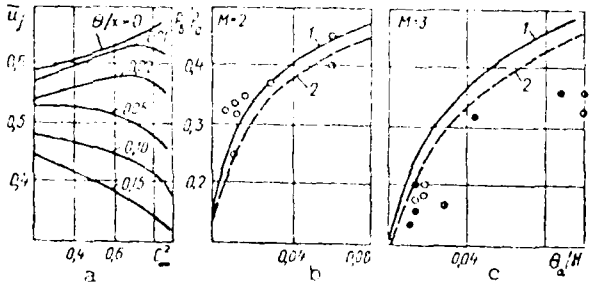

Fig.I.36. Relationship of the value of velocity on dividing stream line to the Crocco number (a) and base pressure to the momentum thickness (b,c) [Tarnopol'skiy and Golikov (1966)] : 1--calculation [Neyland(1969a)] 2--calculation [Tarnopol'skiy and Golikov(1966)] ; marks--experiment [Neyland(1969a)].

Lamb and Hood solution

A simple control analysis of plane turbulent reattachment in an isoenergetic base separated region with no mass bleed was developed by Lamb and Hood (1968) who obtained a wall static pressure distribution prediction in reasonable agreement with experimental data up to M=4.5. This analysis is based on free interaction in the reattachment zone utilizing a numerical search technique to determine the condition.

For the separated flow zone downstream of a rearward facing step, the point of initial interaction is considered as the end of the base region and denoted as the cutoff station of the control volume.

The conditions that must be satisfied at this cut off station are:

a) the zero velocity edge of the mixing zone and reverse flow must coincide.

b) mass flow rate in the free shear layer below the dividing stream line must equal that of the reverse flow.

The former condition determines the relative magnitude of momentum fluxes and pressure forces on the control volume.

Downstream of the dividing stream line reattachment point, boundary layer redevelops causing the wall pressure to approach a nearly uniform value. This redeveloping wall layer is governed primarily by the geometry and inviscid flow downstream of reattachment.

In the past, since only mechanical energy levels are considered in the escape criterion of the Chapman-Korst model, no information about the pressure distribution near the reattachment was obtained. Lamb and Hood (1968), considered the possible isentropic stagnation of the dividing stream line to a downstream static pressure instead of the original Korst model which attributes the downstream static pressure to oblique shock. For the analysis of reattachment, the corner flow effect is neglected and assumed that the lower portion of the shear layer can be treated as if the highly distorted free stream is not present.

Using control volume, momentum integral equations for longitudinal and transverse directions are written.

For the analysis of the pressure distribution downstream of reattachment, which is scarce, Lamb and Hood (1968), developed a simple analysis applicable for all types of external flow or geometric conditions by the first-order approach, assuming free interaction. In the absence of any impingement of shock or expansion waves from the external flow, the pressure distribution downstream of reattachment can be easily determined by the usual coupling of inviscid motion equation with intergral boundary layer equation.

Starting from the reattachment point, a step-wise computation is carried out until the local pressure becomes essentially constant. This simple procedure is justified due to the emphasis of pressure rather than the details of viscous layer. In order to estimate the boundary layer parameters at the reattachment as the initial condition

of developing layer, Lamb and Hood (1968), postulate that due to the extermely large pressure gradient adjacent to the reattachment zone, the growth of the outer portion of the viscous flow is negligible. This implies that the mass flow above the dividing stream line at the cutoff station is equivalent to the mass flow flux at the reattachment. The exact velocity profile at the reattachment is not known, but the integral method permits considerable latitude in profile specification. Because the necessary integrals are available, and its shape is approximately correct, the error function of the shear layer analysis may be chosen so that the shape factor $H = \frac{\delta^*}{\theta}$ for incompressible flow is approximately equal to 2, which is acceptable for separating and reattaching profiles.

Lamb and Hood (1968), confirm the validity of Chapman-Korst isentropic escape criterion as a satisfactory technique for identification of dividing stream line rather than a thermodynamic specification of the dividing stream line stagnation process.

Calculation of the axisymmetric flow

The separation stream line is also used to investigate the separated flow downstream of axisymmetric body by Vereshchagina (1963), Minyatov (1961), Mueller (1968) and Zumwalt (1959). Furthermore, Tagirov (1961, 66) and McDonald (1966) considered the effect of the boundary layer.

Vereshchagina (1963), Korst (1956), Minyatov (1961) and Tagirov (1961) assumed that a mixing layer flow develops at constant pressure

but Mueller (1968) and Zumwalt (1959) considered the streamwise pressure rise.

The flow downstream of axisymmetric bodies is different from that of two-dimensional surfaces and its flow study in the vicinity of the axis of symmetry is difficult because expansion waves in the trailing edge are curved and flow parameters in the expansion region are not only dependent on the angle of inclination, but also on the previous history of upstream flow and the Mach line passing through the point being considered. The boundary of inviscid flow is curvilinear and its shape is determined from the constancy of pressure along this surface. The free surface can not be constructed for the supersonic flow right up to the axis of symmetry.

Zavadskiy and Taganov (1968), studied the axisymmetric laminar flow separation occurring on the leading section of the needle shaped axisymmetric body with a small reattachment zone at supersonic speed. For the reattachment flow at the angle of attack, Chapman-Korst conditions are applied in order to determine the local stream line and the total pressure. The magnitude of pressure in the separation zone was determined from the conservation law of mass. To overcome the difficulties involving axi-symmetric flow, three approaches are proposed: the first is the application of an experimental curve of thickness variation of the wake neck in a function of the Mach number as Gogish (1968) suggests; the second is as Vereshchagina (1963) and Minyatov (1961) did, the radius of the wake neck is approximated to be equal to 0.5 radii of the protuberance not depending on the Mach num-

ber; the third is the position of the shock wave, to be approximated at the intersection of lines of zero velocities (lower boundary of the mixing zone) with the axis of symmetry as Tagirov (1961) proposes. One may approximate pressure in a function of flow turning angle using the Prandtl-Meyer equation taking account of the stream line turning of an axi-symmetric flow as Webb (1968) did.

Kirnasov and Korzhuk (1969a), found that by numerical calculations of the free surface downstream of cones of various half-angles and free stream Mach numbers that the pressure in the base region is constant only for a distance equal to 0.3-0.5 lengths of separation zone. Thus, the flow model with constant mixing layer pressure, oblique shock and isentropic flow applied for two-dimensional cases is doubtful for axi-symmetric flow, because of strong compression requiring a new analytical model.

If the pressure in the base area is assumed constant and corresponding inviscid stream is considered, then its boundary is not straight as the case of two-dimensional flow and reattachment angle θ_c depends on the reattachment position. The boundary of the inviscid flow may be determined by the method of characteristics but one can approximately fix the boundary by a conical surface. Kirnosov and Korzhuk (1969a), used Mangler's transformation for an axi-symmetric mixing layer and obtained a velocity distribution along the separation stream line as seen in Fig.I.37 and the base pressure in Fig.I.38 which is computed assuming isoenergetic flow using conditions of Nash (N = 0.35) and McDonald (1965) of reattachment.

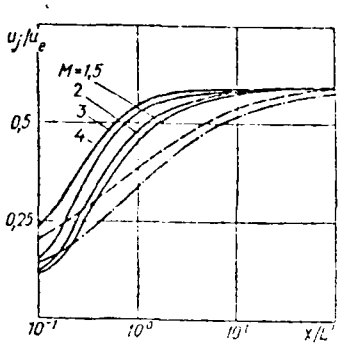

Fig.I.37. Distribution of velocity on separation stream line for free turbulent mixing [Shvets and Shvets (1976)] (dashed line--parabolic profile [Alber and Lees (1968)], dashed-dotted line--Blasius profile).

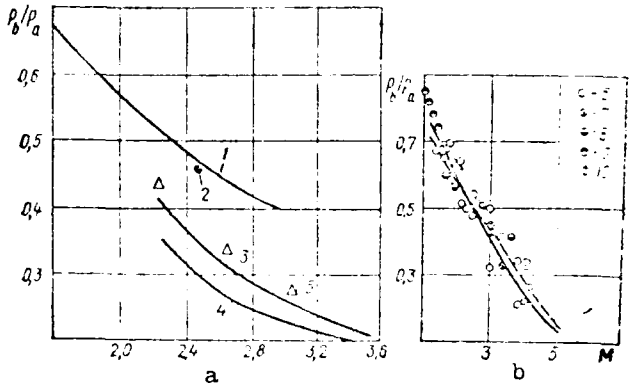

Fig.I.38. Base pressure in an axisymmetric supersonic flow (1--4--calculation; 5--10--experiment): [Shvets and Shvets (1976)] 1--[Minyatov(1961)]; 2--[Vereshchagina(1963)]; 3--[Kirnasov and Korzhuk(1969a)]; 4--[McDonald(1965)]; 5--[Roshko and Thomke(1966)]; 6--$L/r_b = 10$, $Re_L = 3 \cdot 10^6$--$5 \cdot 10^6$ [Chapman(1950)]; 7--$L/r_b = 10$, $Re_L = 3 \cdot 10^6$--$6 \cdot 10^6$ [Chapman(1950)]; 8--$L/r_b = 12$, $Re_L = 2 \cdot 10^6$--$4 \cdot 10^6$ [Chapman(1950)]; 9--$L/r_b = 18$, $Re_L = 9.9 \cdot 10^6$[Graham and Binion(1964)]; 10--$L/r_b = 24$, $Re_L = 5 \cdot 10^6$--$7 \cdot 10^6$ [Potter et al (1959)].

Non-isothermal flow

The complex base flow problems involving heat transfer are not solved at the present time. In the available analysis, the isoenergetic mixing is assumed. Although, due to non-isothermal mixing, this assumption does not correspond to the actual process as Avdu-evskiy, et. al. (1970) state referring to their study on temperature layer of mixing.

Abramovich et. al. (1974), obtained solutions by a self-similar approach for two uniform flows at one temperature but for $Pr = 1$ and $Pr \neq 1$.

For the first case, the solution is simpler because by

$$\frac{i^* - i^*_b}{i^*_e - i_b} = \frac{u}{u_e}$$ the profiles of enthalpy and velocity are related.

Deceleration downstream of the isobaric zone is not adiabatic. Thus, the base pressure is dependent on the base temperature, but based upon the experimental findings, the temperature in the base region may be considered constant, if the thin thermal boundary layer on the wall is neglected. The base temperature is computed using equations of thermal balance between heat of injected gas and heat to the wall in the stagnation zone.

Murzinov (1970), approximated the temperature in the base as shown in Fig.I.39, and compared with Cresci and Zakkay's results reported by Baum et. al. (1964). Murzinov (1970), used the method of mean mass of Lunev (1967) for arbitrary initial profiles of velocity and enthalpy. Using the concept of dividing stream line and computing

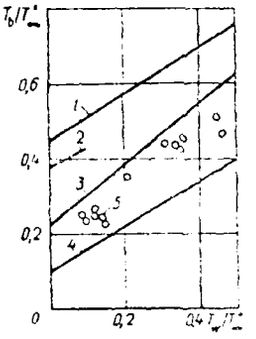

Fig.I.39. Temperature of gas in a base area [Murzinov(1970)]: 1--calculation [Baum et al (1964)] with initial Blasius profile; 2--calculation [Baum et al(1964)] with calculation of turning of the initial profile around the base section; 3--calculation [Murzinov(1970)], cone $\theta = 10^{\circ}$, M = 11.8; 4--calculation taking dissipation into account [Murzinov(1970)]; 5--experiment, cone $\theta = 10^{\circ}$, M = 11.8 [Glick(1964)]

thermal flow and its effect to the base pressure, the following problems are solved: turbulent supersonic flow, (Tagirov (1963)), laminar and turbulent flows past cones and wedges, (Neyland, (1964)), evaluation of effect of turbulent boundary layer thickness at the separation point on the base pressure (Kirnasov and Korzhuk (1969a)), and effect of hypotheses of turbulence to the base pressure.

4. Integral Methods

The ordinary boundary layer theory is not applicable to the separated flow because of the strong interaction of the inviscid flow with the viscous flow close to the body surface or wakes. Hence, it is not possible to determine the distribution of the static pressure for the separated flow region by the inviscid flow solution. Thus, the a priori unknown distribution of the static pressure for the separated flow region must be evaluated by a combined solution of external inviscid flow and viscous flow.

The viscous flow of the separated region involves a reverse flow complicating the problem. For this complex problem, integral methods are applied for its solution. Much of the investigation using the integral methods have been carried out in the U.S.A. For the supersonic flow, the interaction of the inviscid flow with the viscous flow may be studied as follows: The inviscid flow region is considered as isentropic and the viscous flow region is investigated by the boundary layer theory. Then, the parameters on the external edge of the boundary layer are calculated along the boundary of the inviscid flow which is located apart from the solid body at a distance of the boundary layer thickness or displacement thickness.

For the external isentropic supersonic flow, if the inviscid flow is expressed in dimensionless form, the parameters of the outer edge of the viscous region are determined by the local behavior of the boundary.

At first, the development of integral methods, applied to supersonic separated flow in the U.S.A., is briefly outlined and their in-

vestigations in the U.S.S.R. are summarized.

In 1952, Crocco-Lees analytically modeled the inviscid-viscous interaction in two separate fields as shown in Fig.I.40.

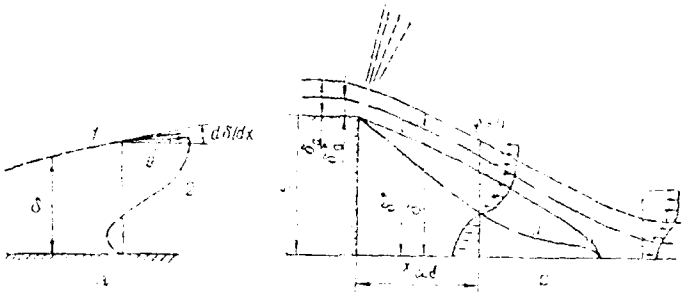

Figure I.40. A diagrammatic concept of isentropic (1) and dissipative (2) flow in a base region [Crocco-Lees (1952)]

The field of the viscous flow has the thickness δ, (here, δ represents the separated flow over the solid body, the physical boundary layer thickness and for the wake downstream of a body, the transverse distance between external boundary of the viscous layer and the axis of symmetry of the body), and its outer boundary is inviscid isentropic flow.

For two-dimensional supersonic steady flow, the distribution of static pressure in the separated flow region is given by the Prandtl-Meyer equation,

$$dp/p = (\gamma M^2/\sqrt{M^2 - 1}) \cdot d\textcircled{H}_c$$

where $\textcircled{H}_c$ is the angle between the flow velocity vector along the external boundary of the viscous layer and the wall. It is assumed that Pr = 1, enthalpy is constant, $M \sim T$ and $\partial p/\partial y = 0$ in the sepa-

rated flow region. As seen later, the assumption of $\partial p/\partial y = 0$ may not be valid in the recompression region [Sharmroth and McDonald) (1972)]. Crocco-Lees (1952), expressed the boundary layer equation in an integral form using a family of parameter $K = (\delta - \delta^* - \theta)/(\delta - \delta^*)$ and determined the static pressure distribution along the external boundary of the viscous layer by establishing a relation between $K(x)$ and local momentum thickness θ, introducing the mixing coefficient $K = (d\delta/dx) - \Theta_c$. This angle Θ_c is determined similar to the physically possible stream line satisfying the condition of passage of the integral curve of the equation through a singular point (whose solution has a family of integral curves expressed in parameters of Θ_c). This singular point is analogous to the throat at Mach number 1 of the converging-diverging nozzle. Although in general, its position may not coincide with the narrowest cross-section of the mixing zone.

Since Crocco-Lees analysis contains the semi-empirical equation for K, Lees and Reeves (1964) proposed to use the additional integral relation of the energy equation instead of the equation of K.

The equation of the stream line inclination along the external boundary of the viscous layer at $y = \delta$, assuming isentropic flow is given by the Prandtl-Meyer relation in a function of

$$\Theta = \nu(M) - \nu(M_e)$$

$$\nu(M_e) = \left(\frac{\gamma+1}{\gamma-1}\right)^{\frac{1}{2}} \left[\arctan\left(\frac{\gamma-1}{\gamma+1}\right)^{\frac{1}{2}} (M_e^2 - 1)^{\frac{1}{2}}\right] - \arctan(M_e^2 - 1)^{\frac{1}{2}}$$

Unknown parameter M which is to be determined by the condition of passage through the singular point. The predicted laminar flow pressure distribution p/p_c, where p_c is pressure at the wake throat, along

the dividing stream line and thickness of a wake δ/H (H is half the base height of the body) for an adiabatic near wake is shown in Fig.I.41.

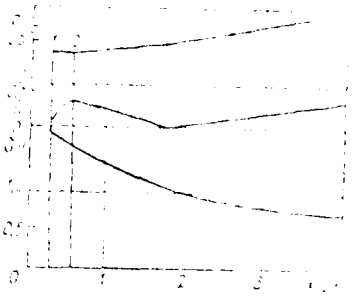

Figure I.41. Distribution of static pressure, velocity along a dividing stream line and thickness of the wake:[Reeves and Lees (1965)]
1--Separation point
2--Section of reattachment together (p_c--is pressure in the region of the neck of the wake.

The process of compression in the laminar separated region is not isentropically affected by Reynolds numbers. Thus, Reeves and Lees (1965), determined the Reynolds number effect caused by non-isentropic compression. The length of compression and the degree of deviation of compression from that of the isentropic one depends mainly on the thickness of the free viscous layer upstream of compression. Therefore, with an increase of Reynolds number, the effectiveness of the compression process and base pressure increases.

Alber and Lees (1968), further investigated the inviscid-viscous interaction of laminar supersonic separated flow downstream of a rearward facing step. A turbulent eddy viscosity is formulated simply by one incompressible constant applicable for both the shear layer and wake, and one reference density ρ_r; i.e.

$$\varepsilon = (\rho_r/\rho_e)^2 K_0 U_e \theta$$

where K_0 is a universal constant amounting to 0.06 ± 0.004. Lees and

AD-A099 165 CATHOLIC UNIV OF AMERICA WASHINGTON D C DEPT OF MECH--ETC F/G 20/4
RECENT DEVELOPMENT IN FLOW SEPARATION.(U)
MAY 80 P K CHANG AFOSR-78-3636

UNCLASSIFIED AFOSR-TR-81-0451 NL

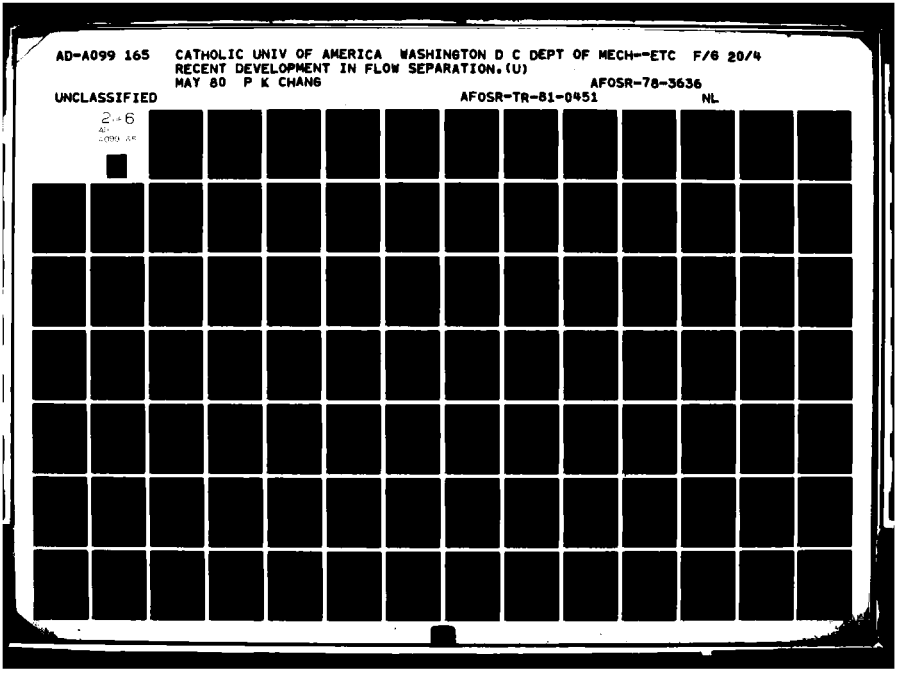

Alber considered that the tip shock separates the outer part of the expanding boundary layer from a new viscous sublayer formed just below the edge of the step. This sublayer, whose thickness amounting to about 10-20% of the initial boundary layer, develops as a free shear layer into a region of recirculating flow at a constant pressure. As the mixing layer approaches the axis, the shear layer turns parallel to the center line and induces a pressure rise in the external flow. The analytical solution is given from a condition of its passage through the critical point and the predicted pressure along the the axis and the position of critical point by Alber and Lees (1968) and the measured data by Badrinarayanan (1961) are shown in Fig.I.42. The measured pressure in the base region is lower than the predicted value because of the non-isentropic actual flow.

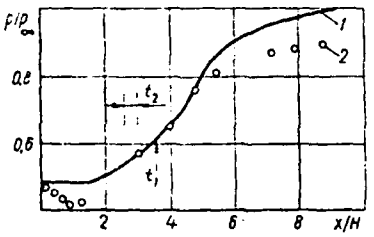

Figure.I.42 Distribution of pressure along the axis for a turbulent flow in a base region when M = 2.07 [Alber and Lees (1968)]
1--Calculation
2--Experiment (position of the trailing critical point: t_1--calculation t_2--experiment [Badrinarayanan (1961)]

Grange, Klineberg and Lees (1967), predicted the a priori unknown location of separation on the blunt body and entire near wake region of laminar compressible flow without the introduction of additional ad hoc assumption or floating parameters. Based upon the Reeves and Lees' (1965) integral method, emphasizing the strong inviscid-viscous interaction, the analysis is carried for the separated flow sketched in Fig.I.43a.

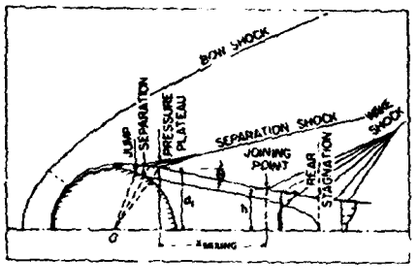

Figure.I.43a Separation and near-wake interaction regions for a blunt body at hypersonic speeds (schematic). [Grange, Klineberg and Lees (1967)]

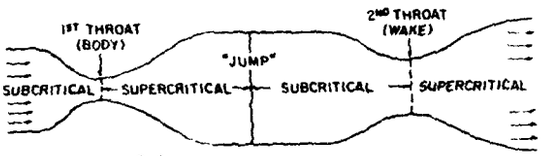

Figure I.43b Schematic representation of interaction viscous flow over blunt body. [Grange, Klineberg and Lees (1967)]

In order to obtain a complete solution to the base flow problem for a blunt body, it is necessary to join the separation region to the constant pressure mixing region and the near interaction zone. The interaction viscous flow over the blunt body is shown schematically analogous to the converging-diverging nozzle in Fig.I.43b. This analogy is based upon the following findings: around the cylinder, the flow becomes supercritical at a point about 97° measured from the forward stagnation point but the flow in the near wake is initially subcritical. Thus, a jump of 97° is required in order to join the supercritical viscous flow over the body to the initially subcritical wake flow. Crocco-Lees (1952), found that the near wake at the rear stagnation point is subcritical, but passes through a throat into the supercritical region downstream of the rear stagnation point.

Rigorous analytical solution requires the evaluation of the boundary layer development starting at the forward stagnation point taking into account the interaction with external flow, but since this problem is a formidable one in itself, Grange, et.al. (1967), instead, adoped the procedure of Reeves and Lees (1965) and regarded $M_e(x)$ as given up

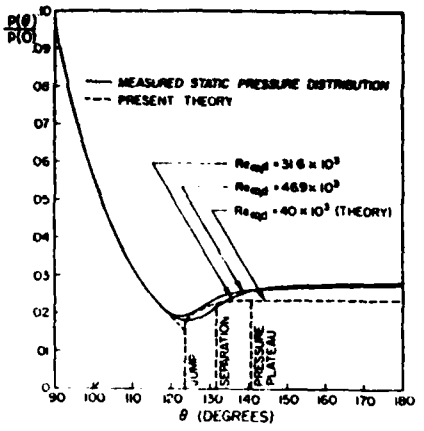

Figure.I.44. Comparison of theory with McCarthy's experiments [Grange, Klinegerg and Lees (1967)]

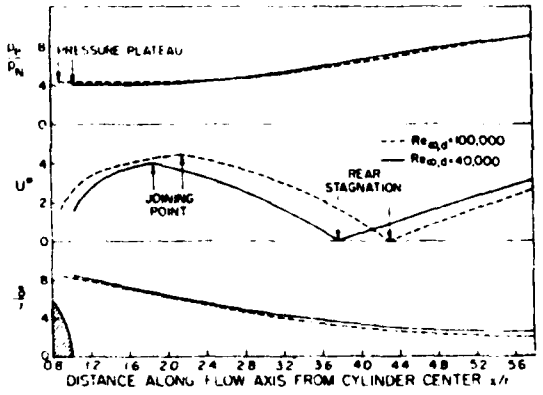

Figure.I.45. Near-wake interaction region. [Grange, Klineberg and Lees(1967)]

to the jump location.

The predicted pressure distribution, velocity and shear layer thickness for the adiabatic circular cylinder at $M_\infty = 6$ and $R_{e_\infty d} = 4 \times 10^4$ compared with ezperimental data of McCarthy (1962) are shown in Fig.I.44 and I.45. The predicted base pressure is somewhat low but the location of the separation point on the cylinder is predicted quite accurately.

Grange, et.al.'s (1967), general method is applicable not only to blunt bodies but also to slender bodies with smooth bases, provided only that the radius of curvature at the base is larger compared to the boundary layer thickness.

In Fig.I.45, the subscript N refers to neck condition, $U^* = U_{\psi=0}/U_e$ and $U = u(a_N/a_e)$ Stewartson's transformed velocity and a is the velocity profile parameter.

Shamroth and McDonald (1972), analyzed the recompression region flow of a supersonic two-dimensional turbulent near wake. Since both

theory and experiment indicate that in the near wake recompression region, even at moderate supersonic Mach numbers, a large transverse pressure gradient exists, particularly in the turbulent flow. Shamroth and McDonald (1972), considered this transverse pressure gradient in their analysis by assuming a proper static pressure profile, improving the other investigator's analysis which assumed a zero transverse pressure gradient.

The governing equations for five parameters $U_m(x)$, $Ue(x)$, $\delta(x)$, $Cp_{CL}(x)$ and $(\partial p/\partial y)_e(x)$ where subscripts m and CL refer to the wake center line are:

for the relation between streamwise and transverse pressure gradients,

$$\partial p_e/\partial x = (-1/\sqrt{M_e^2-1})\ (\partial p/\partial y)_e$$

for the flow angle at the outer edge of the shear layer

$$\tan \nu = (-1/\rho_e Ue) \int_0^\delta \frac{\partial \rho u}{\partial x} \cdot dy$$

for the pressure difference obtained from the transverse momentum equation with the aid of continuity,

$$p(x,0) = \Delta p_{CL}(x) = \frac{d}{dx}\int_0^\delta \rho\ uvdy + \rho_e u_e v_e \left[\tan \textcircled{H}_e - \frac{d\delta}{dx}\right]$$

and two other equations are those derived by Shamroth (1969).

The two usual integral equations are replaced by two new equations obtained from a modified strip method for conservation of streamwise momentum. The said replacement is needed because the Karman momentum integral equation and the kinetic energy integral equation place a physically unrealistic constraint upon the solution.

Although a straightforward treatment of these equations results

in the appearance of a singularity analogous to Crocco-Lees critical point, Shamroth and McDonald (1972), show that two analytical solutions can be obtained which do not exhibit a singular behavior. One solution is given as an initial value problem by properly approximating the term containing the upstream influence and the other as a boundary-value problem in the vicinity of the streamwise station

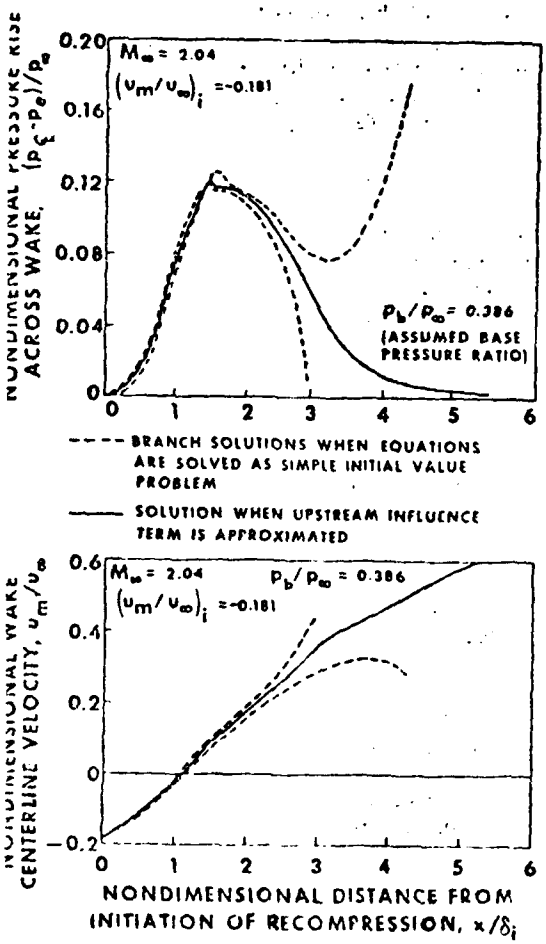

Figure I.46. Predicted streamwise distribution of wake parameters when equations are solved as initial-value problem and term containing upstream influence is approximated [Shamroth and McDonald (1972)]

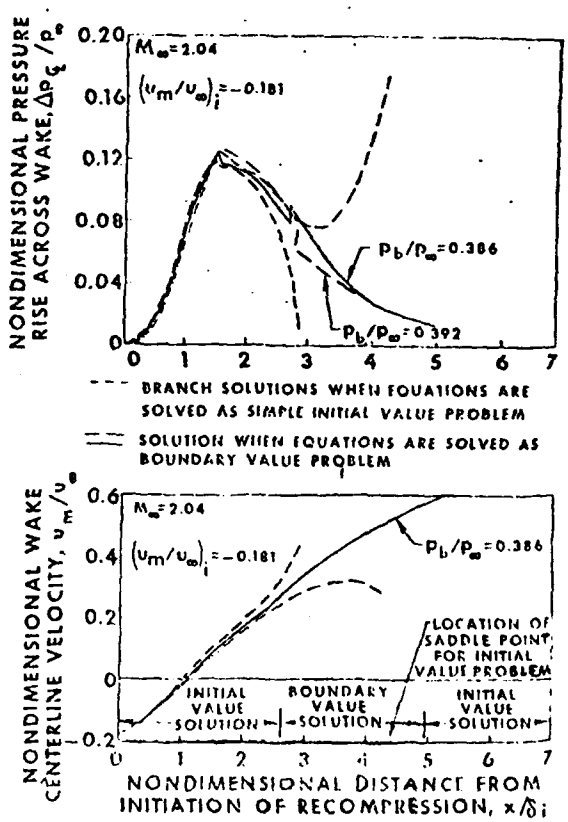

Figure I.47. Predicted streamwise distribution of wake parameters when equations are solved as a boundary-value problem [Shamroth and McDonald (1972)]

where the saddle-point would occur if the equations are definding an initial problems.

Fig.I.46 and I.47, show the predicted distributions of pressure and velocity with no singularity by these two methods.

The static pressure distribution predicted when the problem is treated like that of an initial and upstream influence term and like that of the boundary-value are shown in Fig.I.48, compared with the experimental data of Badrinarayanan (1961). A good agreement exists between the experimental data and the predicted center line static pressure by both methods, for this particular case, but similar agreement may not be obtained for all other cases because of the limitation imposed by the velocity profile family used in the analysis of Shamroth and McDonald (1972).

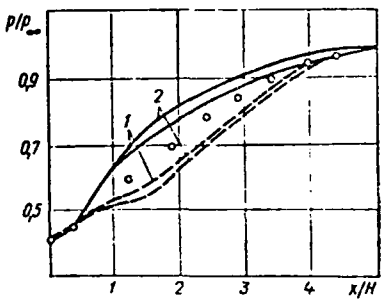

Figure I.49 Distribution of static pressure when M=2.04 [Shamroth and McDonald (1971)] (calculated size θ_a/H =0.052, experimental θ_a/H =0.055; solid line--is the axis of the wake, dashed line--is the external boundary, circles--indicate experiment [Badrinarayanan(1961)] 1--solution of equations with initial data; 2--solution of equations as a boundary-value problem

A theoretical model for the flow field and the convective heat transfer process in the vicinity of the reattachment of supersonic two-dimensional turbulent separated flow has been set up by Lamb and Hood (1972) utilizing multistage control volume and solving the resulting integration by a numerical search technique.

The flow model and numerical technique are the same, developed previously

by Lamb and Hood (1968), for the solution of the reattachment problem presented in Section I.3.

A solution to the reattachment problem is given by momentum balance in both longitudal and transverse directions for the control volume. Assuming the base pressure is known, the Mach number inviscid impingement and conditions at the dividing stream line are determined.

The heat transfer rate which exists at the cutoff station (point of initial interaction at the end of the base pressure region) is taken as characteristic of the entire recirculating zone because the recirculating flow is essentially a constant-flux region as experiments have shown. For the thermal analysis, the almost isobaric near field is employed as a control volume. One of the major uncertainties in any turbulent flow model is the level of turbulence characterized by the spread rate parameter σ which is difficult to estimate from the experimental data with 20% uncertainty. It was found that for a given percentage change in σ, the wall temperature changes correspondingly, while the heat flux changes in the opposite direction.

Lamb and Hood (1972), determined by their analysis the significant parameters in the flow field, the heat transfer distribution, and associated wall temperature of the reattachment surface, obtaining a heat transfer prediction in good agreement with experimental data.

Next, the USSR investigations on separated flow and applications of integral methods are summarized.

Gogish (1968, 1969) and his associates, attempted to predict the separated turbulent flow characteristics at subsonic and supersonic speeds, providing more general precise information compared to the

local methods of dividing stream line by Korst and Chapman. A turbulent boundary layer is expressed by a family of profile of A.S. Ginevskiy,

$$u/u_e = 1 - \lambda f(\eta), \quad f(\eta) = (u_e - u)/(u_e - u_{\textcircled{H}})$$

λ is the shape parameter given by $\lambda = (u_e - u_{\textcircled{H}})/u_e$. The isentropic external flow properties are evaluated for $\textcircled{H} = \nu_\infty - \nu$ given by the Prandtl-Meyer relation. The governing equations are:

$$\frac{d}{dx}\int_0^\delta \rho\, u\, dy = \rho_e u_e \left(\frac{d\delta}{dx} - \tan \textcircled{H}\right)$$

$$\frac{d}{dx}\int_0^\delta \rho u^2 dy = u_e \frac{d}{dx}\int_0^\delta \rho\, u\, dy - \delta \frac{dp}{dx}$$

$$\frac{d}{dx}\int_0^\delta \rho\, u\, dy = k \rho_e u_e \text{ - eq. of ejection}$$

These equations are integrated in a longitudinal direction and the predicted pressure for various Mach numbers are compared with Korst's solution in Fig.I.49.

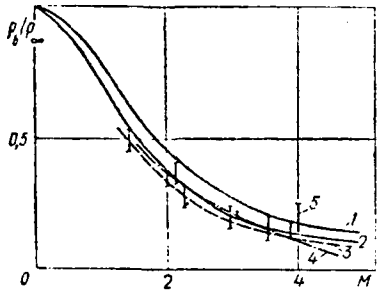

Figure I.49 Calculated (1---4) and experimental (5) values of base pressure in a two-dimensional turbulent supersonic flow: [Shvets and Shvets(1976)] 1-- $\lambda_2 \simeq 1$; 2--$\lambda \simeq 0.5$ [Gogish and Stepanov (1968)]; 3--[Korst, et.al. (1956)]; 4--$(-\alpha)\, K_T = 0.012$ [Gogish and Stepanov (1968)]; 5--[Rom, et.al. (1972)]

For a two-dimensional turbulent wake, using the integral method and considering the compressibility of gas, the following systems of non-linear ordinary differential equations are obtained with respect to λ (x), velocity

$$c(x) = u/u_{max} = M\left(\frac{2}{\gamma - 1} + M^2\right)^{-\frac{1}{2}}$$

and shear thickness δ (x).

$$\frac{d}{dx}\left[c(1-c)^{\frac{1}{\gamma-1}}\ \delta\ (1-H^*)\right] = c(1-c^2)^{\frac{1}{\gamma-1}}\left(\frac{d\delta}{dx} - \tan\textcircled{H}\right)$$

$$\frac{d}{dx}\ln\left(\delta H_k^{**}\right) + \left[(k+1)(H_k+1) + 1 - M^2\right]\frac{d\ln c}{dx} = k(k+1)\frac{1}{\delta_k}\frac{\Delta_k}{H_k^{**}}$$

$$\frac{d\lambda}{dx} + \frac{\lambda(2-\lambda)}{(1-\lambda)(1-c^2)}\frac{d\ln c}{dx} = \frac{\alpha K_T}{\delta}\frac{\lambda^2}{1-\lambda}$$

where $$H_k^{**} = \frac{\theta}{\delta} = \int_0^1 \frac{\rho u}{\rho_e u_e}\left[1 - \left(\frac{u}{u_e}\right)^{k+1}\right] d\eta$$

$$H_k^{*} = \frac{\delta^*}{\delta} = \int_0^1 \left[\left(\frac{u}{u_e}\right)^k - \frac{\rho u}{\rho_e u_e}\right] d\eta ,$$

$$\eta = y/\delta , \quad H_k = H_k^{*}/H_k^{**}$$

$$\Delta_k = \int_0^1 \frac{\tau}{\rho_e u_e}\left(\frac{u}{u_e}\right)^{k-1}\frac{d}{d\eta}\left(\frac{u}{u_e}\right) d\eta ,$$

$\tau = \epsilon\frac{u}{y}$, K_T is a dimensionless coefficient of proportionality

and $\alpha = \left(\frac{d^2 f}{d\eta^2}\right)_H < 0$

These systems of equations have a saddle-point singularity and the initial values are determined from the interaction joining of the near wake region with the constant pressure mixing zone upstream. The joining conditions are derived from those of conservation of δ and δ^* and the mass flow in the constant pressure region. (see Fig.I.40b). Using these conditions, the joining zone x_{ad} is evaluated. The p_b, which is one of the initial values, is determined by the passage of the integral curve through the singular point which

is analogous to the throat of the nozzle.

Perturbation in the external flow effects the pressure at the outer edge and flow in the near wake if they interact upstream of the singular point. The predicted pressure distribution by Gogish, et. al. (1969) along the near wake axis compares favorably with the experimental data of Roshko and Thomke (1966) and Thomann (1958) in Fig.I.50.

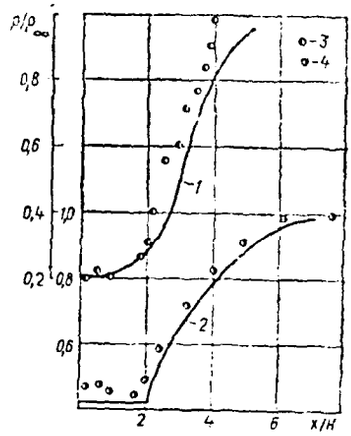

Figure I.50. Distribution of static pressure along the axis of the wake. (1,2--calculations; 3,4--experiment) [Gogish, et.al. (1969)]
1--M = 3.02; 2--M = 1.84 [Gogish, et.al. (1969)]; 3--[Roshko and Thomke (1966)]; 4--[Thomann (1958)].

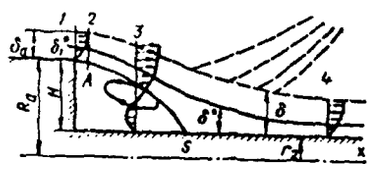

Figure I.51. Diagram of flow behind a protuberance [Antonov (1971)]

Antonov (1971), analyzed the turbulent interaction based upon the base flow model shown in Fig.I.51.

Flow expands in region 1-2 and in region 2-3, the flow is isobaric and interaction begins with the outer of 3. S is the critical point.

The integral momentum equation of the compressible turbulent boundary layer is:

$$\frac{d}{dx}\left(r^m \rho_e u_e^2 \theta\right) + r^m \delta^* \rho_e u_e \frac{du_e}{dx} = r^m \tau_w$$

where r is the radius, m=0 is for two-dimensional flow and m=1 is for axi-symmetric flow. This equation is transformed to an incompressible flow equation. A system of equations for the interaction zone of the boundary layer with the external flow is set up involving a parameter A(M) to be evaluated by experiment.

The predicted pressure distribution using the value of A(M) evaluated by experimental data is shown in Fig.I.52, in close agreement with the measured data of Roshko and Thomke (1966).

Murzinov and Shinkin (1976), computed the basic parameter of the turbulent separated flow region by using an integral method and considering the vorticity separated from the edge, which was not taken account by Gogish, et. al. (1969) and Alber and Lees (1968).

The proposed flow model is as follows: The eddy flow at a corner during the turning and up to subsequent absorption by the viscous layer is assumed inviscid and the subsonic part of the free stream turbulent boundary layer is ignored because of its small dimension, The vorticity for viscous flow field is computed by the method of

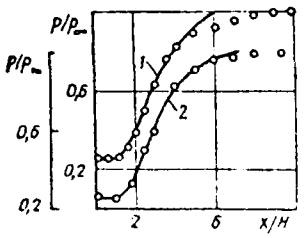

Figure I.52 Distribution of pressure behind an axisymmetric protuberance [Antonov (1971)] (curves--calculation [Antonov (1971)]; signs--experiment [Roshko and Thomke (1966)]: 1--M = 2.56, $\theta/H = 0.05$; 2--M = 3.02, $\theta/H = 0.04$.

Lunev (1967) pointing out that vorticity significantly affects the base pressure.

5. Analytical Solutions by Navier-Stokes Equation

The separated flow problems are solved by applying the Navier-Stokes equations for incompressible and compressible flow, laminar and turbulent flow around blunt bodies, blunt corners, sharp trailing edge corners etc.

The separated flow affects external flow, thus, it is necessary to integrate the characteristics in the flow field, joining the solutions of external, viscous and wake flows and by satisfying the proper boundary conditions. Hence, the analytical solutions are difficult to obtain.

The steady flow problem around a blunt body at alrge Re is not completely solved by the Navier-Stokes equations. Although a number of flow models has been proposed, it is not certain which model is the right one applicable for $Re \to \infty$.

5.1. Asymptotic Methods

In the U.S.S.R. , like Western Countries, asymptotic methods have been applied to solve the difficult problems of separated flows and flow characteristics affected by the boundary layer interaction with an inviscid stream based upon the concept of "free interaction". The "Free interaction" is defined by Chapman et al (1957) as the interaction free from direct influences of downstream geometry as evidenced from the Figure.I.53.

The free interaction occurs because the compression is directly responsible for the thickening boundary layer and its ultimate separation is generated by the outward deflection of the external flow caused by the thickening itself.

In Fig.I.53a, the case of flat plate flow is also shown with the cases of separated flows over a ramp and the forward facing step. The latter cases of separation are well known due to the sharp corner effect involving the streamwise adverse pressure gradient. But, for its flat plate flow, i.e. the separation free inviscid flow, the pressure gradient is zero. Therefore, with its real flow to cause the separation, the stream-wise pressure gradient must be adverse. Consequently, the boundary layer interaction with the supersonic stream must occur upstream of the separation point, inducing a sufficiently large streamwise adverse pressure gradient. A similar interaction mechanism, causing separation, takes place even for a flow with a streamwise inviscid favorable pressure gradient if the Reynolds number is large.

The asymptotic method for $Re \to \infty$ is used for the solution of Navier-Stoke equations. These solutions differ significantly from those obtained from the classical boundary-layer theory and they were successfully applied to a certain degree in evaluating the flow characteristics throughout the separated flow region involving singularities at points of separation and reattachment, further affected by the propagation of downstream disturbance. The problem of flow over the sharp corner and over protuberances placed on the body surface were also solved by asymptotic methods. In the U.S.S.R., much attention is given to the upstream propagation of a downstream disturbance so that more accurate analytical solutions are obtained. In the past, for flow solutions with large Re numbers, applying the Prandtl's boundary layer equations, two regions of flow are considered in order to construct a uniform asymptotic approximation. The flow in one of these regions is formulated by the Euler equation because for large Re the large parts of the flow field are not affected by viscosity. This Euler equation becomes hyperbolic if $M > 1$. The other regions, the viscous boundary layer has a thickness of $O(Re^{-\frac{1}{2}})$ and for this region, the equation becomes parabolic. Thus, the solution involving the disturbance propagation, which is sought, is obtainable from the complete Navier-Stoke equation, but is not obtainable from the classical Prandtl's boundary layer equations. Lighthill (1953a, 1953b), investigated the disturbance propagation for subsonic and supersonic flows. Lighthill (1953a), after reviewing a number of papers, pointed out that the disturbance can have an upstream influence through the agency of the

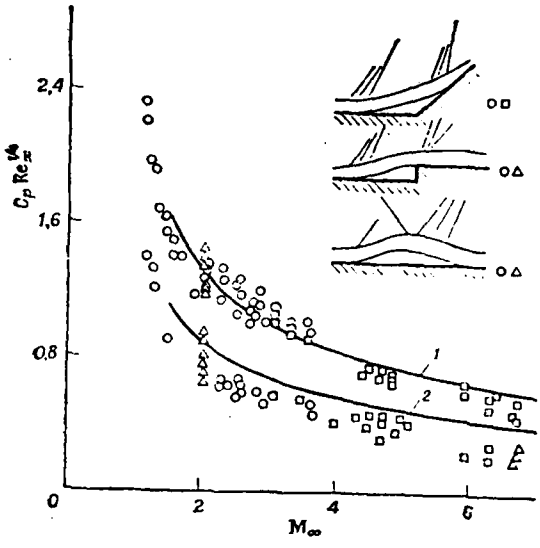

Figure I.53 Comparison of theoretical and experimental pressure coefficients at the separation point and in "plateau" region of the developed separation zone.

—— = Calculation [Neyland. (1971a)]
Experimental data presented in [Erodos and Pallone, (1962)]:
0 = [Chapman, Kuehn, Larson (1957)]
□ = [Sterret, Emory (1960)]
Δ = [Hakkinen, Greber, Trilling, Abarbanel (1959)]
1 = Plateau region:
2 = Separation point.

supersonic boundary layer and two separate mechanisms exist, by means of which the boundary layer, acts to transmit the influence of a disturbance upstream, namely:

(i) a disturbance leading to a positive pressure gradient causes the boundary layer to thicken.

(ii) a sufficiently large compressive disturbance causes separation of the boundary layer. These two mechanisms are not really very different in that the pressure gradient acts in

the same way (reducing the kinetic energy of the slowly moving fluid near the wall) in producing both thickening and separation. However, the presence in the second mechanism of a sizable "dead-air region" of a very slowly moving fluid makes a considerable difference. The mechanism (i) is strictly peculiar to the supersonic flow and the mechanism (ii) is well known in subsonic flow.

Lighthill (1953b), investigated the upstream disturbance propagation for the supersonic flow without separation. He indicates that when any boundary layer on a straight wall is subjected to an expansive steady disturbance due to a sharp corner, then an interaction between the main stream and the boundary layer takes place, but if the flow reflexion is small then the disturbance in the outer viscous sublayer can be neglected, but these are not negligible in an inner viscous sublayer. Furthermore, if the disturbances are Fourier-analyzed longitudinally, then the effect of the inner viscous sublayer on the behavior of each harmonic component outside it is exactly as if there were a solid wall at a certain position in the stream with no flow across it, i.e. $v=0$ and inviscid flow outside it.

Lavrent'yev (1962), set up an ideal model involving separation by dividing the flow field into two areas, the area of vortex motion in the separated flow zone where curl $\bar{v} = -\omega = \text{const}$, where $\bar{v}$ is a velocity vector and ω is the vortex, and the potential flow outside the area where curl $\bar{v} = 0$.

Taganov (1968), attempted, by simplifying the boundary condition

to find a region of incompressible stationary flow within a closed separated zone in a parameter of Re, where Prandtl's equation may hold. It has been pointed out that only with specific boundary conditions, the Kirchhoff's solution is applicable for two-dimensional flow when $Re \to \infty$. The analysis may be used for the formulation of a stable steady flow involving laminar and in certain cases a turbulent separated flow.

Neyland (1969a) and Stewartson and Williams (1969), used the asymptolic methods to solve the Navier-Stoke equation in the following three regions (or triple-desk structure layer): The first-outer region is described in the first approximate by the linear supersonic flow theory. The second region has a thickness of $Re^{-\frac{1}{2}}$. The velocity profiles in this region coincide in the first approximation with the profiles in the undisturbed boundary layer upstream of a free interaction region. Since the disturbances are small, the pressure distribution is sought not to be affected in its first approximation. The third region, the near-wall viscous flow layer has a thickness of $O(Re^{-5/8})$.

Theories of Stewartson and Williams (1969) and Neyland (1969a) are based upon free interaction. Therefore, the separation is considered to be caused by the pressure gradient induced by the change of thickness of the boundary layer. The flow is described by the conventional boundary layer equations, but since the pressure gradient is not given a priori, it must be determined from the compatibility conditions with outer supersonic flow, and Ackeret linear supersonic

flow theory expressed by $\frac{dp_e}{dx} = \frac{\rho_e u_e}{(M_e-1)^{\frac{1}{2}}} \frac{d\delta^*}{dx}$.

The pressure gradient is given in terms of the second derivative of displacement thickness of the viscous flow with respect to the streamwise coordinate region. Therefore, in the boundary layer equations, a higher order (second) derivative with respect to the variable of an unknown function appears. This fact requires another boundary condition in addition to the initial and other conditions on the body surface and at the outer edge of the boundary layer. Since the derivative with respect to the streamwise coordinate is total rather than partial, it is sufficient to specify only a single constant, in this case, the position of separation and not the function. Because the flow downstream of separation may influence the pressure distribution upstream, and thus the position of separation point, it is extremely difficult to assess this influence. The reasons for difficulty in assessing the influence of the downstream separated flow are as follows: For a sufficiently large Re, the boundary layer thickness upstream of separation is of order 0 (λ) where $\lambda = Re^{-\frac{1}{2}}$ and the displacement thickness δ^* is of the same order 0 (λ) but after separation the boundary layer thickness remains of order λ or may become of order unity, affecting the pressure distribution significantly. If the non-dimensional so called "stretched" variable is defined by $\bar{\delta}^* = \delta^*/\lambda$ then this stretched displacement thickness changes from being of order unity before separation to of order λ^{-1} after separation. Thus, in the limit as λ tends to zero, δ^*/λ becomes infinite after separation. In this case, the boundary layer

equation will no longer be valid since the approximations made in forming the boundary layer equation assume that $\bar{\delta}^* = \delta^*/\lambda$ has an order of unity. Therefore, it maybe expected that a singularity will be present in the boundary layer equation at the separation point. The nature of this singularity has been studied by Goldstein (1948), Stewartson (1958), Terrill (1960) Catherall, Stewartson and Williams (1965). At a small distance upstream of the separation point, in place of pressure, the boundary layer displacement thickness distribution in the form of a second- or third-degree polynomial was assumed and the pressure was determined, enabling one to pass through the separation point.

This technique used by Catherall and Mangler (1966) will only work for regions for which the boundary layer thickness remains of order λ . Shallow bubbles within the boundary layer do occur, for example they are often present when a shock wave interacts with the boundary layer and the possibility also remains that the strong thickening of the boundary layer after separation may sometimes occur downstream of the separation point. If this were the case, the method of Catherall and Mangler (1966), would still enable one to integrate the boundary layer equation past the separation point. However, the said method does not apply for flow past bluff bodies at high Re.

Catherall and Mangler (1966), used the Navier-Stokes equation written in terms of a stream function and the velocity and transformation is introduced in which the independent variables are simply connected to the inviscid stream function and velocity potential.

Applied to the problem of infinite Re, since in the limit of Re the displacement surfaces up to separation are coincident with the body, the pressure distribution maybe taken from the potential flow about the body. Applied to a shallow bubble contained inside the boundary layer, no difficulty is encountered at either separation or reattachment. However, the solution after separation is not uniquely determined unless boundary conditions are supplied downstream, because disturbance propagates upstream once the reverse flow sets in.

Neyland (1971a), provided the possibility of passing through the separation point for supersonic flow with free interaction by specifying the analytic connection between the pressure and the derivative of boundary layer displacement thickness in a form of the Ackeret formulation.

The asymptotic analysis refers often to the maximum state of flow in the separation zone at $Re \to \infty$. When $Re \to \infty$, in a closed region of separation, the flow is inviscid with constant vorticity if some of the recirculating stream lines pass through the mixing layer as Prandtl (1904) and Batchelor (1956) indicate. Neyland and Sychev (1970), analyzed the vorticity problem and found that the Re condition can be given by Poisson's equation $\Delta \psi = \omega$ constant where ψ is a stream function. Applying the asymptotic method, the flow characteristics are evaluated in the various separated incompressible flow regions shown in Fig.I.54.

The external inviscid flow region, the mixing layer governed by the Prandtl equation, the inviscid uniform eddy flow in the recircu-

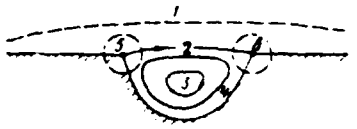

Fig.I.54. Diagram of a separated flow in an incompressible flow [Neyland and Sychev(1970)]:

1--External inviscid flow;

2--Mixing;

3--Inviscid flow in the circulation zone;

4--Boundary layer on the wall of the region of reversed flows;

5 and 6--regions of locally inviscid flow.

lating zone, and a region of locally inviscid flow are characterized by changes of velocity components. The increase of the magnitude of the vorticity causes an increase of friction on the wall but a decrease of friction on the dividing stream line. Based on this flow model, the combined integration of the equation becomes complex, but for a small value of ω, simple algorithms may be used to evaluate flow characteristics and for a small velocity in the region 3, the discontinuity surface linking the up- and downstream corner of the cavity becomes straight, due to a small pressure gradient, thus simplifying the analysis.

Skurin (1972), investigated the asymptotic behavior of an ordinary differential equation. This equation is formulated, based upon empirical findings of turbulance with respect to the distribution of velocity, turbulent energy and mean quadratic values of enthalpy fluctuations along the wake axis.

Sychev, in cooperation with Neyland, achieved successful asymptotic solutions:

Sychev's (1967) asymptotic model involves wake flow with a smaller

velocity than that of the main flow and with length and width of the wake as $O(Re)$ and $O(Re^{\frac{1}{2}})$, respectively. Grove et al (1964) experimentally showed that the stationary flow can be maintained up to $Re \simeq 200$ but it was not possible to obtain the external potential flow characterized by the the model pressure distribution in the wake.

The pressure distribution along the zero stream line in the neighborhood of the separation point is given by

$$p(x) = p_\infty - k(-x)^{\frac{1}{2}} + O(k^2 x) \quad \text{for} \quad x < 0$$

$$p(x) = p_\infty + O(-x)^\beta, \quad \beta > 0, \quad \text{for} \quad x > 0$$

where x is the distance measured from the separation point along the zero stream line.

The pressure gradient

$$\frac{dp}{dx} = \frac{1}{2} k(-x)^{-\frac{1}{2}} - O(k) \quad \text{for} \quad x < 0$$

approaches infinity when $x \to 0$ and $k \neq 0$

The curve of free stream line

$$\varkappa = \frac{d\theta}{dx} = \frac{1}{2} kx^{-\frac{1}{2}} + 0 \quad (1) \quad \text{for} \quad x > 0$$

approaches infinity when $x \to 0$

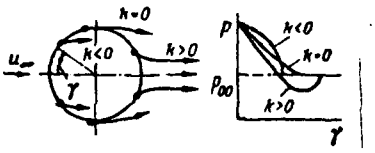

Fig.I.55. Diagram of a field of flow in an ideal fluid [Sychev (1972)]

The case of $k < 0$, is physically impossible because the free stream line intersects with the body surface as seen in Fig.I.55.

The last two equations are for the external flow of a large Re in the neighborhood of the separation point $x = 0$, with external $k > 0$.

The value of k depends on Re but approaches zero when $Re \to \infty$. Hence, it is assumed that $k = \epsilon(Re)ko$ where $Re = u_\infty \cdot L/\nu$ and when $Re \to \infty$, $\epsilon(Re) \to 0$.

The analysis of the laminar flow separation when $Re \to \infty$ shows that a separation takes place due to a large pressure gradient $dp/dx \simeq Re^{1/8}$ in a small distance $\Delta x \simeq Re^{-3/8}$ and such a mechanism of a smaller separation is similar to that of supersonic flow caused by the interaction of a shock wave with the boundary layer as Neyland (1969a) and Stewartson and Williams (1969) observe.

This self-induced pressure rise causing separation can be prevented by neutralizing the effect of the positive pressure gradient.

Sychev (1974), determined the velocity distribution in the region of a positive pressure gradient which provides the laminar incompressible flow attachment up to the trailing critical point. This control technique can be extended to supersonic as well as turbulent flow. For the solution of supersonic separated flow problems the following investigations are cited:

For small but rapidly changing boundary conditions and damping of up- and downstream perturbations affected by the large local perturbations, Neyland (1969a) and Stewartson and Williams (1969) proposed a theory.

Flow in the neighborhood of the body surface is characterized by different asymptotic behaviors in three layers of characteristic thickness of $Re^{-\frac{3}{8}}$, $Re^{-\frac{1}{2}}$ and $Re^{-\frac{5}{8}}$. In the external layer, the flow is approximated by a supersonic linear theory and in the second layer,

the perturbating velocity profile is slightly different from that of an unperturbated one.

In the third layer, close to the wall, the flow phenomena is governed by the first approximation of the incompressible boundary layer ordinary nonlinear equation, because the relative magnitude of perturbation is not small due to the small magnitude of non-perturbating flow. The initial and boundary conditions obtained by the asymptotic approach are joined with the solutions of neighboring regions.

For the hypersonic flow asymptotic analysis, it is necessary to carry out a double maximum approach $Re \to \infty$ and $M \to \infty$ considering the interaction parameter $\chi = M/\sqrt{Re}$.

Neyland (1974), in his book, presents the systematic studies of supersonic viscous flow problems which are not solved by the classical boundary layer theory. Solutions of the Navier-Stokes equations by the asymptotic method and results of the calculation of "free interaction" of supersonic flow with the boundary layer are studied in detail for the following subjects;

Flow around points of separation, location of the boundary layer reattachment, "choking" of perturbation similar to the known phenomena of Laval nozzle, important physical singularities in the neighborhood of the critical point affected by viscosity, results of criteria of similarity for the maximum values of heat transfer etc.

5.2. Similarity Law

The asymptotic solutions of separated flows by the Navier-Stokes equations are obtained for the selected problems, mainly for self-similar ones with small or large flow parameters, due to their mathematical complexity.

As a consequence of the local nature of the asymptotic flow, it is possible to exclude the parameters such as Re, M and temperature from the equations expressed in dimensionless form. Thus, the resulting universal solutions describe all the flows and the formulas for conversion to the physical variables and extablish the similarity laws.

Brown and Stewartson (1969) state in 1969, the use of similarity solutions with reverse flow is probably the best method of coping with

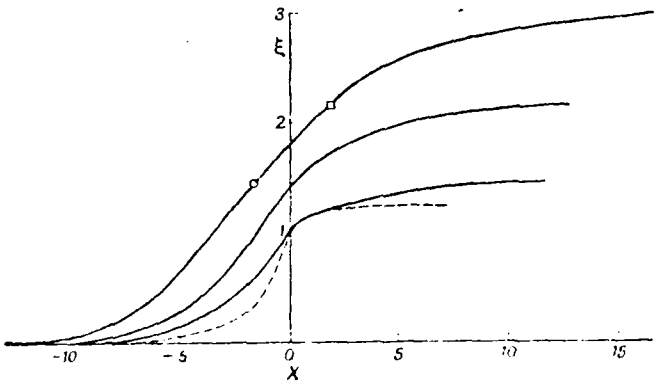

Figure I. 56. Pressure distribution for supersonic viscous gas flow around body contour corner [Neyland 1971b]

$$\xi = 2\, C_p \mathrm{Re}^{\frac{1}{2}} \left[\frac{2B\mu_\infty}{a\mu_w} \right]^{\frac{1}{2}}$$

$$B = (M_\infty - 1)^{\frac{1}{2}}$$

$$X = \frac{x\mathrm{Re}^{3/8}}{l} \left[8\, B^3 \left(\frac{\rho_w}{\rho_\infty} \right)^2 a^5 \frac{\mu_w}{\mu_\infty} \right]^{\frac{1}{2}}$$

$a = (\partial u/\partial y)_w\, l\, \mathrm{Re}^{-\frac{1}{2}}/u_\infty$ - is the pressure gradient calculated in the undisturbed boundary layer ahead of the interaction region.

the main separated region downstream of the separation point. But they are not satisfactory near separation because, due to the rapid pressure rise, viscous forces can be neglected in the major part of the boundary layer.

Neyland (1971b), generalized the similarity and computed the critical pressure rise leading to separation as shown in Fig.I.56.

The similarity law for free-interaction formulated a quite general and relatively simple form of equation. The boundary conditions are satisfactory if the disturbance amplitudes are not too large in the first approximation, leading to a clear understanding of various physical effects. Therefore, the similarity law is applicable for a wider range of following problems as sketched in Fig.I.57 namely (1) flow downstream of a finite length of flat plate (2) flow downstream of the profile (3) flow over flat plate at angle of attack (4) flow over flat plate with a pressure gradient.

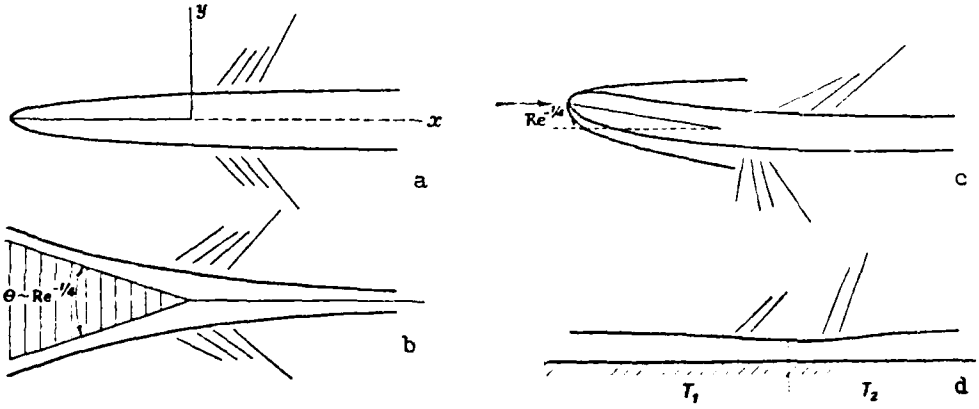

Figure I.57 Supersonic flows described by free-interaction theory. [Neyland (1971b)]

(1) For $x > 0$ the the non-slip condition $u(x,o) = 0$ is replaced by the symmetric condition $u_y(x,o)=0$. Neyland(1969a), investigated the disturbance amplitude and diversions of regions to which the disturbance propagates. Reduction of shear stress to zero on the flow axis leads to acceleration of the stream filaments passing near the plane of symmetry causing a rapid change of displacement thickness and inducing a pressure gradient. Simple estimates using equations of continuity, momentum and linear supersonic flow theory show that near the end of the plate a local free-interaction flow region $x \sim Re^{-3/8}$ of pressure difference $\Delta p \sim Re^{-\frac{1}{4}}$ is formed. A negative pressure gradient is induced near the end of the plate and pressure recovers in the wake, but at $x/Re^{-3/8} \to \infty$, the pressure gradient becomes zero.

(2) Flow over the profile is similar to (1), thus, analogous results are obtained.

(3) For flow over the flat plate at an angle of attack an analogous pattern compared to (1), is valid if the angle of attack is small amounting $\alpha \sim Re^{-\frac{1}{4}}$, as Brown and Stewartson (1970) found.

In this case, the flow turns through the angle $\pm$ upstream of the plate end on the upper and lower surfaces. At sufficiently large α, the flow separates and the critical pressure rise to cause separation is somewhat larger compared to the flow around a corner formed by two walls because the pressure gradient becomes negative due to the flow leaving the plate, as the case of $\alpha = 0$.

(4) For flow over a flat plate with a pressure gradient, the pressure change $\Delta p \sim Re^{-\frac{1}{4}}$ is induced on the length $\Delta x \sim Re^{-3/8}$ according to the linear supersonic flow theory. From the first approximation , it

maybe found that this pressure change Δp in turn influences the near wall layer. The major part of the boundary layer affected by $\Delta p \sim Re^{-\frac{1}{4}}$ changes the magnitude of the displacement thickness by an order of $Re^{-3/4}$ and this change of magnitude is taken into account in the second approximation.

Sychev (1972), shows that in the vicinity of the separation point, a free-interaction zone of the same type of supersonic flow exists, as Neyland (1969a) indicates, but there is also a difference because for the outer inviscid flow region, instead of the linear supersonic flow theory, it is necessary to use the solutions of the classical jet flow theory. Local flow separation is caused by the pressure gradient induced by the free interaction.

Sychev (1972), found that for the incompressible laminar separation, a rational analysis can be carried out if in the neighborhood of the separation point, the external inviscid flow phenomena is described along the ideal fluid free stream line. Then, the mechanism of flow separation becomes similar to the supersonic flow separation caused by the large local pressure gradient.

5.3. Flow over Sharp Corner and Supersonic Flow Reattachment, (Flow with very Large Local Pressure Gradient), Upstream Disturbance Propagation and Flow over Protuberance.

5.3.1. Flow over Corner

Neyland and Sychev (1966), applied the basic concept of asymptotic theory to the flow of very large local pressure gradients. As a

typical example, the expansion flow near a sharp corner at supersonic speed is considered.

Recently, much attention has been paid to the difficult flow problem of a trailing edge with separation, particularly for the supersonic flow. At the sharp corner, where the surface curvature become so great that the boundary layer thickness is comparable with the radius, the boundary layer approximation breaks down. In the corner region, viscous motion maybe applied. Far up- and downstream of the corner, the classical theory is valid, therefore, a local solution around its corner maybe matched with the boundary layer up- and downstream of the corner by the method of asymptotic expansion. But, because its local inviscid solution violates the non-slip condition, a thin secondary boundary sublayer must be added close to the wall. Furthermore, since an upstream propagation of a downstream disturbance occurs, a solution of the full Navier-Stoke's equation is required to solve for the flow in the immediate vicinity of a sharp corner. Since the base pressure downstream of the corner is low and, as Hama's (1966) measurement indicates, that a significant fraction of the pressure drops upstream of the corner, outside the sublayer, the accelerating fluid velocity may reach sonic speed. Thus, in the flow field, a singularity is encountered. This problem, as other many discontinuity problems, belongs to the family of asymptotic or boundary layer phenomena of mathematical physics as stated by Vaglio-Laurin (1960). Neyland (1966), studied the laminar sublayer flow problem by applying the compressible boundary layer equations of accelerating flow which extends to upstream infinity. Integrating the Prandtl boundary layer equa-

tions, the asymptotic behavior of the solutions of Navier-Stokes equations for a large Reynolds number is investigated for the following two cases; (i) for nonuniform velocity and enthalpy profiles in the initial section and (ii) on bodies extending to infinity upward and downward along the flow direction. For case (ii), introducing transformation it is possible to solve the problem involving singularity by self-similar solutions and by well-developed numerical methods of Dorodnitsyn (1956) and Petukhov (1964) as well as by analytical methods of Dorodnitsyn (1942) and Loitsianskiy (1965). For case (i) the following governing equations (Hayes and Probstein (1959)) for compressible laminar boundary layer involving Dorodnitsyn-Lees variables are applied;

momentum:
$$\frac{\partial}{\partial\eta}\left(N\frac{\partial^2 f}{\partial\eta^2}\right) + f\frac{\partial^2 f}{\partial\eta^2} + 2\frac{d\ln u_e}{d\ln\xi}\left[\frac{\rho_e}{\rho} - \left(\frac{\partial f}{\partial\eta}\right)^2\right]$$

$$= 2\xi\left(\frac{\partial f}{\partial\eta}\cdot\frac{\partial^2 f}{\partial\eta\partial\xi} - \frac{\partial f}{\partial\xi}\frac{\partial^2 f}{\partial\eta^2}\right)$$

$$N = \frac{\rho\mu}{(\rho\mu)_w} \qquad f = \int \frac{u}{u_e}\,d\eta, \quad \frac{\partial f}{\partial\eta} = \frac{u}{u_e}$$

energy:
$$\frac{\partial}{\partial\eta}\left(\frac{N}{Pr}\frac{\partial g}{\partial\eta}\right) + f\frac{\partial g}{\partial\eta} + \frac{u_e^2}{He}\frac{\partial}{\partial\eta}\left[N\left(1-\frac{1}{Pr}\right)\frac{\partial f}{\partial\eta}\frac{\partial^2 f}{\partial\eta^2}\right]$$

$$= 2\xi\left(\frac{\partial f}{\partial\xi}\frac{\partial g}{\partial\xi} - \frac{\partial f}{\partial\xi}\frac{\partial g}{\partial\eta}\right)$$

$$g(\xi,\eta) = H/He, \qquad \xi = \xi_0 + \int_0^x (\rho\mu)_w \cdot u_e\, r_w^{2j}\, dx$$

$$\eta = \frac{u_e\, r_w^j}{\sqrt{2\xi}} \int_0^y \rho\, dy$$

For two-dimensional flow, $j = 0$ and for axisymmetric flow, $j = 1$.

For case (ii), Neyland (1966) introduced the following new transformation;

$$\xi = \int_{-\omega}^{x} (\rho\mu)_w F(u_e)dx, \qquad \eta = \rho(u_e) \int_0^y \rho\, dy \tag{22}$$

where functions $F(u_e)$ and $\rho(u_e)$ are to be determines and $F(u_e)$ is to satisfy the convergence of η at $x \to -\infty$.

Then the momentum equation becomes

$$\frac{\partial}{\partial\eta}\left(N\frac{\partial^2 f}{\partial\eta^2}\right) + \alpha f\frac{\partial^2 f}{\partial\eta^2} + \left[2\beta\frac{\rho_0}{\rho} - \left(\frac{\partial f}{\partial\eta}\right)^2\right] = \frac{u_e F(u_e)}{\varphi^2(u_e)}\left[\frac{\partial f}{\partial\eta}\frac{\partial^2 f}{\partial\xi\partial\eta} - \frac{\partial f}{\partial\xi}\frac{\partial^2 f}{\partial\eta^2}\right] \tag{23}$$

$$\alpha = \frac{F(u_e)}{\varphi(u_e)}\frac{d}{d\xi}\left[\frac{u_e}{\varphi(u_e)}\right], \qquad 2\beta = \frac{F(u_e)}{\varphi^2(u_e)}\frac{du_e}{d\xi} \tag{24}$$

At an infinitely distant point $\xi = 0$ and in order to begin the ingegration from $\xi = 0$, it is necessary that the right hand term of eq. (23) must vanish for $\xi = 0$. The eq. (23) will be reduced to the usual form, if the following conditions are satisfied.

$$u_e F(u_e) = 2\xi\varphi^2(u_e)$$

$$\alpha = \text{constant}, \qquad \beta = \text{constant} \qquad (x \to -\infty) \tag{25}$$

Then solutions of eq. (24) and (25) are:

$$u_e + c\xi^{\beta}, \qquad \varphi = Au_e^{\frac{2\beta-\alpha}{2\beta}}$$

$$F = 2A^2 c^{-\frac{1}{\beta}} \cdot u_e^{1+\frac{1-\alpha}{\beta}}$$

From the transformation (??) and above information, $u(x)$ in the neighborhood of point $x \to -\infty$ is given by

$$2\beta A^2 \int (\rho\mu)_w \, dx + \text{const} = \begin{cases} \ln u_e & \text{for } \alpha = \beta \\ \beta/(\alpha-\beta) u_e^{(\alpha-\beta)/\beta} & \text{for } \alpha \neq \beta \end{cases}$$

The self-similar velocity distribution for laminar accelerating flow is

$$u_e = u_e(o) \quad \exp\left[2A^2 \int_o^x (\rho\mu)_w \, dx \right]$$

or

$$u_e = \left[u_e(o)^{\frac{\alpha-\beta}{\beta}} - 2(\beta - \alpha) \cdot A^2 \int_o^x (\rho\mu)_w \, dx \right]^{\frac{-\beta}{\beta-\alpha}}$$

where A, α and β are constants.

This solution leads to the computational procedures similar to those used for the ordinary laminar boundary layer on a finite or semi-infinite body.

For the flow model sketched in Fig.I.58, Matveyeva and Neyland (1967), carried out a one-step calculation by the method of integral relations for the boundary layer upstream of the corner employing Neyland's (1966) analysis. The numerical integration was started at the corner where a pressure ratio of 0.668 (corresponding to a subsonic Mach number) was assumed and continued in the upstream direction. A wall-to-free stream stagnation enthalpy ratio is taken as 0.5. The results obtained by them are plotted in Fig.I.59. and compared with Hama's (1966) data at $M_\infty = 2.35 - 4.02$ as well as Olsson and Messister's (1969) computed values as seen from Fig.I.59.

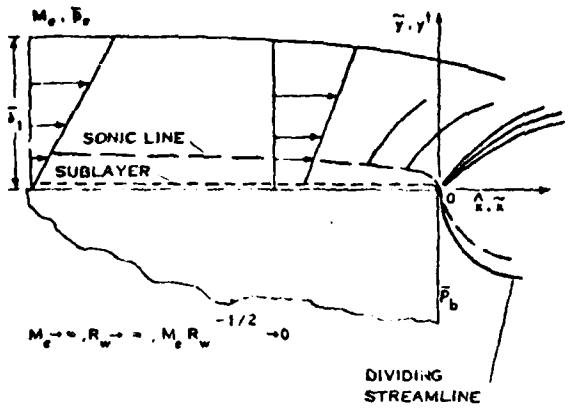

Figure I.3. Acceleration of a hypersonic boundary layer approaching a corner.
[Olsson and Messister (1969)]

Matveyeva and Neyland (1967), applied Neyland and Sychev's (1966), asymptotic analysis and computed the distributions of pressure, friction and heat transfer upstream of a corner of an axisymmetric body over the small distance of several boundary layer thicknesses. Based upon the first approximation, distributions of heat transfer for $Pr \approx 1$, $\epsilon \to 0$ are given in a parameter

$$B = \frac{Pr-1}{Pr} \left[- \frac{\ln \epsilon}{\epsilon} \right]^{\frac{1}{4}}$$

which characterizes the effect of heat conductivity, viscous dissipation and convection. Since Matveyeva and Neyland's (1967) solution is for $|B| \to \infty$, for the actual case of $Re = 10^4 - 10^6$, $Pr = 0.7$, the effect of dissipation to heat transfer is overestimated. Matveyeva and Neyland (1967), predicted pressure distribution more

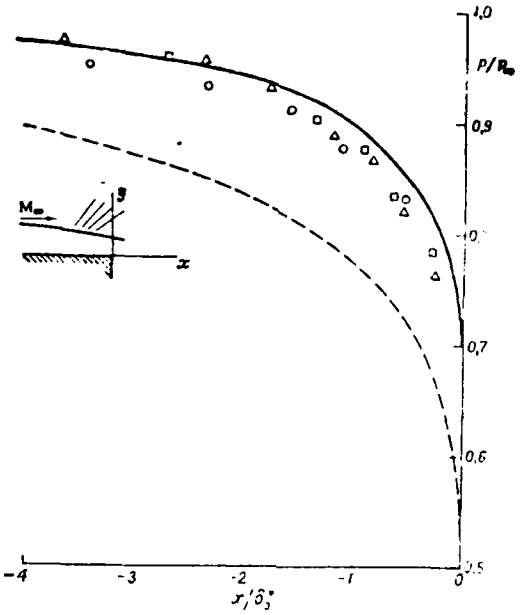

Figure.I.59. Comparison of theoretical and experimental data on pressure distribution ahead of base for two-dimensional supersonic flow.
—— = calculation [Matveyeva dnd Neyland (1967)]
---- = hypersonic approximation [Olsson and Messiter (1969)]:
M_∞ = 3.15: δo^* - laminar boundary layer displacement thickness ahead of interaction region: experimental data [Hama(1966)]:
Δ M_∞ = 4.02, Re = $1.2 \cdot 10^4$: □ M_∞ = 3.15, Re = $1.5 \cdot 10^4$:
o M_∞ = 2.35, Re = $4.4 \cdot 10^4$.

closely with experimental data than Olsson and Messister (1969).

The discrepancies among the computed results of Olsson and Messister and measured data are caused by the following facts: Olsson and Messister's analysis is for hypersonic flow with M_∞, larger than that of the experiment, and effects of viscous interaction and pressure drop distribution cause the errors in the analysis.

No upstream propagation of disturbance is considered.

Olsson and Messister (1969), carried out their analysis employing the asymptotic approach based upon the trip-deck structure of flow layer as described previously and seen in Fig.I.58, by assuming that the upstream flow velocity of the corner is hypersonic and the interaction of the hypersonic flow with bourdary layer is weak. An initial decrease in the pressure causes the boundary layer to become thinner and displacement thickness δ^* continues to decrease until a critical value of the pressure satisfies $d\delta^*/dp=0$. This critical point is located at a distance $O(M_e Re_w \cdot L)$, from the corner, i.e. $\hat{x}=0$, where L is body length. The stretched coordinate system is defined by $\hat{x} = (x-L)/M_e Re_w^{-\frac{1}{2}} \cdot L$, the origin is taken at the corner, the direction of x is parallel to the horizontal surface upstream of the corner and x is positive toward the wake region.

The remaining part of the upstream is given by

$$\hat{x} = (x - L) / Re_w^{-\frac{1}{2}} . L$$

For these two parts, the limits are given by

$$M_e \to \infty , \quad Re_w \to \infty \quad \text{and} \quad M_e Re_w^{-\frac{1}{2}} \to 0.$$

The y coordinate is stretched by $\tilde{y} = y/Re_w^{-\frac{1}{2}} \cdot L$. To obtain the initial upstream condition, it is assumed that for any given flow quantity, the solution obtained in the limit for fixed $\hat{x}$ can be matched asymptotically with the solution obtained in the limit for fixed $\tilde{x}$.

In the first approximation;

$$\tilde{u} (-\infty , \tilde{y}) = \hat{u} (0, \tilde{y}), \quad \tilde{p} (-\infty , \tilde{y}) = \hat{p} (0)$$

$$v (-\infty , \tilde{y}) = 0$$

where superscrips $\wedge$ and $\sim$ refer to coordinate system $\hat{x}$ and $\tilde{x}$.

The so called composit solutions which are uniformly valid approximations in the region of interest $-\infty < \hat{x} \leq 0$ are

$$u/u_e \sim \hat{u}(\hat{x},\hat{y}) + \tilde{u}(\tilde{x},\tilde{y}) - \hat{u}(0,\tilde{y})$$

$$p/p_e \sim \hat{p}(\hat{x}) + \tilde{p}(\tilde{x},\tilde{y}) - \hat{p}(0)$$

$$v/u_e \sim \tilde{v}(\tilde{x},\tilde{y})$$

For the sublayer solution, since the sublayer thickness is $O(Rew^{-3/4}.L)$ the coordinate is formulated by

$$y^+ = y/Rew^{-3/4} \cdot L$$

The limit to be considered is $Rew \to \infty$ with $\tilde{x}$, y^+ and Me fixed. Then the asymptotic representations are:

$$\frac{u}{u_e} \sim U(\tilde{x})\, u^+(\tilde{x}, y^+) + \text{---}$$

$$\frac{p}{\rho_w u_e^2} \sim p^+(\tilde{x}) + \text{---}$$

$$\frac{v}{u_e} \sim Rew^{-\frac{1}{4}}\, U(\tilde{x})\, v^+(\tilde{x}, y^+) + \text{---}$$

$$\frac{\rho}{\rho_w} \sim \rho^+(\tilde{x}, y^+) + \text{---}$$

where $U(\tilde{x})$ is the expansion for u/u_e obtained from the composite solution by setting $\tilde{y} = 0$. The approximate continuity, $\tilde{x}$ - momentum and energy equations are:

$$(\rho^+ Uu^+)_{\tilde{x}} + (\rho^+ Uu^+)_{y^+} = 0$$

$$\rho^+ Uu^+ (Uu^+)_{\tilde{x}} + \rho^+ U^2 v^+ Uy^+ = -dp^+/d\tilde{x} + U(\mu^+ u^+_{y^+})y^+$$

$$U^2 u^+ + \left[2\gamma / (\gamma - 1) \right] p^+ / \rho^+ = 1$$

where $\mu^+ = \mu / \mu_w$

The boundary and matching conditions are

$$u^+ (\tilde{x}, o) = v^+ (\tilde{x}, o) = 0$$

$$u^+ (\tilde{x}, \infty) = 1$$

The sublayer equations are integrated subject to the boundary and matching conditions and the results obtained are

$$u^+ = 1 - e^{-\eta/\theta_o} \quad , \quad \theta_o = 2Mo^{-3} \left[\int_{-\infty}^{\xi} Mo^6 \, d\xi \right]^{\frac{1}{2}}$$

$$y^+ = \frac{1}{2} (\gamma - 1) \theta_o (\gamma U p^+)^{-1} \int_{-\infty}^{u^+} (1 - u^+) \left[1 - u^{+2} U^2 \right] du^+$$

$$\psi^+ = \theta_o \int^{u^+} (1 - u^+)^{-1} \, u^+ \, du^+$$

where

$$\xi = \int_{-\infty}^{\tilde{x}} U \frac{p^+}{pe} \, d\tilde{x} \quad , \quad \eta = U \int_o^{+\eta} \rho^+ \, dy^+$$

and ψ is the stream function and the subscript o refers to $\tilde{y} \to o$.

Neyland (1969a), used the asymptotic solution of the Navier-Stokes equation for the computation of the separated flow characteristics and determined tha amplitude of the pressure perturbation in the attached flow at M = O(1). It was found that the flow remains attached despite the rapid pressure rise when the amplitude of pressure perturbation $\Delta p = C (\epsilon^{\frac{1}{2}})$ prevails in the free interaction region of $\theta (\epsilon^{\frac{3}{8}})$.

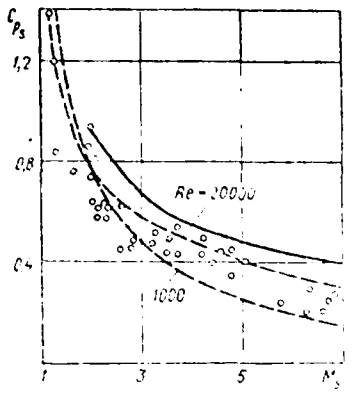

Fig.I.60. Values of the coefficient of pressure at the separation point [Neyland (1969a)] (solid [Neyland (1969a)] and dashed [Yelkin and Neyland (1965)] lines--calculation, circles--experiment [Erdos and Pallone (1962)]

The analysis leads to the existance of a similarity parameter

$$C_p = \frac{\zeta C_{fs}^{\frac{1}{2}}}{(M_s^2 - 1)^{\frac{1}{4}}}$$

where C_{fs} and M_s are coefficients of friction and the Mach number upstream of separation as shown in Fig.I.60.

5.3.2 Upstream Propagation of Disturbance

Brown and Stewartson (1969), Matveyeva and Neyland (1967), and Neyland (1969a), investigated the significant effect of upstream propagation of disturbance to the flow phenomena. Stewartson (1970), found that with no consideration of upstream propagation of disturbance, the reduction of the pressure upstream of the corner is much larger compared to that with consideration of disturbance propagation.

Neyland (1969a), based upon free-interaction theory, found that in order to describe completely the disturbance propagation upstream of a base, it is necessary to extend the upstream region from the

length region $O(Re^{-\frac{1}{2}})$ with pressure change of O (1) up to O $(Re^{-3/8})$ where pressure change of O $(Re^{-\frac{1}{4}})$ prevails. The disturbance propagation phenomena around a corner is characterized by the so called "blocking" effect of the disturbance emanating from the base upon reaching the speed of sound on the local inviscid flow stream line adjacent to the body surface. The acceleration of upstream flow, in the locally inviscid region, equalizing the pressure directly upstream of the base to the base pressure is possible when the ratio of the pressure in the body surface of the disturbed flow region with respect to the pressure in the separated region of the base is less than that corresponding to the sonic pressure change amounting to $(\gamma + 1)/2)^{\frac{\gamma}{\gamma-1}}$ where γ is the ratio of specific heats. In this case, the expansion of the supersonic stream filament takes place as a result of the contraction of the subsonic stream tube lying to the body surface, because the flow acceleration sharply increases the friction stress while the thermal flux to the body surface increases to a lesser degree. However, when the total pressure ratio reaches the previously mentioned critical value, then the Mach number on the body surface (in the locally inviscid part of flow) reaches the sonic value and it is impossible to expand the upstream flow of the corner and a scattered rarefaction wave forms near the corner. Therefore, the upstream flow of a corner is not affected by the further reduction of the base pressure. This writer recalls that this finding of Van Dyke and Nevland (1967) is similar to the well-known isotropic [illegible] barrel flow discharged from a reservoir passing through a [illegible], as a function of the exit pressure level.

Matveyeva and Neyland (1967), considering the propagation of disturbance and formation of the locally inviscid flow region, evaluated the pressure reduction upstream of a corner as 60% of the overall pressure in good agreement with measured date of M. L. Robinson [Stewartson (1970)], at $M_\infty = 2.75$, convex corner angle $\alpha \simeq \frac{1}{4}$ and $Re = 10^6$, compared to the Stewartson's (1970) prediction 90% reduction, not considering the disturbance propagation.

Stewartson (1970), studied the structure of a laminar supersonic flow near a corner and confirmed the triple-deck structure of Matveyeva and Neyland (1967) and improved their analysis by removing the non-uniformity as the influence of the corner dies away upstream and by extending the said analysis to the downstream region of the corner.

The phenomena of disturbance propagation for the case of a strong viscous interaction at hypersonic speed has been investigated progressively in the USSR, but further study is needed to clarify still unclear aspects. At hypersonic speed, the pressure change and the length of interaction region is given in a function of interaction parameter $x = M\tau \gg 1$, namely

$$\Delta p/p \sim x^{1/2} \quad \text{and} \quad x/\ell \sim x^{3/4}$$

where τ is the thickness ratio. Thus, if the interaction is not weak the pressure gradient induced by the external flow around the effective body formed by the boundary layer displacement thickness influences the flow in the boundary layer even in the first approximation. Therefore, the pressure distribution at the outer edge of the boundary layer cannot be considered to be given and must be determined by joint integra-

tion of the equations for hypersonic inviscid flow and the boundary layer. The effects of upstream propagation are dependent on the solution on the edge conditions specified downstream.

Neyland (1970b), realized that no unique solution for moderate and strong interaction regions can be obtained even in the first approximation by specifying the only usual boundary conditions on the body surface and the outer edge of boundary layer as well as initial conditions. Thus, he specified an additional condition in the base pressure or separation point which may be determined from the conditions of compatibility with the solution describing the downstream flow. If this downstream condition is not given, then the following two single-parameter families of nonself-similar boundary layer solutions exist, in addition to the well-known solution obtained by Lees and Stewartson [Hayes and Probstein (1959)],

$$f(\xi,\eta) \sim f_0(\eta) + \xi^{1+a} A_1 f_1(\eta) + \xi^{2(1+a)} f_2(\eta) + \cdots$$

$$p(\xi,\eta) \sim A_0 \xi^{-1} (1 + A_1 \xi^{1+a} + A_2 \xi^{2(1+a)} + \cdots)$$

where ξ, η and f are conventional Dorodnitsyn-Lees variables

$$\xi = \frac{2\gamma}{\gamma-1} \int_0^x \rho dx \ , \quad \eta = (2\xi)^{-1/2} \int_0^y \rho \, dy \ , \quad u = \frac{\partial f}{\partial \eta}$$

The first terms represent the self-similar solution. The non-tribial solution exists only for the "eigen-value" a and is defined to within an arbitrary constant, for example A_1. The subsequent terms are found uniquely for given A_1 from the solution of the linear nonhomogeneous systems of equations. Depending upon the sign of A_1, the pressure for

the nonself-similar solutions is everwhere greater ($A_1 > 0$) or everywhere less ($A_1 < 0$) than that obtainable from the self-similar solution. Kozlova and Mikhaylov (1970), obtained analogous results for the flow over a triangular wing and yawed flat plate when the approaching flow is not normal to the leading edge of the plate. The intensity of disturbance upstream propagation increases with the increase of the yawed angle. For the final solution of the flow over a triangular wing, it is necessary to find out whether the boundary condition is satisfied in the symmetry plane or not.

The eigen value a is the criterion of upstream disturbance propagation intensity as seen from Fig.I.61. The analytical results of Neyland (1971b), Kozlova and Mikhaylov (1971) and Provotorov (1973), indicate that the effect of disturbance propagation decreases with an increase of a. For flow over a flat plate, if gas is injected through the surface of the body, then the effect is increased; while for the cooled surface, the effect decreases markedly. A very important question is the formulation of the additional boundary condition to be used for the unique solution. For example, as Neyland (1970b), indicates for flow near a flat plate base, if the downstream base pressure is given, the solution of the one-parameter family is selected for which the pressure at $x/L = 1$ is equal to the base pressure, where symbol L refers to plate length.

The new similarity law developed recently in USSR is more general compared to that developed by Lunve (1956) and Hayes and Probstein (1959) because these laws do not take account of disturbance propaga-

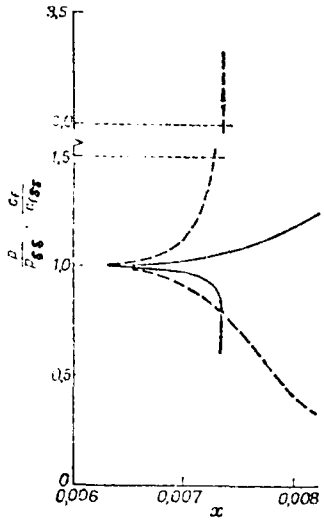

a

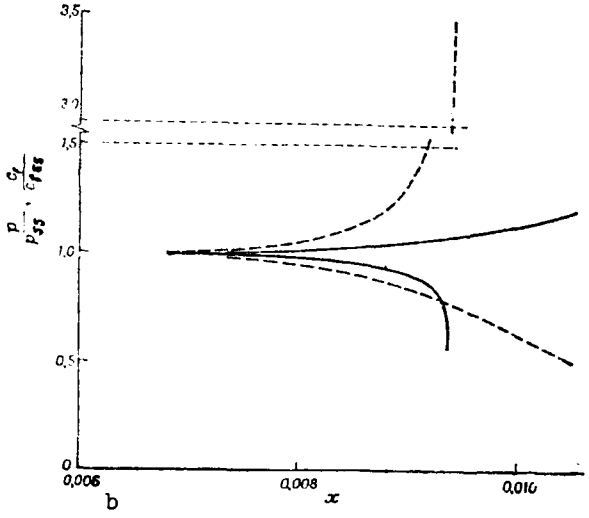

b

Figure I.61. Distribution of pressure and local friction drag coefficient on flat plate for strong hypersonic flow interaction with laminar boundary layer [Neyland (1971b)] .
a- $\gamma = 7/5$, $a \approx 49.6$, b- $\gamma = 5.3$, $a \approx 23$. --- = p/p_{ss} ; --- $C_f/C_{f_{ss}}$; γ = ratio of specific heats; p_{ss}, $C_{f_{ss}}$ = values of parameters for self-similar solution; x-dimensionless length for one of the non-self-similar solution.

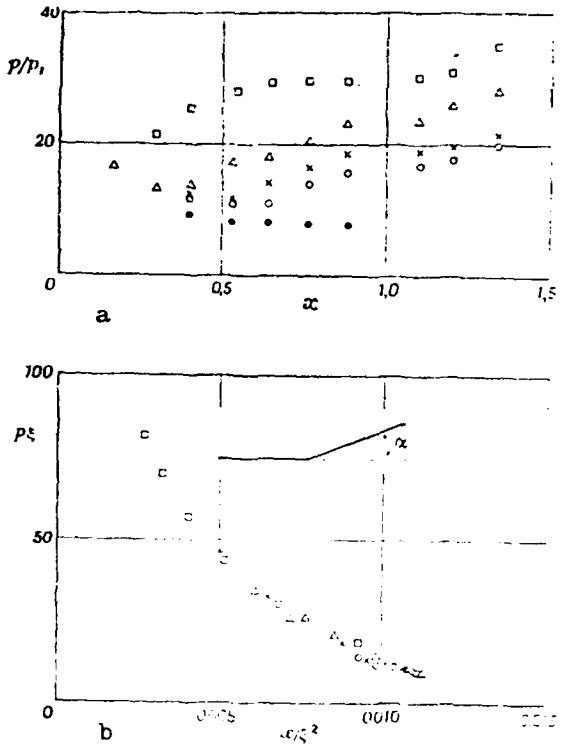

Figure I.62. Experimental verification of similarity law for flows in the regime of strong interaction of hypersonic flow with boundary layer with account for disturbance propagation upstream; M = 23.3, Re = 1.9·10 [Neyland (1970a), and Gorislavskiy and Stepchenkova (1971)].
a) Experimental results; b) Same results in similarity coordinates: • α = 0°; o α = 10°; x α = 11°30'; Δ α = 12°; □ α = 20°; ξ = Dorodnitsyn variable.

tion, although these are useful for regions with only a small disturbance propagation effect.

Kozlova and Mikhaylova (1971), studied the similarity law by taking account of the disturbance propagation and obtained a good agreement with the experimental data of Gorislavskiy and Stepchenkova (1971) and Gorenbukh and Kozlova (1973) for the strong interaction at hypersonic speed as shown in Fig.I.62 and I.63.

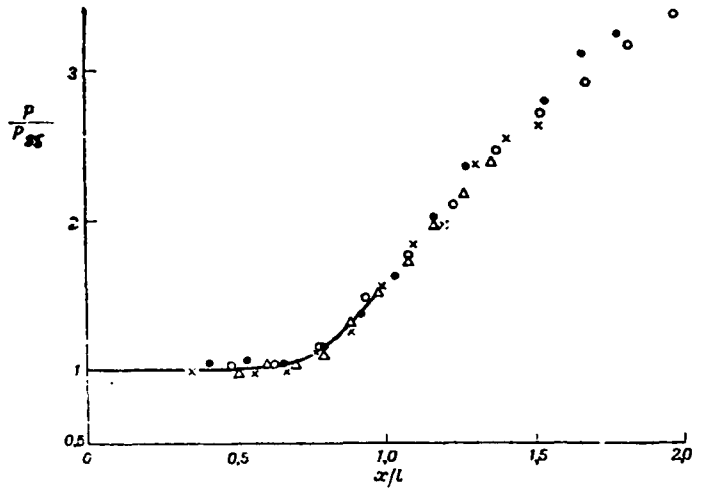

Figure I.63. Comparison of theoretical and experimental data on pressure distribution on flat plate with flap for strong interaction of hypersonic stream with laminar boundary layer;
M = 24.2, X = 10 - 16 [Gorenbukh and Kozlova (1973)].
ℓ = distance from plate leading edge to flap;
p_{ss} = pressure for the self-similar solution;
—— = calculation.
o $\alpha = 90^\circ$, $h/\ell = 0.12$; X $\alpha = 90^\circ$, $h/\ell = 0.08$; Δ $\alpha = 10^\circ$; $\alpha = 0^\circ$
(α = deflection angle of flap mounted on aft part of plate).

5.3.3 Reattachment

The problem of reattachment was studied in USSR for the semi-infinite jet reattachment to the surface of a flat plate as one example of supersonic compression flow with a large local pressure gradient. The flow model is sketched in Fig.I.64. The problem involves the free viscous mixing and it is assumed that the mixing starts at some distance ℓ from the reattachment region. This distance ℓ is used as a length scale and in evaluating Re. Local inviscid flow is described by the Euler's equation as the first approximation. At the end of the mixing zone, the velocity and density profiles are considered the same as those of approaching the undisturbed flow when the asymp-

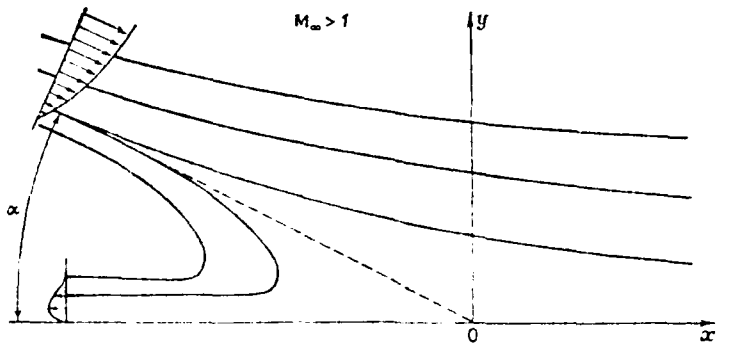

Figure 1.64. Flow scheme in region of semi-infinite two-dimensional supersonic jet attachment to the surface of an infinite flat plate. [Neyland (1970a)]

totic expansion matching principle is used. At the outer edge, the conditions of compatibility with the outer supersonic flow and the zero normal velocity at the body surface are to be satisfied.

Neyland's (1970a) study shows that in the first approximation, the stagnation pressure p_0 of the dividing stream line (stream line incident on the body surface is termed dividing stream line here) at the end of the mixing zone must be equal to the static pressure p at a large distance downstream of the turning region. In reality, however, $p_\infty > p_0$ by an order of magnitude $O\,(Re^{-1/4})$, due to the viscosity effect. If we apply Bernoulli's integral for the inviscid flow, then $p_0 \geqslant p_\infty$. Based upon the vortex theorem of Nickol'skiy (1949) and the arguments presented by Taganov (1968) for analogous incompressible flows, it is shown that if $p_0 = p_\infty$, then the critical point shifts to an infinitely large distance point to the right of the body

surface.

> The so called "critical point" was defined by Crocco-Lees (1952), as a singularity point in the basic differential equation which acts much like the throat of a nozzle in determining the base pressure, for example, or in some cases the surface pressure distribution in a boundary layer shock wave interaction. This property is an important one for the supersonic wake or reattaching supersonic flows directed toward the solid surface. Most of the recompression occours before the critical point is reached.

Neyland (1970a), shows that in a wide range of initial and boundary conditions, $p_0 > p_\infty$ is impossible. If $p_0 > p_\infty$, there must be, to the right of the critical point, an inviscid flow region which does not contain reverse flows and which does not satisfy the condition of compatibility with the outer supersonic flow for $x/Re^{-1/2}_{-} + \infty$. Therefore, Neyland (1970a), proposed the following procedures to solve the reattachment problem. A solution, not containing the critical point, but satisfying the condition of $p_0 = p_\infty$ for the locally inviscid flow, is to be obtained by the first approximation. The consideration of asymptotic behavior of the disturbance decay of this solution leads to the investigation of flow for the region $\chi \sim O(Re^{-3/8})$ where the characteristic pressure change is $O\ (Re^{-1/4})$.
In this region, the pressure rises reaching the limiting value of p_∞. The critical point is also located here and the solution is described by the equations of free-interaction theory. Neyland(1970a), suggests

the Chapman-Korst condition (Chang, 1970) should be corrected in $O(Re^{-1/4})$ although the pressure rise to cause the separation is the same order.

The following Chapman et al (1957), formulation, which is similar to that of Korst, is a simple way to evaluate the reattachment zone pressure:

$$p_{DA} = p_2 \left(1 + \frac{\gamma - 1}{2} M^{*2} \right)^{\frac{-\gamma}{\gamma-1}}$$

where p_{DA} is the pressure in the dead air region, p_2 is the pressure on the wall downstream of the reattachment point and M^* is the Mach number along the dividing stream (the dividing stream is located within the mixing zone, along which $v = 0$ and the circulatory separated region is divided from the streamwise flow field). The velocity along the dividing stream line is $u^* = 0.587\ u_e$.

Brown and Stewartson (1969), raise a number of questions (e.g. is fluid in the dead region almost at rest and is the flow near reattachment so simple?) and comment as follows:

> But, since the agreement with experiment is so good that one is inclined to believe that it contains the principal features controlling the dead air zone and that it may well be worth exploring the assumption further from a more rigrous stand-point. This, however, has not been done.

Neyland (1970a), also studied the heat transfer in addition to pressure at the reattachment. The predicted heat transfer results are favorably compared with the experimental data of Bushnell and Weinstein (1968) as shown in Fig.I.65. For this computation of heat tran-

sfer, the narrow flow regions under the local inviscid flow zone where effects of viscosity and thermal conductivity are significant, have

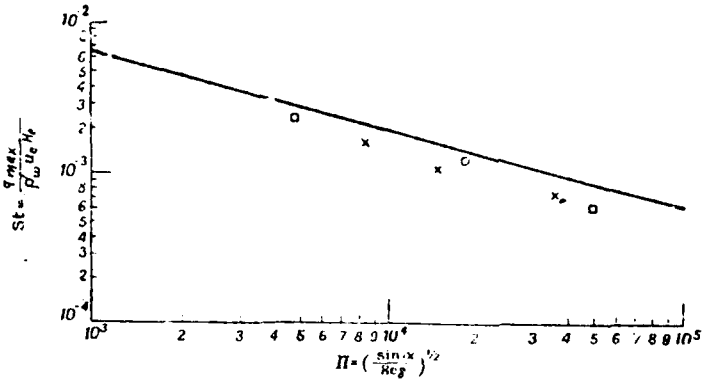

Figure I.65. Comparison of theoretical and experimental data for maximal heat flux in attachment region of laminar separated zone in supersonic flow. [Neyland (1970a)]

x Me = 3, Re = 10^5 , $g^* = 0.5$, $f_w = 0$, $g_w = 0.05$;

o Me = 3, Re = 10^5 , $g^* = 0.9$, $f_w = 0$, $g_w = 0.05$;

□ Me = 3, Re = 10^4 - 10^6, $g^* = 0.5$, $f_w = 0$, $g_w = 0.05$;

• Me = 3, Re = 10^5 , $g^* = 0.5$, $f_w = -0.4$, $g_w = 0.05$.

been considered. To compute the pressure distribution of the inviscid flow numerically, the edge conditions of these regions are used for two strip integrations applying the modified method of Dorodnitsyn (1958), but the computed pressure results were lower than the experimental data of Chapman et al (1957), as shown in Fig.I.66. Neyland (1970a), remarks that in order to improve the agreement of predicted and measured data, the free-interaction region is also to be considered.

Neyland (1970a), extended his asymptotic analysis for an incompressible flow to a compressible separated flow caused by a blunt angle

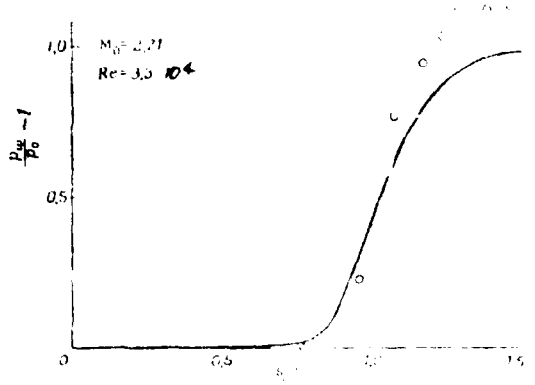

Figure I.66. Pressure distribution in the laminar separated zone attachment region ahead of a flat in supersonic flow. —— Calculation [Neyland (1970b)], o Experiment [Chapman et al. (1957)]; p_w = pressure on the body; p_o = pressure ahead of attachment region.

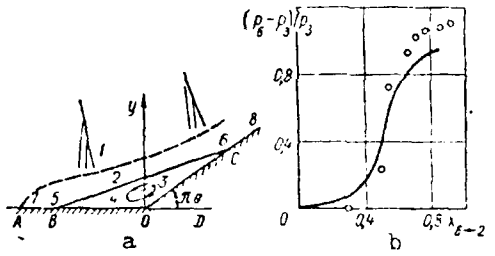

a b

Fig I.67. Diagram of separated flow of a supersonic flow at a blunt angle (a) and calculation of pressure in the field of

1--External inviscid supersonic flow;

2--Zone of mixing;

3--Area of reversed flow;

4--Boundary layer at base of the reversed flow;

5--Area of separation of flow;

6--Area of reattachment of flow;

7--and 8--Boundary layer in front of the area of separation and behind the area of reattachment[Shvets and Shvets (1976)].

Solid line on the graph -- calculation [Neyland (1970a)]; circles -- experiment [Chapman et al (1950)].

$\tau_w = O(\epsilon^{\quad})$ in the following regions (see Fig. [illegible]): external [illegible] supersonic flow, mixing zone of characteristic dimension $x = O($ [illegible] ϵ [illegible] in which the boundary layer equations hold, the region of reversed subsonic flow with a constant vorticity driven by the Euler equation, the boundary layer of thickness $O(\epsilon$ [illegible]) at the base of the reverse flow, region of separated flow of length $O(\epsilon^{3/4})$ along which the pressure distribution is determined by the free interaction of supersonic flow with the boundary layer, the region of flow reattachment of characteristic dimensions of $x = O(\epsilon$ [illegible]), $y = O(\epsilon^{1}$ [illegible]) and the regions of the boundary layer upstream of separation and downstream of reattachment.

In order to compute the incompressible flow in zone 3, it is necessary to define the integral conditions of distributions of pressure and enthalpy of the decelerating flow along the closed stream line. Furthermore, in addition to w, the temperature is also determined from the equations of energy.

If the vorticity is small, a complete solution of flow characteristics in the separated zone is obtainable. Due to the viscosity effect, the computed pressure rise at the reattachment by the Chapman-Korst theory is less than the experimental data by an order of $O(\epsilon^{\frac{1}{2}})$ as shown in Fig. I.67.

5.3.4. Flow Over Protuberance

The asymptotic methods are applied to problems around obstacles or irregularities located on the bottom of a boundary layer. Zubtsov

(1971), analyzed this problem for incompressible flow, and Bogolepov and Neyland (1971), for compressible flow. The results of Zubtosov (1974), show that if the characteristic dimension is of the order of protuberance height, the first approximation reduces to the solution of the Euler equation which does, under certain flow condition, contain a reverse flow region upstream and downstream of protuberance. Bogolepov and Neyland (1971), studied the supersonic flow over a small protuberance for all possible combination of geometrical parameters and the local boundary layer thickness. Tabulated corresponding boundary value and similarity parameters. The results show that a marked increase of friction stress and thermal fluxes to the body surface take place at larger distances exceeding the order of magnitude of the characteristic obstacle dimension. In order to determine the onset of the upstream flow separation on an obstacle whose height and separation zone length are of the same order of magnitude, it is necessary to solve the complete incompressible flow Navier-Stoke equation. If the obstacles are slender, then the separation point and separated region are determined simply using Prandtl's equation. For this case of a slender obstacle, the value of parameter defined by the ratio of obstacle cross-section to characteristic boundary layer section area, amounting Re^{-1} classifies two different upstream pressure fields. If this parameter is small, then the obstacle induces rarefaction and large compression disturbance occurs.

Inger (1974), used the small perturbation theory of a compressible boundary layer to solve the flow problem past a relatively small protu-

berance (or boundary layer control apertures) exposed to high speed laminar flow, assuming Pr and Le are equal to 1, by introducing perturbations u', v', p' and T' caused by the protuberance.
The resulting governing equations are linear differential equations of partial derivatives. If Re is large, one may divide the perturbations into inviscid and viscous components. The viscous component is essentially only in a relatively thin sublayer close to the surface where perturbation motion can be considered as incompressible with negligibly low heat transfer due to viscous dissipation. These assumptions simplify the linearized Navier-Stokes equations of compressible flow.

5.4. Numerical Solutions:

The numerical solutions of the Navier-Stokes equations contributed forwards a better understanding of the separated flow. Babenko et al (1971), pointed out that the problem of the viscous flow over a blunt body is one of the most complex ones due to the significant non-linearity of the Navier-Stokes equations dealing with the reversed flow zone and the phenomena of its instability for larger Re than the critical one. These problems are not self-similar and analytical solutions are too difficult to obtain.

Viviand and Berger (1966) and Kirnasov and Korzhuk (1969a), solved incompressible separated flow problems by the first approximation of the Navier-Stokes equation. The infinite conditions were not rigorously satisfied by this approximation because of the dominant inertia

forces and the obtained solutions are applicable only for a small Re. Fig.I.68 and I.69 show the pressure distribution on the rear wall of a two-dimensional surface in a parameter of $\bar{\delta}$ and stream line configuration in a function of v_H with $\bar{\delta} = 1$, where $\bar{\delta} = \delta/H$, δ is the physical boundary layer thickness and H is the height of the base.

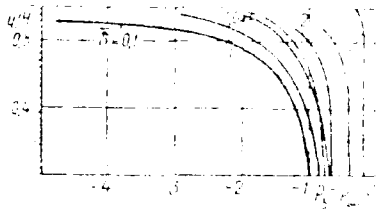

Fig.I.68. Distribution of pressure along the rear wall of the body (solid lines correspond to data of [Kirnasov and Korchuk(1969)], the dashed lines -- to Viviand and Berger (1976) [Shvets and Shvets (1976)]

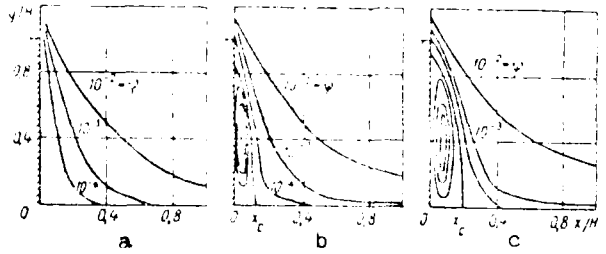

Fig.I.69. Picture of the stream line in a base region [Viviand and Berger (1966)] (x_c -- point of reattachment):
a--$v_H = 0$; b--$v_H = 0.1$; c--$v_H = 0.2$.

v_H = 0, no reverse flow zone is observed. With an increase of v_H to v_H = 0.1, a reverse flow zone becomes apparent and the point of separation shifts from the edge to a point on the rear wall. With an increase of $\bar{\delta}$, the separation point approaches the center and the size of reversed flow region decreases, but with an increase of v_H, the separation point approaches the tailing edge.

Thom (1967), solved the Navier-Stokes equation by a finite difference method in order to investigate the flow downstream of a plate placed perpendicular to the main flow, at a small and average Re. The results indicate that the length of the stagnation zone increased with increase of Re, but its width remained unchanged and the oscillation of the stagnation zone, causing Karman vortex street, was observed at Re = 50 in agreement with experimental results.

Boldyreva and Kuskova (1970), analyzed the flow past a sphere by replacing the infinite condition with an imaginary sphere of large radius. The computation for Re = 1, 5, 10 and 20, shows that with the increase of Re, the flow symmetry breaks down and a noticeable vortex appears when Re = 20.

Dorodnitsyn and Meller (1968), employed the numerical method to solve the viscous incompressible flow in an expanded two-dimensional channel. At each step of iteration, a system of linear algebrac equations was solved indicating that a stagnation appears with a reverse flow.

Pavlov (1968), solved numerically the Navier-Stokes equation for a supersonic flow around a blunt body and completed the flow picture including a shock wave. A formation of vortices downstream of the body was pre-

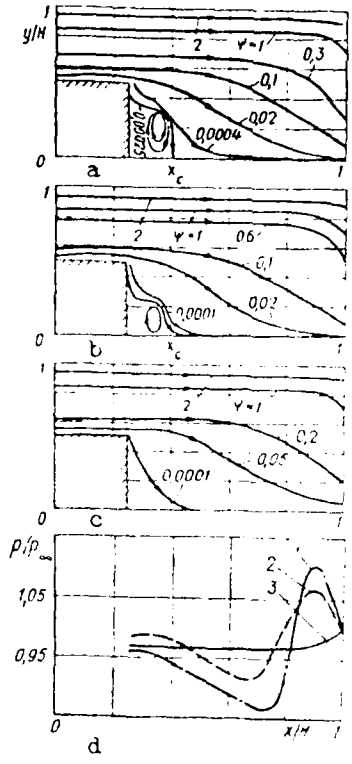

Fig.I.70. Flow of a viscous gas ina wake of a two-dimensional body [Myshenkov (1970)]: a--c--picture of flow (M = 0.288, a--Re = 3, b--Re = 2.1, c--Re = 1.7); d--distributed pressures along the axis of the wake (1--M = 0.288, 2--M = 0.864, 3--M = 1.15)

dicted at Re = 50, but was not detected probably due to the fact that either they were absent in certain conditions or that they were not visible because of the large grid used.

Myshenkov (1970), solved the Navier-Stokes equation by using the Lax-Wendroff method, for subsonic and transonic wakes downstream of a two-dimensional surface at Pr = 0.71, in the range of $1 < Re \leq 1000$. His paper of 1970, shows that at small $Re \leq 1.7$, the flow does not separate and at Re = 1.7 a fairly large zone of small velocity is formed at the rear critical point as seen in Fig.I.70, and with the increase of Re, separation occurs at the base forming a reverse flow region. At the trailing edge, the flow turns at a right angle with no separation affected by viscosity and the separation point is located in the

base region as Weinbaum (1968), theoretically, and Donaldson (1967), experimentally found. With an increase of Re, the dimension of the reversed flow region also increases, the separation point shifts toward the corner and the pressure distribution evens out and at $Re \geq 100$, the base pressure becomes almost constant. When $M \geq 0.864$ the pressure in the separation zone increases reaching $p \geq p_\infty$, caused by the trailing edge shock. However, toward the downstream direction the pressure becomes equal to p_∞.

Myshenkov in 1972, solved the wake flow downstream of a flat plate. At Re = 3, the separation point was located not at the corner, but on the plate base. With an increase of Re, the reversed flow region grows and the separation point moves toward the corner and the pressure variation smooths out. At Re = 100, the pressure becomes almost constant. The base pressure does not vary before separation despite the increase of Re, but after separation the pressure increases sharply, and with a further increase of Re reaching 1000, the base pressure increases monotonically and the wake flow becomes unsteady. The analysis of the Mach number effect in the range of $0.3 \leq M \leq 2$ at Re = 100 shows that with an increase of M from 0.3 to 0.8, the reversed flow region elongated and narrowed. With further increase of M, the reversed flow region contracted in length and width, and if M increases above 1, the flow stabilizes and delays the occurrence of separation.

Brailovskaya (1971b), detected more flow details by solving the two-dimensional supersonic wake flow downstream of a rectangular base. The numerical solution of the Navier-Stokes equation in a small wake region of reversed flow indicates that in the neighborhood of the cor-

ner, the flow expands and the pressure downstream of the wall increases sharply at first, then remains almost constant up to the axis of symmetry. This compression wave is more apparent at large M and Re, and the dimension of the reversed flow region increases almost directly proportionally to Re, but decreases with an increase of M. The interested readers may be aware that the following numerical solutions were achieved elsewhere. Jenson (1959), obtained a solution for the flow around a sphere using the method of relaxation for Re = 5-40 by fixing Re = 17 as the critical Re at which flow remains attached. Son and Hanratty (1969), solved numerically, for the flow around a cylinder at Re = 200 and 500 and Burggaf (1966), numerically analyzed the structure of the separated flow in a rectangular cavity.

5.5 Numerical Experiment

A brief presentation on the numerical experiments, carried out in USSR follows. Recently, at the Computer Center of the Academy of Sciences of the USSR, under the leadership of O. M. Belotserkovskiy, a number of numerical experiments were carried out to investigate the complex fluid flows using various principles of numerical modelling for equations of Euler, Navier-Stokes and Boltzman. Compared to a full scale experiment, the said approach is less expansive and, in a number of cases, it is the only instrument of investigation.

For the numerical experiment, the following steps, which may be correlated to physical experiments are taken:

Selection of a mathematical model, set up of an approximate solution system for the initial differential or integral equation, study of stability

[illegible]

[illegible] experiment is carried out [illegible] resulting [illegible] detailed analysis, correction of a mathematical model and modifi- [illegible] test elements [illegible] compressible flow [illegible] [illegible] equation. [illegible]

[illegible] incompressible [illegible] equation, developed by using stream [illegible] present, but the additional [illegible] condition [illegible] vortex [illegible] numerical algorithms [illegible] around a [illegible] [illegible] parameter [illegible] obtained [illegible] the numerical experiment.

[illegible] isobaric lines and flow characteristics of com- pressible flow separation around a sphere evaluated by the numerical experiment are shown in Fig. [illegible] and Fig. 1.73.

In Fig. 1.73, [illegible] is pressure at the tailing critical point and the location of the separation point on the sphere is given by x_s and the length of the reverse flow region by [illegible]$_s$ along the tailing

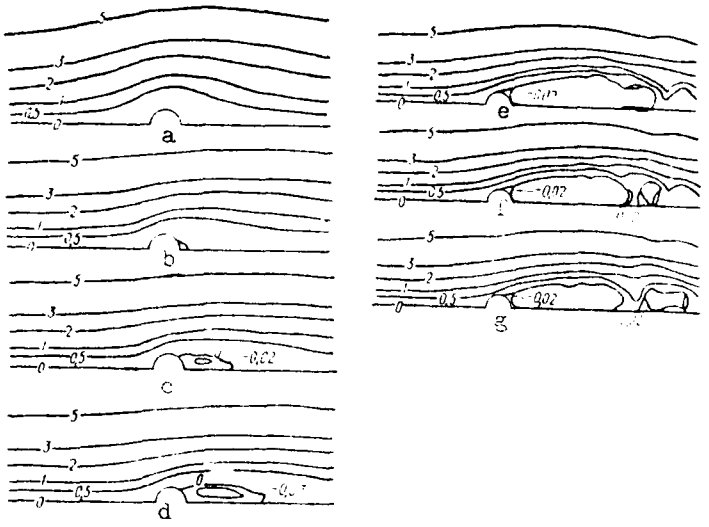

Fig.I.71. Picture of the flow past a round cylinder [Belotserkovskiy et al.(1975)]:
a--Re = 1; b--Re = 10; c--Re = 30; d--Re = 50; e--Re = 10^3, T = 162; f--Re = 10^3, T = 166; g--Re = 10^3, T = 170.

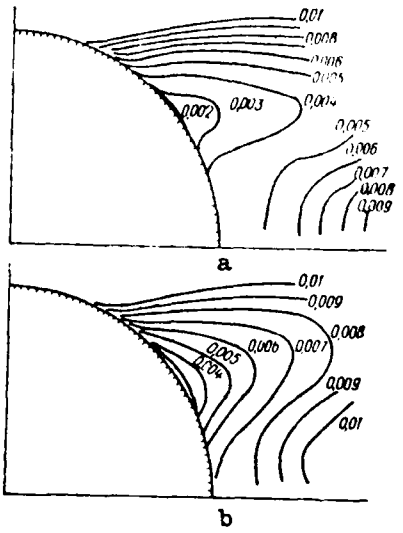

Fig.I.72. Diagram of a separated zone behind a sphere (M=20) [Belotserkovskiy et al. (1975)]:
a--Re = 10^4; b--Re = 1500.

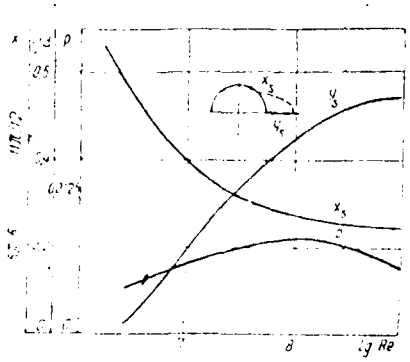

Fig.I.73. Dependence of characteristics of a zone of a reversed circulation flow on the Reynolds number [Belotserkovskiy et al.(1975)].

REFERENCE

[illegible]ramovich, G. N. (1960). Teoriya [illegible], (Theory of turbulent [illegible]reams), Fizmatgiz Press, Moscow

[illegible]ch [illegible] Bakarov [illegible] and [illegible] [illegible] "Tur-[illegible] Wake [illegible] Flow" [illegible] [illegible] Tekhnika" [illegible]

[illegible]

[illegible] Sulayev, [illegible] and [illegible] (196[illegible]) [illegible] Flow [illegible] Behind a Cylinder in a Channel, [illegible] [illegible]Fiziki (Questions of general and applied physics) Nauk[illegible] Press, Moscow

[illegible] "[illegible] Theory [illegible] Turbulent Wake Flows," AIAA [illegible] 34[illegible]

[illegible] "Flow past [illegible]," [illegible] Me-[illegible]nika [illegible]

Ars[illegible] and F. H. [illegible] (196[illegible]) "Numerical Calculation of Super-[illegible] wake flow," AIAA J., Vol. [illegible], No. [illegible]

Antonov, A. N. (19[illegible]) "Calculation of Interaction of a Turbulent Boun-dary Layer with External Supersonic Flow Behind a Protuberance," AN SSSR, M[illegible]

Avduyevskiy, et. al. (1960). Osnovy Teploperedachi v Aviatsionnoy i Raketnoy Tekhnika, (Basis of Heat Exchange in Aviation and Rocket Technology), Oborongiz Press, Moscow.

Babenko, K. I., Vvedenskaya, N. D. and M. G. Orlova (1971). Rezultaty raschyeta obtekaniya beskonechnogo tsilindra vyazkoy zhidkost'yu, (Results of Calculation of Flow past an Infinite Cylinder of Viscous Fluid) , IPM AN SSSR Publishers.

Badrinarayanan, M. A. (1961). "An Experimental Investigation of Base Flows at Supersonic Speeds," J. Roy. Aero. Soc., 65/607.

Bam-Zelikovich, G. M. (1954). Izv. AN SSSR OTN 12.

Batchelor, . K. (1956). "On Steady Laminar Flow with Closed Streamlines at Large Reynolds Number," J. Fluid Mech. 1/2.

Batt, R. and T. Kubota (1969). "Experimental Investigation of Laminar Near Wakes Behind 20° Wedges at $M_\infty = 6$," AIAA J., vol. 6, No. 11.

Baum, E., Denison, M. R., and H. H. King (1964). "Recent Studies of Laminar Base-Flow Region," AIAA J., vol. 2, No. 9.

Bearman, P. W. (1969). "On Vortex Shedding from a Circular Cylinder in the Critical Reynolds Number Regime," J. Fluid Mech. 37/3.

Belotserkovskiy, O. M. and Yu M. Davydov (1971). "Unsteady Method of 'Large Particles" for Gas-Dynamics Calculations," ZhVM i MF 1.

Belotserkovskiy, S. M. and N. I. Nisht (1972). "On Calculating Separated Unsteady Flow around a Slender Profile," Izvestiya AN SSSR No. 3.

Belotserkovskiy, O. M. and L. I. Serverinov (1973). "Conservation Method of Flows and Calculation of Flow Past a Body of Finite Dimensions of a Viscous Heat-Conducting Gas," ZhVM i MF 2.

Belotserkovskiy, O. M. and Yu M. Davydov (1974). "A Numerical Experiment when Studying Gas-Dynamics Flows with Separation or Injection of Flow," in the book Izbrannyye problemy prikladnoy mekhaniki, Selected problems of Applied Mechanics , VINITI AN SSSR Publishers, Moscow.

Belotserkovskiy, O. M., ed. (1974). Chislennoye issledovaniye sovremennykh zadach gazovoy dinamiki, (Numerical Study of Present Day Problems of Gas Dynamics) , Nauka Press, Moscow.

Belotserkovskiy, O. M., Gushchin, V. A. and V. V. Shchennikov (1975), "Method of Splitting Used for Solving Problems of the Dynamics of Viscous Incompressible Fluid," ZhVM i MF 1.

Bespalov, I. V. and B. G. Khudenko (1959). "Structure of a Turbulent Parallel-Plane Wake Behind a Blunt-Body," Univ. Publ. Aviatsionnaya tekhnika 2.

Birkhoff, G. (1955). Hydrodynamics, Dover Publications.

Birkhoff, G. and E. Zarantonello (1957). Jets, Wakes and Cavities, Academic Press.

Bogolepov, V. V. and V. Ya. Neyland (1971). "Supersonic Viscous Gas Flow Around Small Roughness on the Surface of a Body," Trudy TsAGI No. 1363.

Boldyreva, Z. V. and T. V. Kuskova (1970). "The Question of Flow Past a Sphere of a Viscous Incompressible Fluid," Vychislitel'nyye metody i programmirovaniye Computer Methods and Programming , MGU Publishers, Moscow.

Bondarev, Ye N. and M. Ya Yudelovich (1960). "The Possibility of Increasing Base Pressure Behind a Wedge during Flight at Hypersonic Speed," AN SSSR OTN, Mekhanika i mashinostroyeniye 5.

Bondarev, Ye N., (1963). "Time of Establishing Steady Flow in a Base Region," AN SSSR Mekhanika i Mashinostroyeniye, 5.

Bondarev, Ye N. (1964). "Approximate Estimation of the Turbulent Boundary Layer and Influence of Specific Heat Ratio on the Base Pressure Behind a Plane Step," Izvestiya AN SSSR Mech. i Mash. No. 3.

Brailovskaya, I. Yu (1971a). "Explicit Difference Methods for Calculating Separated Viscous Compressible Gas Flows," Collection: Some Applications of the Grid Method in Gasdynamics," Moscow State University Press, vol. 4.

Brailovskaya, I. Yu (1971b) "Flow in a Near Wake," DAN SSSR, 197/3.

Brown, S. N. and K. Stewartson (1969). "Laminar Separation," Annual Review of Fluid Mechanics Vol. 1, Annual Reviews Inc. 4139 El Camino Way. Palo Alto, Calif.

Brown, S. N. and K. Stewartson (1970). "Trailing-edge Stall," J. Fluid J. Fluid Nech. Vol. 42, part 3.

Burggraf, O. R. (1966). "Analytical and Numerical Study of the Structure of Steady Separated Flows," J. Fluid Mech., vol. 24, part 1.

Bushnell, D. M. and L. M. Weinstein (1968). "Correlation of Peak Heating for Reattachment of Separated Flows," J. Spacecraft vol. 5, No. 9.

Calvert, J. (1967). "Experiments on the Low Speed Flow past Cones," J. Fluid Mech. 27/2.

Carriere, P. (1965). "Recent Research Carried Out at ONERA on Problems of Reattachment," 7th Fluid Dynamics Symposium, Jurate, Poland.

Catherall, D. Stewartson, K. and P. G. Williams (1965). "Viscous Flow past Flat Plate with Uniform Injection," Proc. Roy. Soc. A 284 p. 370.

Catherall, D. and K. W. Mangler (1966). "The Integration of the Two-dimensional Laminar Boundary Layer Equations past the Point of Vanishing Skin Friction," J. Fluid. Mech. Vol. 26, part 1. pp. 163-182.

Chang, P. K. (1970). Separation of Flow, Pergamom Press. 1970.

Chang, P. K. (1973). Separation of Flow. MIR Publishers, Moscow 1973), vol. 3. "New Results of Separated Flow Studies" in Russian. pp. 234-302

Chapman, D. R. (1950). "An Analysis of Base Pressure at Supersonic Velocities and Comparison with Experiment," NACA TN 2137.

Chapman, D. R. (1951). "An Analysis for Base Pressure at Supersonic Velocities and Comparison with Experiments," NASA Rept. No. 1051.

Chapman, D. R., Kuchn, D. M. and H. K. Larson (1957), "Investigation of Separated Flows in Supersonic Streams with Emphasis on the Effect of Transition," NACA TN 3869.

Clauser, F. (1959) in the collection Problemy Mekhaniki, Problems in Mechanics , 2nd Ed., Foreign Literature Publishing House, Moscow. "Computation of Turbulent Boundary Layer," 1968, Proceedings AFOSR-IFR of Stanford Conference, vol. 2, 1969.

Crocco, L. and L. Lees (1952). "A Mixing Theory for the Interaction between Dissipative Flows and Nearly Isentropic Streams," J. Aero. Sci., vol.9.

Delany, N. K. and N. E. Sorenson (1953). "Low-Speed Drag of Cylinders of Various Shape," NACA TN 3038.

Denison, M. R. and E. Baum (1963). "Compressible Free Shear Layer with Finite Initial Thickness," AIAA J., vol. 1, No. 2.

Deway, C. F. Jr. (1965). "Near Wake of a Blunt Body at Hypersonic Speeds," AIAA J., vol.3, No. 6.

Donaldson, I. S. (1967). "On the Separation of a Supersonic Flow at a Sharp Corner," AIAA J., vol. 5, No. 6.

Dorodnitsyn, A. A. (1942). "Laminar Boundary Layer in a Compressible Gas," Dokl Akad. Nauk. SSSR vol. 34, pp. 234-242.

Dorodnitsyn, A. A. (1956). "On a Numerical Method for Solving Certain Nonlinear Problems in Aerodynamics," Trudy III. Vses mat S'ezda Izd. Acad. Nauk SSSR. vol. 3, pp. 447-453.

Dorodnitsyn, A. A. (1958). "On a Method for Numerical Solution of Some Nonlinear Problems of Aerodynamics," Proc. Third All-Union Math. Conf. 1956. vol. 3, Izvestiya An SSSR.

Dorodnitsyn, A. A. and N. A. Meller (1968). "On Some Approaches to Solution of the Steady State N-S Equations," ZhVM i MF. vol.8, No. 2.

Dorodnitsyn, A. A. and N. A. Meller (1971). "Application of the Small Parameter Method to Solution of the N-S Equations. Proc. Second. All-Republic Conf. Aerohydromech. Heat Transfer and Mass Transfer," Kiev State University Press.

Dumitrescu, D. and M. D. Cazacu (1970). "Theoretische und experimentelle Betrachtungen über die Strömung zäher Flüssigkeiten um eine Platte bei kleinen und mittleren Reynoldszahlen, " ZAMM vol. 50, pp 257-280.

Eppler, R. (1954). "Beiträge zur Theorie und Anwendung der unstetigen Strömungen," J. Rat. Mech. and Analysis 3/5. pp. 591-64.

Erdos, J. and A. Pallone (1962). "Shock-Boundary Layer Interaction and Flow Separation," Proc. 1962 Heat Trans. and Fluid Mech. Inst., Stanford Univ. Press.

Erdos, J. and V. Zakkay (1971). "Inviscid Solution of the Steady Hypersonic Near Wake by a Time-Dependent Method," AIAA J., vol. 9, No. 7.

Fedyayevskiy, K. K. Ginevskiy, A. S. and A. V. Kolesnikov (1973). Reschet turbulentnogo pogranichnogo cloya v neszhimayemoy zhidkosti Computation of the Turbulent Boundary Layer in an Incompressible Fluid , "Sudostroyeniye" Press, Leningrad,

Fromm, J. (1967). "Unsteady Flow of an Incompressible Viscous Fluid," Vychislitel'nyye metody v gidrodinamike (Computation Methods in Hydrodynamics) .

Gerrard, J. H. (1966). "The Three-Dimensional Structure of the Wake of a Circular Cylinder," J. Fluid Mech. 25/1.

Ginevskiy, A. S. (1969). Teoriya turbulentnykh struy i sledov, (Theory of Turbulent Streams and Wakes) , Mashinostroyeniye Press, Moscow.

Gogish, L. V. and G. Yu. Stepano (1966). "On Calculating Base Pressure in Two-Dimensional Supersonic Flows," Izvestiya AN SSSR MZhG. No. 3.

Gogish, L. V. (1968). "Approximate Calculation of Critical Pressures of Reattachment and Separation of a Turbulent Boundary Layer in a Supersonic Flow," AN SSSR MZhG 4.

Gogish, L. V. and G. Yu Stepanov (1968). "An Integral Method of Calculating Turbulent Separated Flows, in the book Doklad na III Vsesoyuznom S, Yezde po teoreticheskoy i prikladnoy mekhanike (Report on the III All-Union Congress on Theoretical and Applied Mechanics) , Nauka Press, Moscow.

Gogish, L. V. Soboleva, T. S. and G. Yu Stepanov (1969). "Interaction of a Turbulent Wake with an External Flow," AN SSSR MZhG 3.

Gogish, L. V. and G. Yu Stepanov (1971)."Quasi-One-Dimensional Theory of Turbulant Wake Interaction with Supersonic Flow in Channel and Jet," Nauchnye Trudy No. 11. Institute of Mechanics of Moscow State University, Moscow.

Glick, H. S (1964). "Perfected Theory of Crocco-Lees Mixing for Supersonic Flow with Separation and Attachment," Mekhanika 4.

Glotov, G. F., and E. F. Moroz (1970). "Study of Axisymmetric Flows with Sudden Expansion of Sonic Flow," Trudy TsAGI, 1281.

Goldstein, S. (1948). "On Laminar Boundary Layer Flow near a Position of Separation," Quart. J. Mech Appl Math. 1 p. 43.

Golotov, G. F. and G. N. Lavrukhin (1974). "Study of Separated Flow Behind an Axisymmetric Protuberance with Central Rod," Uchyenyye zapiski TsAGI 2.

Gorenbukh, P. I. and I. G. Kozlova (1973). "Experimental Study of Disturbance Propagations Upstream in the Strong Interaction Regime," Uchenyye Zapiski IsAGI, vol.4, No. 2.

Gorislavskiy, V. S. and Z. A. Stepchenkova (1971). "Experimental Study of Separated Zones on a Flat Plate in Hypersonic Gas Flow," Uchenyye Zapiski, TSAGI vol.2, No. 5.

Graham, D. K. and T. W. Binion, Jr. (1964). "Base Drag Measurements on an Ogive-Cylinder Model with Base Nozzle Flow," AEDC-TDR-64-87, Arnold Engineering Development Center.

Grange, J. M., Klineberg, J. M., and L. Lees (1967). "Laminar Boundary-Layer Separation and Near-Wake Flow for a Smooth Blunt Body at Supersonic and Hypersonic Speeds," AIAA J., vol. 5, No. 6, pp. 1089-96.

Grove A. S. Shair E. H. Petersen, E. E. and A. Acrivos (1964). "An Experimental Investigation of the Steady Separated Flow past a Circular Cylinder," J. Fluid Mech. 19/1.

Gurevich, M. I. (1961). Teoriya struy ideal'nov zhidkosti, (Theory of Streams of an Ideal Fluids), Fizmatgiz Press, Moscow.

Gushchin, V. A. and V. V. Shchennikow (1974a). "Solution of Problems of the Dynamics of an Incompressible Viscous Fluid by a Method of Splitting," ZhVM i MF 2.

Gushchin, V. A. and V. V. Shchennikov (1974b). "One Numerical Method of Solution of the Navier-Stokes Equations," ZhVM i MF 2.

Hakkinen, R. J. Greber, I. Trilling, L. and S. S. Abarband (1959). "The Interaction of an Oblique Shock Wave with a Laminar Boundary Layer," NASA Memo 2-18-59w.

Hama, F. R. (1966). "Experimental Investigations of Wedge Base Pressure and Lip Shock," TN 32-1033 Jet Propulsion Lab. Calif. Inst. Tech.

Hayes, W. D. and R. F. Probstein (1959). "Viscous Hypersonic Similitude," Inst. Aero. Sci. Rept. 59-63.

Hayes, W. D. and R. F. Probstein (1959). Hypersonic Flow Theory, Academic Press.

Hill W. G. Jr. (1966). "Initial Development of Compressible Turbulent Free Shear Layers," Ph.D. Thesis. Rutgers, The State University.

Il'ichev, K. P. and Postolovskiy (1972). "Calculation of Unsteady Separated Inviscid Fluid Flow around Blunt-Based Bodies," Izvestiya An SSSR MZhG. No. 2.

Ilizarova, L. I. (1969). "Structure of Fluid Behind a Bluff Body," Promyshlennaya aerodinamika 9.

Inger, G. R. (1972). "Theory of Supersonic Laminar Non-Adiabatic Boundary Layer Flow Past Small Rearward-Facing Steps Including Suction," AIAA J., vol. 12, No. 8, p. 1157. Also Rept. VPI-E-72-71, August, Virginia Polytechnic Inst. & State Univ., Blacksburg, Va.

Jenson, V. G. (1959). "Viscous Flow Around a Sphere at Low Reynolds Number," Proc. Roy. Soc. A., 249/1258.

Kalashnikov, V. N. and A. M. Kudin (1969). "Karman Vortices in Flows of Polymer Solutions Which decreases Friction Drag," AN SSSR MZhG 4.

Keller, H. B. and H. Takami (1960). "Numerical Studies of Steady Viscous Flow About Cylinder. Numerical Solutions of Nonlinear Differential Equations," New York.

Kessler, T. J. (1967). "Two-Stream Mixing with Finite Initial Boundary Layers," AIAA J., vol. 5, No. 2.

Khoroshko, K. S. (1969). "A Hypersonic Wake Behind Blunt Bodies," AN SSSR MZhG 2.

Khudenko, B. G. (1961). "The Use of a System of Potential Flow of an Ideal Fluid for Calculating a Flow of Air with a Zone of Reverse Flows," Izv. vuzov. Aviatgionnaya tekhnika 3.

Khudenko, B. G. (1968). "Calculation of a Turbulent Wake Behind a Blunt Body in a Subsonic Flow," AN SSSR MZhG 4.

Kirk, F. N. (1959). "An Approximate Theory of Base Pressure in Two-Dimensional Flow at Supersonic Speed," Royal Aircraft Establishment. TN Aero 2377.

Kirnasov, B. S. and O. T. Korzhuk (1969a). "Calculation of Parameters of Flow in the Base Region Behind Axisymmetric Bodies in Supersonic Flow," in Doklady na II Respublikanskoy ponferentsii po aerogidromekhanike, (Reports on the II Republic Conference on Aerodynamics) , KGU Publishers, Kiev.

Kirnasov, B. S. and O. T. Korzhuk (1969b). "Stokes Flow in the Base Region and in a Near Wake Behind a Flat Base Section," in Doklady na Respublikanskoy konferentsii po aerogidromekhanike, (Reports on the II Republic Conference on Aerodynamics) , KGU Publishers, Kiev.

Kirnasov, B. S. and V. V. Kudryavtsev (1970). "Flow past a Semi-Infinite Plate in a Channel with Subsonic Flow of Compressible Gas," AN SSSR MZhG 4.

Kline, S. J. (1959). "On the Nature of Stall," J. Basic Eng. Trans. ASME Ser. D. Sept.

Korst, H. H. (1956). "A Theory of Base Pressure in Transonic and Supersonic Flow," J. Appl. Mech. vol.23, No. 4.

Kozlova, I. G. and V. V. Mikhaylov (1970). "On Strong Viscous Interaction on Triangular and Yawed Wings," Izvestiya AN SSSR MZhG No. 6.

Kozlova, I. G. and V. V. Mikhaylov (1971)."On the Influence of Boundary Layer Disturbances on Hypersonic Flow with Viscous Interaction," Izrestiya, AN SSSR MZhG 4.

Krayko, A. N. and R. K. Tagirov (1970). "Construction of the Optimum Stern Section of a Flat Body with Supersonic Speed of Flow," AN SSSR MZhG 3.

Kutateladze, S. S. and A. I. Leont'yev (1962). Turbulentnyy pogranichnyy sloy szhimayemogo gaza. (Turbulent Boundary Layer of a Compressible Gas) , Publishing House of the Siberian Branch of the Soviet Academy of Sciences, Novosibirsk, 1962.

Kuznetsov, O. M. and S. G. Popov (1967). "Discrete Vortices in a Two-Dimensional Wake Behind a Cylinder," AN SSSR MZhG 2.

Kuznetsov, O. M. and S. G. Popov (1968). "Discrete Vortices in a Wake Behind Different Profiles in Subsonic and Supersonic Flow of a Gas," AN SSSR MZhG 5.

Lamb, T. P. and C. G. Hood (1968). "Integral Analysis of Turbulent Reattachment Applied to Plane Supersonic Base Flow," Trans. ASME. J. Eng. for Industry. p. 553.

Korst, H. H. Page, R. H. and M. E. Childs (1955). "A Theory of Base Pressure in Transonic and Supersonic Flow," Univ. Illinois, Exp. Station also ASME Paper 56-APM-30. 1956.

Korst, H. H. and W. L. Chow (1966). "Non-Isoenergetic. Turbulent ($Pr_t = 1$) Jet Mixing Between Two Compressible Streams of Constant Pressure," NASA-CR-419.

Lamb, J. P. and C. G. Hood (1972). "Theoretical Distribution of Heat Transfer Downstream of a Back step in Supersonic Turbulent Flow," Trans. ASME J. Heat Transfer Feb.

Lavrent'yev, M. A. (1962). Variatsionnyy method v krayevykh zadachakhdlya sistem uravneniy ellipticheskogo tipa, (Variation Method in in Boundary Problems for a System of Elliptical Type Equations), AN SSSR Publishers, Moscow.

Lax, P. and B. Wendroff (1960). "Systems of Conservation Laws," Communications in Pure and Applied Mathematics, vol. 13.

Lees, L. and B. L. Reeves (1964). "Supersonic Separated and Reattaching Laminar Flows: I. General Theory and Application to Adiabatic Boundary Layer Shock Wave Interactions," AIAA J., vol. 2, No. 11.

Lighthill, M. J. (1953a). "On Boundary Layers and Upstream Influence. I. A Comparison Between Subsonic and Supersonic Flows," Proc. Roy. Soc. Ser. A. Vol. 217, pp. 344-357.

Lighthill, M. J. (1953b). "On Boundary Layers and Upstream Influence. II. Supersonic Flows Without Separation," Proc. Roy. Soc. Ser. A. Vol. 217, pp. 478-507.

Loitsianskiy, L. G. (1965). "The Universal Equations and Parametric Approximations in the Theory of Laminar Boundary Layer," PMM vol. 29, No. 1.

Lunev, V. V. (1967). "A Method of Mean Mass for a Boundary Layer in an External Flow with Transverse Irregularity," AN SSSR MZhG 1.

Lunve, V. V. (1956). "On Similarity in Viscous Gas Flow Around Slender Bodies at High Hypersonic Speeds," PMM vol. 23, No. 1.

Main, U and D. Maull (1971). "Bluff Bodies and Vortex Shedding - A Report in Euromeh. 17," J. Fluid Mech. Vol. 45, p. 209.

Matveyeva, N. S. and V. Ya. Neyland (1967). "Laminar Boundary Layer near Corner of a Body," Izvestiya AN SSSR, MZhG No. 4.

McCarthy, J. F. Jr. (1962). "Hypersonic Wakes," California Inst. Tech. Grad. Aero. Lab., CALCIT Hypersonic Research Proj. Memo 67.

McDonald, H. (1965). "An Analysis of the Turbulent Base Pressure Problem in Supersonic Axisymmetric Flow," Aero. Quarterly, XVI/2.

McDonald, H. (1966). "The Turbulent Supersonic Base Pressure Problem: A Comparison Between a Theory and Some Experimental Evidence," Aero. Quart., XVII/2.

McErlean, D. and Ch. Przirembel (1970). "The Turbulent Near Wake of an Axisymmetric Body at Subsonic Speeds," AIAA Paper, 70-797.

Mimura, S. (1958). "Phenomenological Free Streamline Theory, Proc. Phys. Soc. 13/11 Japan.

Minyatov, A. Y. (1961). "Calculation of Base Pressure in Supersonic Flow Around Body of Revolution," Izvestiya AN SSSR, OTN. No. 3.

Mueller, T. J. (1968). "Determination of Turbulent Base Pressure in Supersonic Axisymmetric Flow," J. Spacecraft & Rockets, vol. 5, No. 1.

Murzinov, I. N. (1970). "Determining Enthalpy in Stagnant Region of Flow," AN SSSR MZhG, 3.

Murzinov, I. N. and G. P. Skinkin (1976). "Turbulent Flow in Base Region and a Near Wake Taking into Account Eddying of the External Flow," AN SSSR, MZhG. 2.

Myshenkov, V. I. (1970). "Subsonic and Transonic Viscous Gas Flow in Wake of a Flat Body," Izvestiya AN SSSR MZhG No. 2.

Myshenkov, V. I. (1972a). "Numerical Study of Viscous Gas Flows in Blunt-Based Body Wake," ZhVM i MF No. 3.

Myshenkov, V. I. (1972b). "Numerical Solution of the N-S Equations for Gas Flow around a Rectangle," Izvestia AN SSSR MZhG No, 4.

Nash J. F (1962). "The Effect of an Initial Boundary Layer on the Development of a Turbulent Free Shear Layer" Nat. Phys. Lab. Aero. Rept. 1019.

Nash, J. V. Quincey and J. Callinan (1963). "Experiments on Two-Dimensional Base Flow at Subsonic and Transonic Speeds," ARC M 3356.

Nash, J. (1964). "An Analysis of the Subsonic Flow past Symmetrical Blunt Trailing Edge Airfoil Sections at Zero Incidence in the Absence of a Vortex Street," ARC RM 3436.

Neyland, V. Ya (1963). "Hypersonic Viscous Gas Flow over a Flat Plate at Angle of Attack," Inzh. Zhurnal vol. 3, No. 3.

Neyland, V. Ya. (1964). "The Effect of Heat Transfer and Turbulent Flow in the Mixing Field on the Characteristics of Separated Zones," Inzhenernyy Zhurnal. 1.

Neyland, V. Ya. and L. A. Sokolov (1964). "Base Pressure Behind a Wedge at an Angle of Attack in a Supersonic Flow of Gas," Inzhenernyy Zhurnal 2.

Neyland, V. Ya. (1965). "On Calculating Separated Zone Characteristics and Base Pressure with Supersonic Gas Flow Around Bodies," Inzh. Zhurnal vol. 5, No. 1.

Neyland, V. Ya. (1966). "Solving the Equation of a Laminar Boundary Layer Under Arbitrary Conditions, PMM vol. 30, No. 4. pp. 674-78.

Neyland, V. Ya and V. V. Sychev (1966), "Asymptotic Solutions of Navier-Stokes Equations in Fields with Large Local Perturbations", AN SSSR MZhG 4.

Neyland, V. Ya. (1969a). "Supersonic Viscous Gas Flow Near Separation Point," Summaries of Reports of Fluid All-Union Conference on Theroretical and Applied Mechanics, Nauka Press, Moscow. 1968. On the Theory of Laminar Boundary Layer Separation in Supersonic Gas Flow. Izvestiga AN SSSR MZhG No. 4.

Neyland, V. Ya. (1969b). "On the Asymptotic Theory of Heat Flux Calculation near the Corner of a Body," Izvestiya AN SSSR MZhG No. 5.

Neyland, V. Ya. and V. V. Sychev (1970). "Theory of Flows in Steady Separated Zones," Vchyenyye zapiski, TsAGI 1.

Neyland, V. Ya. (1970a). "Asymptotic Theory of Two-Dimensional Steady Supersonic Flows with Separated Zones," AN SSSR MZhG 3.

Neyland, V. Ya. (1970b). "Propagation of Disturbances Upstream in Hypersonic Flow Interaction with a Boundary Layer," Izvestiya AN SSSR MZhG No. 4.

Neyland, V. Ya. (1971a). "Flow Downstream of Boundary Layer Separation point in Supersonic Flow," Izvestiya AN SSSR MZhG No. 3.

Neyland, V. Ya. (1971b). "Over the Asymptotic Theory of Supersonic Flow Interaction with a Boundary Layer," Izvestiya AN SSSR MZhG No. 4.

Neyland, V. Ya. (1974). "Asymptotic Problems of the Theory of Viscous Supersonic Flows," in Trudy TsAGI (Works of TsAGI), TsAGI 1529, Moscow.

Ohrenberger, J. (1968). "Viscous Effects Above the Wake Shock Wave in Laminar Near Wake," AIAA Paper 68-67, Los Angeles, Calif.

Olsson, G. B. and A. F. Messister (1969). "Hypersonic Laminar Boundary Layer Near Base of Slender Body," AIAA J. vol. 7, No. 7, p.1262.

Pavlov, B. M. (1968). "Numerical Solution of Problems of Supersonic Viscous Flow of a Gas Around Blunt Bodies," in Vychislitel'nyye metody i programmirovaniye, (Computation Methods and Programming), 11, MGU, Moscow.

Roshko, A. and J. Lau (1965). "Some Observations on Transition and Reattachment of a Free Shear Layer in Incompressible Flow," Proc. 1965, Heat Transfer and Fluid Mech. Institute, Stanford.

Roshko, A. and G. J. Thomke (1966). "Observations of Turbulent Reattachment Behind an Axisymmetric Downstream-Facing Step in Supersonic Flow," AIAA J., vol. 4, No. 6.

Rotta, I. K. (1967). Turbulentnyy pogranichnyy sloy v neszhimayemoy zhidkosti, (Turbulent Boundary Layer in an Incompressible Fluid), "Sudostroyeniye" Press, Leningrad,

Sananes, F. and L. Masbernat (1966). "Analytical Method of Determining the Shape of a Line of a Discharge Stream on a Step and Taking into Account Friction in the Mixing Zone," C. R. Acad. Sci. 9. AB 262.

Sekundov, A. N. and O. V. Yakovlevskiy (1970). "Experimental Study of Flow in a Wake Behind thin Plates," AN SSSR MZhG 6.

Shamroth, S. J. (1969). "On Integral Method for Predicting Shear Layer Behavior," J. Appl., vol. 36, pp. 673-81.

Shamroth, S. J. and H. McDonald (1972). "A New Solution of the Turbulent Near-Wake Recompression Problem," Aero. Quart., vol. 23, pp. 121-30.

Shvets, A. I. (1972). "Flow in the Base Region of Two-Dimensional Surfaces," AN SSSR MZhG 6.

Shvets, A. I. and I. T. Shvets (1976). "Gas Dynamics of Near Wake," Naukova Dumka Press, Kiev.

Sirieix, M. (1960). "Base Pressure and Process of Turbulent Mixing in Supersonic Plane Reattachment," La Recherche Aeronautique, 78.

Petukhov, I. V. (1964). "Numerical Computation of Two-Dimensional Flows in a Boundary Layer-Numerical Methods for Solving Differential and Integral Equations and Quadrature Formulas," 1zd. Nauka.

Potter, J. L., Whitfield, J. D. and W. T. Strike (1959). "Transition Measurements and the Correlation of Transition Sensitive Data," AEDC-TR-59-4, Arnold Engineering Development Center.

Prandtl, L. (1904). "Fluid Motion with Low Friction," III International Math. Kongr., Heidelberg.

Provotorov, V. P. (1973). "On Disturbance Propagation Through the Axis-symmetric Hypersonic Boundary Layer," Uchenyye Zapiski TsAGI vol.4, No. 1.

Reeves, B. L. and L. Lees (1965). "Theory of Laminar Near Wake of Blunt Bodies in Hypersonic Flow," AIAA J., vol. 3, No. 11.

Relf, E. and L. Simmons (1924). The Frequency of Eddies Generated by Motion of Circular Cylinder," ARC RM 917.

Tibner, H and B. Etkin (1958). "Noise Research in Canada," Proc Int. Congr. Aero. Sci. Madrid.

Tom, J., Seginer, A. Ariely, R. and M. Green (1972). "Heat Transfer in Separated Regions in Supersonic and Hypersonic Flows," ICAS Paper 72-14.

Roshko, A. (1955). "On the Wake and Drag of Bluff Bodies," J. Aero. Sci. Vol. 22, No. 2. pp. 124-132.

Roshko, A. (1961). "Experiments on Flow past a Circular Cylinder at Very High Reynolds Number," J. Fluid Mech. 10/3.

Sirieix, M., Mirande, J., and J. Delery (1966). "Fundamental Experiences on Turbulent Reattachment of a Supersonic Jet," AGARD Conf. Proc. 4.

Sirieix, M. (1967). "Formation and Development of a Wake," Revue francaise de Mechanique, 24.

Skurin, L. I. (1972). "Calculation of Two-Dimensional Wake Behind a Body," IFZh 1.

Son, J. and T. Hanratty (1969). "Numerical Solution for the Flow Around a Cylinder at Re 40, 200 and 500," J. Fluid Mech., 35/2.

Stepanov, G. Yu (1970). "Quasi-unidimensional Calculation of Separated Flows with Large Reynolds Numbers," Tezisy dokladov na nauchnoy konferentsii in-ta mekhanika MGU Thesis. Moscow.

Sterrett, J. R. and J. C. Emory (1960). "Extension of Boundary Layer Separation Criteria to a Mach Number of 6.5 by Utilizing Flat Plates and Forward Facing Steps," NASA TN D-618.

Stewartson, K. (1958). "On Motion of Sphere Along Axis of Rotating Fluid," Quart. J. Mech. Appl. Math. 11. p. 39.

Stewartson, K. and P. G. Williams (1969). "Self-Induced Separation," Proc. Roy. Soc. A., 312.

Stewartson, K. (1970). "On Supersonic Laminar Boundary Layers near Convex Corners, Proc. Roy. Soc. London A 319, pp. 289-305.

Sychev, V. V. (1967). "On Laminar Fluid Flow Behind a Blunt Body at High Reynolds Number," Report to the Symposium on Recent Problems in the Mechanics of Liquid and Gases at Tarda, Poland.

Sychev, V. V. (1972). "Laminar Separation," AN SSSR MZhG 3.

Sychev, V. V. (1974). "Boundary Layer Control to Prevent Its Separation," Uchyenyye zapiski, vol. 4.

Tagirov, R. K. (1961). "Determination of Base Temperature with Sudden Expansion of Sonic and Supersonic Flows," Izvestiya AN SSSR OTN No. 5.

Tagirov, R. K. (1963). "Calculation of Heat Fluxes for Two Different Supersoric Flows over a Back Step," Izvestiya AN SSSR OTN No. 6.

Tagirov, R. K. (1966). "The Effect of the Initial Boundary Layer on Base Pressure," AN SSSR MZhG, 2.

Tani, I. Iuchi, M. and H. Komoda (1961). "Experimental Investigation of Flow Separation Associated with a Step or Groove," Aero. Res. Inst. University of Tokyo, Rept. 204. 27/4.

Tanner, M. (1970). "Druckverteilungsmessungen and Keilen," Z. Flugwiss. 18/6.

Tanner, M. (1973). "Theoretical Prediction of Base Pressure for Steady Base Flow," Progress in Aerospace Sciences 14. Pergamon Press.

Tarnopol'skiy, M. D. and Ye. S. Golikov (1966). "The Question of Determining Base Pressure Behind a Protuberance with Separated Flow," IFZh. 6.

Taganov, G. I. (1968). "On the Theory of Stationary Separated Zones," Izvestiya AN SSSR MZhG No. 5.

Terrill, R. M. (1960). "Laminar Boundary Layer Flow near Separation with and without Suction," Phil, Trans. Roy. Soc. A 253. p.55.

Peterin, M. P. (1964). "The Turbulent Boundary Layer of a Free Stream of Compressible Gas in Wake and Counter Flows," Inzhenernyy Zhurnal 2.

Thomann, H. (1958). "Measurements of Heat Transfer and Recovery Temperature in Regions of Separated Flow at a Mach Number of 1.8," Rept. 82, Aero. Res. Inst. Sweden.

Uknanova, L. N.(1966). "Statistical Characteristics of a Two-Dimensional Turbulent Wake at a Short Distance from a Cylinder," Promyshlennaya aerodinamika 27.

Vaglio-Laurin, R. (1960). "Transonic Rotational Flow over a Convex Cone," J. Fluid Mech. vol.9, pp. 81-103.

Vagramenko, Ya A. and A. F. Puchkova (1973). "Determining Base Pressure with Discharge of an Axisymmetric Supersonic Stream in a Channel," AN SSSR MZHG 6.

Vasil'yev, D. N. (1971). PMTF 5.

Vereshchagina, L. I. (1963). "Base Pressure for Rotating Bodies in Supersonic Flow of Gas," Vestnik Leningradskogo Universiteta, Seriya Matematika, Mekhanika i Astronomiya, 2/13.

Viviand, H. and S. A. Berger (1966). "Base-Flow and Near-Wake Problem at Very Low Reynolds Numbers" J. Fluid. Mech. vol. 23, pt. 3.

Vulis, L. A. (1957). "Motion in a Wake Behind a Blunt Body," Uchyenyye Zapishi Kazakhskogo Universitatea Seriya fiz-mat. 24/4.

Webb, W. H. (1968). "An Approximate Pressure-Angle Relation for Axisymmetric Supersonic Near Wake," AIAA J. vol.6, No.7.

Weinbaum, S. (1966). "Rapid Expansion of a Supersonic Boundary Layer and Its Application to the Near Wake," AIAA J., vol. 4, No. 2.

Weiss, R. F. and S. Weinbaum (1965). "Hypersonic Boundary Layer Separation and the Base Flow Problems," BSD-TR-65-305, Res. Rept., 221, (1965), also AIAA J., vol. 4, No.8, (1966).

Weiss, R. F. and S. Weinbaum (1966). "Hypersonic Boundary Layer and Base Flow Problems," AIAA J., vol. 4, No. 8.

Weiss, R. F. (1967). "A New Theoretical Solution for a Laminar Hypersonic Near Wake," AIAA J., vol. 5, No. 15.

Yudelovich, M. Ya (1965). "Approximate Technique for Calculating Base Pressure for Spherical Bodies," Izvestiya AN SSSR OTN No. 3.

Yel'kin, Yu. G, Nevland, V. Ya. and L. A. Sokolov (1963). "On the Characteristics of Laminar Zones of Separation," Inzhernernyy Zhurnal, 5.

Yurchenok, K. Ye (1968). "Selection of a Hypothesis of Turbulence in the Theory of Base Pressure," AN SSSR MZhG 6.

Zavadskiy, A. Yu and G. I. Taganov (1968). "Calculation of Flow with Non-Symmetric Flow Past an Ellipsoid with Leading Separated Zone of Supersonic Flow," AN SSSR MZhG, 6.

Zuntsov, A. V. (1971). "Influence of Single Roughness on Fluid in the Boundary Layer," Uchenyye Zapiski TsAGI, vol.2, No. 1.

Zumwalt, G. W. (1959). "Analytical and Experimental Study of the Axially Symmetric Supersonic Base Pressure Problem," Ph.D. Dissertation, Dept. Mech. Eng., Univ. Illinois.

CHAPTER II

SYMBOLS

A	Coefficient of calibration
C_{fo}	skin friction coefficient (Squire and Young)
Co	Concentration of active ions
D	diffusion coefficient
d_o	diameter of circular tube
d_p	diameter of probe
F	Faraday number
$f = (\theta/u_e)(du_e/d_x)$	
I	probe current
ℓ_1	length of mixing zone
ℓ_2	total length of cavity wall
u'	fluction of u
u_o	flow velocity at channel axis at 10mm upstream of cavity
v'	fluctuation of v
v*	wall shear velocity
w'	fluctuation of w
$\overline{x} = x/H$	
$y+ = \frac{v^* y}{\nu}$	
$f' = (C_f/C_{fo}) \cdot Re_\theta$	

CHAPTER II

Incompressible Flow Separation

In Chapter I, various analysis for flow separation have been presented. Therefore, in this Chapter II, certain aspects of a separated flow model, experimental investigation of incompressible turbulent flow, affected by adverse pressure gradient involving flow separation, a three-dimensional effect on the separated flow, and the cylinder separated flow phenomena are presented. Although the main content is for subsonic flow, pertinent supersonic phenomena are described for a comparative purpose.

The two-dimensional and axisymmetric boundary layer flow separate if the streamwise adverse pressure gradient is sufficiently large due to the reduction of momentum, especially in the vicinity of a wall surface.

The recent investigations in the USSR on turbulent flow affected by adverse pressure gradient described here may serve for the understanding of flow separation.

1. Effect of Adverse Pressure Gradient on Incompressible Turbulent Flow Involving Separation

1.1 Local Velocity Components and their Fluctuations in the Vicinity of a Wall

Yefimenko and Khafakhpasheva (1976), measured components of local velocity and their fluctuations along the close vicinity of a diffuser wall in order to evaluate effectively the wall turbulence structure up to onset of flow separation. Because, presently most experimental studies were made at a considerable distance from the wall and under conditions

of unlikely flow separation, this investigation is desired to solve the turbulent flow separation problem.

Since the general characteristics of fluid motion is affected by the asymmetry of diffuser shapes used by various investigators, Yefimenko and Khafakhpasheva (1976), instead selected the flat symmetrical diffuser, on whose wall skin friction dropped significantly along the streamwise direction.

The diffuser total divergence angle was 8°, inlet cross section 40 x 100mm, fore section 400mm, and the test Reynolds number at the inlet 5.3×10^{4}. Tests were made at four cross sections 1, 2, 3 and 4, located from the inlet at x = 164mm, 219mm, 274mm and 329mm respectively.

The turbulence characteristics were determined by stroboscope flow visualization and by computer processing of the photographic materials. The electrodiffusion method for the measurement of skin friction applied by Kutateladze, Kashinskiy and Mukhin (1976) uses as the working fluid a solution of sodium hydroxide and potassium ferri - and ferrocyanide in distilled water. This solution is also used for flow visualization because gas bubbles are produced electrolytically due to the chemical reaction of the working fluid with aluminum particles.

The electrodes consisted of platinum wire of 20 μ diameter drawn over the surface of a glass plug inserted into the diffuser wall. The light beam from the Helios-40 IFK-120 electronic stroboscope passed through the plug and illuminated a narrow flow region and the photographs were taken through the parallel walls of the working section. The total

number of instantaneous velocity values amount $(2\text{-}3).10^3$ in the range of $0 < y^+ = \frac{v^* \cdot y}{\nu} < 300$ where v* is wall shear velocity defined by $(\tau_w/\rho_e)^{\frac{1}{2}}$. These instantaneous values are used for computer processing to evaluate flow pattern as a function of time, to analyze the back flow near the wall and to estimate the dimension of separated flow. The magnitude of the wall shear velocity v* was derived from the measured data of Mutateladze, Kashinskiy and Mukhin (1976) using electrodiffusion method.

1.1.1 Results of Measurements

The analysis of the instantaneous flow pattern by visualization and the computer indicates that the upstream of sections 1(x=164mm), and 2(x=219mm), no region of reverse flow existed, but as shown in Fig,II.1, at sections 3(x=274mm), and 4(x=329mm), instantaneous local flow separations in 5% and 8% of the frame, respectively, were observed, though the shape of the averaged velocity profile is still not that of the separation profile. Futhermore, from Figure II.1, it is seen that the values of the transverse velocity components are of the same order of magnitudes as the streamwise velocity components. The separation zones were a few milimeters in diameter. The measured average streamwise velocities at various y^+ are lower than those computed in the viscous sublayer (line I) and in channel or boundary layer (line II) as indicated in Figure II.2.

One example measured transverse velocity v is shown in Figure.II.3. Its absolute value decreases downstream, but the ratio of v/u_o increases downstream and away from the wall. Nevertheless, contribution of v(du/dy)

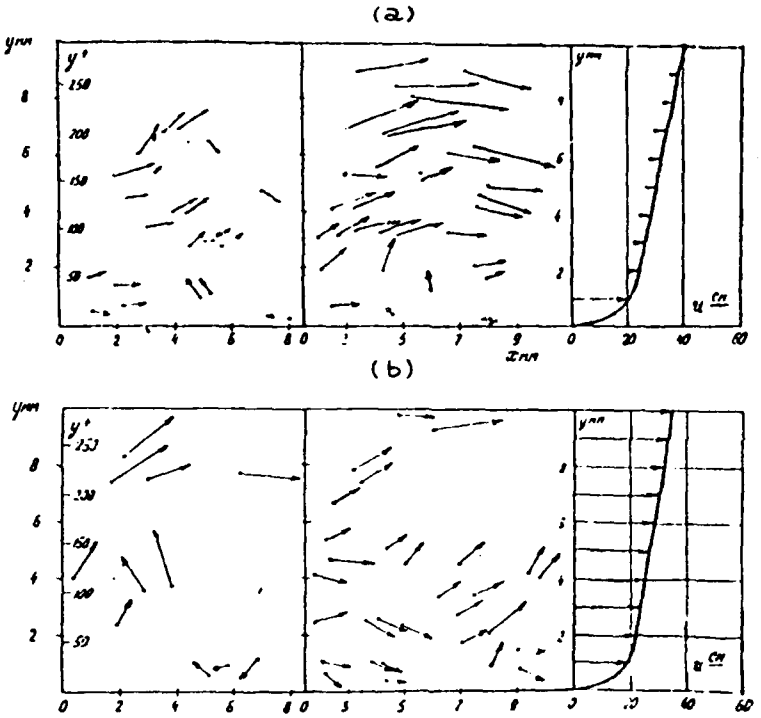

Fig.II.1. Instantaneous flow patterns. (a) x = 0.274 m; (b) x = 0.329 m.
[Refimenko and Khabakhpasheva (1976)]

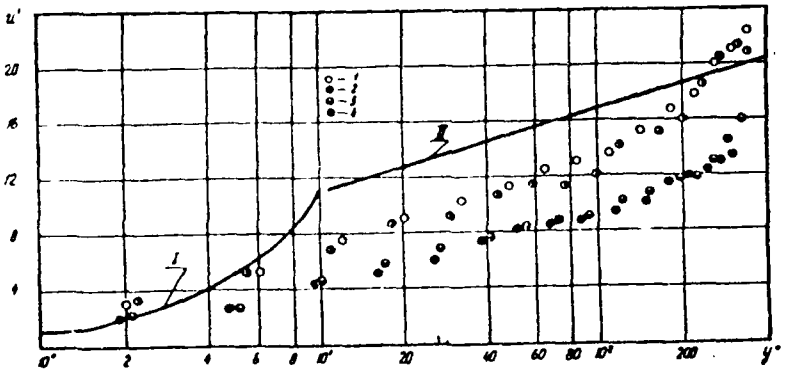

Fig.II.2. Velocity profile in dimensionless coordinates.
I : $u^+ - (u_o \cdot \nu/2v_*^3) \cdot (du_o/dx)y^{+2}$;
II : $u^+ + 5.5 + 5.8 \ln y^+$.
[Yefimenko and Khabakhpasheva (1976)]

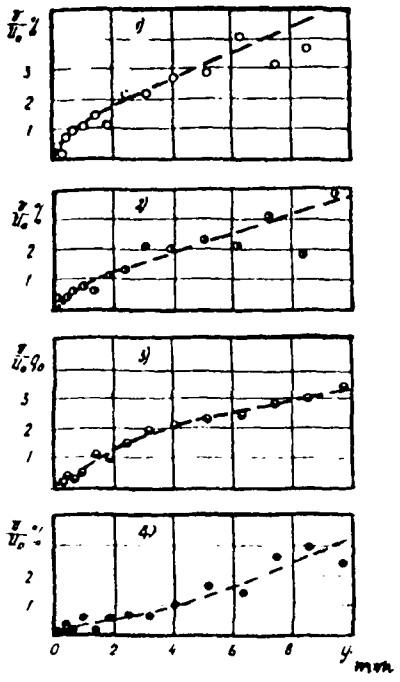

Fig. II.3. Transverse velocity components v/u. [Yefimenko and Khabakhpasheva (1976)] 1,2,3,4, correspond to locations of x = 0.164, 0.219, 0.274, 0.329 m.

to the momentum balance in the wall region may be significant because the streamwise velocity gradient is large.

The three dimensionality of flow was not measured but its existence can be indicated because the measured values of v are larger than those computed by the two dimensional continuity equation.

The measured fluctuating streamwise and transverse velocity $\sqrt{\overline{u'^2}}$ and $\sqrt{\overline{v'^2}}$ normalized by the velocity at the diffuser center line u_o are

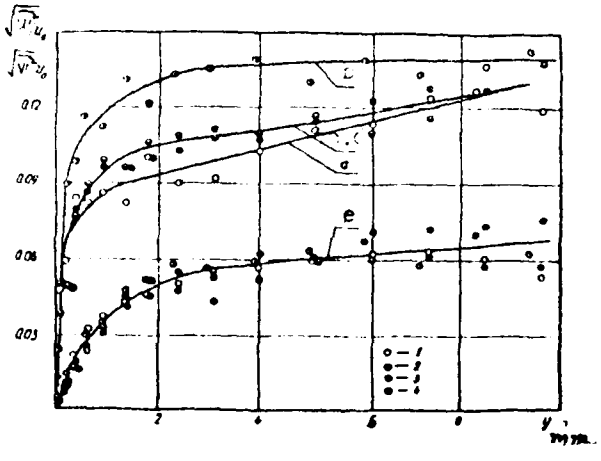

Fig.II.4. Velocity fluctuations. a,b,c,d - $\sqrt{\overline{u'^2}}/u_o$; e - $\sqrt{\overline{v'^2}}/u_o$ [Yefimenko and Khabakhpasheva (1976)] 1,2,3,4, correspond to locations of x = 0.164, 0.219, 0.274, 0.329 m.

shown in Figure II.4. The figure also indicates that the magnitudes of the transverse velocity fluctuation is smaller than that of the streamwise fluctuation.

If the ratio of the streamwise root-mean velocity fluctuation $\sqrt{\overline{u'^2}}$ is plotted with respect to the average local streamwise velocity u as seen in Figure II.5, then this ratio increases downstream and closer to wall.

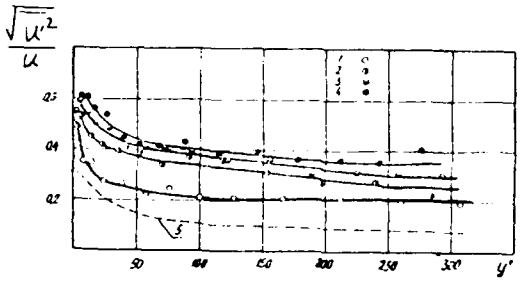

Fig.II.5. The ratio $\sqrt{\overline{u'^2}}/u$. 1,2,3,4, corresponds of location of x = 0.164, 0.219, 0.274, and 0.329 m. ; 5 - plane - parallel channel [Kutateladze et al (1975)]

The normalized streamwise and the transverse velocity fluctuations $\sqrt{\overline{u'^2}}$ / v* and $\sqrt{\overline{v'^2}}$ / v* of diffuser flow and plane parallel channel flow with respect to the wall shear velocity are shown in Figure II.6. Throughout the investigated flow region up to y^+ = 300 - 400 the velocity fluctuations increase with the increase of y^+ and the streamwise velocity fluctuation is larger at small y^+ than the maximum value of the plane parallel flow.

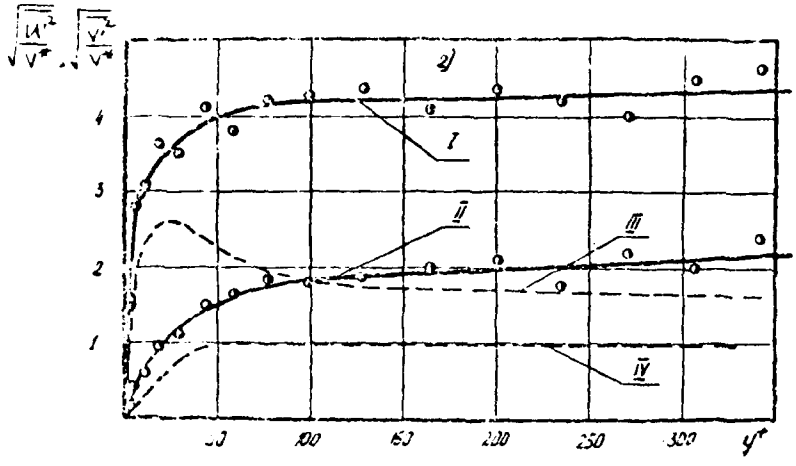

Fig.II.6. Longitudinal (I) and transverse (II) velocity fluctuations. 1,2,3,4, corresponds to locations of x = 0.164, 0.219, 0.274, and 0.329 m. (III),(IV) - plane - parallel channel [Kutateladze et al (1975)]

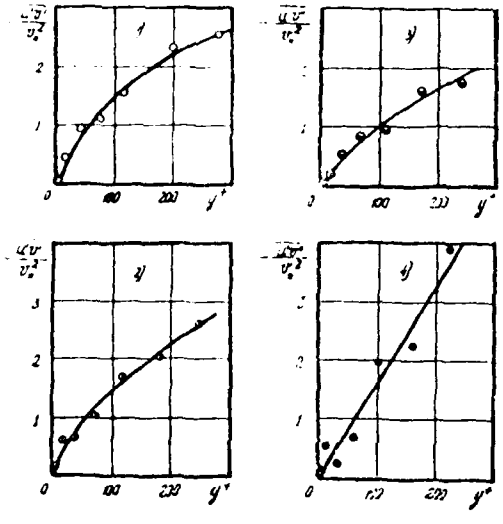

Fig.II.7. Turbulent stresses $\frac{\overline{u'v'}}{v_*^2}$. [Yefimenko and Khabakhpasheva (1976)]

1,2,3,4, correspond to locations of x = 0.164, 0.219, 0.274, 0.329 m.

The behavior of the Reynolds stress is presented by $\overline{u'v'}$ in a function of y^+ in Figure II.7. Although in general, $\overline{u'v'}$ reaches a sharp peak with a long trail, $\overline{u'v'}$ did not reach the maximum under test conditions.

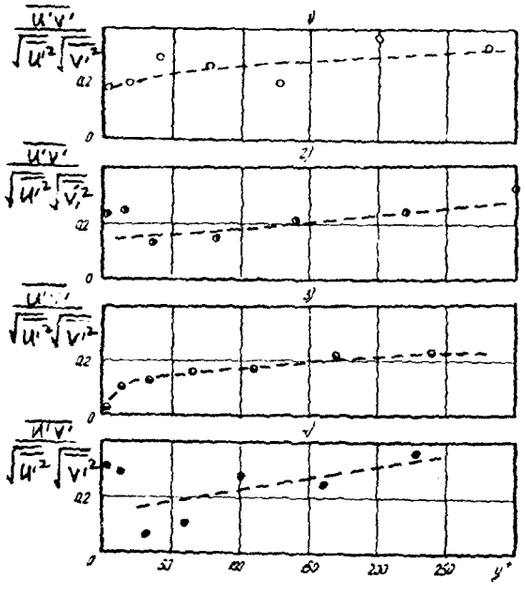

Fig.II.8. Correlation coefficients $\frac{\overline{u'v'}}{\sqrt{\overline{u'^2}}\sqrt{\overline{v'^2}}}$ [Yefimenko and Khabakhpasheva(1976)] 1,2,3,4, correspond to locations of x = 0.164, 0.219, 0.274, 0.329 m.

As indicated in Figure II.8, for diffuser flow, $\overline{u'v'}/\sqrt{\overline{u'^2}}\sqrt{\overline{v'^2}}$ is considerably reduced amounting $\sim$ 0.2 compared to $\sim$ 0.4 - 0.43 for circular pipe flow with dp/dx = 0 in the region of a well-developed turbulent flow.

The relation of $\overline{u'v'}$ with respect to kinetic flow energy along the diffuser center line, $\overline{u'v'}/\frac{1}{2}u_o^2$ in a function of y/δ is not monotonic

as shown in Figure II.9.

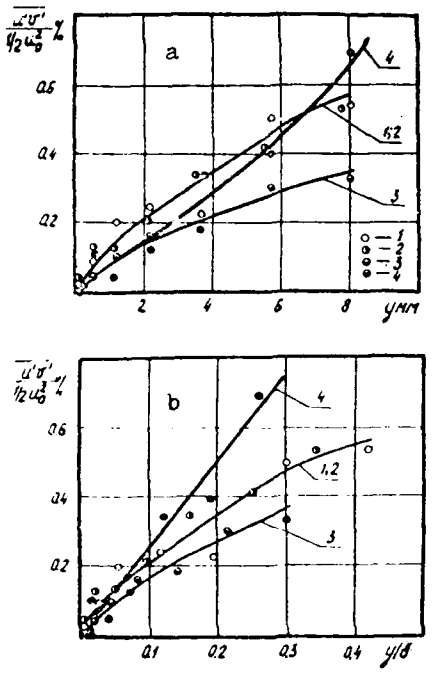

Fig.II.9. Turbulent stresses

$\frac{\overline{u'v'}}{1/2u_o^2}$. [Yefimenko and Khabakhpasheva (1976)]

1,2,3,4, correspond to locations of x = 0.164, 0.219, 0.274, 0.329 m.

In Figure II.9, it is seen that at section 3, the values of $\overline{u'v'}/\frac{1}{2}u_o^2$ are the lowest, while the highest at section 4 at large y, but at sections 1 and 2, almost equal values prevail, independent of the streamwise distance.

The boundary layer thickness used in Fig.II.9, is determined from the velocity profile measured by Kutateladze, Kashinskiy and Mukhin (1976).

1.2. Characteristics of Turbulent Boundary Layer Affected by Adverse Pressure Gradient Involving Separation

Kutateladze, Kashinskiy and Mukhin (1976), accurately measured by applying the electrodiffusion method, the mean and fluctuating components of wall shear stress and flow velocity in a wide range of adverse pressure gradients involving flow separation.

The survey of the present state of art by Kutateladze et. al. shows that: the skin friction computed from the velocity profile measured by Clauser (1954) is not applicable for a strong adverse pressure gradient and only Ludwieg-Tillmann's (1949) equation given by

$$C_f = 0.246 \cdot 10^{-0.678H} (Re_\theta)^{-0.268}$$

is involved with the directly measured skin friction. This equation does not satisfy the separation condition of $C_f = 0$ for $H = H_{cr}$, although this equation provides a very small value of C_f at $H > 3 - 4$. However, the extrapolation technique for $C_f \rightarrow 0$, is often used to determine the separation condition if this equation is selected for simplicity. Ludwieg and Tillmann (1949), installed the thermocouple flush with the wall but it is known that the low reliability of the thermoanemometer readings close to the wall does not yield an accurate determination of the intensity of velocity fluctuation in the viscous sublayer nor of the fluctuation intensity of the wall shear stress.
For the separated turbulent flow, the quantitative information is scare. Therefore, Sandborn and Liu's (1968) instrumental study of structure of the separation zone indicates that the presence of the back flow can be determined with a dual thermoanemometer probe. Khabakhpasheva's (1974)

stroboscope method of visualization showing the higher intensity of shear stress fluctuation on the diffuser wall than on the flat channel may provide more detailed information. The conventional methods which do not allow back flow introduce the indeterminate error.

Thus, in order to contribute to the solution of the essentially unsolved problem of the turbulent boundary layer with streamwise adverse pressure gradient involving separation, Kutateladze et.al. presented the electrodiffusion method, the measured data and their findings.

Electrondiffusion probes, made from platinum wire (50-100μ) or a strip embedded in a chemical glass cylinder of about 0.2m diameter, were inserted into a recess in the wall of the interchangeable working section of the closed flow loop. The working fluid consisted of a solution of 0.5N sodium hydroxide and 0.005N potassium ferri-and ferrocyamide in distilled water.

1.2.1 Measurements of Wall Shear Stress and Flow Velocity

The same technique was used for measurements of wall shear stress and flow velocity. The wall shear stress is related to the probe current by

$$\tau_o = (1.87\mu I^3)/(F^3 C_o^3 D^2 \ell^2 h^3) = AI^3$$

for a rectangular probe and

$$\tau_o = (3.16\mu I^3)/(F^3 C_o^3 D^2 d_o^5)$$

for a circular probe. The symbols mean:

τ_o - wall shear stress

μ - dynamic viscosity

I - probe current

F - Faraday number

C_o - concentration of active ions

D - diffusion coefficient

ℓ - longitudinal dimension of probe

h - transverse dimension of probe

A - coefficient to be determined by calibration

d_o - diameter of circular probe.

These equations are formulated by assuming that the velocity profile close to the wall is linear and the shear stress is steady.

Thus, for the linear velocity profile, if the properties of the electrolyte are known, then steady τ_o can be computed from these equations by measuring current value.

However, with a pressure gradient, it is necessary to take into account the effect of the quadratic term in the series-expansion of velocity near the wall, therefore velocity is computed by

$$u = \tau_o/\mu \cdot y + 1/2\mu\,(dp/dx)\cdot y^2$$

The merit of the electrodiffusion method is readily seen because the thickness of the diffusion layer is small and for the separation $\tau_o \to 0$, consideration of the second term is necessary. For the unsteady wall shear stress involving fluctuation, the following correction is needed.

$$\overline{\tau_o} = \overline{AI^3} \simeq A(\overline{I}^3 + 3\,\overline{I}\,\overline{I'^2})$$

where $\overline{I'^2}$ is mean square value of I fluctuation. The root-mean-square of wall shear stress was determined by

$$\sqrt{\overline{\tau_o'^2}}/\tau_o = 3\sqrt{\overline{I'^2}}/\overline{I}$$

Similarly, the mean velocity is evaluated by

AD-A099 165 CATHOLIC UNIV OF AMERICA WASHINGTON D C DEPT OF MECH--ETC F/G 20/4
RECENT DEVELOPMENT IN FLOW SEPARATION.(U)
MAY 80 P K CHANG AFOSR-78-3636
UNCLASSIFIED AFOSR-TR-81-0451 NL

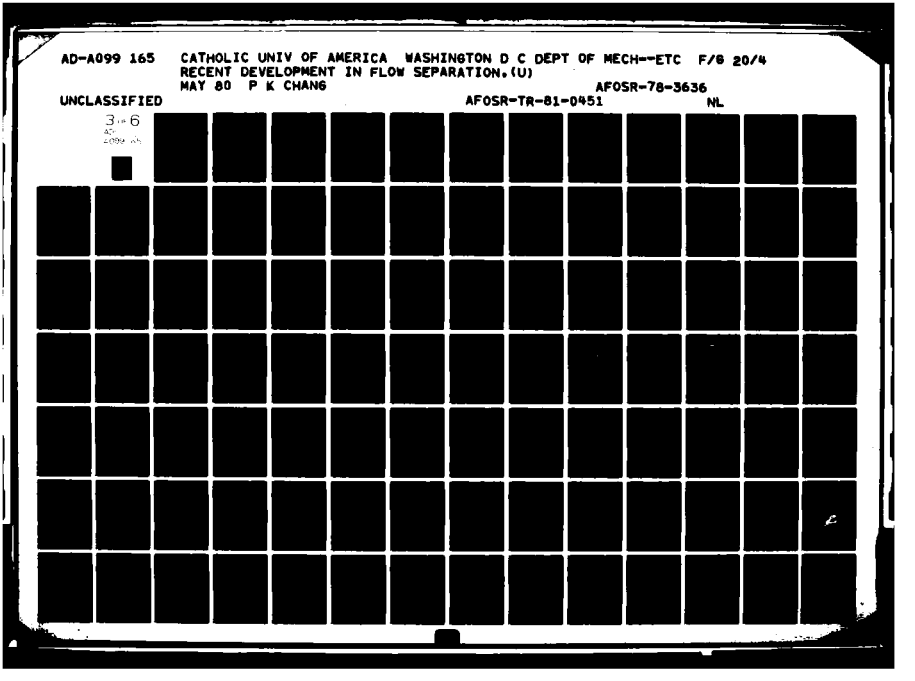

$$u = \tilde{u}\,(1 + \overline{I'^2}/\,I^2)$$

where u is the velocity for no fluctuation and the degree of flow turbulence is given by

$$\varepsilon = \sqrt{\overline{u'^2}}/\,\bar{u} = 2\sqrt{\overline{I'^2}}/\,\bar{I}$$

The electrodiffusion method for velocity measurement is analogous in many respects to constant-temperature hot wire anemometry.

Since the drift of probe characteristics is unavoidable due to contamination in the fluid, a sequence of calibration-measurement-calibration is needed and velocity measurement is calibrated by a laser-Doppler anemometer.

The relative error of mean-value measurement by the electro-diffusion method amounted to 5-7% for wall shear stress, 2.5-3% for local velocity and turbulence intensity and 10-15% for $\varepsilon = 0.5$.

1.2.2 Determination of Characteristics of Separated flow

In order to fix the flow direction, an attempt was made to detect the transitory stall by the modified electrodiffusion method by building a special electronic circuit. The oscillograms of the circuit output are then used to determine the streamwise of the reverse components of the wall shear stress in the transitory stall regime. A dual electro diffusion probe consisting of two closely adjacent rectangular probes is shown in Fig.II.10.

If the source voltage is applied to one probe only, then the probe will show the same current. However, if the voltage is applied to both probes, then the diffusion wake from the upstream probe will form a screen over the second probe which indicates a lower diffusion current.

Fig.II.10. Schematic diagram of dual electrochemical probe.
[Kutateladze et al (1976)]

But, if flow reverses, then the first probe will show a smaller current value. In order to process the probe signals, a special electronic circuit consisting of amplifiers, inverter, commutator, reference-frequency generator, electronic switch and frequency meter were built. The examples of oscillograms of the circuit output recorded with an N 105 oscillograph at scanning rate of 250 mm/sec. in the transitory stall regimes are shown in Figure II.11.

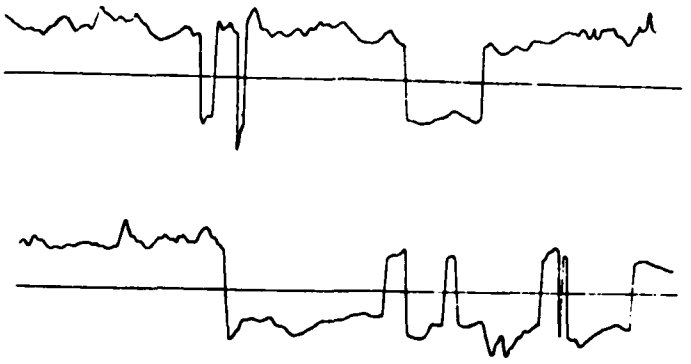

Fig.II.11. Oscillograms of output voltage of measuring circuit. [Kutateladze et al (1976)]

A positive signal polarity on the oscillogram corresponds to a forward direction close to the wall, while a negative polarity corresponds to the back flow. The moments of transition from the positive to the negative signal polarity correspond to the passage of shear stress through the zero point corresponding to the change of the sign, with large absolute value to the probe signal. This is due to the larger error of the wall shear stress measurement by the electro-diffusion method when the instantaneous value of τ_o approaches to zero because the diffusion current of the probe is determined essentially by the second term of the equation

$$u = \tau_o / \mu y + (1/2)\mu \frac{dp}{dx} y^2$$

involving instantaneous pressure gradient. The signal similar to Fig.II.11, can be used to approximate the positive and negative components of the wall shear stress in the transitory stall regime where the intensity of forward and back flows with a rapid transition from one flow direction to the other is high.

1.2.2.1 Results of Measurements

Kutateladze et. al. presented the following semi-empirical formulas:

$$\Psi = 1 + 177f$$

$$H = 1.3 - 177f$$

admitting that these equations do not correlate all the measured data on the various diffuser flows.

The function Ψ is defined by $\Psi = (C_f/C_{f_o}) \cdot Re_\theta$. The value of C_f is evaluated based upon the measured data of wall shear stress

τ_o and the velocity at the outer edge of shear layer u_e. The value of C_{f_o} is computed by using Squire and Young's (1938) equation:

$$C_{f_o} = 2/\left\{5.89 \log_{10}(4.075 \cdot Re_\theta)\right\}^2$$

The symbol f refers to the well-known boundary layer parameter

$$\frac{\theta}{u_e}\frac{du_e}{dx} = f$$

On the other hand, Kutateladze et. al. confirmed that the Ludwieg-Tillmann's equation correlates well with their experimental data. However, the skin friction coefficient evaluated by Clauser (1954) did not correlate well, especially for small values of ψ .

1.2.3 Some Fluctuation Characteristics of Boundary Layer in an Adverse Pressure Gradient

By taking account of fluctuation characteristics of the boundary layer for the adverse pressure gradient flow, the error of measurement can be assessed and the nature of channel flow may be better understood.

The measurement of the channel flow indicates that the streamwise velocity fluctuation u' reaches its maximum at a large distance from the wall. Furthermore, the intensity of the turbulence in the core increases in the flow direction, apparently due to the fluctuations of the instantaneous displacement thickness of the boundary layer at the wall and rate of turbulence increase in the core is dependent upon the degree of blockage of the channel cross-section. This increase of turbulence in the core is considered as a specific internal flow feature distinct from that of external flow. It may be noted that despite the increased turbulence in the core itself remains as a region of constant velocity.

In the transitory stall regime, the back flow coefficient γ_s, defined as the ratio of the life time of the back flow to the total time of measurement, amounted 2.5-15%.

The coventional probes with no correction of back flow responds only to the positive velocity component resulting with an error of the order of γ_s in a given cross-section. Thus, if the value of γ_s is unknown, the error of the measurement is indeterminate. Fig.II.12 shows an example of velocity profile.

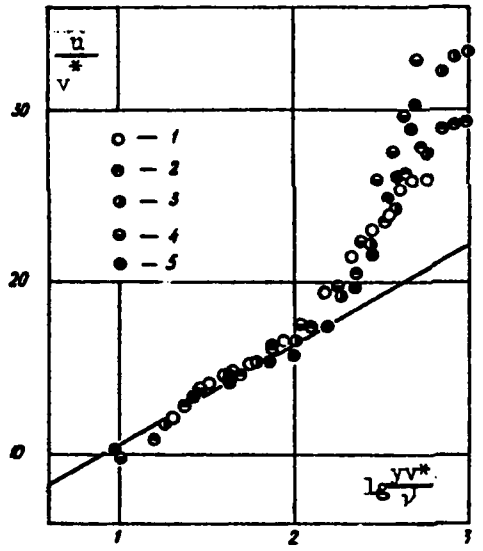

Fig.II.12. Velocity profiles in the boundary layer. Regime 203. 1-x = 0.164 m; 2-x = 0.219 m; 3-x = -.274 m; 4-x = 0.319 m; 5-x = 0.384 m. [Kutateladze et al (1976)]

For small values of $\ln(yv^*/\nu)$, velocity distribution is logarithmic but at its larger values the measured data are error in order of γ_s, thus should be smaller.

The measured data of H and f vary between 1.53-2.00 and $1.8\text{-}6.9\cdot10^{-3}$ respectively as γ_s varies between 0-14.2% indicating that in the internal flow, the back f[illegible] coefficient γ_s does not correlate the conventional aerodynamic parameters.

Kutateladze et.al., confirm the writer's opinion (Chang, 1970) that separation of the internal flow differs from that of the external flow. For the internal flow, as mentioned previously, turbulence increases in the core and the boundary layer thickness near the separation is thick comparable to the channel dimension affecting the stream line displacement by δ^* which in turn strongly increases turbulence in the core as well as characteristics of boundary layer in a given cross-section.

1.2.4 Effect of Three-Dimensionality of Flow

The effect of the three-dimensionality of the flow with an adverse pressure gradient to the flow characteristics, especially to the separated flow, has been assesed by the difference of the measured data by $\Psi_1(x)$ from that of, $\Psi_2(x)$ of the momentum equation. In non-dimensional form,

$$\Psi_1 = \frac{u_e^2\theta}{(u_e^2\theta)_o} - 1 + 1/2 \int_{x_o}^{x} \delta^*/\theta \cdot d\left(\frac{u_e^2}{u_{e_o}^2}\right)$$

$$\Psi_2 = \int_{x_o}^{x} \left(\frac{v^*}{u_e}\right) \cdot d\left(\frac{x}{\theta_o}\right)$$

where subscript o refers to some initial cross-section $x = x_o$.

If the pressure gradient is zero or favorable, then $\Psi_1(x) = \Psi_2(x)$ satisfying the momentum equation as reported at the Stanford Conference (1968), but for flow with adverse pressure gradient difference between $\Psi_1(x)$ and $\Psi_2(x)$ occurs which is attributed to the pressure of the three-dimensional flow.

This three-dimensional effect is evident in the separated flow since it is well-known that the separated flow is multi-dimensional. As shown in Fig.II.13, in the separated flow regime, a large discrepancy exists between the values of $\Psi_1(x)$ and $\Psi_2(x)$, confirming the existence of three-dimensional flow.

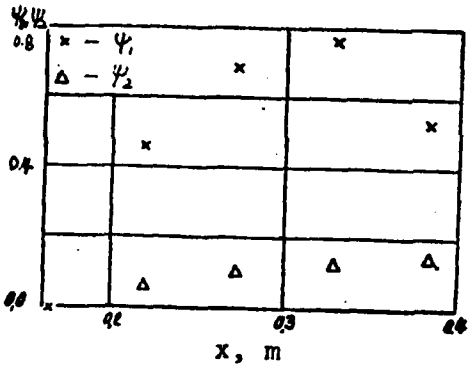

Fig.II.13. Test of relation [Mirskiy (1972)]. Regime 203.

Although, Head and Rechenberg (1962), by using a Preston tube for a pipe flow observed the very substantial and almost periodic variation in skin friction at right angles to the flow direction in the developing turbulent boundary layer, Kutateladze et.al, did not notice perio-

dicity in the wall velocity changes.

2. Cavity Flow

Cavity flow models have been surveyed by A. V. Gorin (1976) in his review paper entitled, "Survey of Models for Calculating the Flow of an Incompressible Fluid in a Square Cavity", Gradient and Separated Flows, (1976), ed. S. S. Kutateladze, Academy of Sciences of the USSR, Siberian Department, Institute of Thermophysics, Novosibirsk, citing mostly twenty nine non-Russian references and seventeen Russian ones, including the USSR experimental investigations. Therefore, only brief remarks on the Russian analytical works on cavity flow model are citied first and then the experimental investigations in the USSR on cavity flow are presented separately.

2.1 Cavity Flow Model

Kochin, Kibel and Roze (1963), attempted to solve the problem of cavity separated flow based on the inviscid flow theory.

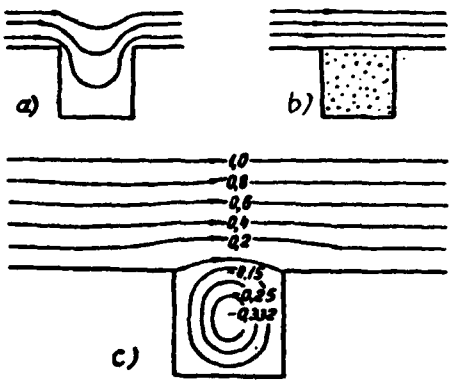

Fig.II.14. "Inviscid" models of flow in a cavity. [Gorin (1976)]

The potential streamlines entering the cavity, as sketched in Fig.II.14a, are considered and the problem is solved by confirmal mapping of the flow field. As an alternative way, based upon the concept of Kirchhoff, as shown in Fig.II.14b the flow field is divided into two; the forward flow field with undisturbed flow velocity u_∞ in the upper plane and a calm flow region in the cavity. These two flow models do not represent the real flow phenomena as experiments indicate, because the magnitude of velocity predicted by these models in the cavity are comparable to u_∞ , contrary to the lower value at the cavity floow (Fig.II.14a model) and equal to zero, (Fig.II.14b model). Furthermore, the analytical solution obtained by Kirchhoff's method is not unique, since for each pressure chosen in the separated flow region, there will be a different interface shape and a new point of separation of the free stream line from the surface.

Gol'dshtik (1962), modeled the cavity flow based on the concept of "composite" motion; the flow is potential outside the separation zone and in the separation zone vorticity is uniform, as indicated in Fig.II.14c. The stream lines evaluated by numerical computation, based on this model, are in a qualitative agreement with those observed by experiment. From the practical viewpoint, these three inviscid flow analysis do not yield, of course, the desired information on friction and heat transfer affected by viscosity.

Neyland and Sychev (1970), based upon the the asymptotic approach, generalized the analysis to be applicable for rotational flow closed by any stream lines. They also explained the physical meaning of the expre-

ssion:

$$\oint u^2 d\ell = \text{const.}$$

obtained by Batchelor (1956) for the two-dimensional recirculating flow within the circular region boundary by a wall, as the balance of shear forces at the fixed and mobile boundaries of the vortex. Thus, the effect of rotation of the vortex core can be neglected since these forces balance out.

Nakoryakov, Badatov and Slin'ko (1970), applied Korst's concept, to solve the problem of rectangular cavity flow. The velocity distribution in the mixing zone was obtained for two constant velocities u_{e_1} and u_{e_2}. The shear stress at the cavity wall, neglecting the corner eddies, and assuming laminar flow over a flat plate, was formulated by

$$\tau = 0.332\mu u_{e_1}^{3/2} (0.74 + 1.1\ \sqrt[3]{\ell_2/\ell_1})^{-3/2} (vx_2)^{-1/2}$$

Where ℓ_1 and ℓ_2 are the length of mixing zone and the total length of the cavity wall respectively and u_{e_1} is undisturbed external flow velocity.

2.2 Experimental Investigations of Cavity Flow

Experimental investigations are carried out for the velocity field, the wall shear stress, and the side wall effect of the cavity flow.

2.2.1 Velocity Field in Cavity

Bogatyrev, Dubnishchev, Mukhin, Nakoroyakov, Sobolev, Utkin and Shmoylov (1976), investigated velocity fields of laminar and turbulent flow in a square cavity by using laser-Doppler anemometry.

Measured data of velocity profiles are correlated in ordinary "jet" coordinates because it is considered that the jet flow prevails after the flow separation from the top edge of the upstream wall. The cavity flow pattern is thus considered as follows: When the jet from the top edge of the upstream wall strikes the downstream wall, a portion of the jet is directed to the bottom corner of the wall forming an eddy and turns from the bottom corner of the downstream wall. The flow then spreads along the floor surface of the cavity toward the upstream wall forming another eddy in the bottom corner of this wall. After flowing away from the floor surface, the jet mixes with the free stream in the mixing zone.

This jet flow model is simple compared to Charwat, et al's(1961b), an experimental mass exchange cavity model which involves three layers in the cavity; shear, buffer and reverse flow layers, and could breathe, i.e. the separating stream line pulsates. A large recompression vortex is observed at the corner of the downstream wall while there is a smaller one at the opposite corner of the upstream wall with the direction of rotation opposite to that of the recompression vortex. For this model, fluid flow is not considered as a jet.

It may be recalled that Kline (1959), observing four different incompressible diffuser flows with a successive increase of divergence angle of wall surface, unstalled flow, transient three-dimensional stall, steady two-dimensional flow and finally at largest divergence angle, tested the jet flow separation from the wall.

Chartwat et al (1961a,b) do not consider their sophisticated mass

exchange model sufficiently complete. Thus, it may be of interest to find out whether the simpler Bogatyrev et al's jet flow cavity model is useful to understand the complex cavity flow problem.

2.2.2 Wall Shear Stress in Cavities

V.Ya Bogatyrev and V. A. Mukhin, measured the mean incompressible turbulent shear stress and reported in the monograph "Gradient and Separated Flows" ed. S. S. Kutateladze, 1976.

Applying the electro-diffusion method, the mean incompressible turbulent shear stresses were measured in rectangular cavities over a range of a Reynolds number of $1.5 - 7.5 \times 10^4$, based upon the mean flow rate in the channel $\bar{W}$ and the channel diameter d, and for various cavity lengths but with its constant depth. The working fluid of the electrolyte was circulated in a closed return loop. The cavity was formed by the sudden axisymmetric expansion of the channel diameter from 31.5 mm to 169.5 mm followed by its equally sudden contraction to the original diameter. This type of cavity geometry ensured the elimination of sidewall effect. The depth of the cavity (H) was kept at a constant 69 mm but the cavity length (L) was varied in a range of L/H = 1.0, 0.7, and 0.5. By providing a sufficient length of the entrance length of 100 calibers it was possible to stabilize the upstream flow of the cavity.

As the sensing element for the measurement of mean shear stress, platinum wire of 0.5 mm diameter was mounted flush with the surface of the probe. The signal from the probe was relayed to a special d.c. amplifier (the EDP-1, electrodiffusion transducer) developed at the Ins-

titute of Thermal Physics of the Siberian Branch of the Soviet Academy of Sciences. In order to keep the physical properties of the working fluid constant, its temperature was maintained at $25 \pm 0.2^{\circ}C$.

The magnitude of shear stress was computed by

$$\tau_w = (3.16 \mu^3 \cdot I^3) / F^3 D^2 Co^3 dp \qquad (1)$$

where μ is dynamic viscosity, I probe current, F Faraday number, D diffusion coefficient, Co concentration of ferricyamide ions outside the diffusion boundary layer and dp the probe diameter. The accuracy of this evaluation was checked within an error of 10% with its value calculated by the Blasius formula.

The measured shear stress distributions on the cavity wall are shown in Fig.II.15, 16, and 17 for L/H = 1, 0.7 and 0.5 and in a parameter of $Re = \bar{W} d/\nu_0$.

Bogatyrev, Dubnishchev et al (1976), found that the shapes of shear stress distributions over the cavity walls correspond to the shapes of velocity distributions of boundary layer on the cavity walls.

As shown in Fig.II.15, 16 and 17, the behavior of shear stress distribution is similar to each other in the range of the Reynolds numbers of the test. The shear stress is maximum near the top edge of the downstream wall and diminishes rapidly toward the bottom of the cavity in a relation of $\tau_w \simeq x^{-\frac{1}{2}}$. This is caused by the wall jet flowing upward toward the mixing zone and striking the downstream wall of the cavity.

From these shear stress distributions the following cavity flow

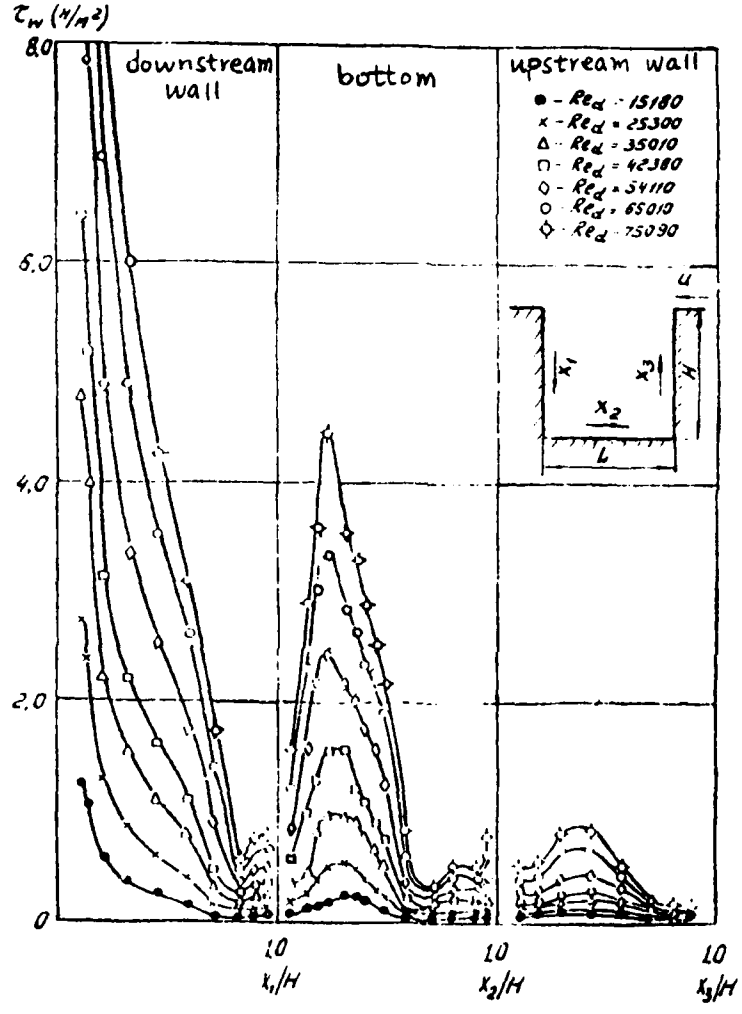

Fig.II.15 Distribution of shear stress along cavity walls (L/H = 1). [Bogatyrev and Mukhin (1976)]

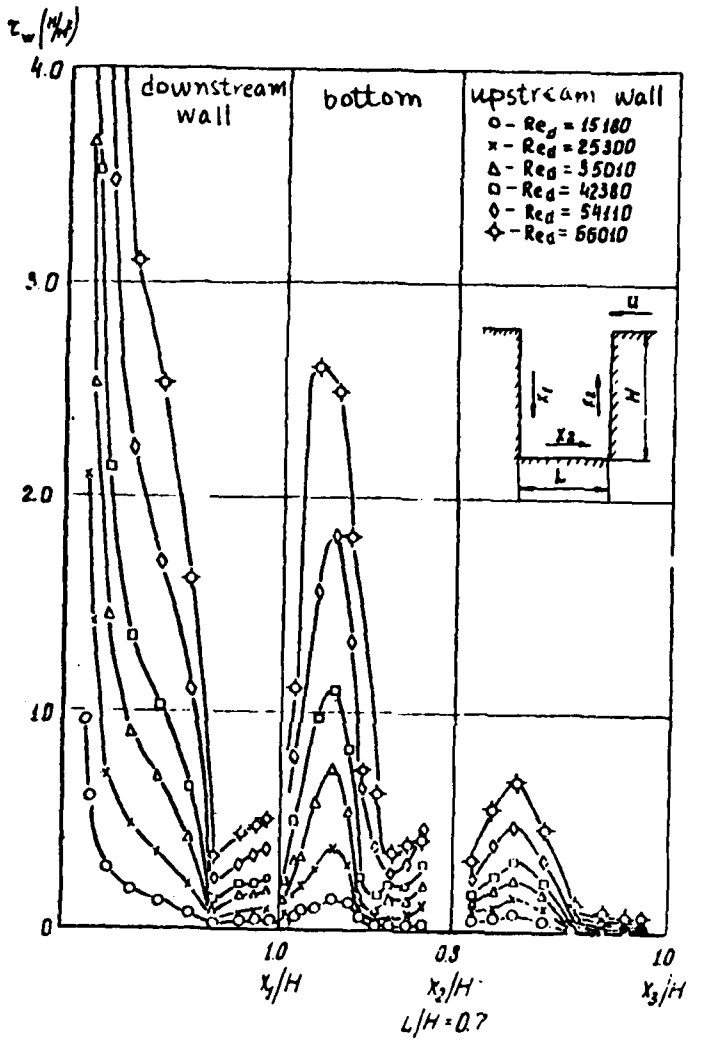

Fig.II.16. Distribution of shear stress along cavity walls (L/H = 0.7). [Bogatyrev and Mukhin (1976)]

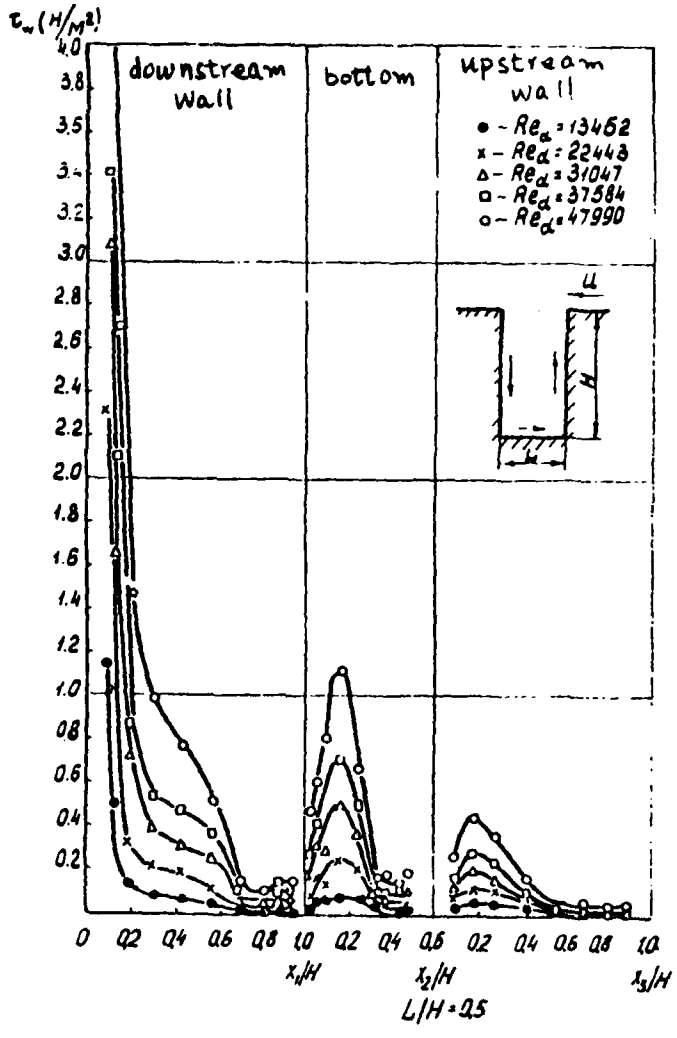

Fig.II.17. Distribution of shear stress along cavity walls (L/H = 0.5). [Bogatyrev anc Mukhin (1976)]

structure is conceived:

The wall jet is divided into two parts; the proper jet region and the wall flow boundary layer.

The boundary layer separation point is located at the position of the minimum shear stress (close to zero) i.e. at $\bar{x} = x/H = 0.8$ for $L/H = 1$, $\bar{x} = 0.7$ for $L/H = 0.7$ and 0.5. The growth of the shear stress after the separation is attributed to the secondary eddies with their rotational directions opposite to those of the primary eddies. Because the probe is insensitive to changes of the flow direction, the skin friction increase is recorded. On the bottom of the cavity, the skin friction is large, then decreases to a smaller value close to zero, followed by a decrease almost to zero at $\bar{x} = 0.6 - 0.7$, indicating that the stagnation zone exists there.

Although limited to *one geometry* of cavity, the measured shear stress data is presented by

$$C_f = 2\,\tau_w/\rho\bar{W}^2 = f(x)\cdot Re_L^{0.23}$$

where $Re_L = \bar{W}\,L/\nu$, as shown in Fig.II.18.

Thus, shear stress distribution may be generalized by the single curve of $C_f\,Re_L^{0.23}$ vs. x/H in a parameter of L/H, for all test Reynolds numbers as shown in Fig.II.19, 20 and 21. The data in these Fig.II.19, 20 and 21 measured by Oka (1969) correlate well with those of Bogatyrev and Mukhin (1976) for two cases of $L/H = 1.0$ and 0.7, but differ for $L/H = 0.5$.

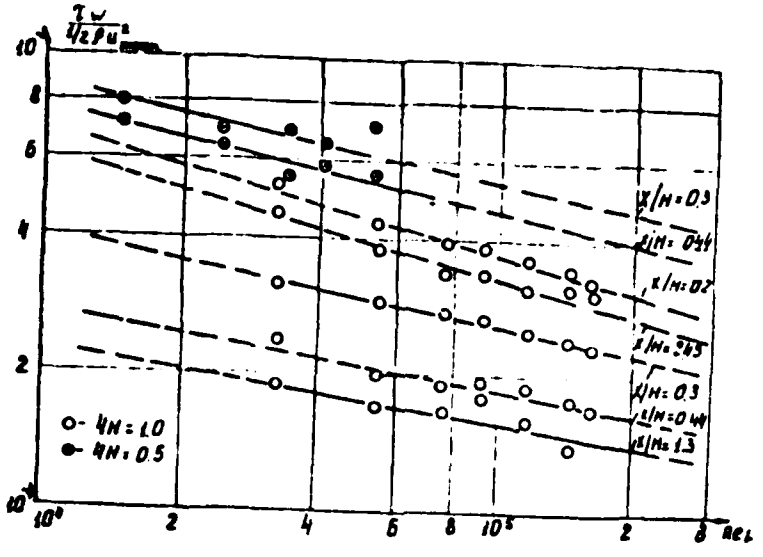

Fig.II.18. Graph of the function $C_f = f(Re_L)$.
[Bogatyrev and Mukhin (1976)]

For such a narrow and deep cavity, it is possible two vortices may be formed in the upper and lower layers in the cavity. Therefore, the discrepancy for L/H = 0.5 may be explained for the possible formation of two eddies, with a larger vorticity for the upper eddy than the lower eddy for the test of Oka (1969); while, for Bogatyrev and Mukhin's (1976) experiment-at-large Reynolds number only one vortex has been formed.

Badatov, Glin'ko and Nakoryakov (1970), compared the experimental data of the turbulent shear stress in a square axisymmetric cavity with those calculated by two-dimensional analysis, neglecting the corner eddies as shown in Fig.II.22.

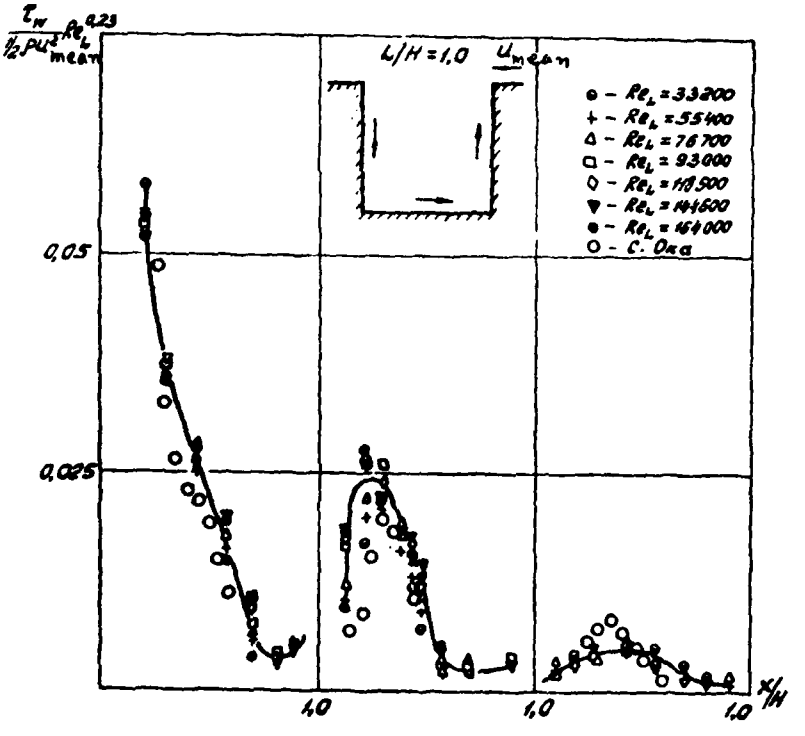

Fig.II.19. Change in generalized friction coefficient along the cavity walls for L/H = 1.
[Bogatyrev and Mukhin (1976)]

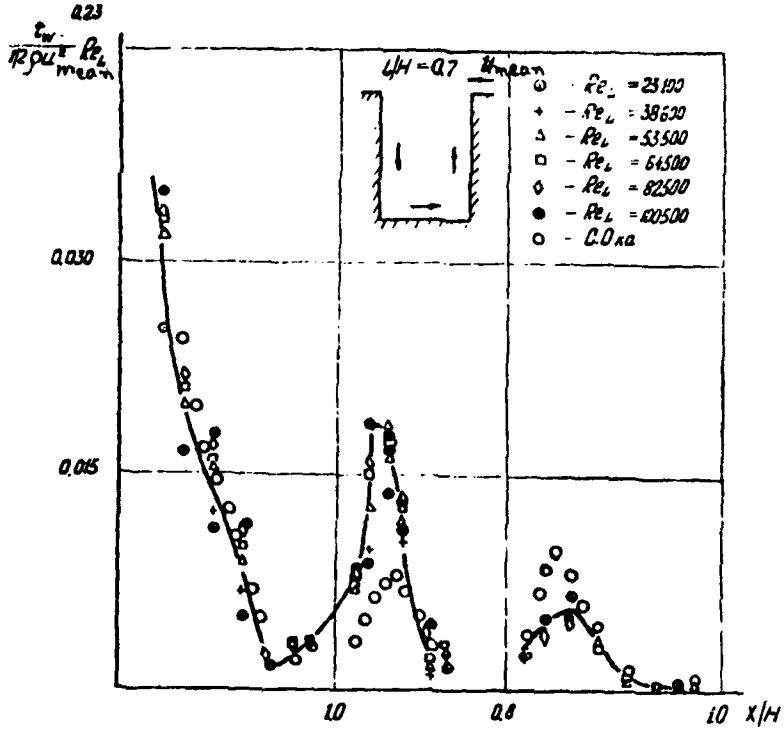

Fig.II.20. Change in generalized friction coefficient along the cavity walls for L/H = 0.7.
[Bogatyrev and Mukhin (1976)]

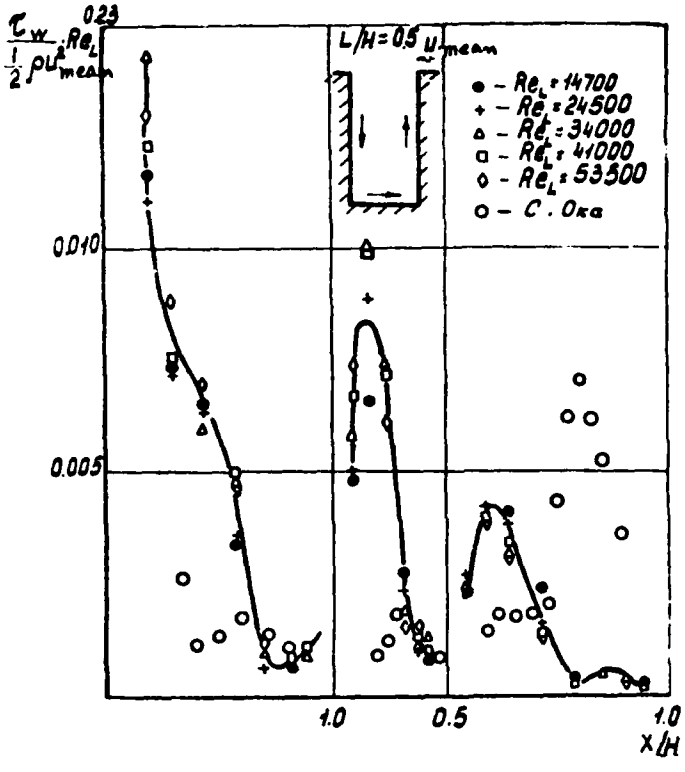

Fig.II.21. Change in generalized friction coefficient along cavity walls for L/H = 0.5.
[Bogatyrev and Mukhin (1976)]

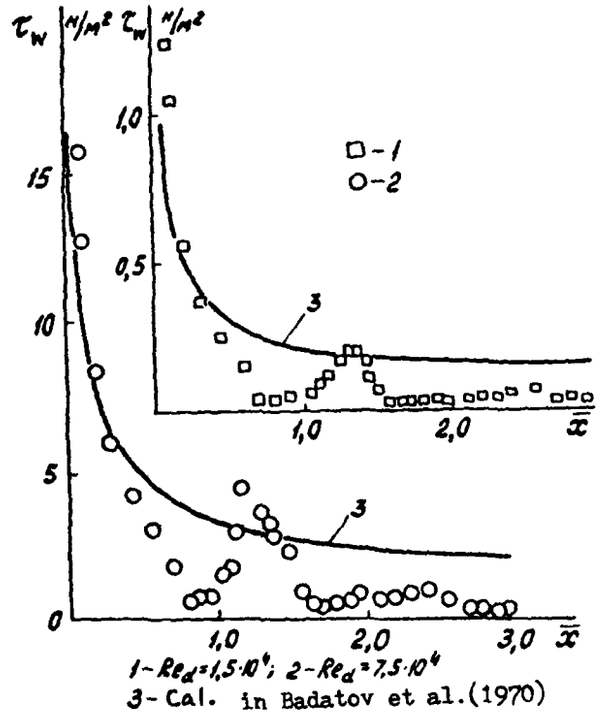

Fig.II.22. Comparison of experimental and calculated data. [Bogatyrev and Mukhin (1976)]

As seen in Fig.II.22, at the small value of $\bar{x}$, i.e. in the upper region of the downstream wall, where the wall jet effect is pronounced but the effect of axisymmetry is not apparent, the measured data is layer than those computed. But at large value of $\bar{x}$, where the effect of channel divergence is appreciable and the flow velocity of the experiment was lower than the plane cavity the measured data is smaller than the calculated values.

Although limited to the rectangular cavity geometry in a range of L/H = 1.0 - 0.5, Bogatyrev and Mukhin's (1976) experimental investigation for the mean turbulent shear stress on the cavity walls is valuable information.

However, in order to understand the complex cavity flow in general, it appears that a wider range of the investigations covering not only a deep but also a shallow cavity flow phenomena are needed, because as Charwat et. al. (1961a), found that a maximum (critical) ratio of L/H exists beyond which the cavity collapses leaving mutually independent separated flow regions at each protrusion.

Chapman et. al. (1957), measured pressure distributions on rectangular cavity walls in a range of L/H = 1.0 ~ 16, Charwat et.al. (1961a) in a range of 0 ~ 13, Tani et.al. (1961), 0.5 ~ 2.5. The shear flow velocity distributions within the cavity were measured by Chapman et.al. (1957), and Charwat et.al. (1961a) and streamwise fluctuating velocity components and Reynolds stresses within the cavity were measured by Tani et.al. (1961). Charwat et.al. (1961b), measured distributions of the drag coefficient, temperature, heat transfer coeffi-

cient and the boundary layer thickness of the cavity flow for a wide range of L/H.

2.2.3 Side-Wall Effects in Rectangular Cavities

The multidimensionality of the separated flow is assessed quantitatively by Bogatyrev and Gorin (1976), through the experimental investigation on the side-wall effects in the rectangular cavities and reported in the monograph "Gradient and Separated Flows" ed. S. S. Kutateladze, 1976.

Kalinin, Dreytser and Yarkho(1972), considered the eddy flow in a square cavity, is not two-dimensional and steady over the entire span of the cavity. Although cavity flow structure may be determined by the two-dimensional eddy cells, three-dimensional ejections of fluid were thought to be taken place in cross-section spaced at roughly equal intervals along the span of the cavity. Through the process of transfer of mass and energy between the eddy flow and main flow, with low and high momentum, it is conjectured that the mass is ejected periodically. On the other hand, experimental investigations of Maull and Easter(1963) Kistler and Tan (1967) Kalinin et.al. (1972), indicate that the three-dimensional flow in the cavity may be caused by the retarding action of the side walls and the sensitivity of internal two-dimensional flow to the disturbances in the mixing zone.

The velocity fields were measured by the laser-Doppler anemometer (LDA) developed at the Institute of Atomic Energy of the Siberian Branch of the Soviet Academy of Sciences.

Bogatyrev and Gorin (1976), measured laminar and turbulent velocity profiles for Re = $u_0 2H/\nu$ = 1500 and 15,000, respectively, (u_0 is flow velocity at the channel axis located 10 mm upstream of the cavity and H = 10 mm is the channel height) in two central sections and at three spans B = 40, 60 and 100 mm of L = H = 40 mm cavity as shown in Fig.II.23 and II.24.

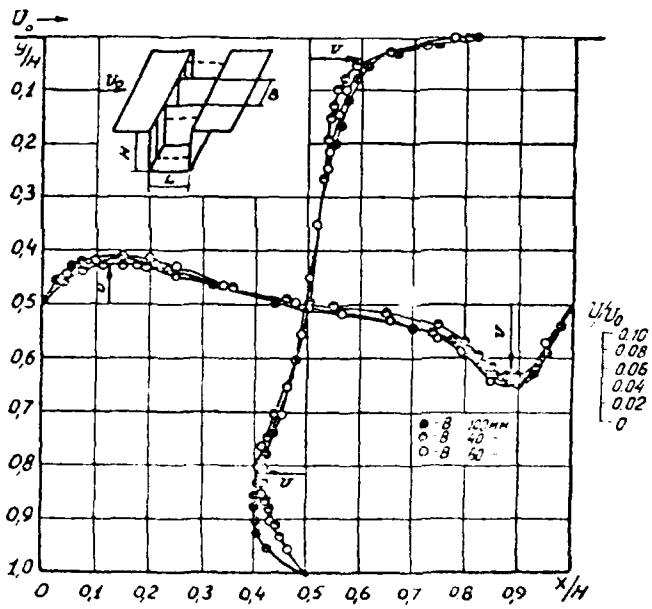

Fig.II.23. Velocity profiles in two central cross-sections of a square cavity for laminar flow regime (Re = $1.5 \cdot 10^3$).
[Bogatyrev and Gorin (1976)]

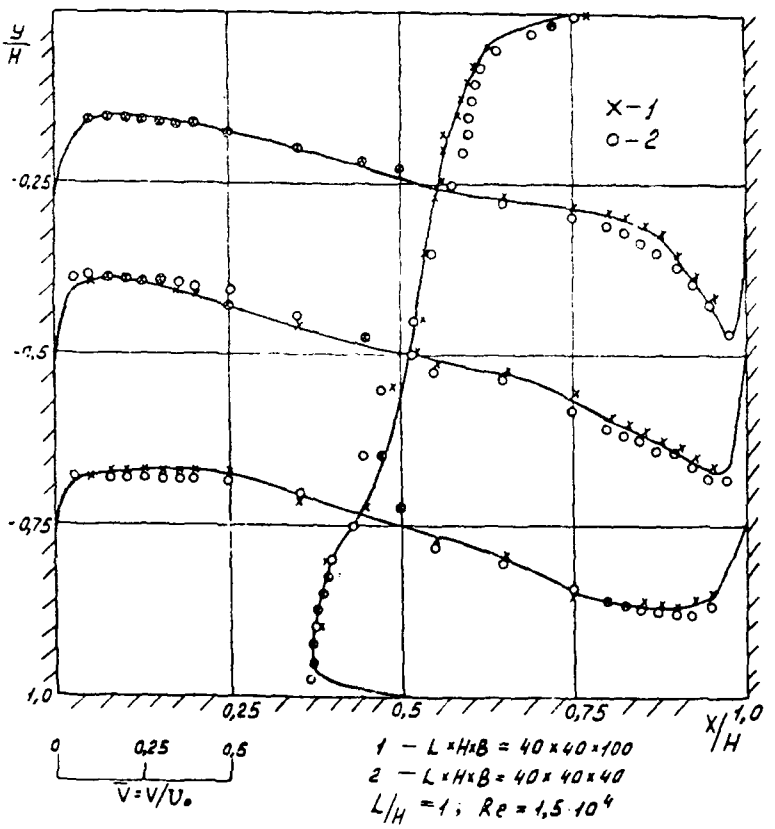

Fig.II.24. Velocity profiles in a square cavity for turbulent flow regime ($Re = 1.5 \cdot 10^4$).
[Bogatyrev and Gorin (1976)]

Evidently the effects of the side walls and the span dimensions may be assessed quantitatively from these figures. Further evidences of effects of the side walls and the span dimensions of the laminar and turbulent cavity flows are indicated in Fig.II.25 and II.26, expressed in the ratio of velocity at the edge of the boundary layer u_m with respect to u_0 and δ /H where δ is boundary layer thickness.

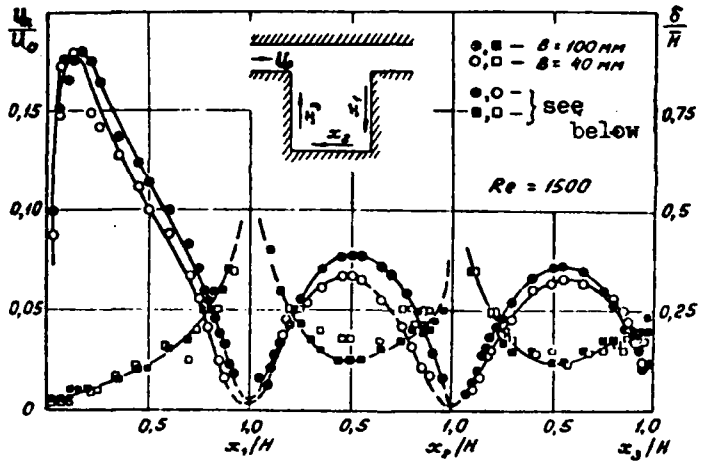

Fig.II.25. Changes in relative velocity u_m/u_0 at edge of the boundary layer and in relative boundary-layer thickness δ /H along cavity walls for Re = 1500.
[Bogatyrev and Gorin (1976)]

Key : a - for velocity; b - for boundary-layer thickness.
●,○ — for speed
■,□ — for boundary layer

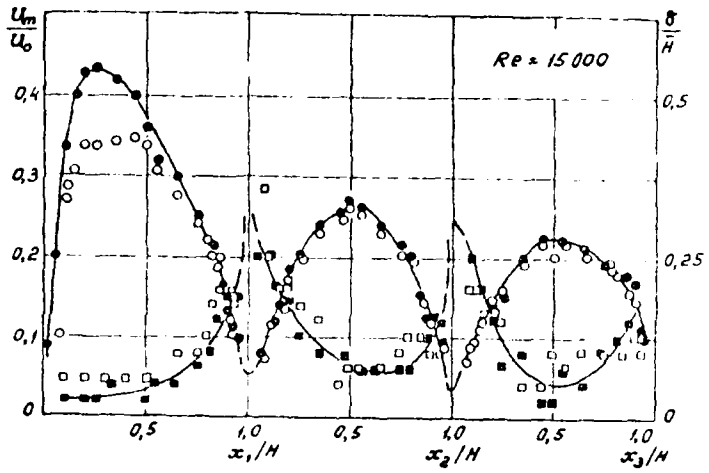

Fig.II.26. Change in the relative velocity u_m/u_o at the edge of boundary layer and in the relative boundary-layer thickness δ/H along cavity walls for Re = 15000.
[Bogatyrev and Gorin (1976)]

Bogatyrev and Gorin's (1976) measurements of flow rates at various depths of the cavity are not uniform, (especially, the disparity is more pronounced at the lower portion), indicating that there is a three-dimensional effect by the corner eddies.

Although the effects of span dimensions on cavity flow can be evaluated by this experiment, in order to assess the side-wall effects it is necessary to obtain further information on the span-wise velocity distribution in the cavity.

3. Flow over a Cylinder

The classical problem of flow over a cylinder with respect to pressure fluctuation and the Strouhal number distribution in a function of the cylinder surface angle measured from the forward stagnation point and in a parameter of the Mach number is briefly presented.

The largest fluctuation of pressure occurs at transonic and low supersonic velocities of external flow not only for, the cylinder flow but also for many other bodies. A combination of intense pressure oscillations and a comparatively high dynamic pressure in this range of velocity may lead to large dynamic loads while the large changes of the flow pattern produce significant changes in the aerodynamic characteristics. By a characteristic value of B defined by $B = (\overline{p^2})^{0.5}/(\overline{p^2})^{0.5}_{st}$ where $(\overline{p^2})^{0.5}$ is a root-mean-square of pressure fluctuation on a cylinder surface and the subscript st refers to forward stagnation point, the relative pressure fluctuation is given in Fig.II.27a. It is seen that at low velocity (M = 0.4) two regions of increased fluctuation appear at $\varphi = 40 - 60^{\circ}$ and $110 - 130^{\circ}$. At M = 0.9, the fluctuation reaches the maximum at $\varphi \sim 90^{\circ}$.

The intense pressure oscillations on the cylinder surface at high subsonic flow velocity are connected with oscillations of the closing compression shocks downstream of the local supersonic regions.

At supersonic velocities, fluctuations are reduced although a slight increase occurs downstream of the separation point due to the oscillation of this point as shown by Kistler (1964) for the separation zone upstream of a step.

The approximate values of the Strouhal number $Sh = \frac{fd}{u_\infty}$ determined from the maxima of fluctuation spectra which are characteristics of the frequency distribution at points round the cylinder surface, are shown in Fig.II.27b. The variation of Sh is more pronounced with the decrease of the Mach number. At subsonic velocities the minimum values of Sh are found at $\varphi = 40 - 60^\circ$, and higher frequencies occur at higher angle of φ. At supersonic velocities the minimum values of Sh are obtained in the region of $\varphi = 90^\circ$.

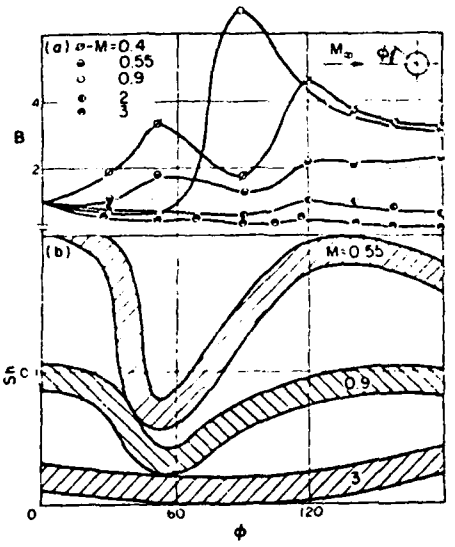

Fig.II.27. Distribution of the pressure fluctuation on the surface of a cylinder and position of the maximum in the spectrum. [Shvets (1978)]

References

Badatov, Ye. V. Slin'ko M. G. and V. Ye. Nakoryakov (1970), Teoret. osnovy khim. tekhnologii 4/6.

Batchelor, G. K. (1956). "On Steady Laminar Flow with Closed Stream-lines at large Reynolds Number," J. Fluid Mech. 1, Pt. 2.

Bogatyrev, V. Ya. and V. A. Mukhin (1976). "Experimental Study of Wall Shear Stress in Cavities," Gradient and Separated Flows, ed. S. S. Kutateladze, Academy of Sciences of USSR, Novosibirsk.

Bogatyrev, V. Ya. and A. V. Gorin (1976). "On Side-Wall Effects in Rectangular Cavities, "Gradient and Separated Flows" ed. S. S. Kutateladze, Acad. Sci. USSR, Siberian Branch, Novosibirsk.

Bogatyrev, V. V. Ya. Dubnishchev, Yu. N. Mukhin, V. A. Nakoryakov, V. Ye. Sobolev, V. S. Utkin, Ye. N. and N. F. Shmoylov (1976). "Experimental Study of Flow in a Cavity," PMTF 2.

Chang, P. K. (1970). Separation of Flow, Pergamon Press. also Otryvnyye Techeniyye, (Separation of Flow), MIR Publishers, Moscow, 1972.

Chapman, D. R. Kuehn, D. M. and H. K. Larson (1957). "Investigation of Separated Flows in Supersonic Streams with Emphasis on the Effect of Transition," NACA TN 3869.

Charwat, A. F. Dewey, C. F. Roos, J. N and J. A. Hitz (1961a). "An Investigation of Separated Flows —— Part I. The Pressure Field," J. Aero. Sci. vol. 28, June. pp. 457-470.

Charwat, A. F. Dewey, C. F. Roos, J. N. and J. A. Hitz (1961b) "An Investigation of Separated Flows —— Part II. Flow in the Cavity and Heat Transfer," J. Aero. Sci. July, pp. 513-527.

Clauser, F. (1954). "Turbulent Boundary Layers in Adverse Pressure Gradient," J. Aero. Sci. 21, 91-108.

Col'dshtik, M. A. (1962). "Mathematical Model of Separated Flows in Incompressible Fluid, "Dokl. Akad. Nauk SSSR 147/6.

Gorin, A. V. (1976). "Survey of Models for Calculating the Flow of an Incompressible Fluid in a Square Cavity," Gradient and Separated Flows," ed. S. S. Kutateladze, Acad. Sci. USSR Siberian Branch, Novosibirsk.

Head, M. R. and I. Rechenberg (1962). "The Preston Tube as a Means of Measuring Skin Friction," J. Fluid Mech. 14/1 (1962).

Kalinin, E. K., Dreytser G. A. and S. A. Yarkho, (1972). Intensifikatsiya teploobmena v kanalakh (Intensification of Heat Transfer in Channels), "Mashinostroyeniye" Press, Moscow.

Khabakhpasheva, Ye. M. (1974). Nekotoryye dannyye o strukture techeniya v vyazkom podsloye. Problemy teplofiziki i fizicheskoy gidrodinamiki (Data on the Structure of Flow in the Viscous Sublayer. Problems of Thermophysics and Physical Hydrodynamics), Nauk Press, Novosibirsk.

Kistler, A. J. (1964). "Fluctuating Wall Pressure under a Separated Supersonic Flow," J. Acoust. Soc. Am. 36(3).

Kistler, A. L. and F. C. Tan (1967). "Some Properties of Turbulent Separated Flows," Phys. Fluids,10/9, Pt. 2.

Kline, S. J. (1959). "On the Nature of Stall," J. Basic Eng. Trans ASME Ser D. Sept.

Kochin, N. Ye. Kibel, M. A. and N. V. Roze (1963). Teoreticheskaya gidromekhanika, (Theoretical Hydromechanics), Part 1, "Fizmatgiz" Press, Moscow.

Kutateladze, S. S. Mirnov, B. P. Nakoryakov, V. Ye. and Ye. M. Khabakhpaskeva (1975). "Eksperimental'noye issledovaniye pristennykh turbulentnykh techeniy, ("Experimental Study of Turbulent Flows Close to the Wall), Nauka Press, Novosibirsk.

Kutateladze, S. S. Kashinskiy, O. N. and V. A. Mukhin (1976). "Experimental Investigation of the Characteristics of Turbulent Boundary Layer with Adverse Pressure Gradient Involving Separation," Gradient and Separated Flows. ed. S. S. Kutateladze, Acad. Science U S.S.R., Siberian Branch, Novosibirsk.

Ludwieg, H. and W. Tillmann (1949). "Investigations of Wall Shear Stress in Turbulent Friction Layers," Ing.-Arch. 17, 288-299.

Maull, D. J. and L. F. East (1963). "Three-dimensional Flow in Cavities," J. Fluid Mech. 16, Pt. 4.

Mirskiy G. Ya (1972). "Apparaturnoye opredeleniye kharakteristik Sluchaynykh protsessov," (Instrumental Measurements of the Characteristics of Random Processes). Energia Press, Moscow.

Nakoryakov, V. Ye. Badatov, Ye. V. and M. G. Slin'ko (1970). "Mathematical Modeling of Heat and Mass Transfer Processes in Separated Flows with Laminar and Turbulent Mixing Regions," Teor. osnovy khim. tekhnologii 4/5,6.

Neyland, V. Ya. and V. V. Sychev (1970). "On the Theory of Flow in Steady Stalled Zones, "Uchen. zap. TsAGI 1/1.

Oka, S. (1969). "Wall Shear Stress in a Rectangular Cavity," Int. Seminar on Heat and Mass Transfer in Flow with Separated Regions and Measurement Techniques, Herceg-Novi, Sept.. pp. 1-13.

Sandborn, V. A. and C. V. Liu (1968). "On Turbulent Boundary-layer Separation," J. Fluid Mech. 32, Pt. 2 (1968).

Shvets, A. I. (1978). "Base Flow," Prog. Aerospace. Sci. vol. 18, Pergamon Press.

Stanford Conference, "Computation of Turbulent Boundary Layers," (1968). 1968 AFOSR IFP Stanford Univ., Stanford, California, vol. 1,2.

Squire, H. B. and A. D. Young (1938). "The Calculation of the Profile Drag of Aerofoils," R M No. 1838, British A.R.C.

Tani, I. Iuchi, M. and H. Komoda (1961). "Experimental Investigation of a Flow Separation Associated with a Step or a Grove," Rept. N 364, Aeronaut. Research Inst. Univ. Tokyo.

Yefimenko, G. I. and Ye. M. Khafakhpaskeva (1976). "Effect of Adverse Pressure Gradient on Wall Turbulence Structure," Gradient and Separated Flows, ed. S. S. Kutateladze, Acad. Sci. USSR, Siberian Branch, Novosibirsk.

CHAPTER III

SYMBOLS

b	mixing layer thickness
$\dot{m}$	injected mass flow rate
$(C_p)_c$	reattachment pressure coefficient
f	frequency
H	step height
L	model height
ℓ_m	total mixing shear length
Mr	Mach number of reverse flow
M_θ	Mach number along the wake axis
Δm	mixing width near compression
$\overline{p_j^*}$	ratio of total pressure on the separation stream line to the total pressure of undisturbed flow
$\bar{u}$	$\bar{u} = u_j/u_e$
u_j	velocity along the dividing stream line
x_c	position of deceleration downstream of a neck
x_s	distance measured from the separation point
β	angle between separation shock and base surface
γ	boat-tail angle
θ	body surface inclination angle or angle between boundary of inviscid flow and base surface or wake closure angle
$\overline{\omega^2}$	spectral density of fluctuation

CHAPTER III

Compressible Flow Separation

Since the problems of supersonic flow involving separation are important for the development of missile, aerospace crafts and satellites, etc., many investigations have been carried out in the past and reported widely. In this Chapter the recent developments emphasizing supersonic flow which have not been presented in the writer's books, Separation of Flow, (Pergamon Press, 1970) and Control of Flow Separation, (McGraw-Hill Book Co., New York, 1976) are reported. The USSR contributions presented by A. I. Shvets and I. T. Shvets in their book, Gasdynamics of Near Wake, (1976, Naukova Dumka Press, Kiev) are particularly reviewed here. For convenience, the problems of flow separation at hypersonic speed range are presented separately later, although some hypersonic phenomena are treated in this section. The content is mainly for experimental investigations concerning separation of external flow, base flow, separated flow over a two dimensional surface and an axisymmetric body, and between two bodies, etc. The problems of base pressure will be presented in Chapter IV. but, some information on base pressure which is pertinent to particular problems of compressible flow separation are also given in this chapter. Several introductory presentations are made before the classifications of problems to be treated here.

More recent information on reattachment and lip shock are described briefly.

Erdix (1967) plotted the pressure distribution of a supersonic turbulent flow past the walls of a nonsymmetric converging and diver-

ging channel with a sharp corner and an inclined flat surface, downstream, as seen in Fig.III.1.

The positions of separation are either known apriori or not. In the case of the position known apriori, at the sharp corner, pressure in the separated region is almost maintained equal to that upstream of separation as seen in Fig.III.1a.

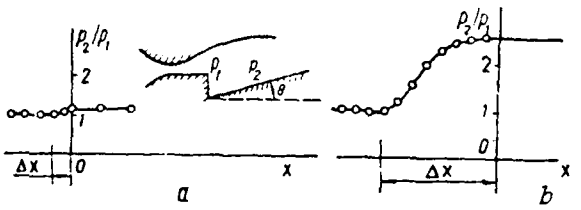

Fig.III.1. Pressure on the walls of a nozzle and behind a step [Sirieix (1967)].

In the case of apriori an unknown separation point, the pressure in the separation zone is also to be considered in a relation of pressure upstream of separation, and p_{max} is not dependent on the reattachment condition. If the shock wave strength increases in the region of shock wave and boundary layer interaction region Δx, then $(p_2-p_1)/\Delta x$ reaches its critical value and the boundary layer separates upstream of the step.

The pressure distribution in this case, shown in Fig.III.1b, indicates the continuous compression, downstream separation, reaching p_{max}. When θ increases, the separation point moves upstream,

the magnitude of p_{max} changes, and reattachment pressure p_2 increases. But, at certain value of θ , the difference of $p_2 - p_1$ becomes zero.

Reattachment flow behavior, downstream of an axisymmetric downstream facing step with a finite initial turbulent boundary layer, is described by pressure distribution by Roshko and Thomke (1966), as seen in Fig.III.2.

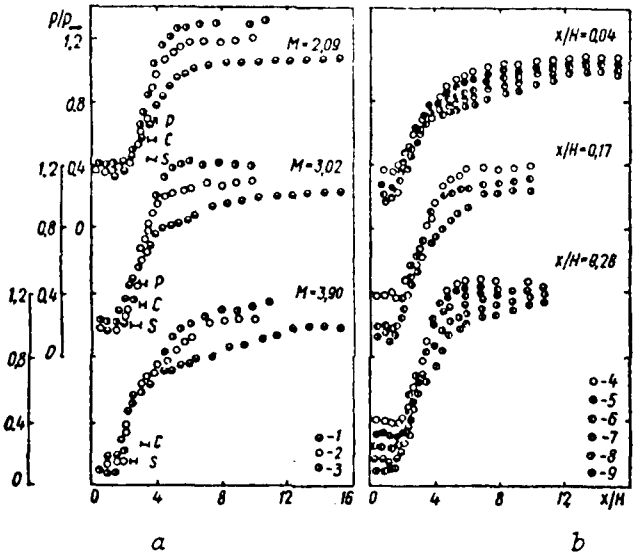

Fig.III.2. The effect of the height of the protuberance (a) and the M number (b) on distribution of pressure in a function of x/H [Ribner and Etkin (1958)]. (P--is the peak distribution of pressure; S--is the point reversed flow occurs; C--is the position of the joining point):

1--H/R = 0.042; 2--H/R = 0.17; 3--H/R = 0.28;

4--M = 2.09; 5--M = 2.56; 6--M = 3.02;

7--M = 3.49; 8--M = 3.90; 9--M = 4.37;

The initial pressure rise to reattachment may be presented by a single curve independently from M and x/H. Furthermore, point P, the position of the peak pressure and C, the location of reattachment are fixed for all M; but S, the initial point of reverse flow shifts toward the step if M increases. It is clearly seen that the pressure downstream of reattachment is effected significantly by the geometry of the step and M.

The reattachment pressure of a two-dimensional turbulent flow is predicted in a simplified manner by Batham (1969) based upon the concept of free interaction in a good agreement with experimental data up to M = 3.2, as shown in Fig.III.3.

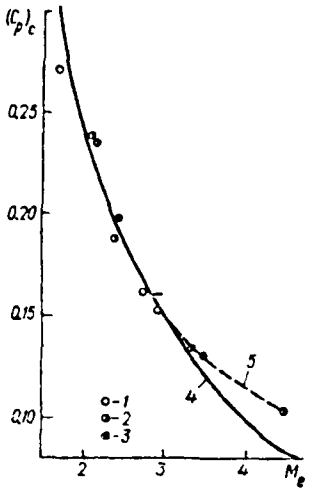

Fig.III.3. Coefficient of pressure with repeated reattachment [Batham (1969)] : 1--Protuberance; 2--Base flow; 3--Incident discontinuity; 4,5--Calculation.

The discrepancy at M > 3.2 may be attributed to the application of the linearized Prandtl-Meyer equation. For analysis it is assumed that the dividing streamline is straight and the variation of flow

parameters in the free-interaction region is similar and depends only on the state of the interaction.

Hama (1968) investigated "lip shock" (also called "separation shock") emanating from the separation edge of a 6° half-angle wedge by means of optical observations as well as by surface and pitot pressure measurements in the ranges of M = 2-4.5 and $0.2 \times 10^{6} \leq Re \leq 2 \times 10^{6}$, showing that lip shock effects the reattachment. Lip shock strength is quite substantial in contrast to the usual belief that lip shock is as weak as the sound wave. The pressure of a lip shock of substantial strength means that the expansion process at the separation edge is more complicated than the usually assumed Prandtl-Meyer expansion. The flow actually overexpands first, then is recompressed by the lip shocks, and this is caused essentially by a viscous separation effect similar to the separation shock emanating from a circular cylinder, rather than being caused by inviscid rotational-field phenomena.

In the near wake of the wedge two shocks, lip and wake shock occur and these shocks interact directly influencing the pressure recovery process and distorting the near wake velocity profile. Contrary to turbulent reattachment, the effect of the lip shock-wave shock interaction is absent and pressure is smoothly recovered. At lower Mach numbers, the lip shock can be clearly distinguished from the wake shock, and if the Reynolds number is sufficiently large, a slip stream parallel to the free stream direction emerges from the intersection point of two shocks. At higher Mach numbers, the two shocks merge to form one continuous shock, particularly with laminar flow of a lower Reynolds number.

If the separation edge is smoothly tapered so that a proper boattail angle leads the flow direction upstream of the separation almost parallel to free shear layer direction, then no expansion is involved at the separation and slip shock is eliminated or its strength is reduced. Under these conditions, the anomalous behavior in the static pressure recovery distribution along the wake center line, such as peak and hump, disappears.

1. Characteristics of Compressible Flow Separation

1.1 Mixing Layer and Reversed Flow

Su and Wu (1971) identified the satisfactory correlating parameters, based upon the so-called reduced Re_c in the mixing region, and proposed a base pressure correlation for a two-dimensional reward facing step.

For the definition of Re, it is customary to use the characteristic length of the body L, and its height H, but since such Re does not yield proper physical meaning, Su and Wu (1971) instead referred to the total mixing shear length ℓ_m and mixing width at near compression Δ_m. Although they are not known apriori, these two lengths are correlated to the model length L, upstream of the two-dimensional rearward facing step, and its height H. Then, L is related to δ, the physical boundary layer thickness upstream of separation, and H to Δ_m, which is related to ℓ_m. By taking the ratio of inertia to viscous forces in the mixing region:

$$Re_c = \rho_\infty u_\infty (u_\infty/\ell_m)\Big/\mu_\infty(um/\Delta m^2) = (\rho_\infty u_\infty \ell_m/\mu_\infty)(\Delta m/\ell_m)^2$$

by assuming $\ell_m \sim H$

$$\frac{\Delta m}{\delta} \sim \left(\frac{\ell m}{\delta}\right)^n \sim \left(\frac{H}{\delta}\right)^{n(Re_{\infty L}, M_\infty)}$$

$$Re_c = \frac{\rho_\infty u_\infty H}{\mu_\infty}\left(\frac{H}{\delta}\right)^{2n-2}$$

If the dependence of δ on Mach number is neglected, then

$$\frac{\rho_\infty u_\infty H}{\mu_\infty} = \left(\frac{\rho_\infty u_\infty L}{\mu_\infty}\right)\left(\frac{H}{L}\right) \sim \left(\frac{H}{\delta}\right)^m \left(\frac{L}{H}\right)^m \left(\frac{L}{H}\right)^{-1}$$

and

$$Re_c = \left(H/\delta\right)^{m+2n-2} \left(L/H\right)^{m-1}$$

where n and m depend on whether flow is laminar, transitional or turbulent. For laminar and turbulent flow, m = 2 and 5 respectively. For transitional wake, taking m = 2 and n = 0.9

$$Re_c \sim \left(\frac{H}{\delta}\right)^{1.8} \left(\frac{L}{H}\right) \sim \left(Re_{\infty H}\right)^{0.9} \left(\frac{L}{H}\right)^{0.1}$$

By correlating with experimental data in the regions of $0.05 \times 10^6 < Re_{\infty L} < 1.8 \times 10^6$, $2 < M_\infty < 3.55$, $5.33 < L/H < 3.14$, 0.0072 in $< H < 0.75$ in.

Su and Wu (1971) proposed the base pressure prediction of a two-dimensional rearward facing step by

$$p_b/p_\infty = Re_c\, e(-6.97 + 0.745D - 0.1136D^2)$$

where $D = \ell m(Re_c)$.

Tagirov (1969) clarified, by his detailed experiment, a number of characteristics of turbulent supersonic flow, mixing downstream of two-dimensional protuberance, to be used for the analysis of separated flow. The validity of the hypothesis on the conservation of total pre-

ssure along the stream line is confirmed by measuring the boundary layer characteristics up- and downstream of the expansion fan, and zero velocity lines are determined by measuring pressure, as seen in Fig.III.4.

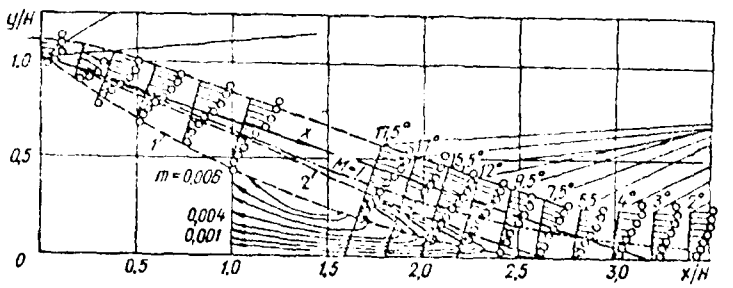

Fig.III.4. Field of Mach numbers behind a two-dimensional protuberance with M = 1.97 [Tagirov (1969)]:
1--lines of zero velocity; 2--lines of constant mass.

This Fig.III.4 indicates also the profile of the Mach number, including M = 1 and the lines of constant mass evaluated, based upon the velocity of the mixing zone.

The mixing layer thickness designated by b is given by Abramovich (1969) as

$$b/x_s = C \frac{\bar{\rho}_2 + 1}{2} \cdot \frac{1 - m}{1 + \bar{\rho}_2 m}$$

assuming the initial boundary layer thickness is equal to zero, where x_s is distance measured from the separation point,

$\bar{\rho}_2 = \rho_2 / \rho_1$ and $C \simeq 0.27$ is an empirical constant.

Neyland and Taganov (1963) formulated the pressure at the re-

attachment of a separating stream line on the trailing body by

$$\frac{\bar{p}_j^*}{\bar{p}_p} = \left[\frac{1 + \frac{\gamma-1}{2} Me^2}{1 + \frac{\gamma-1}{2}(1-\bar{u}^2)Me^2}\right]^{\frac{\gamma}{\gamma-1}}$$

where $\bar{p}_j^*$ is the ratio of the total pressure on the separating stream line to the total pressure of undisturbed flow, $\bar{u} = u_j/u_e = 0.587$ (u_j is the velocity along the dviding stream line) M_e is the Mach number along the external boundary of the mixing zone, taken equal to the Mach number over the equivalent cone.

The measured relative velocities in the mixing layer and in the reverse flow area are shown in Fig.III.5. In Fig.III.5 the horizontal axis is $\varphi = u/u_o$, and the vertical axis is $\eta = (t-to)/(\delta-to)$ where δ and to are coordinates of external and internal boundaries of the mixing zone and t is a variable coordinate measured from the wall. The internal boundary is determined by the line of zero velocity. The reverse flow is correlated by

$$\varphi = 1 - \eta^3 \quad , \quad \varphi = u/u_{max} \quad \text{and} \quad \eta = y/y_\varphi$$

From Fig.III.5 it may also be noted that a counter rotational flow exists in addition to the main circulating flow.

Shvets and Panov (1970) and Shvets (1970, 1971) investigated the near wake structure by measuring static and total pressure through optical and flow visualized observations, using a plate mounted downstream of the base. By observing a number of detailed characteristics by Töpler instrument, the field of the maximum density gradient corresponding to that of the expansion wave, jet boundary and trailing shock,

etc., are determined. A comparison of the results obtained by pressure measurement and optical and flow visualized observation reveals the precise flow structure and enables one to fix the boundary lines as shown in Fig.III.6.

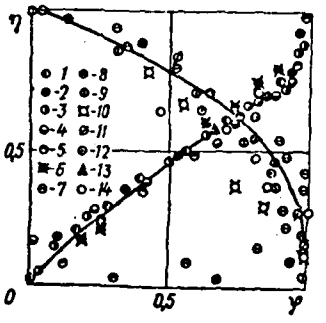

Fig.III.5. Relative velocities in the mixing layer (1--6) and in the reversed flow (7-14) [Tagirov (1969)]:
1--$\theta = 17.5^{\circ}$; 2--$\theta = 17^{\circ}$; 3--$\theta = 15.5^{\circ}$;
4--$\theta = 12^{\circ}$; 5--$\theta = 9.5^{\circ}$; 6--$\theta = 7.5^{\circ}$;
7--$\ell/H = 0.56$; 8--$\ell/H = 0.97$; 9--$\ell/H = 1.37$;
10--$\ell/H = 1.5$; 11--$\ell/H = 1.6$; 12--$\ell/H = 1.7$;
13--$\ell/H = 1.77$; 14--$\ell/H = 1.9$.

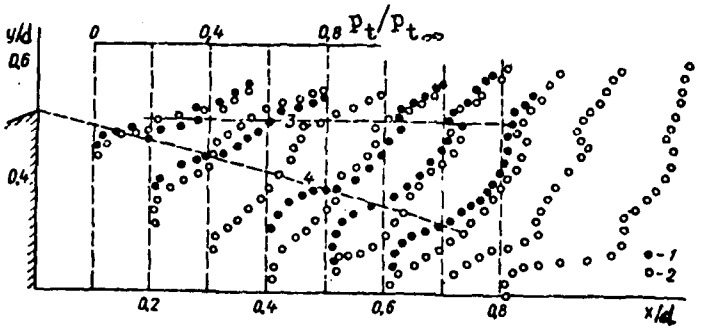

Fig.III.6. Field of pressure behind a cone ($\theta = 20^{\circ}$, M = 3):
1,2--Cone on strand wires and pylon;
3--Boundary discontinuities; 4--Boundary of the viscous layer.
[Shvets and Shvets (1976)]

Bauer (1967) measured the pitot pressure downstream of cones at M = 3.035 and $Re_d = 1.13 \times 10^5$ based on the cone base diameter in order to find flow parameter in functions of Re and cone angle to relate the base pressure. Furthermore, the movement of the rearmost stagnation point effected by the injection rate was studied.

The structure of the base flow may be obtained by a pitot pressure "map" of the flow field with no injection, in Fig.III.7. The flow expansion around the cone corner and the corner lip shock are clearly evident. The lip shock appears as a small increase in pitot pressure in the streamwise direction. The recirculation region is largely within the line labeled "0.2" and the shear layer is just outside the recirculation zone. Although the neck region is not located precisely, it is in the neighborhood of x/d = 1.5, where x/d is the ratio of the downstream distance of base to the diameter of the cone base. The wake shock emerges from the neck region as a strip of high pitot pressure gradient. The effect of injection was to widen the wake picture, as shown in Fig.III.7.

The edge of the shear layer in the plane x/d = 1.5 moved outward from y/d = 0.32 to y/d = 0.44 as $\dot{C}_m$ increased from 0 to 1.2 %. In the recirculation region, the pitot pressure was smaller than the static pressure, in as much as the flow past the pitot head was reversed from its usual direction, and this reverse flow phenomena persisted as $\dot{C}_m$ was increased from 0 to 3.0 %. When $\dot{C}_m$ was increased to 3.6 %, the reverse flow had just disappeared and some flow unsteadiness was noticed. The recirculation zone does not move downstream with increa-

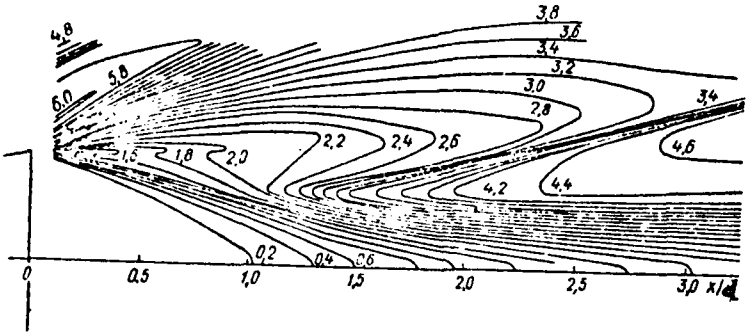

Fig.III.7. Diagram of the lines of constant pressure measured with a piot tube in the wake behind a cone ($\theta = 12^{\circ}$, M = 3.03, $Re_d = 1.1\ 10^5$, $\delta/d = 0.026$ [Bauer (1967)] ; dimensionless values presented along each line are obtained by dividing the measured pressure by 0.044 at technical atmosphere .

sing injection rate but shrinks until some critically small size is attained, below which it can not be maintained in its closed-stream-line form.

Shvets (1970) accurately determined the shock boundary, the zero velocity line and the coordinate of the dividing stream line (based upon the mass conservation of the circulating flow given by $\int_0^y \rho u dy = 0$ (assuming T = const.) and by measuring the pressure as shown in Fig. III.8. The obtained data was compared with those of optical and flow visualized observations. Optically measured, and by flow visualization, observed curves 7 and 6 indicate the boundary dividing the low pressure region from that of constant static pressure and the external boundary of the mixing layer respectively. The propagation of the expansion wave to separation shock is indicated by the approach of curve

7 to curve 1. Curve 5 appears sharply in flow schlieren photographs and the dividing streamline 3 is close to line 6.

The isobars of total pressure in the base region in Fig.III.9 indicate the discontinuities of total pressure characterizing the shock waves. A turning region of total pressure curves may be noticed at the location immediately above the shocks, indicating the position of the substantial over-expansion of the flow. Curves of total pressure close to the curve of $p_t/p_{t\infty} = 0.3$ are close each other, indicating that this area is a viscous flow region.

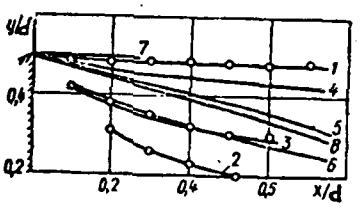

Fig.III.8. Near wake (cone on stranded wires, $\theta = 20^\circ$, $M = 3$):
1-3--Measurement of pressure;
4-6--Visualization; 7-8--Optical measurement;
1--Boundary discontinuity; 2-- $u_x = 0$;
3-- $\psi = 0$; 7--End of the expansion wave;
8--Boundary of the mixing layer [Shvets and Shvets (1976)].

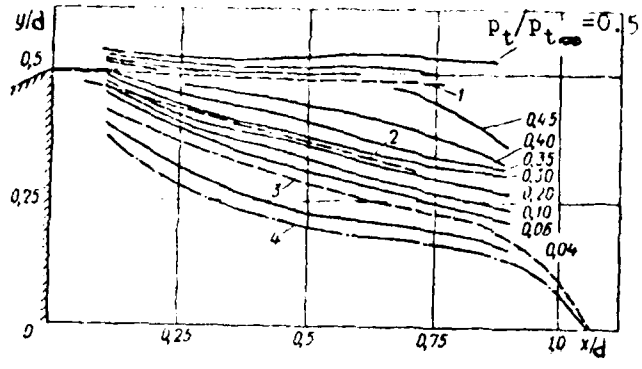

Fig.III.9. Isobars of total pressures ($\theta = 20^{\circ}$, $M = 3$) [Shvets and Shvets (1976)]:
1--Boundary discontinuity; 2--Boundary at the mixing layer; 3-- $\psi = 0$; 4-- $u_x = 0$.

Fig.III.10 is a photograph of flow visualization using a mixture of soot, oil and kerosene. The mixing zone appears light above region 3 washed by the mixture. The upper boundary line 2 is dividing stream line. Downstream of body, velocity and Mach number along the dividing streamline increase due to the momentum transfer. Obeying the law of mass conservation, all streamlines below $\psi = 0$ reverse their directions toward the base because of the compression taking place at the neck region, but above $\psi = 0$, stream lines maintain their directions downstreamwise through the neck region with reduced velocity.

The reversed flow phenomena involving reattachment downstream of a cone were also investigated by optical and flow visualized ob-

Fig.III.10. Visualization of flow on a plate behind a cone:
1--Inviscid flow; 2--Boundary of the viscous layer; 3--Toroidal circulation flow; 4--Point of deceleration; 5--Reversed flow; 6--Line of run-off; 7--Compression zone. [Shvets and Shvets (1976)] .

servations by Shvets (1970, 1971). In order to take photographs a plate was placed in the near wake region. Although the pressure of the plate on which boundary layer accumulates and its mounting device decreases the width of recirculating region, the fundamental features of recirculation and reattachment are retained in the photographs.

Stream line of flow over the corner is directed toward the central axis after turning, and pressure on the body base immediately below the corner is smaller than the pressure predicted by the Prandtl-Meyer equation due to its overexpansion. Since this low pressure increases to

higher base pressure, flow moving toward the base center separates. The external viscous flow does not separate from the corner edge and tends around the local annular separation zone. The point of the external flow separation is located on the external boundary of the annular separation zone and the point of internal radial flow separation is located on the internal boundary of this zone. The flow lines approaching the run off line 6, form a cylindrical layer whose density and pressure are increased at a certain distance downstream of the base. The density gradients of these lines are approximately equal to that of line 6. When the reverse flow approaches the base, flow decelerates and forms a pressurized zone from which the fluid particles scatter in a radial direction. Thus, from the central area of the base section (y/d = 0.1-0.3) radial flow goes out from the base and forms an another run-off line (x/d = 0.1) located parallel to the base section.

Fig.III.11. of tuft flow visualization shows areas of vortex 1 and central flow 2. The central flow along the plate is fed into the stagnation zone, the spreading area 3. Having reached the cone base, flow spreads in a radial direction and is ejected by the main flow. Then, part of fluid flows between 2 and 6 (Fig.III.10). Thus, as Korst states, stagnation zone is open and fluid is pumped from it toward the plate surface. The reverse flow phenomena in the stagnation zone may be summarized as follows: if the reverse flow is induced by vortex, then its velocity reaches its maximum value at the position where the streamline direction on the internal boundary of the vortex coincides with the stream direction. The flow directed in two directions; one along the

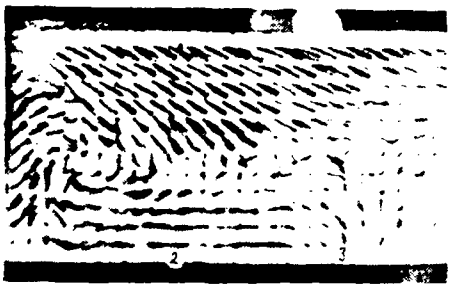

Fig.III.11. Photographs of a plate behind a base [Shvets and Shvets (1976)]:
1--Toroidal flow; 2--Reversed flow;
3--Point of deceleration.

main flow direction and another approaches to the stagnation zone in a form of a cylindrical stream.

Realizing that no static pressure distribution along the normal direction to the near wake was investigated in the past, due to difficulties in measurements and due to a strongly curved stream line, Isayev and Shvets (1970) measured the static pressure in a semi-plane, normal to the axis of wake, using a thin trapezoidal plate as shown in Fig.III.12. Such information is needed to understand the flow structure, to evaluate the Mach number and to establish a reliable computational system.

The base flow is effected by the pressure of the plate, and the boundary layer on it distorts the measured pressure. Neverthless, the main features of flow are retained and it was possible to study the pressure gradient. From Fig III.12 it is seen that although static

pressure varies insignificantly in the reserved flow zone, the pressure gradient is substantial in the mixing layer. The static pressure increases from the lower part of y/d and reaches the maximum at approximately 0.2, then with increase of y/d, pressure decreases and levels off downstream of the trailing shock.

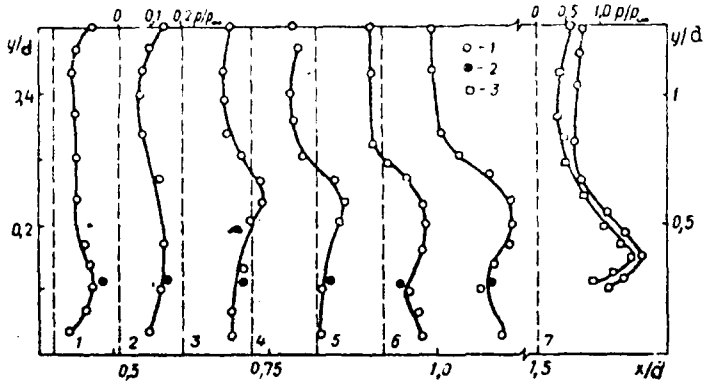

Fig.III.12. Distribution of static pressure behind a cone [Shvets and Shvets (1976)]:
1--$\theta = 10^{\circ}$, M = 3; 2--Base holder; 3--$\theta = 30^{\circ}$, M = 3.

Data on the pressure distribution in the neck region is illustrated in Fig.III.13. Upstream of the neck, say at x/d = 0.5, pressure gadient in y/d is relatively smooth, compared to x/d = 0.8 where compression begins and flow turns.

The flow phenomena of near wake effected by various body shapes were studied by Isayev and Shvets (1970) and Shvets and Panov (1970) by measuring the total pressure downstream of sharp and blunt cones

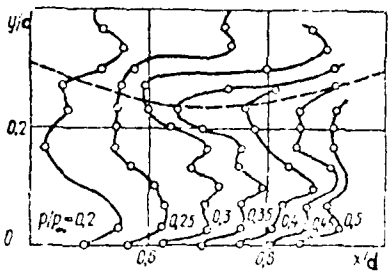

Fig.III.13. Isobars of static pressures ($\theta = 10^{\circ}$, $M = 3$) (dashed line corresponds to the wake boundary) [Shvets and Shvets (1976)].

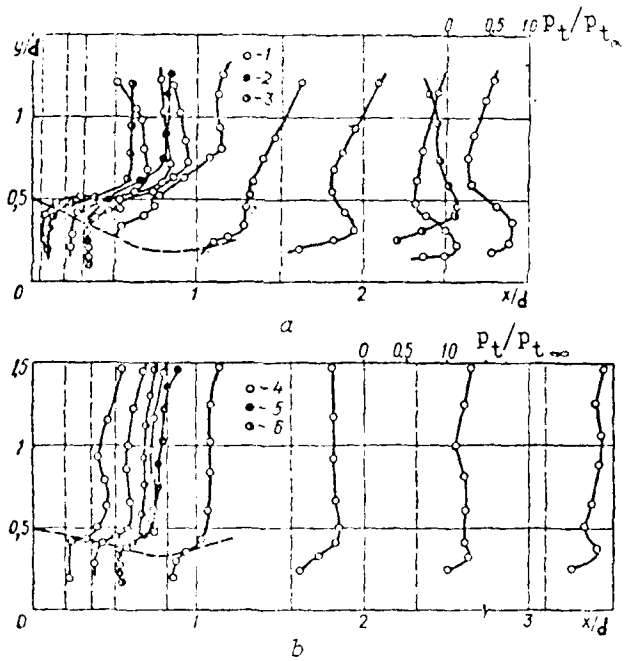

Fig.III.14. Distributions of full pressure in a near wake (dashed curves correspond to the boundary of the wake; 4-6--Sector bodies) [Shvets and Shvets (1976)]:
1--Cone $\theta = 10^{\circ}$, $M = 3$; 2--Blunt, $r/R = 0.4$, $M = 3$; 3--$r/R = 0.4$, $M = 2$; 4--$t = 0.2$, $M = 3$; 5--$t = 1$, $M = 3$; 6--$t = 1$, $M = 4$.

of half angles θ , amounting to 10°, 20° and 30° and a reverse cone of $\theta = 5^{\circ}$ with elliptical leading section (L/d = 1).

As shown in Fig.III.14 a slight reduction of pressure in the recirculation zone is achieved by blunting, although $p_t/p_{t\infty}$ increases about 10-20 % for $y/d > 0.8$ if ellipsoid with ratio of axis, $t = 0.2$ is changed to a sphere in the leading section.

The geometrical configurations in β , δ and distance between the base and neck($\ell' = \ell/d$) of near wake behind cones determined by Töpler photographs in a function of Mach number are shown in Fig.III.15 including those of hypersonic speeds. In the supersonic Mach number region, with increase of M, angle β decreases and contracts the wake neck, whereas in hypersonic Mach number region, with the increase of M, magnitudes of β , $d' = \bar{d}/d$ and ℓ' increase, indicating that flow characteristics are different in supersonic and hypersonic regions.

The diameter of wake neck $d' = \bar{d}/d$ and angle β effected by a cone half angle are shown in Fig.III.16.

Panov and Shvets (1965) noticed the hysteresis phenomena of separation occurring on the circumferential surface of blunt bodies. If the angle of attack α is increased from 0°, then at certain angle of attack α_1, flow separates but if the angle of attack is decreased from a larger angle to a smaller one, then separation disappears at α_2 which is smaller than α_1. For example, at M = 3, flow around a reverse cone of $\theta = 5^{\circ}20'$ with spherical blunting, when the angle of attack was increased, separation occurred at $\alpha_1 = 8^{\circ}$, but by decreasing , separation was retained up to $\alpha_1 = 5^{\circ}$.

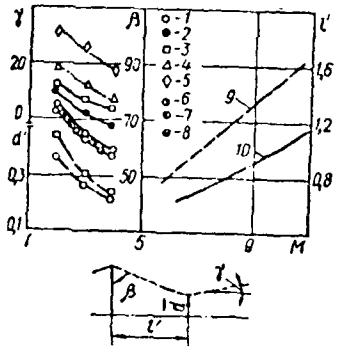

Fig.III.15. Configuration of a near wake (solid curve means β, dashed-- ℓ', dashed-dot--d') [Shvets and Shvets (1976)]:
1--Cone, $\theta = 10^\circ$ on pylons; 2--Cone, $\theta = 10^\circ$ on base holder; 3--Sector body, t = 0.2; 4-- γ, cone, $\theta = 10^\circ$ on pylons; 5-- β, boundary discontinuity; 6--Calculation [Chapman (1950)]; 7,8--Calculation for two-dimensional and axisymmetric flows [Thomann (1959)]; 9, 10--Ballistic testing, M = 6-11, $Re = 1 \cdot 10^6$ [Waldbusser (1966)].

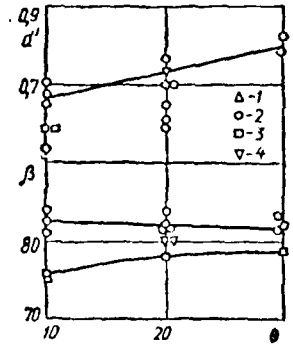

Fig.III.16. The effect of the angle of the semi-apex of the cone on the diameter of the wake neck $d' = \bar{d}/d$ and angle θ:
1--M = 1.7; 2--M = 2; 3--M = 3; 4--M = 4.
[Shvets and Shvets (1976)]

1.2. Flow Parameters Along the Wake Axis

The information on the flow parameters along the wake axis is important to establish the accurate flow system of the near wake, thus, in the past pertinent parameters have been measured. One of the parameters which determines the viscous effect in the base region is $\bar{\delta} = \delta/d$. If $\bar{\delta}$ is small in correspondence to a large Re, then the viscous effects are significant only in the thin mixing layer; but with a large $\bar{\delta}$, the large part of the stagnant zone becomes viscous. For the fixed value of Re, $\bar{\delta}$ is proportional to ℓ/d and the thinner the body, the more important are the viscous effects in the base area.

The measured pressure distribution and M_θ, the Mach number along the wake axis downstream of a cone, are shown in Fig.III.17. The position of deceleration is determined at the point of the intersection of curves p_t and p_{tr} where subsript r refers to reverse flow. If boundary layer thickness increases, then the deceleration point moves toward the cone.

The experimentally determined point of deceleration and the Mach number of the maximum velocity of the reversed flow are shown in Fig.III.18. The reverse flow velocity Mach number increases linearly to $M_r \simeq 0.8$ at $M = 6$. If the free stream velocity approaches to sonic ($M \simeq 0.95$), then the critical point moves downstream. If M increases subsequently to 5, then the critical point approaches to this point, but at a hypersonic Mach number no significant shift is noted.

The pressure close to the body and downstream of the deceleration

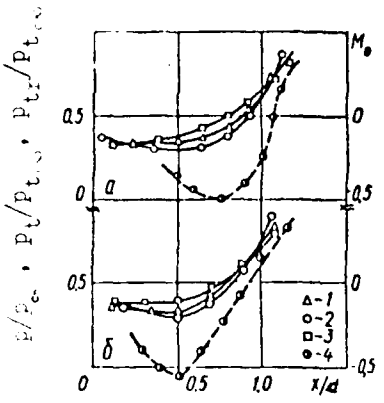

Fig.III.17. Distribution of pressure and the M numbers along the axis of the wake behind a cone ($\theta = 20^\circ$, $M = 3$; $\bar{\sigma} = 0.01$ (a) and $\bar{\sigma} = 0.04$ (b): 1--p--static pressure; 2 and 3--p_t and p_{tr}--pressure measured by an attachment directed upstream and downstream; 4--M_θ--Mach number on the axis of the wake. [Shvets and Shvets (1976)].

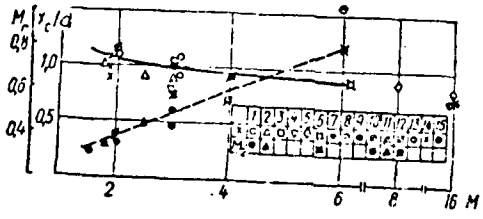

Fig.III.18. Position of the deceleration point x_c/d and maximum velocity of reversed flow M_r for a cone (1-8), a wedge (9-13) and a cylinder (14, 15) [Shvets and Shvets (1976)]:
1--$\theta = 10^\circ$, $Re = 4 \cdot 10^6$; 2--$\theta = 11^\circ$, $Re = 3 \cdot 10^6$ (data of A.S. Boyko, V.S. Trusov, and A.A. Yasnov); 3--$\theta = 10^\circ$ [Bauer (1967)]; 4--$Re = 1.1 \cdot 10^5$ [Collins, Lees and Roshko (1970)]; 5--$\theta = 5^\circ$, $Re = 9 \cdot 10^6$ [Zakkay and Cresci (1966)]; 6--$\theta = 10^\circ$, $Re = 2 \cdot 10^7$ [Martellucci, Trucco and Agnone (1966)]; 7,8--$\theta = 10^\circ$, $Re = 10^5$ [Todisco and Pallone (1965)]; 9--$\theta = 15^\circ$, $Re = 2 \cdot 10^6$ [Badrinarayanan (1961)]; 10--$\theta = 15^\circ$, $Re = 1 \cdot 10^6$ [Badrinarayanan (1961)]; 11--$Re = 6 \cdot 10^6$ [Larson et al (1962)]; 12--$\theta = 6^\circ$, $Re = 3 \cdot 10^5$ [Lewis and Behrens (1969)]; 14--$Re = 1 \cdot 10^6$; 15--[Herzog (1964)].

point are effected by Mach number. The pressure in the recirculation zone and in the neck decrease with of Mach numbers up to x/d = 1.3 but further downstream with increase of M, pressure also increased as shown in Fig.III.19. The position of the critical point depends on Re, and Van Hise (1959) found that with perturbation in the range of Re = 5 x 10^4 - 7 x 10^5, the critical point approaches to the body if Re increases.

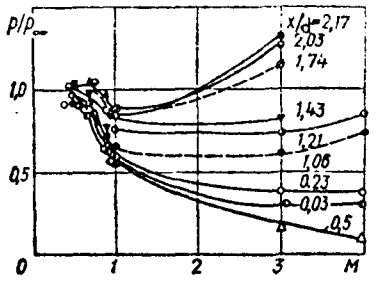

Fig.III.19. The effect of the M number on pressure along the axis of a wake ($\theta = 10^{o}$) [Shvets and Shvets (1976)].

The measured pressure distributions along the wake axis effected by various shapes of bodies are illustrated in Fig.III.20. The pressure increases from x/d = 0.5, and with an increasing conical angle, static pressure in the compression zone also increases. The position of deceleration downstream of neck is determined at x_c/d = 1.1, taking the total, and static pressure becomes equal, but the flow visualization indicates its location at x_c/d = 1.0. The pressure begins to increase upstream of the neck and ends at a distance of more than two

diameters downstream from the base section. In the region of increased pressure, magnitude of pressure grows more sharply at M = 4 compared to M = 3 and with increase of Re from Re = 1 x 10^7 to 2.5 x 10^7. The pressure in the compression zone also increases strongly compared to the region close to the body.

Martelluci, Trucco and Agnone (1966) carried out the detailed measurements of the distributions of static, and total pressure and temperature, Mach number, and stagnation point location along the wake center line downstream of a 10° half angle circular cone at M = 6, stagnation pressure 800 psi and free stream Re = 6.15 x 10^6 based upon the diameter.

The boundary layer at the cone shoulder was turbulent for the entire test series. Considerable efforts were made to optimize the method of model support by using a tow-rod band so that wake properties, with a minimum of support interference, could be obtained.

The measured center line pressure distribution are shown in Fig.III.21. The base pressure was maximum at the center line with slight decrease in the radial direction, and a minimum is reached at a radial position r/d = 0.25 where d is the model base diameter. The static pressure reaches its maximum at $x/d \simeq 1.5$ but its minimum is located at $x/d \simeq 0.5$. The location of the downstream stagnation point was determined from u = 0 line measurements. The stagnation point was located $x/d \simeq 0.88$ from the model base as shown in Fig.III.22. The u = 0 line was normally straight except in the vicinity of the axis, at an angle of 25° with the cone axis.

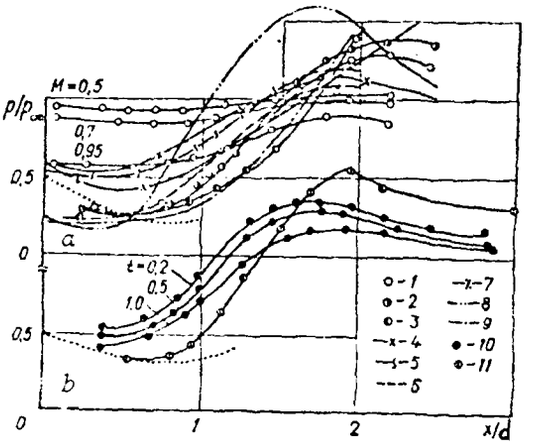

Fig.III.20. Static pressure along the axis of a wake (dashed lines correspond to the boundary of the wake; 1-3, 5-9--Conical bodies; 4--Cylinderical protuberance; 10--Sector body; 11--Disk) [Shvets and Shvets (1976)]:

1--$\theta = 10^{\circ}$, M = 3; 2--$\theta = 20^{\circ}$, M = 3; 3--$\theta = 10^{\circ}$, M = 4; 4--M = 1.85, Re = $1.5 \cdot 10^6$ [Badrinarayanan (1961)]; 5--$\theta = 10^{\circ}$, M = 1.49, Re = $2 \cdot 10^6$ [Zakkay and Sinha (1965)]; 6--$\theta = 10^{\circ}$, M = 3, Re = $2 \cdot 10^6$ [Zakkay and Sinha]; 7--$\theta = 5^{\circ}$, M = 4, Re = $4 \cdot 10^7$ (data of A.S. Boyko, V.S. Trusov, and A.A. Yasnov); 8--$\theta = 10^{\circ}$, M = 6.2, Re= $2 \cdot 10^7$ [Martellucci, Trucco, and Agnone (1966)]; 9--$\theta = 10^{\circ}$, M = 8, Re = $1.7 \cdot 10^6$ [Zakkay and Cresci (1966)]; 10--M = 3; 11--M = 3.

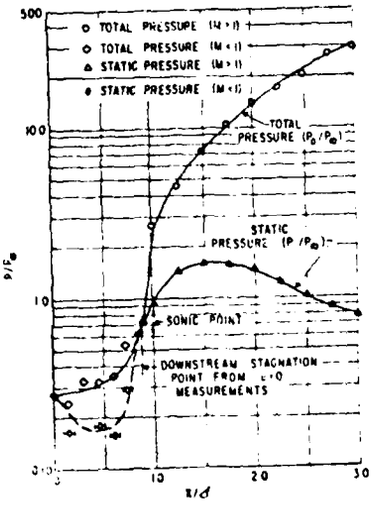

Fig.III.21. Centerline pressure distribution [Martellucci, Trucco and Agnone (1966)].

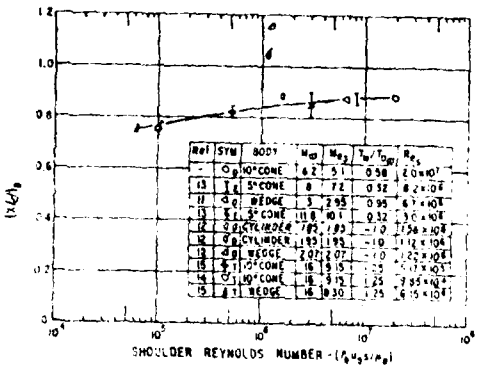

Fig.III.22. Distance to the downstream stagnation point for bluff base bodies [Martellucci, Trucco and Agnone (1966)].

The throat of the basic wake structure, defined as the position where the local Mach number is 1.0 along the wake axis of symmetry, was located at x/d = 0.98 from the model base, but the neck of the wake structure was located at x/d = 1.75. The maximum subsonic Mach number along the axis of the recirculation zone was not small, amounting to $M_{CL\cdot max} \simeq 0.8$. The vortex created in the recirculation zone is energized by the shear face imparted via the dividing stream line, and since the air density in the recirculation zone is small, this shear face can cause a high velocity or Mach number.

Zakkay and Cresci (1966) measured distributions of pressure and of temperature along the wake axis, as well as normal to this axis downstream of a 5° half-angle circular cone, at Mach numbers of 11.8 and 8.0.

The Mach 11.8 tests were carried out at a free stream Reynolds number of 6.10×10^5/ft and a stagnation temperature of 1700°R. The boundary layer near the model base was laminar. The center line pressure distribution was evaluated successfully. However, due to very small differences of pressure in the recirculation zone because of the sonic velocity there, it was not possible to determine the local velocity accurately from the measured pressure data. The measured center line variations of stagnation temperature are shown in Fig.III.23 indicating gradual increase of stagnation temperature downstream.

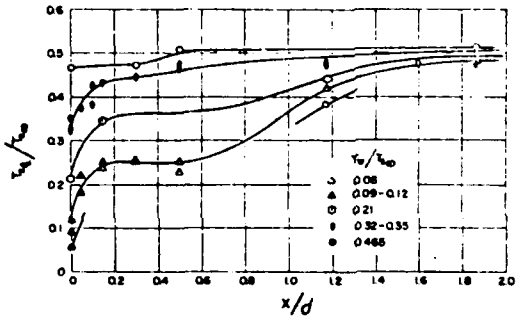

Fig.III.23. Centerline variation of stagnation temperature (M_∞ = 11.8) [Zakkay and Cresci (1966)].

The stagnation temperature profiles in a parameter of x/d are shown in Fig.III.24, where $\bar{r}$ = r/D non-dimensionalized radial distance, measured from the model center line. The increasing fullness of the profiles is observed along with the increasing temperature of the viscous core as the wake progresses downstream. The Mach 8.0 tests

were conducted at free stream Reynolds numbers of 0.3 and 1.7 x 10^6. For these conditions, the boundary layer on the cone surface at the model base was a completely laminar and a fully developed turbulent, respectively, although the flow in the entire near wake was probably laminar in nature.

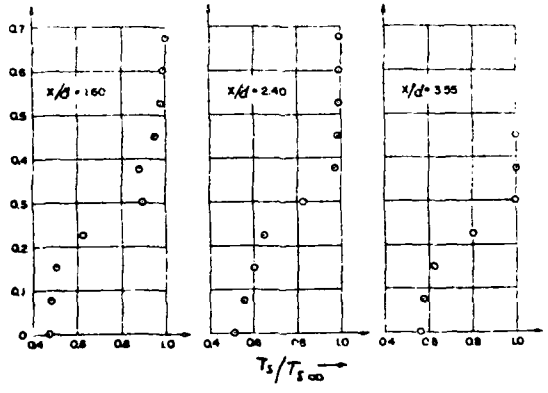

Fig.III.24. Stagnation temperature profiles (M_∞ = 11.8, $T_w/T_{w\infty}$ = 0.32, Re_∞ = 6.0 x 10^5/ft) [Zakkay and Cresci (1966)].

The base pressure distribution and radial distribution of static pressure are shown in Fig.III.25 and III.26, respectively. The base pressure data in Fig.III.25 are only repeatable to within $\pm$ 10 % because of the extreamely low pressure in the base region. The abrupt changes in static pressure in Fig.III.26 correspond to weak shock.

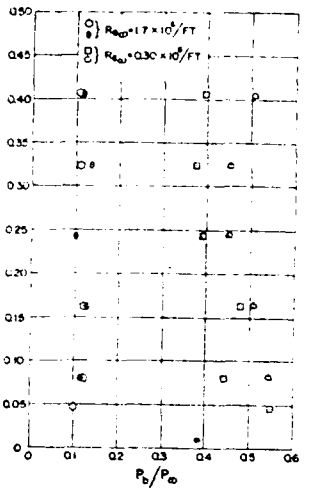

Fig.III.25. Base pressure distribution (M_∞ = 8.0) [Zakkay and Cresci (1966)].

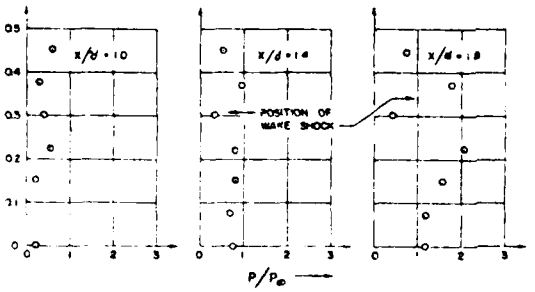

Fig.III.26. Radial distribution of static pressure (M_∞ = 8.0) Re_∞ = 1.7 x 10^6/ft.
Zakkay and Cresci (1966) .

The center line variation of stagnation temperature and radial distribution of stagnation temperature are shown in Fig.III.27 and [illegible], respectively

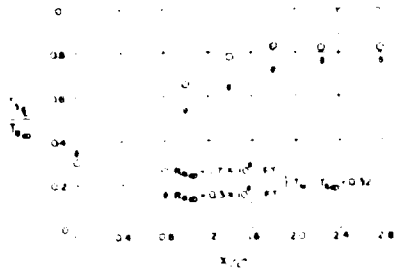

Fig.III.27 Centerline variation of stagnation temperature (M_∞ = 8.0) [Cakkay and Cresci (1966)].

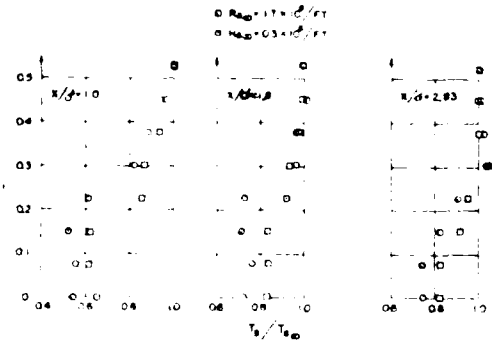

Fig.III.28. Radial distribution of stagnation temperature (M_∞ = 8) [Cakkay and Cresci (1966)].

In Fig.III.27, center line variation of stagnation temperature for both a laminar and turbulent flow condition on the model base indicates that the stagnation temperature in the recirculation zone did not vary much within the Reynolds number range tested. As seen in Fig.III.28, the profiles corresponding to the turbulent boundary layer at the body shoulder become fuller than those corresonding to a laminar boundary layer.

Furthermore, the following facts were obtained from the experiments. Downstream of the sonic point, temperature profiles are essentially unaffected by the model surface temperature. The $u_{CL} = 0$ in the recirculation zone is located at $x/d = 0.8$. The base pressure decreases substantially with increasing Reynolds number, from a value of $p_b/p_\infty = 0.8$ for Re_∞/ft of 6.0×10^5/ft to a value of $p_b/p_\infty = 0.10$ for Re_∞/ft of 1.7×10^6/ft. The static temperature in the near wake seems to be fairly constant and not strongly dependent on the free stream Mach number and Reynolds number. The temperature in the recirculation zone is effected strongly by the wall temperature.

1.3. Separation Shock (Lip Shock)

At the beginning of Chapter III, Hama's (1966) experimental investigation for the lip shock were presented. Further details of this shock wave structure and its effect on the flow field were described here. The analysis of the inviscid expansion of the boundary layer at the trailing edge of a slender blunt-based body was reported by Weinbaum (1966) and Weiss and Weinbaum (1966).

Weiss (1967) coupled this inviscid expansion to models of the shear layer and the recompression zone and thus obtained the complete solution of the near wake for a given base pressure. However, in these analyses, the upstream influence of the base pressure, the wave interaction in the supersonic rotational flow due to the expansion upstream, and subsonic region were neglected. The initial sonic stream line was simply expanded to the base pressure, and its final flow angle determined the initial inclination of the dividing stream line. In these analyses, the velocity and temperature profiles which layer near not be calculated, and this resulted in less accurate initial conditions for the shear layer analysis. Therefore, in order to remove these limitations and omissions, Weiss and Nelson (1968) developed a theoretical model and computed the pressure distribution upstream of a corner of blunt-base effected by the base pressure. The entire expansion is assumed to be inviscid, and the subsonic and supersonic regions of the boundary layer are treated with stream tube approximation and Prandtl-Meyer relation. By matching the stream function and the pressure on the initially sonic stream line, the expansion process upstream of the trailing edge and its location are determined. The extent of the upstream expansion increases linearly with the Mach number at the edge of the boundary for a Mach number greater than five. The base pressure influences the expansion process at a trailing edge for many boundary layer thicknesses upstream, [illegible] in a good agreement with the experimental data [illegible]. That, the computed pressure distribution upstream of

the corner can be used as the boundary condition for a detailed characteristic solution of the supersonic portion of the boundary layer.

Scherberg and Smith (1967) conducted an experimental investigation of the flow pressure structure of a supersonic flow over a rearward facing step. The results indicate that the corner expansion fan is not the linear Prandtl-Meyer fan, and lip shock emerging from the

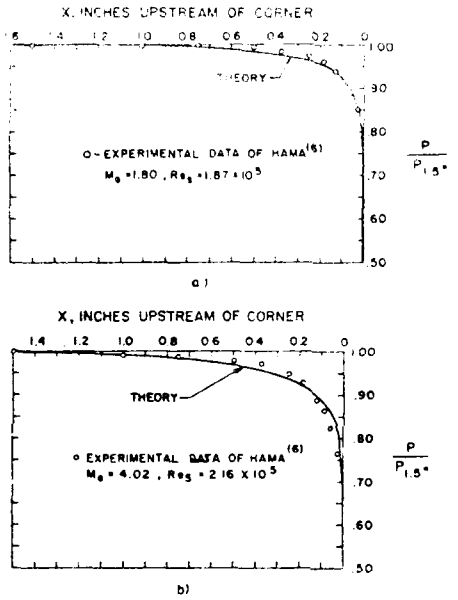

Fig.III.29. Comparison of the theoretical and experimental pressure distributions [Weiss and Nelson (1968)]. Experimental data [Hama (1966)]

separated shear layer may not be neglected. These findings are in agreement with those of Hama's (1968). Furthermore, the base pressure influence on the upstream flow of the corner was noted, and its magnitude was evaluated by Weiss and Nelson (1968).

The lip-shock flow structure was studied by means of shadow-

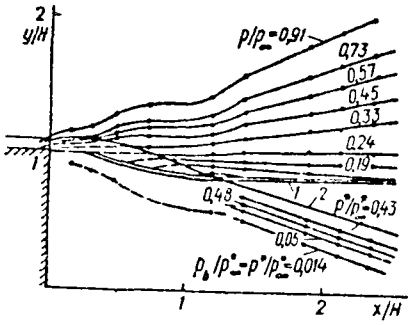

Fig.III.30. Field of pressure in the neighborhood of the protuberance when M = 2.5 [Chapman (1950)] (H = 11.26 mm):
1--Shock wave; 2--Boundary of the viscous layer.

graph photographs at M = 3.5, which show the lip-shock interaction with the shear layer downstream of the step and with reattachment shock. A strong pressure gradient from base pressure to free stream pressure was noticed in both horizontal and vertical directions immediately upstream and above the corner. The strength of the lip shock varied along its length, and its maximum strength was reached in the vicinity of the shock shear-layer intersection. The required flow development is that of overexpansion and pressure recovery through a shock, but the degree of overexpansion varies with the free stream pressure, the free stream Reynolds number and the step height.

Shvets and Shvets (1976) found the strength of separation shock for models with an after-body of varying degrees of converging slope. If the angle of convergence is smaller than the Prandtl-Meyer angle

required to reach the base pressure, then at the trailing edge the expansion is insignificant. Thus, the shock strength is small. If the angle of slope is larger than angle of expansion, then separation occurs, forming the shock wave. If the angle of slope is equal to the angle of expansion, i.e. base pressure is equal to the pressure in the boundary layer upstream of the trailing edge, then the flow separates with no formation of shock. The large overexpansion position is located over the area where the pressure curves bend, as shown in Fig.III.30.

The effect of turbulent boundary layer thickness on the pressure distribution downstream of a cone is shown in Fig.III.31 and indicates that with the increase of the turbulent boundary layer thickness, total pressure decreases.

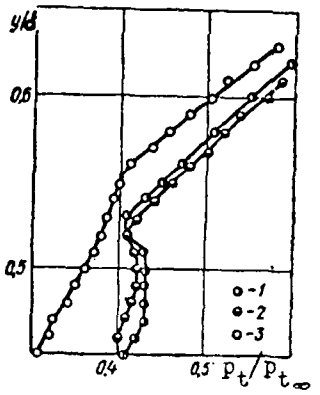

Fig.III.31. Profiles of pressure behind a cone ($\theta = 20^\circ$, $x/d = 0.5$, $M = 3$) [Shvets and Shvets (1976)]; 1-- $\delta/d = 0.02$; 2-- $\delta/d = 0.03$; 3-- $\delta/d = 0.05$.

The separation shock wave behavior at supersonic speed downstream of a wedge is compared with that of a cylinder. As Weinbaum (1966) indicates, the strength of the separation shock is attributed to the reflection of expansion in an entropy layer and the gradient entropy is caused by the vorticity of the inviscid flow and the presence of the viscous layer. The strength of shock of a cylinder is lower than that of a wedge because of smaller entropy and entropy layer by the shock wave, and its origin is located inside the viscous layer which is formed as the result of rotation of viscous flow and the shifting of the point of separation. For a cylinder, the expansion occurring close to the separation point is stronger compared to a wedge, a compression wave causing an initial section of more intense shock occurs.

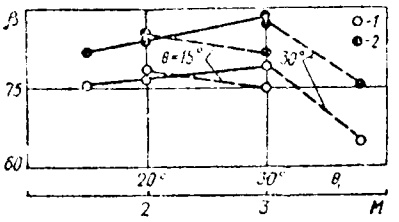

Fig.III.32. Values of angles between the boundary of an inviscid flow and a base section (1) and between a boundary discontinuity and a base section (2) (the solid lines correspond to $\beta = f(\theta)$, M = 3, the dashed lines -- $\beta = f(M)$ [Shvets and Shvets (1976)].

[illegible] the geometrical configuration of the wake downstream of wedge at various Mach numbers is shown in Fig.I.I.3(). With the same angle θ, between the boundary of inviscid flow and the base surface, the angle β between the separation [illegible] and the base surface decreases with increase of M, whereas [illegible] increases with increase of θ.

[illegible] upstream of a Step

[illegible] investigations on flow separation upstream of the step have been reported in past. Recently, further experimental [illegible] on this subject have been conducted in the USSR. Panov and Shvets (1966a, 1967) carried out experiments on flow separation upstream of a two-dimensional forward-facing step at subsonic, transonic and supersonic speeds, and with various step heights. As the pressure distribution in *Fig.III.33* shows, pressure upstream and close to the step is larger than that of the free stream in contrast to the lower base pressure downstream of the body.

In Fig.III.33 the pressure distributions at subsonic and transonic speeds show that the same step height H = 25 mm and $\delta_1/H = 0.1$, with increase of Mach number, p/p_∞ also increases. Furthermore, it is indicated that at M = 2.9 with the same boundary layer thickness $\delta = 5$ mm, if the shock wave interacts with the boundary layer, pressure rises more rapidly with the increase of the step height, starting from the lower pressure, compared to that of a lower step height, but at a location of x/δ_1, the values of p/p_∞ are the same, independent of H/δ_1.

Shvets and Shvets (1976) mention in their book that if the shock wave interaction with the boundary layer is absent, then the separated region spreads upstream, increasing the inclination angle θ, and likewise increases the pressure rise sharply, as compared to the case of a lower θ, although no separation point is indicated in the graph to support this remark.

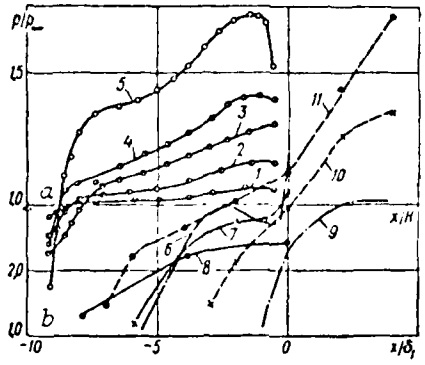

Fig.III.33. Distribution of pressure on the wall in front of a step (a) (H = 25 mm, $\delta_1/H = 0.1$)(1—5)(b), with flow past steps (δ_1--5 mm, M = 2.9)(6—8) and drop of discontinuity on the boundary layer (δ_1 = 5 mm, M = 2.9) (9--11) [Bogdonoff and Kepler (1955)].
1--M = 0.39; 2--M = 0.63; 3--M = 0.83; 4--M = 0.93; 5--M = 1.1; 6--H/δ_1 = 1.0; 8--H/δ_1 = 0.4; 9--θ = 7°; 10--θ = 11°; 11--θ = 15°.

Fig.III.34 shows the critical pressure drops in a function of the Mach number for flows past the forward facing step, the incidence shock, and the nozzle. This finding is presented by Panov and Shvets

(Mirels) by a straight line approximation in the range of $1.3 \leq M \leq 4$ as $p_2/p_1 = 0.315 + 0.675\,M$. Such a straight line relationship is confirmed by Petrov et al (1952) and Petrov (1969).

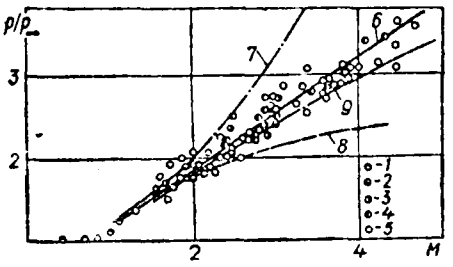

Fig.III.34. Dependence of a critical drop of pressure on the Mach number [Shvets and Shvets (1976)]: 1--separation in front of the step (M number equals 0.39; 0.63; 0.83 and 1.1); 2--data of G. Gedd, D. Kholder, A. Rigan; 3--data of R. Leyndzh, Kh. Roy [Panov and Shvets (1966a)]; 4--incidence of discontinuity; 5--separation of flow in nozzles (data of Arens, Spiegler, Foster, Stevens et al) [Panov and Shvets (1966a)]; 7-[Eggink (1950)]; 8--[Mager (1956)]; 9-[Arens and Spiegler (1963)].

1.5. Flow Separation Due to Short Blunt Bodies

Experimental programs to evaluate the base pressure effected by body configuration, Mach number and Reynolds number were carried out by flight tests so that model support interference in wind-tunnel tests may be eliminated and reliable data could be obtained for useful analysis.

Cassanto (1965) found that for a hemispheric nose cone at zero

[illegible] of attack, exposed to turbulent super- and hypersonic flow [illegible] base pressure is affected strongly by both cone angle and bluntness and the base pressure is governed largely by the local flow [illegible] the base [illegible] [illegible] given bluntness and free stream [illegible] [illegible] has a [illegible] [illegible] because the [illegible] [illegible] [illegible] local Mach number of a sharp [illegible] [illegible] [illegible] of base to free stream pressure is [illegible] higher or [illegible] the ratio of the local cone pressure to the free stream pressure for a blunt body can be slightly lower or higher than for a sharp body, depending upon bluntness. Thus, the product of these two ratios $(p_b/p_l)(p_l/p_\infty)$ where the subscript l refers to local on the cone, is such that a blunt body generally has a higher base pressure than a sharp body. The free-flight base center line pressure data of cones at zero angle of attack and M = 4–19 were correlated by Cassanto, Rasmusser and Coats [illegible].

For a sharp cone, the base pressure is strongly dependent on the Reynolds number and base pressure decreases with increasing the Reynolds number for laminar and turbulent flows, whereas for blunt cone base pressure it is relatively insensitive to the Reynolds number. Using the local Mach number, Reynolds number, physical and displacement thickness of a boundary layer, test data of p_b/p_l, is correlated in a function of M^2_δ (Re_δ) by a single curve for various bluntnesses and M = 4–19.

[illegible] measured the base pressure downstream of slender cone with a continuous dome after-body and compared it with base pressure downstream of slender cone with a flat [illegible] for the laminar flow, and at zero [illegible] base pressure is a function of r_{dome}/R_{base} [illegible] dome radius. Base pressure [illegible] base pressure was 20 % lower than [illegible] This behavior is not fully [illegible] explained in the [illegible] associated with the flow [illegible] for a flat surface, separation occurs at the sharp [illegible] of the juncture of the cone and base, but for a model with a dome, flow tends to follow the contour and stays attached longer before finally separating. Hama (1968) measured the base pressure increase with increasing dome radius at M = 4.5 on a two dimensional wedge having laminar or transitional flow and had results contrary to Cassanto et al's (1969) findings for M = 11.9 on a free-flight model in a laminar flow. A higher local Mach number tends to cause a higher flow turning angle, and hence the base pressure is lower for the dome model than for the flat base.

Using cone models of r/R = 0.25, $\theta = 50^{\circ}$, 60°, and 70° with axisymmetric boat-tailed after body (boat-tail angle $\gamma = 20^{\circ}$, 25° and [illegible]$^{\circ}$ experiments were carried out to evaluate the base pressure, the streamwise pressure gradient in the wake at supersonic, trasonic and subsonic speeds by Cassanto and Buce (1971).

At supersonic speeds as shown in Fig.III.35(a) , in all tests, with

an increase of the angle of attack, the base pressure decreases significantly.

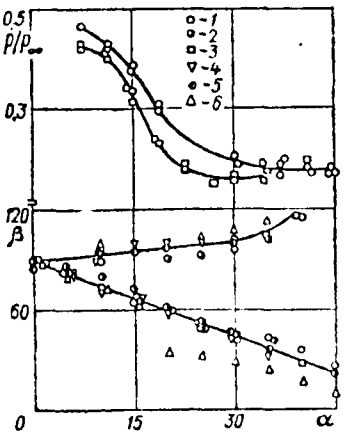

Fig.III.35. Dependencies of base pressure (a) and the position of the free viscous layer (b) on the angle of attack (M = 3) [Shvets and Shvets (1976)]:
1--θ = 50°; 2--θ = 60°; 3--θ = 70°;
4-- γ = 20°; 5-- γ = 25°; 6-- γ = 30°.

However, at transonic and subsonic speeds, as shown in Fig.III.36, values of static pressure, total pressure and reversed flow total pressure increase smoothly, although in the region of x/d = 1-2, they decrease slightly and then finally approach the magnitudes of static pressure of free stream at the reattachment.

In Fig.III.35(b), it is shown that variation of angle β, which is defined as the angle between the base section and tangent to the outer boundary of viscous layer at a distance of 0.25 d from the base section. On the windward side β decreases, approximately linearly, with increasing α, whereas on the leeward side, up to $\alpha = 30^\circ$, increases linearly with increase of α.

It was found also that the shape of models has little effect on β,

and therefore the position of the free viscous layer close to the short cone model of large angle can be determined approximately from the curves of Fig.III.36.

With the external supersonic flow, the static pressure in the recirculation zone is maintained approximately constant as seen in Fig. III.37. For pointed bodies, with an increase of free stream velocity, pressure in the compression zone increases sharply, shifting the maximum pressure zone close to the body.

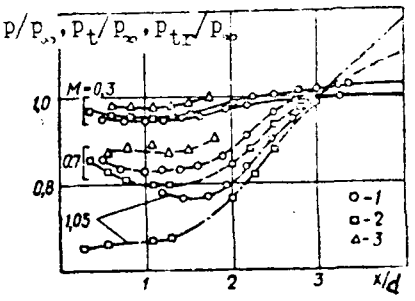

Fig.III.36. Pressures on the axis of a wake with subsonic and transonic flow (cone $\theta = 60^\circ$, $r/R = 0.25$) [Shvets and Shvets (1976)]:
1-- p --Static pressure;
2-- p_t --Direct flow;
3--p_{tr}--Reversed flow.

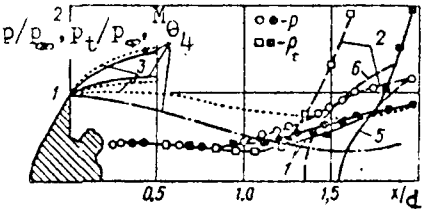

Fig.III.37. A near wake behind a blunt cone ($\theta = 60^\circ$, $r/R = 0.25$) [Shvets and Shvets (1976)]:
1--M = 2; 2--M = 3; 3,4--Boundaries of expansion waves and a viscous layer when M = 2 and M = 3; 5,6--Distribution of the Mach number on the axis of a wake when M = 2 and M = 3.

The pressure field at subsonic speed, shown in Fig. III.36, reveals the following phenomena: zero velocity line originates at the [illegible] the maximum thickness of the reverse flow zone is located at x/d = 1 and the maximum pressure gradient prevails in the mixing layer. The thickness of the viscous layer grows not much at transonic speeds.

The [illegible] subsonic flow pressure distribution [illegible] as it is shown in Fig. III.36. Toward the downstream the total pressure increases. Although within the viscous layer the total pressure is nearly constant normal to wake axis, its magnitude increases sharply above the viscous layer.

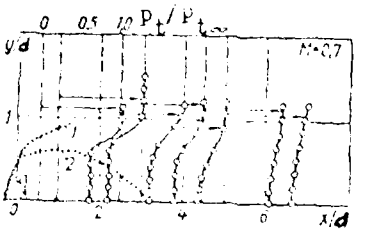

Fig. III.36. Fields of total pressure with subsonic flow (φ = [illegible], x/B = 0.25) [Shvets and Shvets (1976)]: 1--boundary of the wake region according to photographs of flow; 2--line u_x = 0 constructed according to measurements of p_t and $p_{t\infty}$.

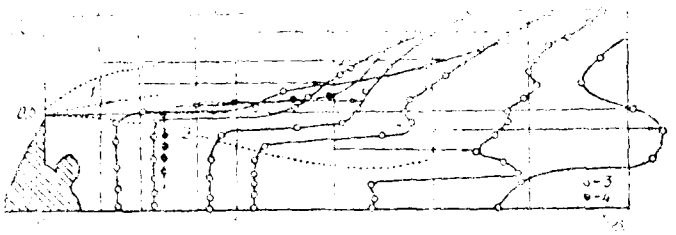

...s of ...ota... ...essures with supersonic
...he viscous layer

The photograph of Fig.III.40 shows clearly the curved expansion wave, viscous layer and trailing shock. Flow separated, at the corner, at all velocities tested. At subsonic speed, free vortices caused by separation are transferred downstream in a turbulent vortex layer. At transonic speed, flow velocity reached locally to supersonic velocity at the external boundary of the mixing layer and formed zones closed by the shock wave. At supersonic speeds, the separation zone dimension is reduced significantly.

Isayev and Shvets (1970), Panov and Shvets (1966b) and Shvets and Panov (1973) carried out experimental tests for two series of bodies in a wind tunnel.

One series of models consists of a basic cylindrical section and a leading section of various shapes such as conical, elliptical, flat faced with rounded leading lateral edges, in a range of r/R = 0-1, where r is the radius of the rounding of the leading edge and R is

[illegible] of the basic cylindar section, but the length of the main part of the models were equal to the diameters.

Another series of models consist of a body with a cone shaped [illegible] frustum, with 8^{o} conical angle, and leading segments of spheri- [illegible] form.

The measured base pressure data are compared with data obtained [illegible] and wind-tunnel tests are illustrated in Fig.III.41, where [illegible] a parameter of M, are shown in Fig. III.42.

In Fig.III [illegible] the measured M in a function of M_a for the el- [illegible] gional leading section are compared with the predicted data of Chu- [illegible]kin and Shulishnina (1961) for similar models.

Fig. III.40. Photographs of flow in a base region (cone $\theta = 10^{o}$, $r_b/r = 0.25$, M = 3, $Re = 2e^{5}$) [Shvets and Shvets (1976)]: 1--expansion wave; 2--viscous layer; 3--trailing edge discontinuity

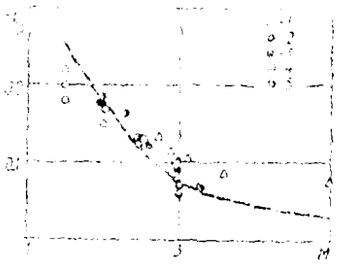

Fig.III.41. Base pressure for a body with small elongation [Shvets and Shvets (1976)].
1--elliptical leading section; 2--rounded section; 3--sectors of a body; 4--free flight [Chapman (1950)]; 5--tunnel testing [Chapman (1950)].

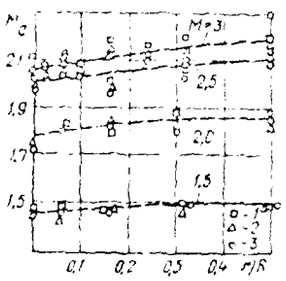

Fig.III.42. Dependence of the M_a number on the parameter of rounding r/R [Shvets and Shvets (1976)]:
1--0.4 R; 2--0.24 R; 3--0.12 R.

Fig.III.43. M_a number for elliptical leading section (dashed line--experiment, solid line--calculation [Chushkin and Shulishnina (1961)], t--ratio of semi-axes of an ellipsoid).

for a fixed value of t-, the ratio of semi-axis of ellipsoid- o
Ma increases with the increase of M. At the beginning the increase
is large, and then smaller, approaching to the asymptotic value for
$\infty \longrightarrow$ [illegible]. The asymptotic values of Ma are 2.5, 2.7 and 3.0 for
= [illegible] 1.0 [illegible] respectively.

[illegible] the base pressure [illegible]
[illegible] were [illegible] the [illegible]
[illegible] of Ma. The value of [illegible] corresponds to the
[illegible] of [illegible] Ma = 3., indicating that the base pressure of short bodies may
be determined, based upon the flow parameters on the trailing section
of the body.

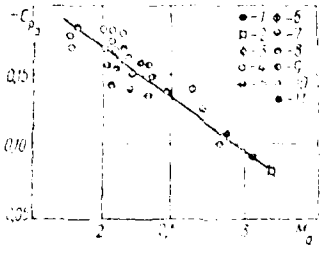

Fig. [illegible] Derived coefficient of base pressure (1--3--conical leading sections, 4--round sections, 5--11--elliptical sections) [Chvets and Chvets (1976)]:
1--θ = 10°; 2--θ = 30°; 3--θ = 60°; 5--t = 0.2; 6--t = 0.3; 7--t = 0.5; 8--t = 1.0; 9--t = 1.5; 10--t = 2.0; 11--t = 3.0.

[illegible] of flow between bodies

The problem of flow between the space of two bodies involving separation and reattachment is of practical interest to aircraft [illegible]. Recently in the USSR, attention has been paid to the [illegible] between two bodies, but omitting the upstream phenomena of [illegible]. If the front body is placed on the solid surface, then [illegible] separate on the surface, [illegible] of the front [illegible] to the [illegible] of the front body. Not considering this phenomena and concentrating on the problem downstream of a front body, Shilov (1969) studied supersonic flow around a disk (rear body) of smaller height behind the front body of larger height. Diagrams of such flows are shown in Fig.III.45.

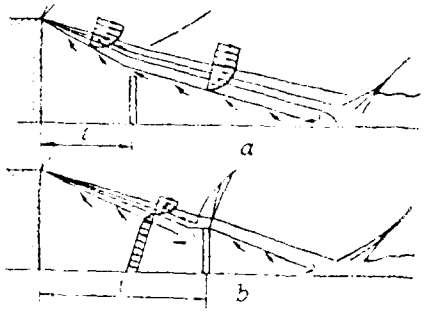

Fig.III.45. Diagram of flow past two closely positioned bodies [Shilov (1969)]; (l —Distance between bodies).

If the distance l between the front body base and disk is small, and is totally submerged into the separation zone as indicated in Fig.III.45a, then downstream of the disk, the flow behavior is considered to be that of the ordinary base flow, involving flow from the reattachment as well as upstream flow effected by the flow through

the gap between the external edge of the disk and the mixing zone. The turning of the external supersonic flow at the trailing edge of the front body, and pressure on both sides of the disk, are determined referring to the equilibrium position of the free boundary layer taking into the flow rate in the separation zone. If the distance ℓ is increased and flow rate through the gap is small, then external flow structure changes in the upstream area of the disk and flow reattaches to the disk as indicated in Fig.III.45b. Flow downstream of the disk is also considered as ordinary base flow, although the initial boundary layer thickness is thicker. The force acting on the disk increases, due to the change of flow momentum in the boundary layer entering the separation zone in front of the disk. But at a cetain length ℓ, the flow rate reaches its maximum due to the reverse flow. If this flow rate is smaller than that required to maintain the flow rate in the separation zone, then flow behavior suddenly changes and flow downstream of the front body becomes that of ordinary base flow and the disk is exposed to a non-uniform supersonic flow. Based upon such a model, the drag coefficient of the disk is computed in a function of ℓ and compared with experimental data as seen in Fig.III.46.

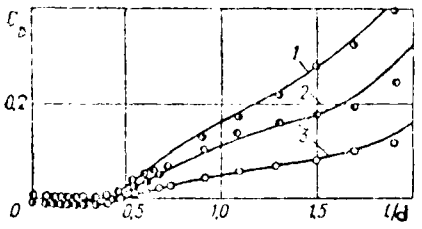

Fig.III.46. Drag coefficient of a disk with varying distance from a body (curves--calculations, [Shilov (1969)]: 1--M = 2, 2--M = 2.5; 3--M = 3.6.

Semonkevich (1969), in the study of supersonic flow between two bodies, assumed that the external inviscid flow separating from the trailing edge of the front body mixes with the fluid existing between the two bodies and forms a free boundary layer.

At the reattachment point on the rear body, the boundary layer flow is divided into two parts-one part flows away as external flow and another part, after impinging on the rear body, turns and forms a recirculatory flow, and its velocity depends on the body heights. In order to cause such a reverse flow, the reversed flow rate must be equal to the entrained flow rate along the internal boundary of the boundary layer.

Karpov et al (1968) and Cherkez et al (1970) computed the flow characteristics in the separation zone between two closely positioned coaxial bodies and found an equilibrium position of a free boundary layer.

The spread of this free boundary layer passing the rear body provides a flow rate in the separation zone equal to that entrained along the internal boundary of the boundary layer. Based upon this conjecture the angle of flow turning at the separation and a change in pressure are evaluated. For this analysis, flow parameters upstream of the separation are assumed to be known as evaluated by the external flow calculation over the front body. In order to describe the continuity, it is necessary to find the flow rate along the internal boundary according to boundary layer characteristics, to determine the relationship between the position of the boundary

layer relative to rear body, and to evaluate the flow rate entrained into the separation zone.

Fig.III.47, shows the base pressure coefficient, downstream of the front body, in a function of ℓ/d_{front} and in a parameter of d_{rear}/d_{front}, the ratio of diameters of rear to front body, referring to static pressure on the front body upstream of separation point. If $d_{rear} > d_{front}$, then with the increase of ℓ/d_{front}, the flow turning angle at the separation and base pressure decreases.

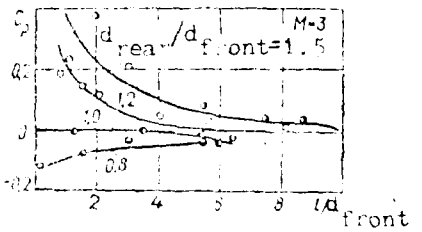

Fig.III.47. Dependence of the coefficient of base pressure on the distance between bodies (d_{read}/d_{front} -- relationship of the diameters of two bodies [Karpov, Semenkevich and Cherkez (1968)].

The non-dimensional critical length $\bar{\ell}_{cr} = \ell_{cr}/d_{front}$ at which the single separation zone is divided into two (because of the reattachment and subsquent reseparation on the floor surface or symmetry axis) is shown in Fig.III.48, in a function of M and in a parameter of d_{rear}/d_{front} by [Karpov et al (1968)].

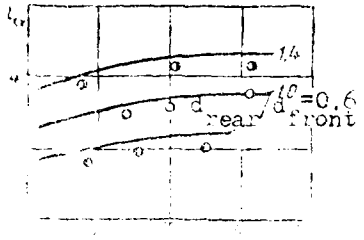

Fig.III.48. Value of the critical distance between bodies at which restructuring of flow occurs [Karpov, Semenkevich and Cherkez (1968)]

Gudryavtsev et al (1969) investigated the quasi-steady supersonic flow over closely positioned coaxial bodies. The flow parameters in the separated zone between two bodies depend on the velocity of separation, even if its velocity is very small compared to that of free stream flow.

Study of aeroballistic experimental results indicates that the restructuring process of cavity flow, from a single separated zone to two separated zones, is gradual, and $l_{cr} = 5 - 6\ d_{front}$, while for the statically model exposed to high speed flow, $l_{cr} = 3.5 - 4$ in agreement with the predicted value suggested by Karpov et al (1968).

Nikolaev (1971, 1973) established the engineering method to compute the pressure downstream of the body, and in the neighborhood of axisymmetry, by assuming that the inclination angle of the dividing stream line does not differ significantly from the inclination of tangential to the edges of two bodies.

Shvets (1971) obtained experimental data on flow in the space

between a cone and cylinder whose diameters and lengths were same, and plotted the pressure distribution on the support which holds the cone and the cylinder, as shown in Fig.III.49.

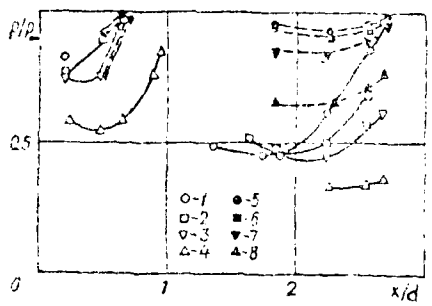

Fig.III.49. Pressure on the holder between a cone ($\theta = 10^{\circ}$) and a cylinder (solid lines correspond to M = 3, dashed lines correspond to $\bar{\ell} = L/d = 0.75$) [Shvets and Shvets (1976)]:
1— $\bar{\ell} = 0.2$; 2— $\bar{\ell} = 0.5$; 3— $\bar{\ell} = 0.7$; 4— $\bar{\ell} = 1.0$; 5—M = 0.4; 6—M = 0.7; 7—M = 0.8; 8—M = 0.9.

With approximately same ℓ/d, at supersonic speed, the pressure variation is more pronounced, compared to subsonic speed. For example, with $\ell/d = 0.7$, at M = 3, p/p_{∞} reaches its minimum value of $\sim$ 0.45 at x/d $\sim$ 2.2 and increases p/p_{∞} to 0.62 at x/d $\sim$ 2.75, whereas with $\ell/d = 0.75$, at M = 0.7, the minimum value of $p/p_{\infty} \sim$ 0.85 is reached at x/d $\sim$ 2.25 and $p/p_{\infty} \sim$ 1.0 is at x/d $\sim$ 2.75.

The Structure of Flow at Hypersonic Speeds

The separated flow at hypersonic speeds is characterized by certain [illegible] from those at a lower Mach number [illegible] separated flow phenomena, especially wake [illegible]

[illegible] explained as hypersonic [illegible] length. Since the near [illegible] is [illegible] the flow can be studied by using boundary layer equations.

Chernyshov, Fedotkin and Tolchkin (1977) systematically presented the investigations of other countries on hypersonic wakes in the "TsAGI Review of the Central Aero-Hydrodynamic Institute" (Tsentral'nyy aerogidrodinamicheskiy).

Shvets and Shvets (1976) described the hypersonic separated flow in their book Gasdynamic of Near Wake , frequently referring to recent articles of the AIAA Journal.

The significant changes in the structure of a laminar near wake [illegible] the Mach number varies from its small numbers to $M \simeq 7$, [illegible] hypersonic wake structure as McLaughlin et al (1971) [illegible]

[illegible] (1972) experimentally determined the streamlines, lines of constant total pressure, and temperature and positions of shock waves in the cross-stream of a slender cone, at $M_\infty = 7$ and at various angles of attack.

An attempt will be briefly made to describe the various features of hypersonic wake such as laminar, turbulent, shape, and heat transfer at the angle of attack.

.1 Laminar Wake

Lyman (1967) carried out the experimental studies of fluid mechanical structure of a laminar hypersonic wake downstream of a 9° half-angle sharp circular cone which was magnetically suspended and exposed to M = 16 helium flow at zero angle of attack. The emphasis of the investigation has been on gaining a fundamental understanding of the initial phases of development of the wake and to provide the information needed to construct fluid mechanical models.

The measured data of velocity, Mach number, temperature and pressure along the axis are shown in Fig.III.50, and III.51, and indicate the following flow features. No appreciable extent of constant axial static pressure in the recirculation zone exists. A maximum axial static pressure of 2.4 p_∞ is located at x/d = 0.75 where x and d are axial distance from the base of the cone and d is the diameter of base. Downstream of this, the pressure decreased to the free stream level at x/d ≃ 5. Downstream of x/d = 5, pressure remains approximately constant at a level about 15 % higher than normal p_∞. The base pressure is 1.58 p_∞. The wake stagnation point is upstream of x/d = 1 and sonic point on the axis at x/d ≃ 1.6. A rapid acceleration of axial flow downstream of the stagnation point takes place, due to a favorable pressure gradient and viscous mixing

At x/d = [illegible] the [illegible] velocity reaches [illegible] magnitude of 70 – 80 [illegible] the free stream value. The trailing shock wave originates at x/d = [illegible] [illegible] it emerges from the viscous wake at x/d = [illegible]. The far wake region [illegible] at x/d = [illegible] several wake diameters downstream of [illegible] where the trailing shock emerges from the viscous wake. The [illegible] far wake [illegible] only 20 [illegible] the viscous [illegible] is greater [illegible] order of magnitude. [illegible] assumption may be applied to analyze the [illegible] wake.

2.2 Turbulent Wake

The turbulent wake downstream of a cone at M = 6, and Re_{∞} = [illegible] x 10^{7} was investigated by Martellucci, Trucco and Agnone (1966) and the reached the following conclusions.

[illegible] of u = [illegible] is straight everywhere except on the symmetry axis and the angle of inclination to the symmetry axis is [illegible]°. Positions [illegible] the local Mach number equal to unity is at x/d = [illegible], wake neck [illegible] = [illegible], and the local critical point at x_c/d = [illegible] when Re_a = [illegible] and at x_c/d = 0.87 when $Re_a = 10^{7}$, indicating that x_c/d does not depend significantly on the Reynolds number. The subscript a refers to the condition on the trailing edge of the body. The shock was also straight and its inclination angle to the axis is 4°. It is noted also that the maximum static pressure on the wake axis is larger than p_{∞}.

2.3. Two-Dimensional Separation Flow

[illegible], Hankey and Dwoyer (1971) investigated laminar separated

[illegible] downstream of the rearward facing step, analytically and experimentally [illegible] separated flow. The pronounced downstream dis- [illegible]

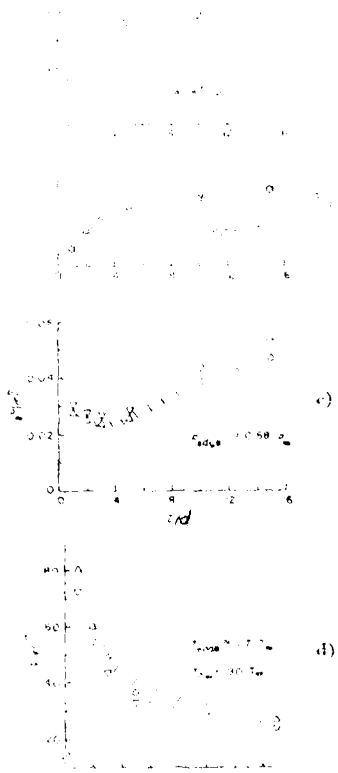

Fig. [illegible] Distribution of relative velocity [illegible], the M number, relative temperature T/T and pressure [illegible] along the axis of the wake [illegible] [Murman (1960)] [illegible] $M_e \approx$ 1.[illegible] $T_e \approx 1.7\ T_\infty$ [illegible] $p^*_\infty =$ [illegible]

[illegible]. However small, this "upstream" feeding will [illegible] the flow near the trailing edge of the wedge. The [illegible] [illegible] the expanding [illegible]

[illegible] flow field [illegible] characterized by a strong [illegible] inviscid interaction and the inertia and viscous effects are of equal order of magnitude. In the viscid dominated region the method of rotational characteristics is applied for their analysis by assuming that the straight stream line is parallel to the trailing plate, preceded by a straight dividing stream line. The impact pressure distributions downstream of the step are calculated from the characteristics solution. The experiment shows that the separation point is located at a distance [illegible] 0.063 in. downstream of the corner [illegible] the vertical face of 0.35 in. height, and the reattachment [illegible] in. downstream of the step.

[illegible], show the pressure distributions along the inviscid [illegible] downstream of the step. It is [illegible] [illegible] [illegible] that [illegible] rather [illegible] [illegible] the pressure to a peak beyond which it approaches [illegible]. The [illegible] deviation of pressure data at the [illegible]

discontinuity in ... [illegible] ... probably due to the inter-
action between the ... [illegible] ... and this pressure dif-
ference ... [illegible] ... flow.
However, the ... [illegible] ... adjacent
... downstream ... [illegible] ... boundary
layer ... [illegible] ...
... flow downstream ... the forward ... [illegible] ...
... conventional boundary layer analysis.

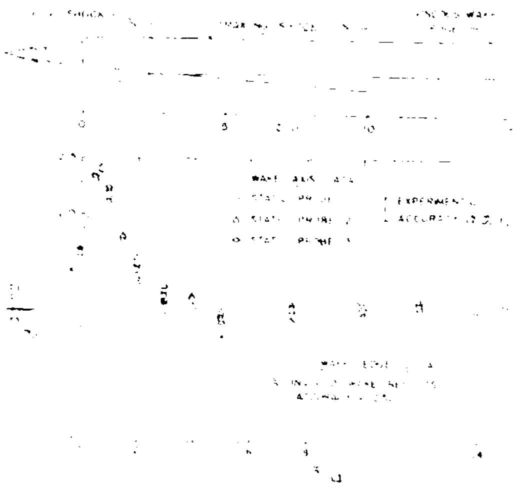

Fig. [illegible]. Change in static pressure along the axis of the wake ... [illegible] ... [Murman ([illegible])].

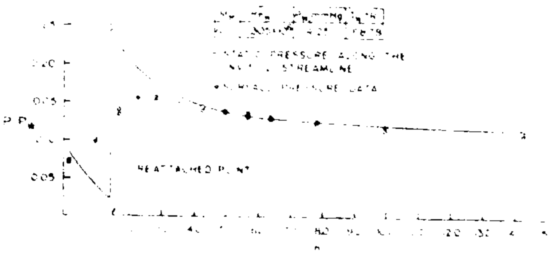

Fig. [illegible]. Change in static pressure downstream from a protuberance (M = [illegible], Re = 0.31·10^[illegible], H = 8.9 mm) [Shang, [illegible]sey and [illegible]wover (1971)] (solid lines--calculation of static pressure along the boundary line of the current of an inviscid flow; dots--experimental data on pressure on the surface; C--the point of reattachment).

AD-A099 165 CATHOLIC UNIV OF AMERICA WASHINGTON D C DEPT OF MECH--ETC F/G 20/4
RECENT DEVELOPMENT IN FLOW SEPARATION.(U)
MAY 80 P K CHANG AFOSR-78-3636

UNCLASSIFIED AFOSR-TR-81-0451 NL

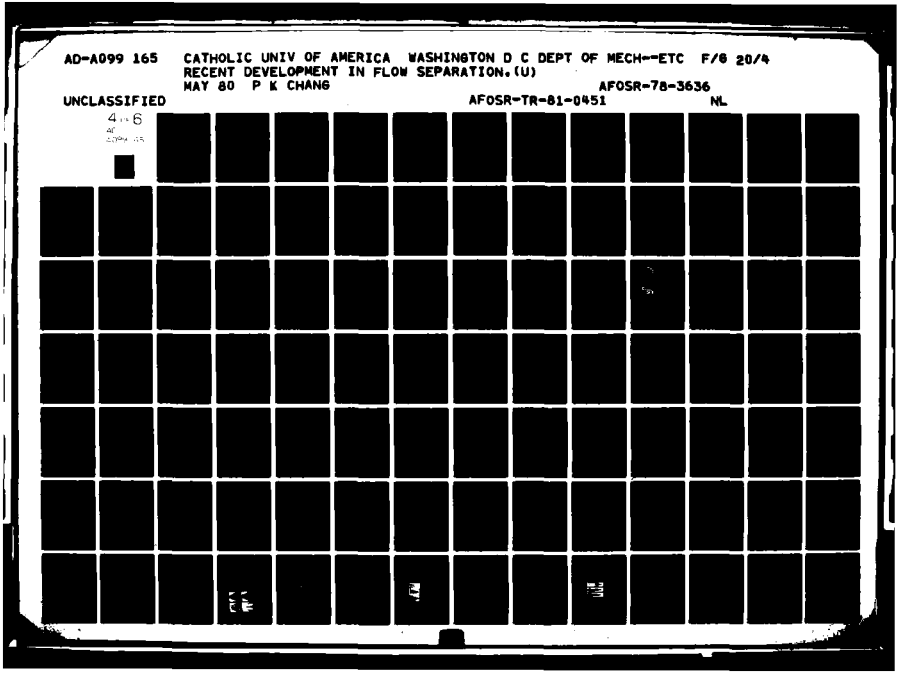

Impact pressure comparison between experimental and rotational characteristics computations show that the majority of the separated flow field is primarily an inviscid phenomena and the viscous dominated region is rather limited, but the separated flow region exerts an influence over the entire flow field. Although the rotational characteristics can be applied successfully for inviscid flow, the complete flow field must be determined by a numerical matching scheme between the imbedded viscous flow, evaluated by the Navier-Stokes' equations.

It was noticed that in the separated region, except for the leading-edge shock, no obvious shock waves were detected. A single reattachment shock wave was barely detectable and its strength increased as it propagated downstream. The expansion fan emerging from the corner eventually reaches the leading edge shock, and the gradient of the impact pressure in the plane perpendicular to the testing surface decreased considerably. No uniform flow field existed between the leading shock and reattachment shock.

Shang and Korkegi (1968) measured the pressure distribution downstream of a rearward facing step at angles of attack. The model consisted of a wedge of 12° half-angle, followed by a flat plate, recessed to form a step with respect to the wedge base.

Fig.III.53, shows p/p_w, in a function of x/H for $5 < M_w < 7.5$ at various angles of attack. The subscipt w, refers to wedge and symbols x and H refer to distance from the base and height of the base, respectively.

The following significant facts may be noted. The distributions of the non-dimensionalized pressure, with respect to wedge pressure, are essentially coincident up to a point, beyond the peak value. Furthermore, the reattachment point appears insensitive to the variation in the Mach number after the initial decrease following the peak pressure, the levels of the various curves tend to approach different asymptotes. For purposes of comparison, the isentropic asymptotes for the various configurations are indicated in Fig.III.53.

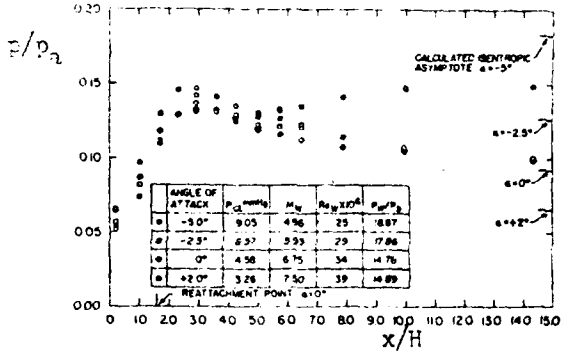

Fig.III.53. Pressure distribution downstream of the rear-facing step at various incidences [Shang and Korkegi (1968)] .

Dewey (1965) measured, at hypersonic speeds, the surface pressure distribution on a circular cylinder as a function of Re_{od} (based on stagnation conditions and diameter) as shown Fig.III.54.
The most striking feature is the diminishing extent and finally, the disappearance of the region of constant pressure as the Reynolds number decreases. The assumption of constant pressure mixing implies that the surface pressure downstream of separation is constant and equal to

the value at the outer edge of the shear layer. As seen in Fig.III.53, this assumption is not valid at the lowest Reynolds number tested, but a large region of constant pressure is anticipated for $Re_d \geq 5 \times 10^4$. A second important result is that the separation point, which is located very close to the surface pressure minimum, moves aft with a decreasing Reynolds number. The pressure rise required to separate the boundary layer increases with a decreasing Reynolds number, allowing the boundary layer to penetrate more and more deeply into the base region. The third significant finding is that there is a small pressure rise downstream of the cylinder. This region of increased pressure extends about $\pm$ 15° on either side of the axis, indicating that the reverse flow stagnates in the base region.

2.4. Effects of the Angle of Attack

Wu and Behrens (1972) measured mean flow properties of hypersonic wakes downstream of a 20° total angle wedge at M = 6, Reynolds numbers 7000 - 55000 based upon wedge base height and at various angles of attack up to 25°.

The near and far wake structures, as well as streamlines and velocity profiles over a downstream distance of 60 base heights, were determined. Separation on the leeward surface occurs at $\alpha > 17°$, and the near wake flow field changes accordingly. In the laminar wake flows, the wake width, minimum velocities and maximum temperature change little with the angle of attack. In the transitional wake, a

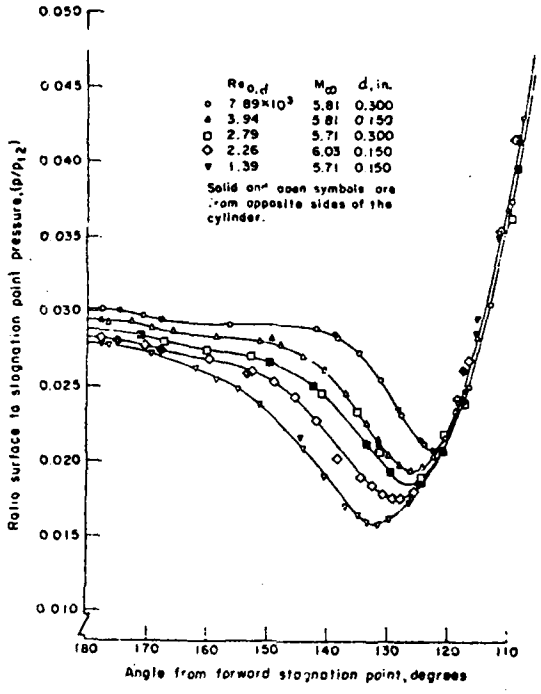

Fig.III.54. Distribution of pressure on the surface of a cylinder in the area of separated flow (M = 5.8) [Dewey (1965)]:
1--$Re_d = 7.8 \cdot 10^3$;
2--$Re_d = 3.9 \cdot 10^3$;
3--$Re_d = 2.7 \cdot 10^3$;
4--$Re_d = 2.2 \cdot 10^3$;
5--$Re_d = 1.3 \cdot 10^3$.

"breakaway" phenomena is observed and the transition moves flow upstream as the angle of attack increases. At the angle of attack, the flow phenomena over a two-dimensional surface and axisymmetric body are quantitatively different. Flow over the cones causes a very thick boundary layer on the leeward side even at a relatively small angle of attack. Thus, in the near wake, steeper gradients in velocity and temperature occur on the windward side, but not on the leeward side when they occur in the wake flow of a wedge at angle of attack. Tje inviscid wake flow parameters: wake static pressure, velocities, Mach number, and temperature at the edge as well as the flow inclination in real flow compare favorably with the simple inviscid shock expansion model for $M = 6$ and $\alpha \leq 25^{\circ}$.

The close correspondence between the simple inviscid shock-expansion model and the real wake outside the viscous wake for $M = 6$, $\alpha \leq 25^{\circ}$, indicates that the inviscid far wake is determined mainly by the relative strengths of the leading edge shocks. The locations of wake edges are determined by the intersection of the tangent of the maximum transverse gradients and the wake edge levels of the pitot pressure traces. The wake thickness is obtained as the width between these intersections on the leeward and windward sides. The transition moves upstream as the angle of attack is increased for the same Reynolds number. At a small angle of attack, the near wake structure is very similar to that of a symmetric wake. The boundary

layers separate at both trailing edges of the wedges and coalesce at about three-quarters of the base height downstream, and as the angle of attack increases, the recirculation region moves toward the leeward side. When $\alpha > 17.5^{\circ}$, flow separates on the leeward surface and the recirculation region extends from base to leeward side. Separation moves upstream with an increase of the Reynolds number.

The structure of a typical near-wake flow field at $\alpha = 25^{\circ}$ is shown in Fig.III.55.

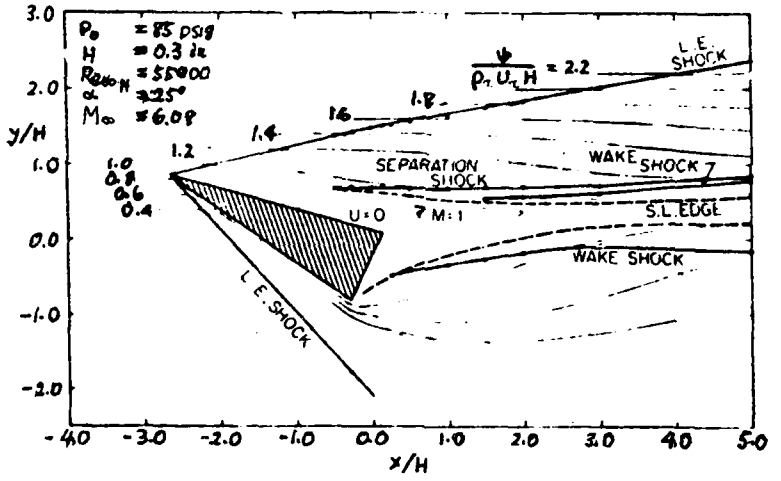

Fig.III.55. Flow in a wake behind a wedge with an angle of attack 25° ($\theta = 10^{\circ}$, M = 6, Re_H = 55,000) Wu and Behrens (1972) : 1--shock in a wake; 2--boundary of the field of viscous flow; 3--shock caused by separation.

Some important features of the wake geometry, such as the shock wave location, the shear layer edges, the sonic line contour of zero-velocity and the stream lines are seen in Fig.III.55. The stream line curvature near the windward trailing corner clearly indicates the strong pressure gradients in this region. At four or five base heights downstream of the base, the flow in the viscous wake is nearly parallel to the free stream direction. In the far wake flow field, the overshoot of a wake static pressure exists which depends strongly on the angle of attack; the higher the angle of attack, the larger the overshoot. The viscous wake edge values of the velocity, the Mach number and the temperature are very close to the upstream conditions for all angles of attack on the leeward side, and change considerably on the windward side with the angle of attack.

2.5. Shape of Wake

Waldbusser (1966) investigated the geometry of the laminar wakes downstream of three cones: one pointed cone and two blunted cones with a nose-to-base radius ratios of 0.035 and 0.3.

The diameter and location of the neck in showngraph photographs were determined at the intersection of the trailing wake shock and edge of the viscous core. Measured neck data indicate that neck diameter is strongly effected by M_∞, the ambient pressure and the model size but neck diameter normalized by the base diameter δ/d is a function only of M_∞ and $Re_{d\infty}$ as shown in Fig.III.56. An increase of $Re_{d\infty}$ at

constant $Re_{d\infty}$ results in a decreased δ/d. No effect of the cone angle, the bluntness ratio, the nose shape or the body size was discernible within the limits of tests available. Distance to the neck increases linearly with increasing M_∞, not effected by $Re_{d\infty}$, nose bluntness, body size, cone angle or nose shape in the range of $6.5 \times 10^4 \leq Re_d \leq 1.2 \times 10^6$. The shock origin is located at the

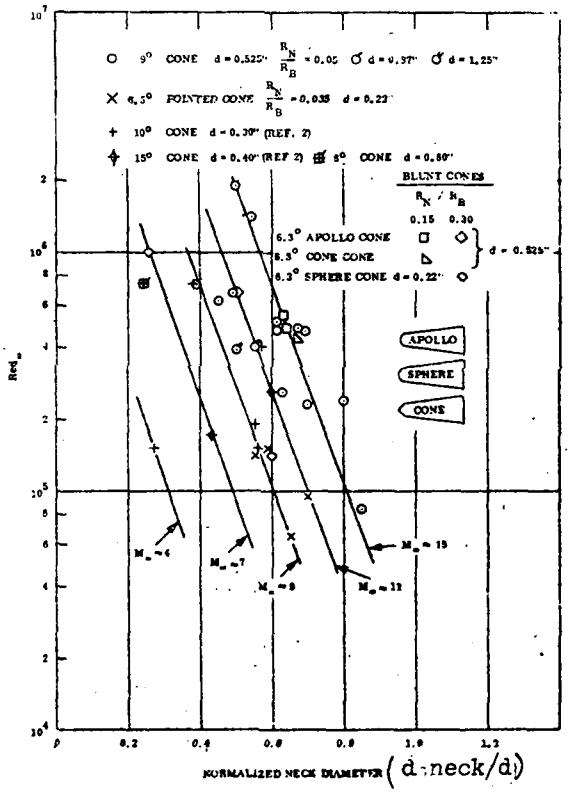

Fig.III.56. Diameter of the wake neck behind cones (θ = 6-9°, r/R = 0.15-0.3) [Waldbusser(1966)] ; 1--M = 4; 2--M = 7; 3--M = 9; 4--M = 11; 5--M = 15.

point where the continually coalescing compression waves (was not visible on a shadowgraph) produce a density gradient large enough to become observable on the photograph. Distance to the shock origin increases with increasing M_∞ . The shock origin with respect to the circumference of the model is located by the angle, which is defined as an angle in a meridional plane between the straight line from the aft end of the conical surface parallel to the body axis, and the line from this same point to the origin of the wake shock.

With an increase of M_∞ , γ decreases. The shear layer is approximated by the flow region which is bounded by a line between the edge of the boundary layer and the edge of the neck and a line between the cone shoulder and a point somewhat upstream of the measured shock origin.

Levensteins and Krumins (1967) studied the base flow geometry by optical observation using titanium cones of a 9° half-angle with various bluntnesses in the range of $6 < M < 15$ and $2 \times 10^4 < Re_d < 1.3 \times 10^6$. The origin of recompression shock and location of neck are given by

x_s--- axial distance from the base to origin of the recompression shock, which is considered to be indicative of the location of the rear stagnation point.

x_n--- axial distance from the base to the wake neck.

The widths of wake flow at x_s and x_n are denoted by δ_s and δ_n respectively:

Then, x_s/d and x_n/d, δ_s/d and δ_n/d are plotted in a function of

Re for cone of 6.3° half-angle at M ≃ 9, for laminar and turbulent flow as shown Fig.III.57.

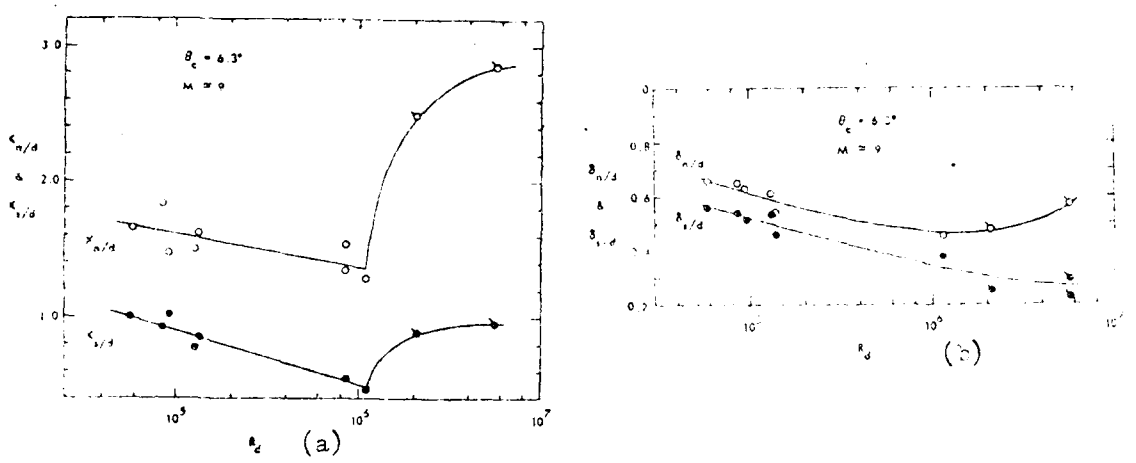

Fig.III.57. The effect of the Re number calculated according to the diameter of the basic of a cone on the geometry of flow in the base region (θ = 6°18′, r/R = 0.05, M = 9) [Levensteins and Krumins (1967)] 1--laminar flow, x_s/d, δ_s/d; 2--laminar flow, x_n/d, δ_n/d; 3--boundary layer on the cone is turbulent.

As long as flow is laminar, the whole base region decreases in size with the increasing body Reynolds number, but the size of the base region increases when the boundary layer on the cone is turbulent. The distance between the recompression shocks at their origins δ_s/d decreases with increasing Re_d, even in the turbulent base flow where other three distances x_n/d, x_s/d and δ_n/d increase with Re_d.

Koch (1967), using schlieren photographs, studied the wake neck geometry downstream of 10° half-angle cone of 1.75 in a base diameter with a 0.005 in. nose radius at the average free stream Mach number of 5.2, $3.8 \times 10^4 < Re_d < 4.65 \times 10^6$, and at average angle of attack less than 2°. The velocity was selected so as to attain hypersonic con-

ditions without causing the bow shock to lie so near the model surface that boundary layer details would be difficult to see in schlieren picture.

Koch (1967) found that wake-neck geometry was effected by the Reynolds numbers, as shown in Fig.III.58.

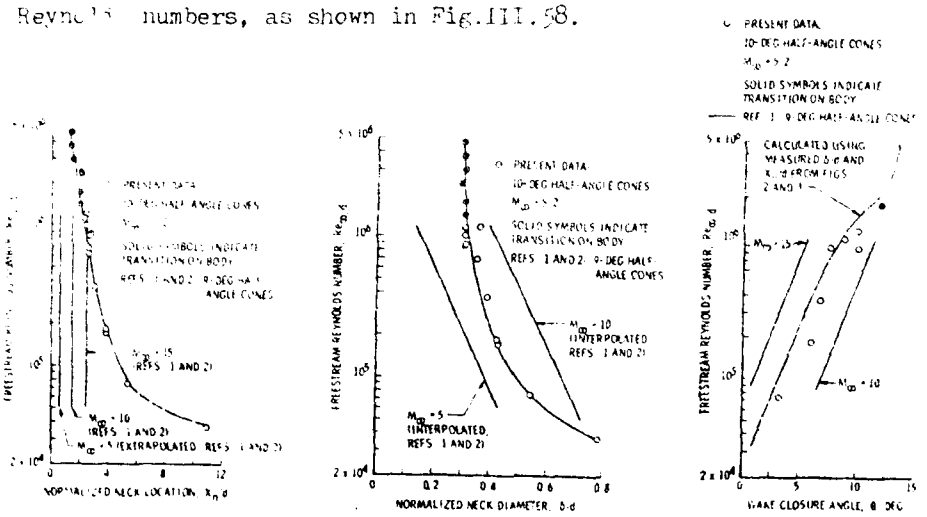

Fig.III.58. Configuration of a wake behind a cone as a function of the Re number of an unperturbed flow (cone with half-angle 10°, M=5.2, θ--angle of contraction [Koch (1967)]. Ref 1 - [Waldbusser, E(1964)] "Geometry of the Near Wake of Pointed and Blunt Cones" General Electic Fluid Mechanics Component Data Memo 1:19. Ref 2 - [Waldbusser (1966)]

As seen in Fig.III.58a the neck location is considerably moved rearward as Reynolds number decreases, but Waldbusser (1966) did not indicate such a movement. The normalized neck diameter tends to remain constant at about 0.3 above a free stream Reynolds number of one million, as Fig.III.58 indicates. The wake-closure angle, measured at the midpoint of the distance between the body base and the neck, is shown in Fig.III.58c. If the free shear layer is assumed to be straight,

then this angle can be calculated from the measured neck diameter, and its location using the following equation:

$$\gamma = \tan^{-1}\left[\frac{(1-\delta/d)/2}{x_n/d}\right]$$

A comparison of the measured and calculated values indicates that the assumption of a straight shear layer is a reasonable simplication for the tested flight conditions.

3. Oscillation in a Near Wake Boundary Layer

In the separation zone, and base downstream of a body, oscillation of pressure and dynamic pressure occur, causing significant dynamic load, and effecting the aerodynamic characteristics. For a rocket, the thrust force is affected by base pressure change, which depends on many factors, such as, boundary layer separation from the body, the downstream stagnation zone, the jet engine exhaust gas and their interaction with external flow, etc.

V.W.Kuptsov, Yu D.Vinogradov and A.F.Kulyabin, et al, studied base pressure, analyzing the possible causes and characteristics of oscillations.

Since the problem of near wake flow oscillation is complex, it is advisable to investigate separately the effects of different factors on the base pressure.

The free viscous layer in near wake is formed by the boundary layer flow on the upstream body surface.

Associated with the irregular turbulent motion is not only an aero-

dynamic noise, but also a fluctuating pressure field, and the pressure on the material surface can produce a significant effect if flight vehicles operate in the regimes of large dynamic pressure. Random forces may cause fatigue failure in a structure as well as undesirable levels of structural vibrations.

Hence, the following investigations of Willmarth and Wooldridge (1962) and Kistler and Chen (1963) are of interest. Willmarth and Wooldridge (1962) measured mean square pressure, the power spectrum of pressure, the space-time correlation of the pressure parallel to the stream and the spatial correlation of pressure traverse to the stream, etc. of the turbulent pressure field at a wall, beneath a five-inche thick turbulent boundary layer, produced by natural transition on a smooth surface. The root-mean-square (rms) wall pressure was 2.19 times the wall shear stress and the power spectra of the pressure were to scale with the free stream speed and the boundary layer displacement thickness.

The space-time correlation measurements parallel to the stream direction exhibit maxima, at certain time delays, corresponding to the convection of the pressure-producing eddies at speeds varying from 0.56 to 0.83 times the stream speed. The convection speed u_c may be defined as the quatient of the transducer separation Δx and the time delay at the maximum of the correlation. The lower convection speeds are measured at small spatial separation of the pressure transducers, or when only the pressure fluctuations at high frequencies are correlated and higher convection speeds at large spatial separation of the pressure transducers, and/or, when only low frequencies are correlated. A pre-

ssure-producing eddy of large or small wave length λ decays and disappears after travelling a distance of about 6λ .

Both the transverse and the longitudinal scale of the pressure fluctuations were of the order of the boundary layer displacement thickness, and the transverse and longitudinal scales of both large-and small-scale wall pressure fluctuations were approximately the same. The results of Kistler and Chen's (1963) measurements of the pressure fluctuations by a turbulent boundary layer on a solid in a range of M = 1.33 - 5.0 are as follows.

The major effect of increasing the Mach number is to decrease the length scale of the pressure field, and the integral scale of the pressure field and the integral scale of the wall-pressure fluctuations change, from 16% of the boundary layer thickness at M = 1.33, to 0.06% at M = 4.54. The root-mean square (rms.) values of the pressure are proportional to the local mean shear for all Mach numbers, and the proportionality constant changes from about 3 for subsonic boundary layer to about 5 for Mach numbers greater than 2. The space-time correlation with space separation in the direction of the mean flow are characterized by a convection speed, and this speed falls from 0.8, if the free stream velocity at M = 1.33, to 0.6 at M = 5. The peak value of the correlation coefficient falls to one-half for a spatial separation of the measuring points of two-tenth of boundary layer thickness.

The intensity of fluctuation increases in the transition region and grows significantly in the flow passing over protuberance on the surface and forming the local separation zone. For supersonic flow,

strong pressure fluctuation occurs if shock wave interacts with boundary layer. Because the pressure fluctuation in the boundary layer effects the base pressure fluctuation, it is necessary to investigate the fluctuation phenomena on the body surface to analyze the base pressure problem.

Schloemer (1967) investigated the effects of pressure-gradient on turbulent boundary layer wall-pressure fluctuations in a low-turbulence subsonic wind tunnel.

By examining the effects of mild pressure-gradients, both adverse and favorable, on the turbulent boundary layer pressure fluctuations and comparing with zero pressure-gradient, it was found that:

1) The most stricking differences are the change in convection velocities due to a distortion of the mean velocity profiles which are caused by the imposed pressure-gradients. Convection velocity ratios u_c/u were higher in the favorable pressure-gradient and lower in the adverse pressure-gradient, when compared to zero pressure-gradient.
2) Convection velocity increases with longitudinal separation, and decreases with the increasing frequency for adverse and favorable pressure-gradients as well as the zero pressure-gradient.
3) Loss of coherence, or decay of a particular frequency component along the longitudinal direction, was faster in the adverse case compared to zero pressure-gradient. The decay rate is slower in the favorable pressure-gradient.

4) Lateral decay of a particular frequency component is not affected by pressure-gradient.

5) Root-mean-square pressure-fluctuation levels for broad frequency bands are larger in the adverse pressure-gradient and less in favorable compared to zero pressure-gradient.

6) The spectral density is altered reflecting the changes in longitudinal turbulent intensity with distance from the wall affected by the pressure distribution. When non-dimensionalized by δ^*, the adverse pressure-gradient spectrum is higher at lower non-diminsional frequencies than the zero pressure-gradient spectrum. Blyndze and Dokuchayev (1969) measured the spectra of pressure fluctuation in non-self-similar boundary layer of negative mean pressure-gradient showing that a non-dimensional spectral density is smaller the larger is the absolute value of the mean pressure-gradient, and this tendency prevails mainly at high frequencies. Downstream of fully developed turbulent boundary layer of zero pressure-gradient, redistribution of the energy of the pulsation motion occurs between the small-scale and large-scale components.

Smolyakov and Tkachenko (1969) studied the streamwise, transverse and diagonal spectra and phase velocities of turbulent pressure pulsations at zero mean pressure-gradient on the wall at $Re = 0.35\text{-}1.1 \cdot 10^8$.

The fluctuations in a thick boundary layer of natural transition from laminar to turbulent flow investigated by Kistler and Chen (1963)

are shown in Fig.III.59 , and space-time correlation in Fig.III.60.

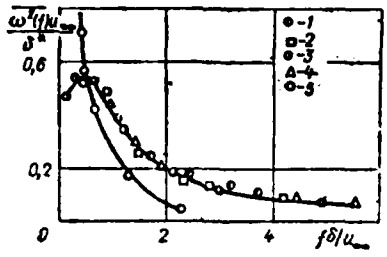

Fig.III.59. Fluctuation in a thick boundary layer: [Kistler and Chen (1963)]
1--M = 2.6, Re = $1.51 \cdot 10^4$;
2--M = 3.5, Re = $1.55 \cdot 10^4$;
3--M = 3.99, Re = $1.65 \cdot 10^4$;
4--M = 4.54, Re = $1.47 \cdot 10^4$;
5--M = 1, Re = 0.045 X 10^4.

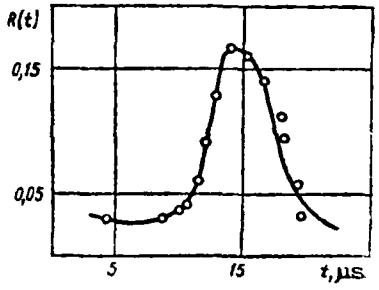

Fig.III.60. Graph of space-time correlation.
[Kistler and Chen (1963)]

In Fig.III.59 it is seen that $\omega^2(f)u_\infty/\delta$ is proportional to the distribution of oscillation energy in a function of the frequency, $f\delta/u_\infty$ where ω = 2π x frequency, δ is geometrical boundary layer thickness, and f is measured frequency and in Fig.III.60, t is time and R(t) is the correlation.

Fiszdon and Mello-Christensen (1960) and Trilling (1958) studied the oscillation in the interaction zone of shock wave with boundary layer.

Oscillations of a shock wave were forced and induced by a special device with a prescribed frequency. Such an experiment made it posible to model and study more precisely the oscillation parameters in the separation zone caused by oscillation of the incident shock.

Kistler (1964) measured the pressure fluctuations under a turbu-

lent, separated region upstream of a forward-facing step at Mach numbers of 3.01 and 4.54, finding that these pressures are considerably larger than the pressures produced by an attached boundary layer. It was shown that pressure fluctuations originate from two distinct causes; fluctuations due to turbulent free shear layer.

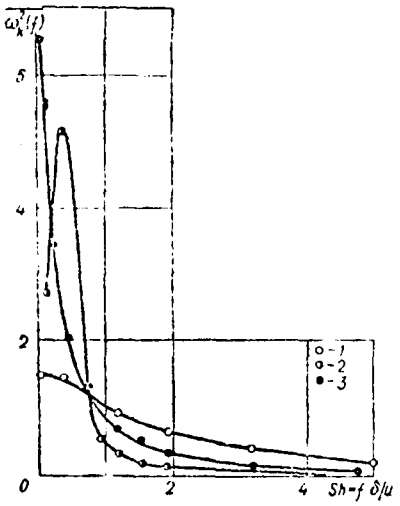

Fig.III.61. Fluctuation of pressure in front of a step (M = 3.01, u/δ = 16,000 1/s, $\omega_K^2(f)$ -- is a qualitative evaluation of distribution of energy of fluctuation according to frequency) [Kistler (1964)]
1--Boundary layer;
2--x/H - 0.8;
3--x/H - 3.

Kistler (1964) measured the spectra in the M = 3.01 separated flow at x = 1.55 and 6.06 in. and also upstream of the separation as shown in Fig.III.61 . In this figure in order to make the relative shapes more apparent, the ordinate is constructed so that the areas under the spectra are equal. The actual power spectra of the pressure can be obtained through normalization and multiplication by the value of p'^2, where p' is rms pressure level corresponding to the particular location.

It is apparent from these spectral shapes that there is more energy at the low frequencies in the separated region than in the attached boundary layer. The various spectra are not similar (affinely related). No spectra were obtained near the separation point because due to the

large fluctuations in the spectra at these low frequencies etc. and thus, it was difficult to obtain the quantitative measurements.

Kistler and Chen (1963) found that at M = 5 the convection velocity of the attached boundary layer is 0.6 of the free stream velocity. The remarkable result noted by Kistler (1964) is that the convection speed for the separated flow, which can be roughly described as the speed of the turbulent eddies most efficacious in producing the wall pressure, is in the direction of the external stream.

Vehicles involving flow separation at supersonic speed are effected by the large, time-dependent forces, and these forces are resolved into two components, a low frequency buffeting caused by changes in the geometry of the separated region, and wide-band fluctuations orginating in the free shear layer of the separated region. The magnitude of loading preduced by each component can be estimated by Kistler's (1964) analysis. The magnitide of the component of these forces may be minimized if the location of the separation line is fixed by tripping the small ramp so that the high pressure region has a fixed area and does not contribute an additional fluctuating force.

The fluctuating pressure occurring within the separated region are due to the combined action of the turbulent shear-layer and the recirculating flow, and therefore it appears that no method exists to drastically modify the fluctuation levels other than by avoiding the separation itself.

A high frequency of oscillation is recorded in the stagnation zone where probably the main source of oscillation is turbulent pulsation

in the stagnation zone boundary. The volume of fluid in the stagnation zone acts as "buffer" cushion, convecting and partially damping the oscillation parameters.

Measured data of pressure fluctuation of the turbulent flow on the wall by flight tests carried out by Speaker and Ailman (1966), Willmarth and Roos (1965), and by Bull (1963) and Kistler (1964) are shown in Fig.III.62.

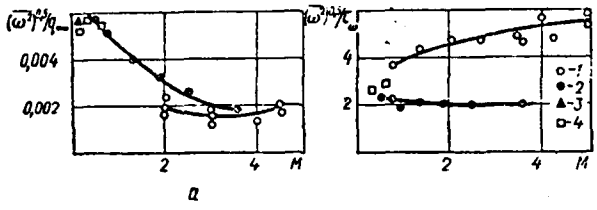

a

Fig.III.62. Data measurement of fluctuation of pressure on the wall with a turbulent boundary layer: [Shvets and Shvets (1976)]
1--[Kistler (1964)] ; 2--[Speaker and Ailman (1966)] ; 3--[Willmarth and Ross (1965)] ; 4--[Bull (1963)].

As the Mach number increases, $\overline{\omega^2}^{0.5}/q_\infty$ -value decreases, and this relationship can be approximated by

$$\overline{\omega^2}^{0.5}/q_\infty = 3.25\cdot10^{-4} + [5 + (M - 4)^2].$$

Speaker and Ailman (1966) investigated the pressure fluctuation on the wall downstream of protuberances at conditions of H/δ = 0.92-2.2 (where H is height of the protuberance and δ is boundary layer thickness) and M = 1.4 and 3.5. The mean quadratic value of fluctuation, directly downstream of the protuberance, was close to the value of turbulent boundary layer upstream of the protuberance.Fig.III.63

shows fluctuations downstream of projection of $H/\delta = 0.2\text{-}0.5$, exposed to an incompressible flow and downstream of protuberances. With the increase of the downstream distance from the protuberance, fluctuations increase, reaching a maximum value close to the reattachment point and then slowly decrease. The ratio of fluctuations at the reattachment point, to that upstream of the protuberance, can be evaluated by the following equation,

$$\frac{\overline{\omega^2}^{0.5}_{max}}{\overline{\omega^2}^{0.5}_{boundary\ layer}} = 1.356\sqrt{H/\delta^* + 1}$$

Fricke and Stevenson (1968) experimentally investigated the pressure fluctuations in a separated flow behind a thin fence, identifying the noise source with the flow. The similar relations of sound levels to frequencies and free stream velocities set up in the near field of a jet, or a conventional boundary layer, give reasonably accurate predictions of sound levels behind the fences. It was further found that the frequency spectra alter considerably with distance behind the fence, and that the maximum sound level behind a fence is about eight times that in a turbulent boundary layer with the same free stream dynamic head.

Yefimtsov and Karaushev (1970) and Yefimtsov and Shubin (1974) measured non-dimensional spectral density pulsation on the fuselage surface in a range of $0.5 \leq M \leq 1.6$.

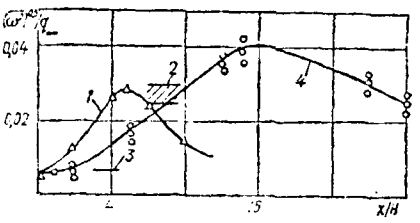

Fig.III.63. Distribution of fluctuations behind projections and protuberances :
1--M = 1.14 [Speaker and Ailman (1966)] ;
2--M = 0 [Greshilov et al (1969)] ;
3--Unperturbed boundary area, M = 1.4 [Speaker and Ailman (1966)] ;
4--M = 0 [Fricke and Stevenson (1968)] .

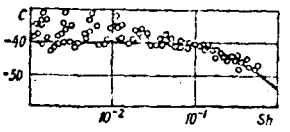

Fig.III.64. Dimensionless spectra of fluctuations of pressure near the walls in a turbulent boundary layer ($c = 10 \log \frac{\overline{w^2(f)}\, u}{q^2 \delta^*}$)·Sh = $f\delta^*/u$ [Yefimtosov and Karaushev (1970)] .

From Fig.III.64, it is apparent that a universal curve of $C = 10 \log \frac{\overline{w^2(f)}\, u}{q^2 \delta^*}$ with respect to $Sh = f\delta^*/u_\infty$ may be drawn in the range of $Sh > 0.3 \cdot 10^{-2}$, which corresponds to the range of $0.9 \leq M \leq 2$ of flight measurement by Belcher (1965).

In the range of $Sh \leq 0.3 \cdot 10^{-2}$ of supersonic flight regime, the scattering of the experimental data due to low-frequency pressure fluctuation increases, but it appears that the following equation may approximate the experimenta data.

$$\overline{w^2(f)}\quad u_\infty / q^2 \delta^* = A \left[1 + (f/fo)^2\right]^{-1}$$

where fo is the frequency at which spectral density drops by 3 db, $fo \approx 0.2\, u_\infty / \delta^*$ and $A = 10^{-4}$.

References

Abramovich, G. N. (1969), Prikladnaya gazovaya dinamika, (Applied Gasdynamics), Nauka Press, Moscow.

Arens, M. and E. Spiegler(1963), "Boundary Layer Separation in Over-expanded Conical Exhaust Nozzles," AIAA J., Vol. 1, No. 3.

Badrinarayanan M. A. (1961)."An Experimental Investigation of Base Flows at Supersonic Speeds,"J. Roy. Aero. Soc. 65/607

Batham, J. P. (1969), "A Reattachment Criterion for the Turbulent Supersonic Separated Flows," AIAA J., Vol. 7, No. 1, TN.

Bauer, A. B. (1967), "Some Experiments in the Near Wake of Cones," AIAA J., Vol. 5, No. 7, TN.

Blyudze Yu G and O. N. Dokuchayev (1969)."Measurements of Pulsation of Velocity and Pressure in Turbulent Boundary Layers,"AN SSSR MZhG 5.

Bogdonoff, S. M. and C. E. Kepler (1955), "Separation of a Supersonic Turbulent Boundary Layer," J. Aero. Sci., Vol. 22, No. 6.

Bull, M. K (1963),"Properties of the Fluctuating Wall Pressure Field of a Turbulent Boundary Layer," AGARD Dept. 455

Cassanto, J. M. (1965), "Ratio on Base Pressure," AIAA J., Vol. 3, No. 12.

Cassanto, J. M, Rasmussen, N. S. and J. D. Coats (1969), "Correlation of Free-Flight Base Pressure Data for M = 4 to M = 19," AIAA J., Vol. 7, No. 6.

Cassanto, J. M, Schiff, J. and E. J. Softley (1969), "Base Pressure Measurements on Slender Cones with Domed Afterbodies," AIAA J., Vol. 7, No. 8.

Cassanto, J. M. and P. Buce (1971), "Free Fall Stability and Base Pressure Drop Tests for Planetary Entry Configurations," J. Spacecraft and Rockets, p-790.

Chapman, D. R. (1950)."An Analysis of Base Pressure at Supersonic Velocities and Comparison with Experiments,"NACA TN 2137

Cherkez A. Ya et al (1970), "The Use of the Theory of Turbulent Streams for Analysis of Separated Flow Between two Bodies," Turbulentnyye techeniya,(Turbulent Flows) , Nauka Press, Moscow.

Chushkin, P. I. and N. P. Shulishnina (1961), "Tables of Supersonic Flow Around Blunt Cones," Tablitsy sverkhzvukovogo techeniya okolo zatuplennykh konusov , AN SSSR Publishers, Moscow.

Collins, D. J. Lees L. and A. Roshko "Near Wake of a Hypersonic Blunt Body with Mass Addition," AIAA J. Vol. 8, No. 5.

Dewey, C. F., Jr. (1965)."Near Wake of a Blunt Body at Hypersonic Speeds," AIAA J., Vol. 3, No. 6.

Eggink, H. (1950), "The Improvement in Pressure Recovery in Supersonic Wind Tunnels," ARC Tech. Rept., R & M. 2703.

Fiszdon W. and Mollo-Christensen (1960)."An Experimental on Oscillating Shock Wave Boundary Layer Interaction," JASS 1.

Fricke F. R and D. C. Stevenson (1968)."Pressure Fluctuations in a Separated Flow Region,"J. Aconst. Soc. America. 44/5

Greshilov,Ye.M. Yevtushenko and L. M. Lyamshev (1969)."Spectral Characteristics of Pulsations of Pressure near the Walls with Separation of the Boundary Layer Behind a Protuberance on a Smooth Wall," Akusticheskiy zhurnal 1.

Hama, R. R. (1966), "Experimental Investigations of Wedge Base Pressure and Lip Shock," TR 32-1033, Jet Propulsion Lab.

Hama H. R. (1968), "Experimental Studies on Lip Shock," AIAA J., Vol. 6, No. 2.

Herzog R. T. (1964)."Nitrogen Injection into Base Region of a Hypersonic Body," GALCIT Hypersonic Res. Proj. Memo 71 Calif. Inst. Techn.

Isayev, S. P. and A. I. Shvets (1970), "Flow in the Base Region with Supersonic Flow past Bodies," AN SSSR MZhG 1.

Karpov Yu L., Semenkevich Yu and A. Ya Cherkez (1968), "Calculation of Separated Flow between two Bodies," AN SSSR MZhG 3.

Khlebnikov, V. S. (1971), "Study of Flow in Front of a Sphere placed in the Wake of a Body with Supersonic Flow," Uchyenyye zapiski TsAGI, 1.

Khlebnikov, V. S. (1973), "An Engineering Method of Calculation of Pressure and Heat Flow with Combined Supersonic Flow past two Bodies," Trudy TsAGI Works of TsAGI , TsAGI Publishers, Moscow.

Kistler A and W. Chen (1963)."The Fluctuating Pressure Field in a Supersonic Turbulent Boundary Layer," J. Fluid Mech. 16. 1.

Kistler A. L. (1964)."Fluctuating Wall Pressure under a Separated Flow," J. Aconst. Soc. America 36/3

Koch, K. E. (1967)."Supersonic Cone Wake-Neck Geometry," AIAA J., Vol. 5, No. 11.

Krivtsov V. N., Cherkez, A. Ya, and V. A. Shilov (1969), "Study of Hypersonic Flow past two Separated Bodies," AN SSSR MZhG 2.

Kuznetsov, V. M., Podobin, V. P., and T. A. Tolokina (1973), "Study of Hydrosonic Wakes," Uzor TsAGI, (TsAGI Review).

Larson H. E, Scott C. J, Elgin, D. A. and R. E. Seiver (1962), "Turbulent Base Flow Investigations at Mach Number 3," Univ. Minnesota Rosemount Aeron. Labs. Research Rept. 183.

Levensteins, J. J., and M. V. Krumins (1967), "Aerodynamic Characteristics of Hypersonic Wakes," AIAA J., Vol. 5, No. 9.

Lewis J. E. and W. Behrens (1969) "Fluctuation Measurements in the Near Wake of a Wedge with and without Base Injection," AIAA J. Vol. 7, No. 4.

McLaughlin, D. K., Carter, J. E., Finston, M., and J. A. Forney (1971), "Experimental Investigation of the Mean Flow of the Laminar Supersonic Cone Wake," AIAA J., Vol 9, No. 3.

Mager, A. (1956), "On the Model of the Free Shock-Separated Turbulent Boundary Layer," J. Aero. Sci., Vol. 23, No. 2.

Marcillat J. (1974), "An Experimental Study of the Near Wake of Slender Cone at Varying Incidence at $M_\infty = 7$," J. Fluid Mech. 1.

Martelluci, A., Trucco, H., and A. Agnone (1966), "Measurements of the Turbulent Near Wake of a Cone at M = 6," AIAA J., Vol. 4, No. 3.

Murman, E. M. (1969), "Experimental Studies of a Laminar Hypersonic Cone Wake," AIAA J., Vol. 7, No. 9.

Neyland, V. Ya and G. I. Taganov (1963), "Configurations of Leading Separated Zones with Symmetric Flow past Bodies by a Supersonic Flow of Gas," Inzhenernyy zhurnal 3.

Panov, Yu A. and A. I. Shvets (1965), "Experimental Study of Flow in Stagnation Zones," Vestnik KPI, Kiev 2.

Panov Yu A. and A. I. Shvets (1966a), "Separation of a Turbulent Boundary Layer in Supersonic Flow," Prikladnaya meklanika 1.

Panov, Yu A. and A. I. Shvets (1966b), "Study of Base Pressure close to the Trailing Edges of Axisymmetric Bodies in a Supersonic Flow," Prikladnaya mekhanika 2/6.

Panov Yu A. and A. I. Shvets (1967), "Methods of Calculation of Interaction of Shock Waves with a Boundary Layer," Giroaero mekhanika i teoriya uprugosti 6.

Petrov, G. I. et al (1952), "The Effect of Viscosity on Supersonic Flow with Shock Waves," Trudy TsIAM Works of TsIAM , Oborongiz Press, Moscow.

Petrov, G. I. (1969), "Determination of the Position of the Supersonic Flow Causing Shock Wave in the Channels of an Air-Breathing Jet Engines," Space Engineering, Dordrecht, Holland.

Ribner, H. and B. Etkin (1958), "Noise Research in Canada," Pro. 1st Int. Congr., Aero. Sci., Madrid.

Roshko, A and G. J. Thomke (1966), "Observations of Turbulent Reattachment behind an Axisymmetric Downstream Facing Step in Supersonic Flow," AIAA J., Vol. 4, No. 6.

Scherberg, M. G. and H. E. Smith (1967), "An Eperimental Study of Supersonic Flow over a Rearward Facing Step," AIAA J., Vol. 5, No. 1.

Schloemer H. H. (1967)."Effects of Pressure Gradients on Turbulent Boundary Layer Wall-Pressure Fluctuations, J. Aconst Soc. America 42/1

Semenkevich Yu. P. (1969), "Restructuring of Supersonic Separated Flow between Bodies," Trudy I Respublikanskoy konferentsii po aerogidromekhanika, KGU Publishers, Kiev.

Shang, J. S. and R. H. Korkegi (1968)."Investigation of Flow Separation over a Rearward-Facing Step in a Hypersonic Stream,"AIAA J., Vol. 6, No. 5.

Shang, J. S., Hankey, W. L., and D. L. Dwoyer (1971)."Hypersonic Flow over a Rearward Facing Step", AIAA J., Vol. 9, No. 10.

Shvets, A. I. and Yu A. Panov (1963), Study of Flow behind a Body with Supersonic Velocity of Flight , Sbornik nauchnykh rabot (A Collection of Scientific Works) , KGU Publishers, Vol. 1.

Shvets, A. I. (1970), "The Near Wake in Supersonic Flow", IX International Symposium of Fluid Dynamics", Poland, Fluid Dynamics Transactions (Warsaw) V.

Shvets, A. I. and Yu A. Panov (1970), "An Investigation of Stream behind Bodies in a Supersonic Flow", Academy of Science, Warsaw, Poland, Archiwum budowy maszyn XV.

Shvets, A. I. (1971), "Near Wake", X International Symposium of Fluiddynamics, Poland, 1971, Fluid Dynamics Transactions(Warsaw) VI, 1972.

Shvets, A. I. and I. T. Shvets (1976), Gas Dynamics of Near Wake, Naukova Dumka Press, Kiev.

Shilov, V. A. (1969), "The Pecularities of Flow in a Base Region of a Body Moving at Supersonic Velocity Separated from a Disk Body," Trudy I Respublikanskoy Konferentsii po aerogidromekhanika, Works of the I Republic Conference on Aerodynamics, KGU Publishers, Kiev.

Sirieix, M (1967), "Formation and Development of a Wake," Revue francaise de mechanique, 24.

Smolyakov A. V. and V. M. Tkachenko (1969)."Results of Measurement of Reciprocal Spectra of Turbulent Pulsations of Pressure," AN SSSR MZhG 1.

Speaker W. V. and C. M. Ailman (1966)."Static and Fluctuating Pressure in Regions of Separated Flow," AIAA Paper 66-456

Su M. W. and J. M. Wu (1971), "Base Pressure Correlation in Supersonic Flow," AIAA J., Vol. 9, No. 7, TN.

Tagirov R. K (1969), "Experimental Research on Separated Flows behind Flat Protuberances when M = 1.97," AN SSSR MZhG 4.

Thomann, H (1959)."Measurements of Heat Transfer and Recovery Temperature in Regions of Separated Flow at Mach Number 1.8,"Aeronautical Research Institute of Sweden, Report 82.

Todisco A and A. Pallone (1965)."Near-wake Flow field Measurements," AVCO Corp. Tech. Memo. RAD-TM-65-21.

Trilling, L (1958)."Oscillating Shock Boundary Layer Interaction,"JASS 5

Van Hise, V. (1959), "Investigation of Variation in Base Pressure over the Reynolds Number Range in which Wake Transition occurs for Two-Dimensional Bodies at Mach Numbers from 1.05 to 2.92," NASA TND-167.

Waldbusser, E. (1966), "Geometry of the Near Wake of Pointed and Blunt Hypersonic Cones," AIAA J., Vol. 4, No. 10.

Weinbaum, S.(1966), "The Rapid Expansion of a Supersonic Boundary Layer and its Application to the Near Wake," AIAA J., Vol. 4, No. 2.

Weiss, R. F. and S. Weinbaum (1966), "Hypersonic Boundary Layer Separation and Base Flow Problem," AIAA J., Vol. 4, No. 8.

Weiss, R. F. (1967), "A New Theoretical Solution of the Laminar Hypersonic Near Wake," AIAA J., Vol. 5, No. 12.

Weiss, R. F. and W. Nelson (1968), "Upstream Influence of the Base Pressure," AIAA J., Vol. 6, No. 3.

Willmarth W. W. and T. E. Woodridge (1962)."Measurements of the Fluctuating Pressure at the Wall Beneath a Thick Turbulent Boundary Layer,"J. Fluid Mech. 14/2

Willmarth W. W. and F. W. Ross(1965)."Resolution and Structure of the Wall Pressure Field Beneath a Turbulent Boundary Layer," J. Fluid Mech. 22/1

Wu, J. J., and W. Behrens (1972)."An Experimental Study of Hypersonic Wakes behind Wedges at Angle of Attack," AIAA J., Vol. 10, No. 12.

Yefimtosov B. M and G. P. Karaushev (1970). "Flight Study of Noise in a Boundary Layer," Trudy TsAGI (Works of TsAGI) p 1207

Yefimtsov B. M and S. Ye Shubin (1974). "Reciprocal Spectra of Pulsations of Pressure near the Wall of a Turbulent Boundary Layer," Trudy TsAGI, p 1539

Zakkay, V and R. Sinha (1965). "Measurements in the Near Base with Injection," New York University, AA - 65 - 12.

Zakkay, V. and C. R. Cresci (1966). "An Experimental Investigation of the Near Wake of a Slender Cone at $M_\infty = 8$ and 12," AIAA J., Vol. 4, No. 1.

CHAPTER IV

SYMBOLS

b_o	wake width
i_θ	enthalpy on the wake axis
k	coefficient of proportionality
S	area of aperture in the perforation
$\tilde{S}$	penetrability of perforation
Vo	volume
u'	fluctuating velocity component in x-direction
v'	fluctuating velocity component in y-direction
φ	angle measured from the forward stagnation point
θ	momentum thickness or wedge angle
Δ	width of mixing layer

subscript

cp	mean for laminar flow in the body surface and in the near wake

CHAPTER IV

Base Flow and Wake

Much attention has been paid in the USSR to the problems of steady and unsteady base flow, downstream of two-dimensional, axisymmetric configurations at various ranges of speed.

At first, the problems of steady base pressure are presented referring to Shvets' book, Gas Dynamics of Near Wake. Then, the unsteady base pressure investigations are described with reference to Shvets' article, "Base Flow" , Prog. Aerospace Sci., vol. 18, Pergamon Press, 1978.

1. Steady Base Flow

The positions of flow separation on smoothly curved configurations at various Mach numbers are not known a priori. Thus, Shvets (1970) set up a simplified computational method, to determine the position of flow separation.

Assuming a certain point where the tangent to a smooth configuration surface becomes parallel to the free-stream direction, pressure at the position is equal to the pressure of the undisturbed free stream. Then, determine the pressure distribution on the trailing section of the surface by the expansion wave equation. The point of the separation is determined at a point where the computed pressure becomes equal to the base pressure, considering that pressure downstream of the separation is equal to the base pressure. For example, on a cylinder with surface pressure at $\varphi = 90^{\circ}$, measured from the forward stagnation point,

is approximate to that of an undisturbed free-stream. Then, by using the method of Panov and Shvets (1966) for evaluation of $c_p = f(X)$, the point of separation is determined at $\varphi = 112^\circ$, in a good agreement with experimental data.

4.4 Base Pressure at Supersonic Speeds

Shvets (1972) conducted experimental investigations of base flow, downstream of a cylinder and a wedge of various half angles, and differentiated the base flow phenomena of a cylinder from those of a wedge.

If a cylinder is placed in a supersonic flow stream and the Mach number is increased, then the base pressure decreases, and at $M \simeq 0.5$, a local supersonic zone is formed on the cylinder surface. At a point located at $\varphi = 80^\circ$, the pressure first decreases, and then increases to equal the value of the base section of the cylinder.

If a cylinder is placed in a supersonic free-stream, the base pressure becomes small, as evidenced in Fig.IV,1b for M = 3. Flow over the surface expands; thus, pressure becomes low, as shown in the first pressure minimum in Fig.IV.1b. The subsequent pressure increase, from over-expansion to base pressure, causing the boundary layer seperation, located at $\varphi = 115^\circ$. By Töpler photograph, the pressure minimum point is determined at $\varphi = 115^\circ$. A second minimum of pressure at $\varphi = 145 - 155^\circ$ is due to the circulatory flow directed to this zone along the surface of a cylinder, originating at $\varphi = 180^\circ$.

For the wedge of $\theta = 15^\circ$, the measured pressure distribution along the base section at M = 3 shows that pressure is maintained almost constant, equaling $p/p_{t_\infty} = 0.027$. But with increase of Re, the

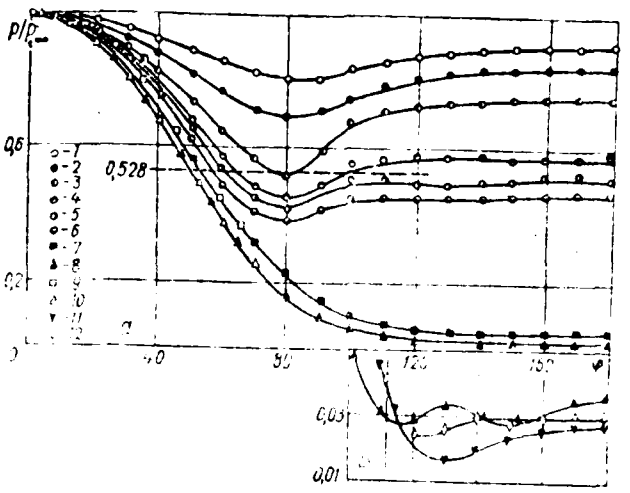

Fig. IV.1. Distribution of pressure on the surface of a cylinder (dashed line corresponds to calculations of the separation point): [Shvets and Shvets (1976)].
1--M = 0.32; 2--M = 0.44; 3--M = 0.54; 4--M = 0.68; 5--M = 0.81; 6--M = 0.88; 7--M = 2.0; 8--M = 3.0; 9--calculation, M = ∞; 10--calculation, M = 3 [Vas, Murman, and Bogdonoff (1965)]; 11--M = 5.8, Re = 1.4 · 10³ [Dewey (1965)]; 12--M = 6.8, Re = 4.10 [Dewey (1965)].

laminar base pressure decreases, whereas the base pressure downstream of a cylinder increases slightly, if Re increases. If it is assumed that the pressure on the body surface exposed to the separation region is constant and equal to the pressure of the external boundary of the mixing layer, then it becomes apparent that as the Reynolds number decreases, the dimension of the separation zone decreases, shifting the separation point toward the trailing edge of the configuration.

The measured total pressure, downstream of the wedge and the cylinder, indicating the position of separation shock, the external boundary of a free, viscous layer and trailing edge shock, are shown in Fig.IV.2.

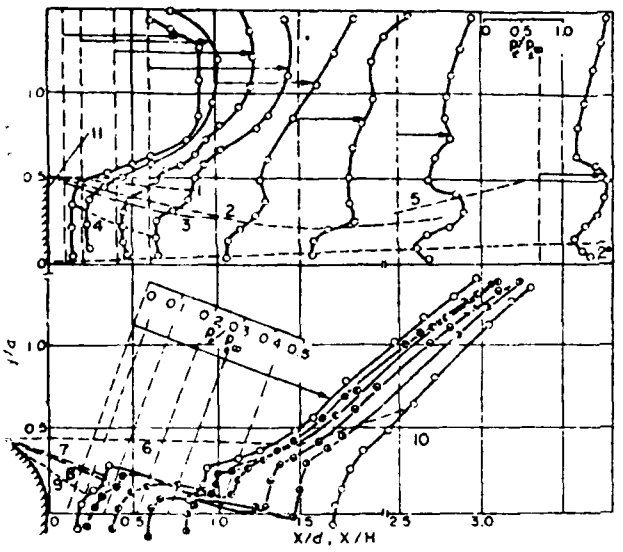

Fig.IV.2. The fields of total pressures behind a wedge (a) and a cylinder (b) (M = 3): [Shvets (1978)] 1, 2, 5, 6, 7, 10--optical measurements; 3, 8--visualization on a plate; 4, 9--measurements of pressure, $u_x = 0$; 1, 6--boundary discontinuity; 2, 3, 7, 8--boundary of a free viscous layer, 5, 8--trailing-edge discontinuity.

For the wedge, the largest pressure-gradient occurs close to its edge, and the maximum pressure area corresponding to Prandtl-Meyer expansion, is located further apart from the wake axis. Starting from the neck on the external section of boundary-layer pressure increases, due to compression in the trailing shock and after compression the boundary layer thickens considerably, forms the vortex layer, and makes up the basic part of the near wake.

Downstream of the cylinder, the area between the separation shock and mixing layer, is an inviscid flow-field extending to the trailing-edge shock. The location of this area corresponds to constant $p_t/p_{t\infty}$ on the pressure curve. Ahead of separation-shock in the non-viscous flow, the most important pressure-gradient can be found not far from the cylinder, where due to the curvature of the bow shock wave, the flow is highly rotational.

Shvets (1972) differentiated the base flow of a cylinder from that of a wedge, using Fig,IV.3 and Fig,IV.4. Fig,IV.3 to show an expansion wave, mixing layer and wake neck. It is clearly seen that the separation point is located on the rear surface of the wedge, downward about

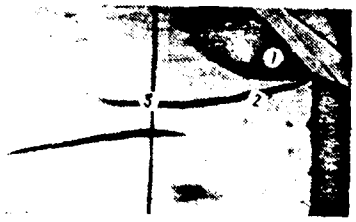

Fig.IV,3: A photograph of flow behind a wedge ($\theta = 15^{o}$, M = 3): [Shvets and Shvets (1976)] 1--expansion waves; 2--mixing layer; 3--wake neck.

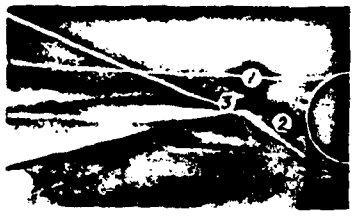

Fig.IV,4: Photograph of flow behind a cylinder (M = 3): [Shvets and Shvets (1976)] 1--boundary discontinuity; 2--mixing layer; 3--neck of the wake.

0.1 H/2 from the corner tip, where the strong pressure-gradient from the base to wedge pressure prevails, indicated by the large density-gradient in the photograph. Wake neck is located at a distance ~ 1.7H from the base section and its width is 0.4H and the angle between the trailing-edge shock and symmetry-axis is 14^{o}. Shvets (1971) found that, compared to the cone wake, the wedge wake boundary, downstream of the neck, expands more slowly.

For the cylinder, as shown in Fig.IV,4 the width of wake neck is ~ 0.25d, located at a distance ~ 0.9d from the base section. The trailing-edge shock originates in the proximity of the neck, and the angle between this shock and symmetry axis is 19^{o}.

By comparing Fig.IV,3 and Fig.IV,4 the following significant differences between the wakes of a cylinder and a wedge are noted. For a cylinder, the neck is narrower and located closer to the base, as compared to a wedge, and the separation shock is straight and the trailing-edge shock is strong and much more inclined, as compared to wedge. For a cylinder, the stream lines downstream of expansion are approximately

parallel, and a free viscous layer conserves the boundary layer structure. On the other hand, a wedge involves expansion, and so divergent rotational flow is formed, and leads to the destruction of the boundary-layer structure inside the free, viscous layer.

Base flow downstream of cones has been investigated experimentally. Fig.IV,5, shows the measured, base pressure data of cone models with turbulent flows at their trailing edges at $M_\infty = 3$, with a slight blunting of the nose, p_b/p_∞ decreases slightly, whereas, with a strong blunting, base pressure increases.

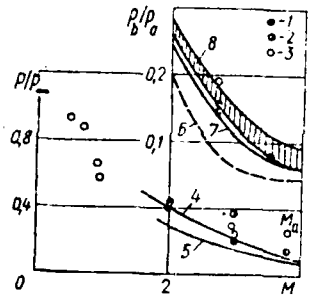

Fig.IV,5: Dependence of a base pressure for models of cones: [Shvets and Shvets (1976)] 1-Cone on lateral pylong, θ = 10°, H/d = 0.07 (H-thickness of the pylon); 2-Cone on stranded wires, θ = 20°, d'/d = 0.02 (d'-diameter of the stranded wire); 3-Cone on a base holder, θ = 10°, d'/d = 0.25 (d'- diameter of the holder); 4-Calculation [Isayev & Shvets (1970)], cone θ = 10°; 5-Calculation, wedge θ = 10°; 6-[Cassanto, Rasmussen & Coats (1969)]; 8-Calculation (see Chapter 2 [Stepanov and Gogish (1973)]

The value of p_b/p_∞ decreases with the increase of the Mach number approaching a certain value. But with an increase of velocity at hypersonic speed range, the base pressure increases as Bondarev and Yudelovich (1960) and Cassanto, et.al. (1969) indicated in their wind tunnel and flight tests. Stepanov and Gogish (1973) predicted the lower value of the base pressure compared to that in Fig.IV.5, but if the thickness of the initial boundary layer is taken into account in the calculations, then the value of the base pressure becomes larger and better, correlating with the experimental data.

Grodzovskiy, et.al. (1972) investigated experimentally the base drag of an axisymmetric-perforated nozzle in the range of $1.75 < M < 4.9$. The flow characteristics depend on the penetrability of perforation $\tilde{S}$ defined as $\tilde{S} = S/(\pi d^2/4)$, where S is the area of aperture in the perforation and d is the diameter of the midsection of the nozzle. If $\tilde{S} \ll 1$, an ordinary type of near wake occurs on the trailing edge of the nozzle, but with an increase of $\tilde{S}$, the base pressure increases. If $\tilde{S} \simeq 1$, then the flow passing through the perforation remains supersonic within the nozzle and with the decrease of $\tilde{S}$, the total pressure loss as well as the base pressure increases. A maximum decrease in the base drag is achieved with $\tilde{S}_{opt} \simeq 0.05$ and the best effect of perforation is expected in the range of $1.75 < M < 3.0$.

A flow control technique for a body of revolution with a blunt after section, utilizes the interaction of the stream normal to lateral surface of the body with base flow.

If the external flow Mach number exceeds 1.9, then such lateral flow decreases the base pressure with the increase of the Mach number as Zhdanov and Born (1974) found. The extent of this low pressure zone reaches 3-4 radii of the body and the maximum base pressure decreases in an amount of 25-30% of the value with no lateral flow at $M \geq 2.9$.

1.2 Base Pressure at Hypersonic Speeds

Shvets and Shvets (1976) in their book, presented hypersonic wake problems, mostly referring to the Western references.

The flight test of a wake downstream of blunt cones at hypersonic speed by Wilson (1972) indicated that two distinct wakes develop, as

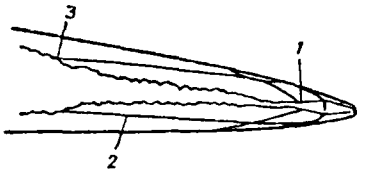

Fig.IV.6: Diagram of flow past a blunt cone miving at hypersonic velocity [Wilson (1967)]
1--Viscous wake; 2--Boundary of the inviscid wake; 3--Field of separation of the inviscid wake.

seen in Fig.IV.6. One is a viscous wake which forms as a result of heating the air caused by viscous friction on the body surface, and the other, is an inviscid wake which forms as a result of heating the air during the passage of the bar shock wave. The viscous wake develops only from one part of the boundary layer located close to the body surface and an inviscid wake forms the other part of the boundary layer.

The friction between the recirculation area and the separation stream line causes the recirculatory flow. The flow model may be conceived as follows. The external flow is such that the boundary layer on the body develops as inviscid up to the pressure level equal to the base pressure and rotational flow develops along the separation stream line. Then, in this vortex flow a new viscous layer of thickness δ develops whose magnitude can be approximated using the formula for the boundary layer on a plate.

The hypersonic wake has basic peculiar characteristics effecting the base pressure compared to that of the supersonic one.

4.3 Reynolds Number Effect

Four regimes of the base pressure may be classified in a function of a Reynolds number as Lees (1964) found and is shown in Fig.IV.7 and IV.8. At small Re_L based on the length of the model, the boundary layer

on the body is laminar and with an increase of Re_L, the intensity of laminar mixing decreases and the base pressure increases slowly. With the increase of Re_L, the transition point moves toward the edge increasing the local mixing significantly. Having reached a maximum value, the base pressure decreases sharply. If Re_L grows fairly large, then the transition point shifts toward the trailing edge of the body and with a further increase in Re_L, the mixing intensity changes insignificantly, but the thickness of the boundary layer increases. Therefore, the base pressure increases at first, reaching a certain maximum. Then, it begins to decrease. If Re_L is very large, the transition point is practically stable; and, with a subsequent increase of Re_L, the base pressure decreases because of a decrease of the boundary layer thickness on the trailing edge.

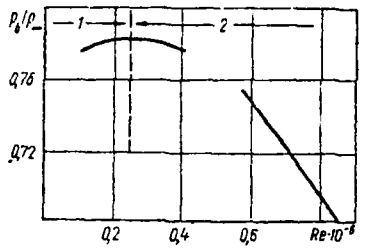

Fig.IV.7: Dependence of the base pressure on the Re number [Crocco and Lees (1952)]. 1--Laminar wake; 2--Point of transition shifts along the wake.

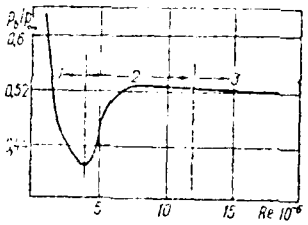

Fig.IV.8: Dependence of base pressure on the Re number [Crocco and Lees (1952)] 1--Boundary layer on a laminar body, transition point in the wake; 2--Turbulent wake, transition point in the boundary layer; 3--Turbulent regime.

The base pressure at hypersonic speed for various bluntness of the body is given in a good correlation with one of the important parameters, the Mach number, on the trailing edge as shown in Fig.IV.9 by Cassanto, et.al. (1969) and Cassanto (1965). The test results

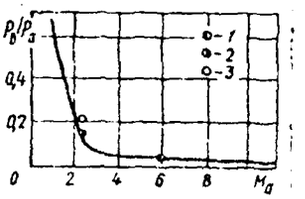

Fig.IV.9: Base pressure in a turbulent flow [Cassanto, Rasmussen, and Coats (1969)] (curve--dependence [Cassanto, 1965])
1--r/R = 0; 2--r/R = 0.3; 3--r/R = 0.6

for a series of cones (θ = 10-90°) in a helium tube at M = 10-26, Re = 0.16 - $4 \cdot 10^6$ are given by Artonkin (1972) as a linear equation:

$$(P_b)_{cp}/p_\infty = -0.09 + 2.82\, M^2/\sqrt{Re}$$

where subscript cp refers to mean for the laminar flow in the body surface and in the near wake.

1.4 Effect of Body Shape

Lockman (1967) measured the base pressure downstream of sharp and blunt cones in a shock tube at M = 14. As seen in Fig.IV.10, the base pressure of a cone of a half-angle 15° is higher than that of 10° and the base pressure increases with the increase of blunting.

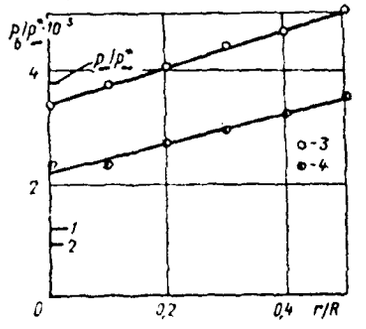

Fig.IV.10: The effect of half angle and the degree of blunting of the cone on base pressure (with cone with radius of base 1.9 cm, r/R= 0--0.5, M = 14) [Lockman (1967)] 1--calculation, θ = 15° (see chapter II [Vas, Murman and Bogdonoff (1965)]; 2--calculation, θ = 10° (see chapter II [Vas, Murman, and Bogdonoff (1965)]; 3--θ = 15°; 4--θ = 10°

The measured base pressure magnitude was almost equal to the static pressure of an undisturbed flow p_∞, but it is larger than the base pressure computed for a sharp cone, based upon the thin boundary layer. The effect of a base surface shape on the base pressure is measured by Cassanto, Schiff and Softley (1969) as seen in Fig.IV.11. With the dome shaped base surface, the base pressure is decreased about 20% compared to the plane base

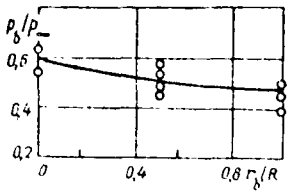

Fig. IV.11: The effect of the shape of the base of a cone on base pressure ($r_б$--radius of roundin of the base of the cone, M = 10, Re = 1.7 $\cdot 10^6$ [Cassanto, Seiff and others (1969)]

affected by the flow separation phenomenon. With the flat base, the flow separates in the neighborhood of the tip where the body surface and base surface are joined, but for the rounded base surface, the point of seperation is shifted downstream because the flow remains attached up to a certain distance, downstream of the joint of both surfaces. The local Mach number increases with the increase of a flow angle of bending at the separation point. Thus, on the models with a rounded base, the pressure becomes lower compared to a flat base.

4.5 Radial Gradient of Base Pressure

Cassanto (1967), measured by a flight test, the laminar base pressure downstream of 10° cone at M = 20 along the axisymmetric line and at points of 0.66 R from this center, so that the radial gradient of the base pressure may be assessed.

From IV.11, it is seen that at $Re_L < 10^6$, and the base pressure along the center line is twice the base pressure at 0.66 R, but with the increase, the magnitudes of the base pressure as well as the difference of the two base pressures decrease.

Artonkin (1972) found that the pressure distribution along the base surface downstream of cones at M = 10-26, Re = 0.16 - 4×10^6 is approximately parabolic and its value at the center line is about three

times larger than it is at the edge. The empirical formula for this base pressure distribution is

$$p_b/(p_b)_{cp} = 1.34 - 0.88\,(r/R)^3$$

where cp refers to mean.

1.6 Effect of the Angle of Attack

Wu and Behrens (1972) measured the base pressure downstream of a wedge at M = 6 and at various angles of attack. At small angles of attack, the base pressure decreases slightly with an increase of an angle of attack and Re. However, at larger angles of attack, the base pressure increases significantly except for the smallest $Re_{\infty H} = 7000$. When $\alpha > 17.5^{\circ}$ flow separates, and the pressure on the surface in the area of separated flow becomes approximately equal to the base pressure. The reason for this base pressure behavior of the angle of attack and Re is not clear.

[illegible] Unsteady Base Flow

It is important to understand the unsteady forces in the base and the separated flow region, since most vehicles have separated flows over at least part of their boundaries.

Despite of the numerous investigations on a near wake, the flow [illegible] downstream of the base has not been studied in [illegible] this section, pressure fluctuations downstream of axi- [illegible] are presented. The experiments [illegible] parallel with study of the flow structure down- [illegible] used for the

analysis of unsteady process in the base region.

If the body is exposed to fluid flow, in general, the amplitudes of fluctuation are the largest at transonic and low supersonic velocities.

A combination of intense fluctuation of pressure and comparatively large dynamic pressure in this range of velocities may result in a significant dynamic load and due to abrupt restructuring of flow aerodynamic characteristics may change.

Distribution of the pressure fluctuation on the cylinder surface given by $B = (\overline{p^2})^{0.5}/(\overline{p^2})^{0.5}_{st}$ in a function of angle φ measured from the forward stagnation point is already shown in Fig.II.27a. The symbol $(\overline{p^2})^{0.5}$ refers to the root-mean-square (rms) of pressure fluctuation. Kistler (1964) studied the fluctuation increase in the region of the separation point due to the oscillation of this point and for the separation zone upstream of the forward facing step. The fluctuation increase in the region of the rear sonic point depends on the effect of the reversed flow.

It may be noted from the Fig.II.27a that at $\varphi = 90^{\circ}$, by approaching to sonic speed, B value increases and at supersonic speed the fluctuation on the entire cylinder surface including the base region decreases if the fluid velocity changes from M = 2 to 3. The distribution of the Strouhal number on the cylinder surface which characterizes that of frequency is shown in Fig.II.27b. The velocity increase in the surface from the forward stagnation point is accompanied by a decrease fluctuation frequency. In the range of subsonic speed, the minimum values of the Strouhal number are observed at $\varphi = 40 - 60^{\circ}$ and at supersonic speed, the minimum value is reached in the region of $\varphi = 90^{\circ}$.

Fluctuation of the pressure is measured using gas-discharge and induction [illegible] fluctuation of the velocity by [illegible] sensor and glow-discharge

sensors. The oscillations of the wake boundary are studied by the high-speed multiple photography of flow.

In order to measure the pressure fluctuation a special gas-discharge sensor is developed based on the relationship of parameters of corona discharge in a gas to pressure. This sensor has the following characteristics : rearrangement of space charge which determines the reaction of the charge to change in pressure is the result of restructuring the regime of the electron avalanche and the time for this process is less than 10^{-6} sec. Thermal velocities of the molecules are small, thus practically ignored. The sensor is placed in an aluminum chamber and a platinum spike is mounted in its center insulated by a porcelain tube. The output signal with the gas-discharge sensor, through the cathode repeater, is fed to the input of parallel three-octave spectrometers and to the input of the sequential analyzer. The mean quadratic value and the maximum amplitude of fluctuation are simultaenously measured. Since the sensor is not designed to measure the mean pressures but only to measure the fluctuation the effect of temperature can be ignored. Shvets et al (1968) notes that the most intensive pressure fluctuations of flow rate originates in the wake throat region are transmitted to the body by the reverse flow. Fig.VI.12 shows the effect of body elongation (aspect ratio) on the base pressure fluctuations. At subsonic speeds and low supersonic speed downstream of small elongation the fluctuations are considerably larger than those of larger elongation. But, at M = 2 and 3 the fluctuations are almost independent of body elongation.

2.1 Fluctuation Spectra

The base pressure fluctuation of rockets depend on a number of factors. Expecially the following factors are influential: quasi-steady restructuring of flow in multi-nozzle units or annual flow, acoustical radiations of flow

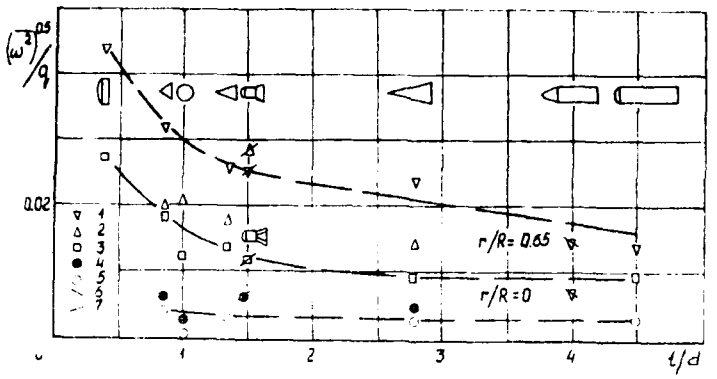

Fig.IV.12. Effect of body elongation(aspect ratio) on base pressure fluctuations. [Shvets and Shvets (1976)].
1: M = 0.6, 2: M = 0.9, 3: M = 1.2, 4: M = 2, 5: M = 3, 6:Eldred (1961) 7: Kistler and Chen (1963)

and flow unsteadiness in the region.

Fig.VI.13 shows the non-dimensional spectral density of the base pressure fluctuations defined by

$$S_1 = \frac{\overline{\omega^2}(f)\, u}{q^2\, d} \quad \text{and} \quad S_2 = \frac{\overline{\omega^2}(f)\, u}{\overline{p^2}\, d}$$

in a function of Strouhal number defined by $Sh = \frac{f \cdot d}{u}$

The basic energy of base pressure fluctuation is concentrated in the region of low frequencies. The model tests at low subsonic speed indicate that the spectral density at lower frequencies is higher in the vicinity of base surface, whereas at supersonic speed it is higher in the center of the surface.

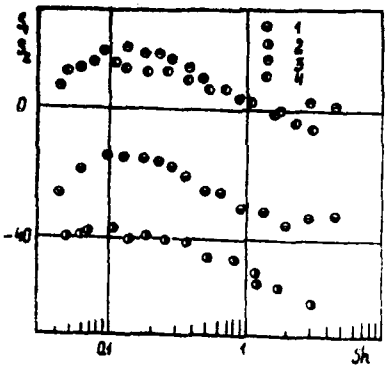

Fig.IV.13. Spectral density of pressure fluctuations for base point 0.5 R of the blunt body ($\theta = 30^{\circ}$)
[Shvets and Shvets (1976)]
1; S_1 , M = 0.4, 2; S_1 , M = 2 3; S_2 , M = 0.4
4; S_2 = M = 2.

Mabey (1972) divided the intensity of base pressure fluctuation into three groups by values of $\sqrt{Sh.\ F(Sh)}$, where the function of F(Sh) is determined by

$$(\Delta p)^2 / q_\infty^2 = \int Sh \cdot F(Sh)\, d(\ln Sh).$$

and Δp is base pressure difference from Δ f band with frequency f.

weak oscillation : $\sqrt{Sh\ F(Sh)} \leq 0.004$

average oscillation : $\sqrt{Sh\ F(Sh)} \leq 0.008$

strong oscillation : $\sqrt{Sh\ F(Sh)} \simeq 0.016.$

Rossiter and Kurn (1967) noted that the intensity of the fluctuation

decreased approximately by a factor of 2 when subsonic flow becomes supersonic, (M = 2). The experimental data indicates that the turbulent boundary layer fluctuation amplitude increase with an increase of Re.

. ...upsov and A. V. Antonov presented the pressure fluctuation in ... layer, upstream separation region, and the downstream of protuberance and base in Fig.IV.14.

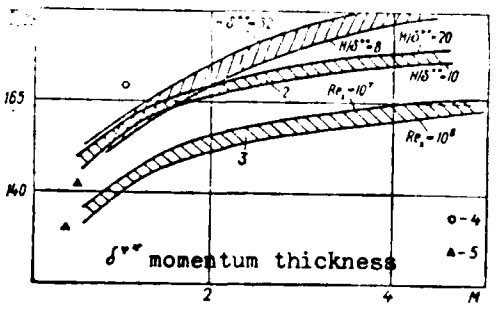

Fig.IV.14. Fluctuation of pressure in separation zones (B--total level of fluctuations reduced to pressure p_∞ =1 at):
1--separation in front of a protuberance; 2--maximum pulsation behind a projection; 3--boundary layer; 4, 5--base pressure [Rossiter and Kurn (1967)]; 5-- [Eldred (1961)].

The value of $\bar{B}$, the total level of fluctuation reduced to pressure p = 1 atm. is determined by these authors based upon the value of $\bar{\omega}^2 \, a_s / \tau_w$ = 2-6, for turbulent boundary layer. It is shown that with increase of M, values of $\bar{B}$ also increase. [Figure IV.14]

Speaker and Ailman (1966) presented the following empirical equation for maximum fluctuation in the range of M = 1.4 and 3.5 as well as H/δ = 0.5 - 1.8.

$$\bar{\omega}^{2\,0.5}_{max} / \bar{\omega}^{2\,0.5}_{b.l} = 1.2 \sqrt{(M - 1)\,(H/\delta^* + 1)}$$

indicating that the maximum values of fluctuation in the separation

zone is much larger than $\bar{\omega}^2_{b\ell}$ of the boundary layer.

Computation of the maximum fluctuation at the reattachment point downstream of a projection reveals that at small Mach numbers, the value of $\bar{B}$ is in a same magnitude at separation upstream of the protuberance, but if M > 2, the fluctuation upstream of the protuberance is higher. The slope of the maximum of protuberance is gentle in a range of $\bar{B} \simeq 0.1 - 0.2$ as Greshilov, Yevtushenko and Lyamshev (1969), Fricke (1971) Fricke and Stevenson (1967) and Speaker and Ailman (1966) found.

A comparison of $\bar{B}$ data in the base region with those of a separated turbulent boundary layer upstream and downstream of protuberance, indicates that at M = 1, the level of these base fluctuations is comparable to the level of fluctuations of the boundary layer separation upstream and downstream of protuberance, but at M > 2.5 the fluctuations in the base region are smaller.

The volume of the stagnation zone in the base region may be used to characterize the unsteady process as shown in Fig.IV.15 which presents $k\ \bar{\omega}^2 / q_\infty$, where k is a coefficient of proportionality amounting $k \simeq 0.006$ in a function of stagnation volume V with respect to a fixed volume $Vo = \frac{1}{6} \pi d^3$.

The volume of the stagnation zone is approximately equal to the volume of a circular section of a cone with a diameter of a base equal to the wake neck diameter d with height H equal to the distance from the neck

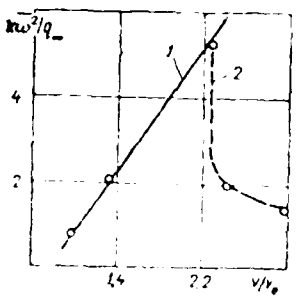

Fig.IV.15. The effect of the volume of the stagnant zone on pressure fluctuations (cone, $\theta = 10^{o}$, M=3): [Shvets and Shvets (1976)] 1--"Active volume"; 2--"Passive volume."

to the cone base. The values of d and H are determined by the optical flow visualization. The fluctuation may be reduced by providing a damping cavity in the trailing edge section as shown in Fig.IV.15. By placing a "passive" volume of cylindrical cavities in the cone base, fluctuation is reduced while the "active" volume of the staguation zone increases fluctuation. In the region of a large pressure gradient where the viscosity effect is significant (for example, close to trailing edge shock) an intense fluctuation occurs.

2.2 Strouhal number

The Strouhal number, defined by frequency corresponding to the maximum amplitude, is an important parameter for the study of unsteady wake flow. The velocity of potential flow u_e is used as a characteristic velocity because the flow in the base region depends on the flow parameters on the rear section of the body and the flow process on the base region has a large effect on fluctuation. As a characteristic dimension of the Strouhal number, the diameter of the body is usually used, but as u_e increases a near wake diameter does not vary monotonically and wake

diameters differ depending upon the different shapes of bodies. Therefore, for the supersonic flow, the Strouhal number is to be formulated, not based upon body diameter but by wake diameter, the neck diameter d'. However, for a low velocity less than 50 m/sec, the characteristic dimension of the near wake is also the wake diameter as Kasnko (1970) indicates.

The experimental results of the Strouhal number $Sh = f\,d/u_\infty$, in a function of M for composite body of a blunt cone and cylinder and other shapes are shown in Fig.IV.[illegible]. For the Sh, the frequency of oscillation f is taken approximately by the frequency corresponding to the maximum amplitude of the spectrum, diameter d of body and velocity of undisturbed flow u_∞ as the characteristics. For all bodies tested, Sh decreases as the undisturbed flow velocity increases. For the smallest supersonic velocities, the Strouhal numbers are maximum. The Strouhal numbers measured in the base for $M > 3$ by Shvets et al (1968) and Eldred (1961) agree with those downstream of propuberance measured by Speaker and Ailman (1966).

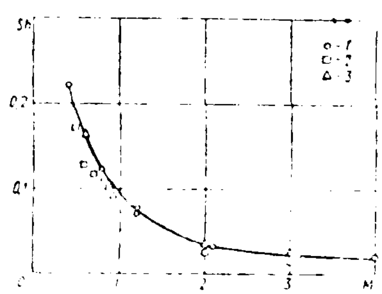

Fig. IV.[illegible] Dependence of the Sh number of fluctuation of base pressure on the M number:
1-- Composite model (blunt cone and cylinder); 2--Model for injection (cone and cylinder); 3--Cylinder located normal to the direction of flow. [Shvets and Shvets (197[illegible])]

It has been observed that an intense vibration accompanies the extension of dive brakes and other high-drag devices on aircraft and missiles.

Also, a considerable vibration at the fundamental longitudinal mode and at the internal resonance frequencies of a vehicle which had a blunt base was noted during the maximum dynamic pressure phase of flight. Eldred (1961) in order to study this phenomena measured the base pressure fluctuations at two base positions on a small body of revolution at eleven points in the velocity range of 68-352 ft/sec. The results show that (a) the ratio of $\left[\overline{p^2}/\overline{q^2}\right]^{\frac{1}{2}}$ varies between 0.007 at the center of the base to 0.015 at 65% radius (b) the spectrum of the pressure fluctuations depends on body Strouhal number (c) variation of observed vibration response with flight parameters can be predicted from the base pressure fluctuation data.

Lien and Eckerman (1966) studied the fluctuations in the turbulent wakes of slender cones and spheres in the ballistic field, employing the Mach-Zehnder interferometer, finding the existence of some periodicities in the turbulent wake at hypersonic speeds. The most distinct difference between cone wakes and sphere wakes is the existence of the large amplitude regular periodic structure in the former. The periodic structure persists up to several hundred diameters length downstream in cone wakes and the sphere wake periodicity having a much smaller amplitude is found to disappear at an earlier stage. The periodicity in terms of the Strouhal number (Sh defined by taking the ratio of the cone base to the wave length instead of counting the periodicity of the regular fluctuations) increases with the increase of Re_d, described by the Rayleigh Strouhal formula with an asymptotic limit estimated to be 0.55-0.6. It is indicated that the correlation length ℓ of the turbulent density fluctuation

(with respect to axial separation distance) decreases with increasing Re_d, and indicated also for hypersonic cone wake the tendency exists to approach self-preservation at high Re_d although in the range of $8 \times 10^5 < Re_d < 2 \times 10^6$ no state of self-preservation was observed. In this range of Re_d, the % rms density fluctuation scatters in between 4 and 11%.

3.3. Types of Oscillations

The sketch of the base flow structure, presented in Fig.IV.17, may serve to clarify the factors to cause the supersonic base pressure fluctuation. On the boundary of stagnation zone, the external flow interacts with recirculating supersonic flow. The flow in the wake neck region, where additionaly the mixing of external flow with gas ejected from the stagnation zone occurs, affects the flow in the stagnation zone. Fluctuation of the base pressure is caused by a number of interconnected factors. In particular, quasi-steady regimes with relaxation fluctuation, flow-rate variation in the stagnation zone, instability of reverse flow, shifting of separation and reattachment points, acoustic oscillations in resonance, and large eddy and turbulence.

The flow of the mass of the external region and the mass of gas, ejected from the stagnation zone, is slowed down in the neck region and scattered in two directions. Part of the gas with total pressure larger than the pressure in the compression region passes downstream, while other parts of gas with a total pressure less than the pressure in this region is turned into the stagnation zone. Due to a pressure drop between the com-

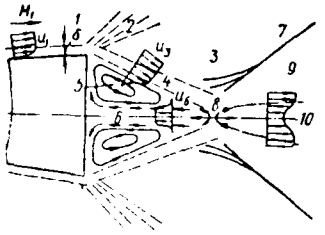

Fig. IV.17. Diagram of flow in a base region:
1--Flow close to the trailing edges; 2--Rarefaction wave; 3--Inviscid flow after expansion; 4--Mixing layer; 5--Toroidal flow; 6--Reversed stream; 7--Trailing, edge discontinuity; 8--Deceleration point; 9--Inviscid wake; 10--Viscous wake.
[Shvets and Shvets (1976)]

pression region and stagnation zone gas is accelerated to a higher velocity and approaches to base as an axisymmetric flow.

All perturbations of flow parameters occur in the wake neck, causing oscillation of trailing edge shock, and fluctuations of pressure in the compression zone and amount of gas if the reversed flow occurs. They also cause the turbulent fluctuation in the flow boundary of stagnation zone and deceleration and mixing in the wake neck region. It may be assumed that mean-quadratic value of the base pressure fluctuation is proportional to the dynamic pressure of the reversed flow toward the base.

The occurance of flow-rate variation may be explained as follows: Although the oscillations of the body due to dynamics of flight or by external perturbation are insignificant, neverthless a bow shock wave oscillation causes a variation of flow parameters such as Mach number, flow direction behind the wave. Because of variation of a trailing edge shock, pressure on the dividing stream line affects on the variation of base pressure.

It is to be noted that, the initial perturbation may produce amplitude and frequency. However, if flow rate variation occurs, it is due to volume and flow parameters in the stagnation zone. These factors cause an unsteady process.

Fluctuations of stagnation boundaries, dimension of neck and position of trailing edge shock affect the flow through the neck. G. I. Petrov indicates that if the fluctuation of the flow rate occurs downstream of a neck at supersonic speed, then a large scale vortex is formed in the wake.

Fluctuations of the base pressure, with a frequency of several kilohertz (M=3, Sh $\simeq$ 0.1 - 0.6), cause flow instability at the separation and reattachment regions due to the fluctuation of reversed flow and oscillations in the stagnant zone. In general, the zones of separation involving local shock wave are the locations to cause flow parameter pulsations. Kistler (1964) observed the stronger pressure fluctuation close to the separation point up stream of a step compared to those in the stagnation zone.

The high-frequency fluctuations of the base pressure are caused by a large scale eddy and a turbulence in the viscous layer of external flow. In pictures taken at short time exposure ($t \simeq 5\,\mu s$), the eddy is visible in the external viscous layer and in the wake neck.

V. M. Kuptsov (see Theory of Turbulent Streams G. M. Abramovich, Fizmat-

giz Press. Moscow 1960) evaluated theoretically the maximum value of turbulent fluctuation of the transverse velocity component as $\overline{v}'=0.2\cdot\overline{u}'$, the mean length as $\ell \simeq 0.1\,\Delta$, where Δ is width of mixing layer and mean frequency of fluctuation by $f \simeq \overline{v}'/\ell$.

A stagnation zone with a large fluid volume of relatively low fluid velocities probably causes lower frequencies. By adding a passive volume of a cylindrical groove in the base, the level of fluctuation may be lowered resulting in a shift toward the reduced frequency. However by increasing active volume (increase in the area of high total pressure) not only the level of frequency of fluctuation is increased but also the frequency range is expanded. The part of the energy required for low-frequency fluctuation decreases with an increase of active volume.

The base pressure fluctuation is caused also by an oscillation of shock wave incident on the circulating flow. For the clarification in physical sense about the instability, particular, the principles of flow-rate fluctuation, it is necessary to study the space-time correlation of fluctuation.

3. Wake

In this section only some results of pressure fluctuation, and fluctuating velocity components are given separately for subsonic, supersonic and hypersonic speeds relating them to downstream wake distance x.

3.1 Subsonic Wake Flow

As pointed out by Birkhoff and Zarantonello (1959), the fluctuation in a wake is accompanied by the fluctuation shift of the separation point on the body. Thus, if the trailing edge of the body is sharp, then fluctuations are absent.

Sekundov and Yakovlevskiy (1972) analyzed the wake flow fluctuation and compiled the experimental data, analysis of turbulent transition, and fluctuation intensity.

The fluctuating velocity components $\overline{u}'$ and $\overline{v}'$ behind a thin plate are shown in Fig.IV.18 by Chevray and Kovasznay (1969).

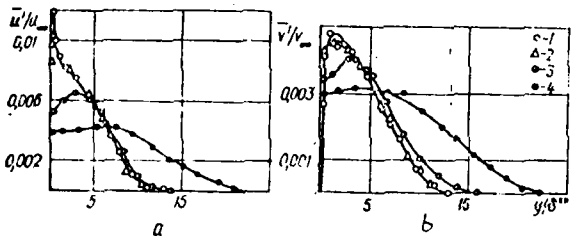

Fig.IV.18. Intensity of fluctuation a longitudinal (a) and lateral (b) component of velocity: [Chevray and Kovasznay (1969)]

1--x/ θ = 0; 2--x/ θ = 8.6; 3--x/ θ = 86; 4--x/ θ = 414.

The maximum values of these two components prevail at locations far from the symmetry axis, close to the zone of maximum shear.

Close to the trailing edge value of $\overline{u}'$ is approximately two times that of $\overline{v}'$ and this difference becomes smaller downstream approaching zero.

3.2 Supersonic Wake Flow

Lewis and Behrens (1969) indicate that the structure of the wake flow downstream of a wedge is characterized by an internal shear in the circulating flow zone. In this region, no noticeable unsteady signals from the hot wire anemometer were observed. Therefore, it was concluded that the reversed flow area is laminar, flow in it is stable, and the turbulent boundary layer does not affect it. Basically at $Re_H = 2.7 \cdot 10^4$ where H is base height, wake flow downstream of the wedge is two-dimensional up to $x/H < 8$. This flow is unsteady and the small perturbation increase is predicted by the linear theory of instability. An increase in Re_H to $8.7 \cdot 10^4$ results in a transition from the laminar to the turbulent flow close to the wake neck located at $x/H = 3.5$. At x/H, where the turbulence is fairly well developed, frequencies were also high as shown in Fig.IV.19.

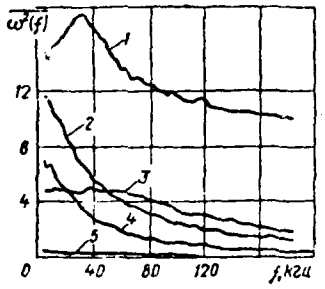

Fig.IV.19. Distribution of frequencies (boundary layer with generated vortices, $Re = 3 \cdot 10^5$):
1--x/H = 8; 2--x/H = 1.1; 3--x/H = 2.5; 4--x/H = 0.8; 5--x/H = 0.2 (external flow). [Shvets and Shvets (1976)]

The spectrum is not uniform compared to the turbulent boundary layer and the turbulence in the various positions of the wake is not yet self-similar. Apparently the shear layers are formed only from the internal part of the boundary layer. They are unstable as the small but increasing flow fluctuation shows. The maximum value of fluctuation measured by the hotwire anemometer increased rapidly between x/H = 1-4.

Pirri (1972) presented a theoretical study of the decay of the fluctuating velocities in the supersonic near wake expansion of a boundary layer turbulence.

Since the expansion is very rapid, the applicable linearized analysis is used to the boundary layer mean flow stream lines as the boundary expands into the near wake to predict a change of the fluctuation levels and turbulent scale sizes. The vortex is assumed to be initially circular of length scale Λ , and large values of Λ would correspond to turbulence scales at a low wave number end of the spectrum.

The turbulence is generated primarily in the high shear region of the viscous sublayer and wall-dominated turbulence layer and diffuses into the outer region where turbulence is nearly balanced by dissipation creating nearly homogenous field.

Including the effect of compressibility of the mean flow, mean properties are calculated by the characteristic method. The results indicate that the decay rate is strongly dependent on proper specification of the anistropic boundary layer turbulence and the decay is not caused by dissipation but by contraction of a distribution of vorticity filament by mean flow.

A comparison of analytical results with the only existing measured data of the boundary layer turbulence decay in the near wake expansion region of a slender body of Lewis and Behrens (1969) may result in a good agreement when a realistic choice of boundary layer turbulent energy spectrum and velocity fluctuation levels is made.

Demetriades (1964) investigated experimentally the viscous wake of seven right-angle two-dimensional wedges by using the hot-wire anemometer at M = 6, emphasizing the transition to turbulent and lateral spreading of the turbulent wake. The laminar near wake thickness was constant for very slender wedges (5^{o} included angle), but upon transition the wake spreads laterally rapidly and almost linearly within the first 100 effective base height. Transition to turbulence moves rapidly upstream as the pressure increases but eventually gets "stuck" at some characteristic distance behind the body. This sticking distance increases with an increasing slenderness and / or an increasing flight Mach number. The near wake of the wedge is strongly stabilized by the large lateral Mach number gradient and the transition Reynolds number was independent of the body size but dependent on the wedge angle. The minimum Reynolds number for transition based on an effective body size was about 10,000. The wake seems to be free of fluctuations at the beginning but further downstream a signal appreciable magnitude develops. Although the signals could be partly due to the changing sensitivity of the instrument as it traverses the wake, they also indicate the pressure of actual flow fluctuations. In the light of a small disturbance stability theory, a spectral analysis of these signals would be of interest, particularly in the wake region immediately preceding transition.
Zubkov and Shvets et al (1972) studied base pressure fluctuations and measured dynamic pressure in the reversed flow of cone. In a range of subsonic velocities, fluctuations of large amplitude were observed in a broad range of frequencies (Sh = 0.05-0.1) and as the speed of sound was

approached, fluctuations of dynamic pressure increase. At supersonic speeds, the first maximum of the spectrum of dynamic pressure fluctuations is found at the same frequencies as the frequencies of pressure fluctuation. ($M = 3$, $Sh \simeq 0.4$, $M = 4$, $Sh \simeq 0.02$)
Similar to pressure fluctuation, by going over from M=3 to M=4, the dynamic pressure fluctuations decrease at the first maximum. But, there is a distinct difference of spectra of dynamic pressure fluctuation occuring only one maximum at Sh = 0.2-0.4 from that of pressure spectra.

For the purpose of clarification of flow dynamics in the base region, optical flow visualization is made by taking 3-6 thousand frames of pictures per second. Fluctuation of the free viscous layer was observed as periodic changes of dimensions of toroidal vortex and fluctuation of this vortex close to the wake boundary. The region of circulating flow is surrounded by a flow of large velocity gradient, and the internal viscous layer is unsteady. The fluctuations are caused by a flow rate fluctuation in the stagnation zone and coincide in frequency with fluctuation corresponding to maximum amplitude of pressure fluctuations as Panov, Shvets and Khazen (1966) noted.

Chevray and Kovasznay (1969) measured the turbulence in the wake of a thin aluminum flat plate with constant thickness of 0.160 cm except the last 60 cm where it was machined down symmetrically on both sides so that the thickness was tapered linearly down to h = 0.025 cm at the trailing edge. Coil springs were used upstream as turbulence generators which

produced a thick and stable turbulent boundary layer near the trailing edge and its Reynolds number $Re = \delta u_\infty / \nu = 1.5 \times 10^4$ was in all tests. No detectable periodic components were found in the wake at any downstream station. Turbulence intensities given as rms value of streamwise and normal components of the velocity fluctuations show that the maximum intensity moves away from the axis of symmetry and it occurs near the zone of maximum shear.

The low level of fluctuation in the circulation zone downstream of a wedge is due to reverse transition from the turbulent to the laminar caused by sudden expansion of flow.

3.3 Hypersonic Wake

The region of a hypersonic wake in an atmosphere is divided into two areas: viscous internal and inviscid external. The internal region increases its dimension downstream by absorbing the external fluid and turbulence contributing to the mixing with turbulent core.

The analogies exist between compressible and incompressible flow in the following characteristics frequency of pulsation; relationship between Sh and Re number, coincidence of origins of vortex formation and the occurrence of turbulence in the wake and development of large scale vortices in small-scale turbulence.

Therefore, for the study of dynamic characteristies of hypersonic wakes, measured data of incompressible subsonic wakes are often used because due to the large coefficient of turbulent diffusion of motion, fluid velocity in the wake, rapidly decreases to a subsonic level.

Behrens and Ko (1971) investigated experimentally at M=6, Re=30.000 - 230.000/in. and stagnation temperature 275°F the stability behavior of natural flow fluctuations in both linear and nonlinear instability region in the wake of 10° half angle wedges and a flat plate with sharp leading and trailing edge. By measuring hot-wire fluctuation, the growth and decay of flow fluctuations and development of frequency spectra are to be determined. Measured mean flow and fluctuations are divided into linear and nonlinear instability region. The inviscid linear stability theory predicts well the growth of the fluctuation and amplitude distribution in the linear region. In the nonlinear region similarities with low-speed wake exist. The fluctuations grow on the wake axis. As the wake becomes nonlinear, the signal on the axis starts to grow rapidly. In order to investigate the fluctuation, which causes the break down of the steady laminar flow field, frequency distributions of fluctuation were taken at points in the wake where the fluctuation signals are maximum and on the wake axis. Near the flat plate the fluctuation intensity monotonically decays with an increasing frequency and as the flow moves downstream a peak in the spectrum develops. Further downstream a peak in the spectrum decreases rapidly. The most unstable frequency is called the fundamental frequency, and twice this frequency, the first harmonic. A further increase of a fundamental frequency component and a further tuning about this frequency is observed at the beginning of the nonlinear region. On the wake axis, a maximum is observed at twice the fundamental frequency (first harmonic). On the wake axis, a most dramatic rise in the fluctuating intensity occurs as the wake becomes nonlinear.

The linear instability region (in which the mean flow is laminar) is followed by a nonlinear instability and the fluctuation spectrum undergoes dramatic changes. In none of the Behrens and Ko's (1971) investigations was it possible to make measurements far enough downstream to reach "fully developed turbulent flow".

Based upon the measured peak frequencies, a nearly universal Strouhal number of $f\, b_o/u_\infty = 0.3$ where b_o is wake width, was found for both incompressible and hypersonic flows. The prediction for the development of mean flow and flow fluctuation in the nonlinear region by Ko, Kubota and Lees (1970) for an incompressible wake is applicable for a hypersonic wake. Employing the integral method, this theory was used for the study of the interaction between a two-dimensional, single frequency finite amplitude disturbance in a laminar incompressible wake behind a flat plate at zero incidence. A similar procedure can be applied to flow of inviscid nature and governed by two-dimensional disturbances.

Assuming the small fluctuation compared to mean values obtained from equations of energy and state and ignoring the energy dissipation, the density fluctuation is given by

$$\bar{\rho}'/\rho = a^{0.5} (1 - i_e / i_\theta)$$

where $\bar{\rho}'$ is fluctuation of density, $a = 0.2$ is a coustant, i_e and i_θ are enthalpy on the boundary and on the wake axis respectively.

The maximum fluctuation occurs if $i_e/i_\theta \rightarrow 0$ i.e. $(\bar{p}'/p)_{max} \rightarrow a^{0.5}$.

If it is assumed that fluctuations of density and velocity are self-pre-

serving, then

$$\left(\overline{\rho'} / \rho \right)^2 = a \left[\left(\rho_e - \rho \right) / \rho_e \right]^2$$

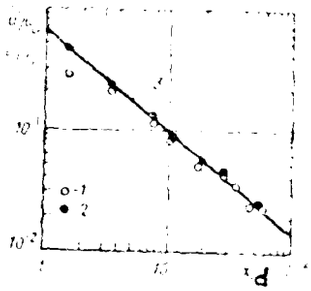

Fig.IV.20. Fluctuations on the axis of a wake: [Gibson et al (1968)]
1- $\overline{u'}/u_\theta$; 2- $\overline{u'}/u_\infty$ -0.85
3- $\overline{u'}/u_\theta = 0.16\ (x/d)$

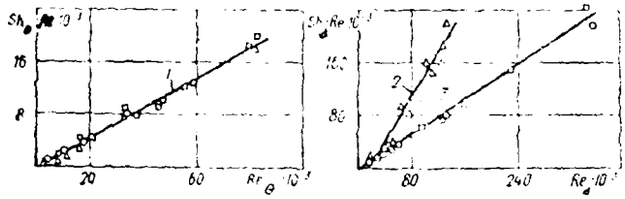

Fig.IV.21. The Strouhal number for hypersonic wakes behind a sphere (squares) and cones (triangles) (M = 14). [Fox et al (1967)]

Gibson, Chen and Lin (1968) measured the decay of a mean variance and a gradient variance of temperature and velocity in the initially heated sphere wake in a water tunnel. It was found that the dissipation rate of kinetic energy and the temparature variance both decrease approximately as $x^{-2.4}$ for the first 60 diameters downstream of the sphere and small scale temperature and velocity fluctuations were approximately homogencous for cross-sections of the wake normal to flow.

No region of continuous turbulence was found even on the wake axis, and a velocity spectrum measured on the wake axis normalized using the measured viscous-dissipation rate was in a good agreement with spectra from other turbulent systems normalized by the Kolmogoroff scaling.

For experimental investigation instead of air, water is often used because much more sensitive temperature sensors may be used in water and high spatial resolution, frequency response and sensitivity to temperature fluctuation can be achieved by using "single-electrode" conductivity probes in dilute electrolyte solution.

The mean square fluctuation velocity u' in x-direction normalized with the upstream velocity u_∞ and central line velicity u along the x-distance up to 60 diameters at Re = 65,000 is given by

$$\overline{u}'/u_\theta = 0.66\ (x/d)^{-0.85}$$

as whown in Fig.IV.20.

Fox et al (1967) expressed universal relationship between $Sh_\theta \cdot Re$ and Re_θ as well as $Sh_d \cdot Re$ and Re_d for a hypersonic wake downstream of a sphere and a cone as shown in Fig.IV.21 which were approximately given by ;

For line 1 ; $Sh_\theta \cdot Re \cdot 10^{-3} = 0.229 \left[1 - (1820/Re_\theta) \right]$

For line 2 ; $Sh_d \cdot Re \cdot 10^{-3} = 1.72 \left(1 - 18100/Re_d \right)$ (for cones)

For line 3 ; $Sh_d \cdot Re \cdot 10^{-3} = 0.66 \left(1 - 3180/Re_d \right)$ (for spheres)

References

Artonkin, V. G. (1972). "Base Pressure Behind a Cone with Hypersonic Velocities," Uchyenyye zapiski, TsAGI, 3.

Behrens, W. and D. C. S. Ko (1971). "Experimental Stability Studies in Wakes of Two-Dimensional Slender Bodies at Hypersonic Speeds," AIAA J. vol 9, No. 5.

Birkhoff, G. and E. Zarantonello (1957). Jets, Wakes and Cavities, Academic Press.

Bontarev, Ye N., and M. Ya Yudelovich (1960). "The Possibility of Increasing Base Pressure Behind a Wedge during Flight at Hypersonic Speed," AN SSSR OTN, Mekhanika i Mashinotroyeniye, 5.

Cassanto, J. M. (1965). "Ratio on Base Pressure," AIAA J., Vol. 3, No. 12.

Cassanto, J. M. (1967). "Radial Base Pressure Gradients in Laminar Flow," AIAA J., Vol. 5, No. 12.

Cassanto, J. M., Rasmussen, N. S., and J. D. Coats (1969). "Correlation of Free-Flight Base Pressure Data for M=4 to M=19," AIAA J., Vol. 7, No. 6.

Cassanto, J. M., Schiff, J., and E. J. Softley (1969). "Base Pressure Measurements on Slender Cones with Domed Afterbodies," AIAA J., Vol. 7, No. 8.

Chevray, R and L. S. G. Kovasznay (1969). "Turbulence Measurements in the Wake of a Thin Flat Plate," AIAA J. vol. 7, No. 8.

Crocco, L. and L. Lees (1952). "A Mixing Theory for the Interaction Between Dissipative Flows and Nearly Isentropic Streams," J. Aeron. Sci. vol. 19, No. 10.

Demetriades, A. (1964). "Hot-Wire Measurements in the Hypersonic Wakes of Slender Bodies," AIAA J. vol 2, No. 2.

Dewey, C. F. Jr (1965). "Near Wake of a Blunt Body at Hypersonic Speeds," AIAA J. vol.3, No.6.

Eldred, K. M. (1961). "Base Pressure Fluctuations," J. Aconst. Soc. America 33/1.

Fricke, F. R. and L. C. Stevenson (1968). "Pressure Fluctuations in a Separated Flow Region," J. Aconst. Soc. America. 44/5.

Fricke, F. R (1971). "Separated Flow Noise," Proc. 7th Intern. Congress on Acoustics. vol.2, M-P-U. (Physical Acoustics Sec Budapest).

Fox, J. Webb, W. H. Jones, B. C and A. G. Hammitt (1967). "Hot-Wire Measurements of Wake Turbulence in a Ballistic Range," AIAA J. vol.5, No.1.

Gibson, C. H. Chen, C. C. and S. C. Lin (1969). "Measurements of Turbulent Velocity and Temperature Fluctuations in the Wake of a Sphere," AIAA J. vol.6, No.4.

Greshilov, Ye. M. Yevtushenko, and L. M. Lyamshev (1969). "Spectral Characteristics of Pulsations of Pressure near the Walls with Separation of the Boundary Layer Behind a Protuberance on a Smooth Wall," Akusticheskiy zhurnal 1.

Grodzovskiy, G. L. Lashkov, Yu. A. Svishchev, G. P. and I. N. Sokolova (1972). 'Study of the Effect of Perforated Nozzles with Longitudinal Slots on Base Resistance of a Body of Revolution with Supersonic Velocities," Uchyenyye Zapiski, TsAGI, 2.

Isayev, S. P. and A. I. Shvets (1970). "Flow in the Base Region with Supersonic Flow past Bodies," AN SSSR MZhG 1.

Kiknadze, A. V. (1970) "Variation of Flow in Wakes Behind Disks and Sphere," AN SSSR MZhG 3.

Kistler, A. L. and W. Chen (1963) "The Fluctuating Pressure Field in a Supersonic Turbulent Boundary Layer" J. Fluid Mech. vol.16.1.

Kistler, A. L. (1964). "Fluctuating Wall Pressure under a Separated Flow," J. Aconst. Soc. America 36/3.

Ko, D. R. S. Kubota, T. and L. Lees (1970). "Finite Disturbance Effect on the Stability of a Laminar Incompressible Wake Behind a Flat Plate," J. Fluid Mech. vol.40, pt.2. pp.315-341.

Lees, L. (1964). "Hypersonic Wakes and Trails," AIAA J., vol.2, No.3.

Lewis, J. E. and W. Behrens (1969). "Fluctuation Measurements in the Near Wake of a Wedge with and without Base Injection," AIAA J. vol.7, No.4.

Lien, H. and J. Eckerman (1966). "Interferometric Analysis of Density Fluctuations in Hypersonic Turbulent Wakes," AIAA J. vol.4, No.11.

Lockman, W. K. (1967). "Free-Flight Base Pressure and Heating Measurements on sharp and blunt Cones in a Shock Tunnel," AIAA J., vol.5, No.10.

Mabey, D. G. (1972). "Some Measurements of Base Pressure Fluctuations at Subsonic and Supersonic Speeds," ARC CP 1204.

Panov, Yu A., and A. I. Shvets (1966). "Study of Base Pressure close to the Trailing Edges of Axisymmetric Bodies in a Supersonic Flow," Prikladnaya Mekhanika, 26.

Panov, Yu A, Shvets, A. I. and A. M. Khazen (1966). "Study of Variation of Base Pressure Behind a Cone in a Supersonic Flow," AN SSSR MZhG 6.

Pirri, A. N. (1972). "Decay of Boundary-Layer Turbulence in Near Wake of a Slender Body," AIAA J. vol.10, No.5.

Rossiter, J. E. and A. G. Kurn (1967). "Wind Tunnel Measurements of the Effect of a Jet on the Time Average and Unsteady Pressures on the Base of a Blunt After body. LD," ARC CP 903.

Sekundov, A. N. and O. V. Yakovlevskiy (1972). "Transition Regime of Flow in a Two-Dimensional Wake Behind a Thin Plate and Cylinder," AN SSSR MZhG 3.

Shvets, et al. (1968). "The Effect of the Mach Number on Variation of Base Pressure behind a Cone," Vestnik M G U Matematika i Mekhanika 1.

Shvets, A. I. (1970). "Flow past a Compressed Rotational Ellipsoid along the large Axis," AN SSSR MZhG. 2.

Shvets, A. I. (1971). "Near Wake," X International Symposium of Fluid Dynamics Transactions, (Warsaw), 1972.

Shvets, A. I. (1972). "Flow in the Base Region of Two-dimensional Bodies," AN SSSR M hG. 6.

Shvets, A. I. and I. T. Shvets (1976). Gas Dynamics of Near Wake, Naukova Dumka Press. Kiev.

Shvets, A. I. (1978). "Base Flow" Prog Aerospace Sci, vol.18. Pergamon Press.

Speaker, W. V. and C. M. Ailman (1966). "Static and Fluctuating Pressure in Regions of Separated Flow," AIAA Paper 66-456.

Stepanov, G. Yu, and L. L. Gogish (1973). Kvaziodnomernaya gazodinamika sopel rakyetnykh dvigateley, (Quasiunidimensional Gasdynamics of Jet Engine Nozzles), Mashinstroyeniye Press, Moscow.

Vas, I. E. Murman, E. M. and S. M. Bogdonoff (1965). "Studies of Wakes of Support-free Spheres at M=16 in Helium," AIAA J., Vol.3, No. 7.

Wilson, L. N. (1967). "Far-wake Behavior of Hypersonic Blunted Cones," AIAA J., Vol. 5, No. 8.

Wu, J. J. and W. Behrens (1972). "An Experimental Study of Hypersonic Wakes behind Wedges at Angle of Attack," AIAA J., Vol. 10, No. 12.

Zhdanov, V. T. and L. Ye. Born (1974). "Experimental Study of Interaction of a Stream of Inert Gas Flowing Normal to the Lateral Surface and Flow in the Base Region of an Axisymmetric Body," Trudy, TsAGI, (Works of TsAGI).

Zubkov, A. I. and A. I. Shvets, et al. (1972). "Study of Separated Turbulent Separated Flows," Doklady na XIII Mezhdunarodom kongresse po teoreticheskov i prikladnoy mekhanike (Reports on the XIII International Congress on Theoretical and Applied Mechanics) Nauka Press, Moscow.

CHAPTER V

SYMBOLS

i	enthalpy
K	constant
q	heat flux
$\bar{q}$	thermal flux along cross-section of downwind convex side of semi-cone
q_o	heat flux at stagnation point
Rx	Reynolds number based upon x
λ_o	Coefficient of thermal conduction
θ	wedge angle
θ_K	semi-cone angle
μ_o	Coefficient of viscosity corresponding to stagnation temperature

CHAPTER V

Thermal Effects on Flow Separation and Reattachment

Separating and reattaching flows at high speed are affected by aerodynamic heating.

Most of the investigations of these problems are experimental. Thus, presentations made here are for experiments. Although, some analytical investigations are reported.

For convenience, heat transfers of separated flow and reattached flow are presented separately.

1. Experimental Investigation of Wake Heat Transfer

The problems of wake heat transfer are divided into heat transfer of near wake, far wake and transition.

1.1 Near Wake

Muntz and Softley (1966) carried out two sets of experiments on the near wake downstream of 0.05 nose bluntness ratio, 10° half angle sphere cone at hypersonic speeds. One group involved the simultaneous measurements of density and static temperature and another group involved base pressure and base heat transfer.

The static temperature and density were measured directly using an electron beam excitation technique. The results indicated that the near wake static temperatures are sensitive functions of both Re and

model surface temperature but not of Mach number as shown in Fig.V.1.

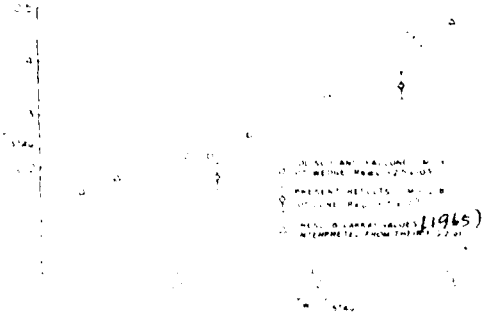

Fig.V.1. Temperature at the trailing critical point of a wake depending on temperature of the surface of a model [Muntz and Softley (1966)]:
1--cone, $\theta = 10^{\circ}$, $M = 12.8$, $Re_{\infty,L} = 7 \cdot 10^5$; 2--wedge, $\theta = 10^{\circ}$, $M = 16$, $Re_{\infty,L} = 2.5 \cdot 10^5$; 3--cone, $\theta = 5^{\circ}$, $M = 8$-12 [Lykoudis (1966)].

Static temperatures of the wake flow decrease with an increase of Re, but with a decrease in temperature of the wall of the body. The maximum temperature in the wakes increased with increasing the nose bluntness ratio. Fig.V.2 shows the distribution of static pressure along the axis of wake downstream of a cone. The critical point is located close to the point of maximum wake temperature.

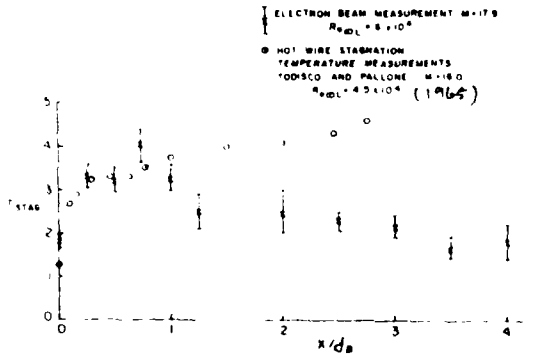

Fig.V.2. Distribution of static temperature along the axis of a wake ($\theta = 10^{\circ}$, $r/R = 0.05$, $M = 12.8$, $Re_L = 7 \cdot 10^5$, $T^* = 1100^{\circ}K$ [Muntz and Softley (1966)]: 1--according to deexcitatation of perturbed atoms; 2--according to measurement of base pressure.

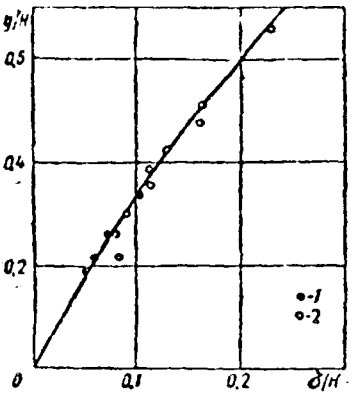

The measurement of Batt and Kubota (1969) indicated that in the laminar wake downstream of a wedge, the wake neck width can be correlated by a single curve irrespectively whether the wedge wall is cold or adiabatic as shown in Fig.V.3.

Fig.V.3. Results of measurement of the width of a wake neck (wedge $\theta = 20^{\circ}$, M = 6) [Stepanov (1969)]; 1--cold wall, H = 7.62 mm; 2--adiabatic wall, H = 3.81 and 7.62 mm.

1.2 Far Wake

Martin (1969) presented fairly completely in his monograph "Entry into the Atmosphere" (Vkhod v atmosferu) MIR Press, Moscow, on the boundary of wake, turbulence, transfer of mass and heat, chemical reaction, wake and its interaction with electromagnetic waves.

Shvets and Shvets (1976) therefore described the certain aspects of far wake gasdynamics from the U.S.A., recent references in their monograph "Gasdynamics of Near Wake" Kiev.

Levensteins and Krumins (1967) measured the laminar and turbulent wake growth downstream of cones of various half-angle 9° - 40° at $M \simeq 10$ as shown Fig.V.4.

The laminar wake, marked by open circle in this Fig.V.4, indicates that the laminar wake does not grow monotonically and there are oscillations in the wake width. The straight line about which the oscillations occur

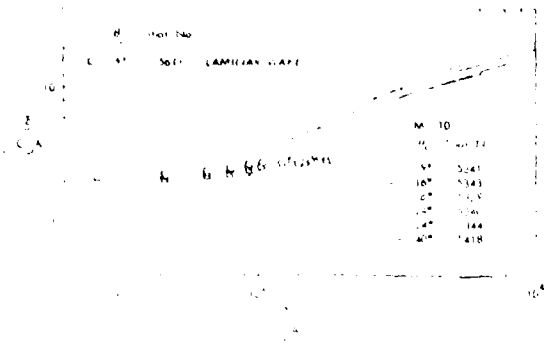

Fig.V.4. Increase in the width of a turbulent wake behind a cone when M = 10 [Levensteins and Krumins (1967)] (marks apply to cone, $\theta = 9^0$, laminar wake).

has a relationship of $\delta \propto x^{0.1}$ and the period of these oscillations is about 50 body diameters. The turbulent wake growth downstream of 4 cones of different half-angles are also shown in Fig. V.4. The turbulent wake growth downstream of a 9^o half-angle cone is given by 1/3 power growth and for far wakes of all 4 cones in the coordination defined are of the same size and grow at the same rate. For the larger angle cone, the near wake width decreases and the growth rate increases with increasing drag coefficient.

1.3 Transition

Lees (1964) summarized the tentative picture of the transition in the wake at hypersonic speeds as follows:

Below a certain minimum critical Reynolds number, the wake is laminar. Above this limit the transition first appears at about 40 - 50 diameters downstream of the body if the body is blunt and then moves upstream as the ambient pressure increases maintaining a constant value of $(Re_{xf})_{TR} = 5.6 \times 10^4$ where the subscript f refers to turbulent front, independent of body diameter. When the transition reaches the neck, it gets "stuck" there until Re_L exceeds $(Re_L)_{TR}$ for the free shear layer,

and eventually appears in the boundary layer on the body. For a sharp-nosed slender body, the transition first appears in the wake at lower ambient pressure and somewhat further back in terms of body diameters than a blunt body, especially at lower hypersonic speeds. Again the transition moves rapidly upstream as the ambient pressure increases but this forward motion slows down when the location of the transition approaches the neck.

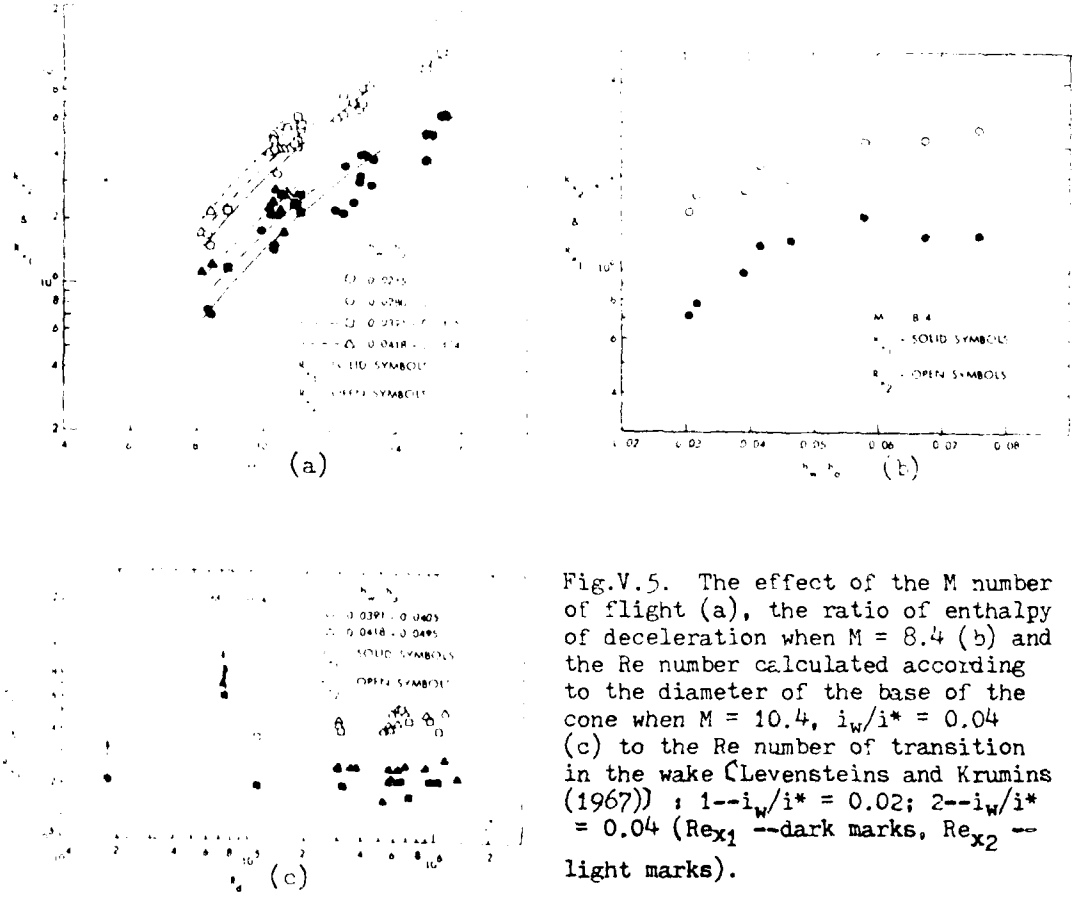

Fig.V.5. The effect of the M number of flight (a), the ratio of enthalpy of deceleration when M = 8.4 (b) and the Re number calculated according to the diameter of the base of the cone when M = 10.4, $i_w/i^* = 0.04$ (c) to the Re number of transition in the wake (Levensteins and Krumins (1967)) ; 1--$i_w/i^* = 0.02$; 2--$i_w/i^* = 0.04$ (Re_{x_1} --dark marks, Re_{x_2} -- light marks).

The wake flow transition is effected by the Mach number, wall to stagnation enthalpy ratio and the body Reynolds number which as Levensteins and Krumins (1967) reported is shown in Fig.V.5. In this Fig.V.5, Re_{x_1} and Re_{x_2} are based upon x_1 and x_2 and defined as an axial distance from the model base to the very first appearance of laminar waves in the viscous wake and to the first appearance of fully turbulent flow respectively

The wake flow transition downstream of cones in a function of the Mach number is shown in Fig. . a. The data for nearly the same wall-to-stagnation enthalpy ratios are considered as a group. In the region of $8 < M < 16$ the wake transition Reynolds number increases with increasing the Mach number, due to the decrease of an amplification rate of small disturbances with increasing the Mach number as seen in Fig.V.5b for $M = 8.4$.

Wake flow transition Reynolds numbers increase with an increase of the wall-to-stagnation enthalpy; or decreasing heat transfer rates at the surface of the body. If $\Delta T = (T_m - T_e)/T_e$ where subscrips m and e refer to wake center line and at the edge of wake, for a given Mach number, ΔT increases as the heat-transfer rate on the body surface decreases and with increasing ΔT, the amplication rates for small disturbances decrease. From Fig.V.5c, it is seen that at low Reynolds numbers the wake transition Reynolds numbers increase with decreasing body Reynolds numbers.

2. Viscosity-Diffusivity Models

Zakkay and Fox (1967) carried out a theoretical and experimental investigation of the turbulent far wake and found that among the available several viscosity-diffusivity models, the eddy viscosity that best correlates the experimental results is based upon the product of the wake half-radius and the mass flux at the center line $(\rho u)_{CL}$.

For the laminar far wake, since the diffusion processes are well defined, standard techniques are available for the prediction of the flow field, but for the turbulent flow, the transport properties are not well defined and some assumptions are to be made to define e.g. a turbulent viscosity for use in the laminar equation in order to solve the problem.

Zakkay and Fox (1967) used an approach similar to that applied for the problems of mixing based upon the basic equations in the modified von Mises plane for the analysis of far wake flow field. The investigation was conducted at hypersonic speeds, but at a relatively low temperature, so that for the understanding of turbulent transport properties no complications due to dissociation or chemical reaction arise. The test was conducted using a flat faced cylinderical model exposed to M = 12 flow of stagnation pressure 450 psi and a stagnation temperature of 2000°K just high enough to prevent condensation. The Reynolds number based on a free stream condition was 4.5×10^5/ft and model wall-to-stagnation temperature ratio was 0.265. The measured profiles are used as imput data in the solution of the set of boundary layer equations in an implicit finite difference scheme for an IBM 7094

computer. With the measured profiles, a straight forward marching downstream of the solution was obtained using the assumed form of the eddy viscosity of various models. The final profiles obtained from the machine are compared to the ones of experiments. Thus, a systematic evaluation of various models was made. The results indicate that the model that best describes the wake is that which also describes coaxial mixing. The viscosity-diffusivity models considered are:

model 1, $\mu = K \rho_{CL} u_{CL} r_{1/2}$

model 2, $\mu = K (\rho_e u_e - \rho_{CL} u_{CL}) r_{1/2}$

model 2A, $\mu = K \rho_e (u_e - u_{CL}) r_{1/2}$

model 3, $\mu = K \rho_{CL} u_{CL} r_{1/2} \left[\left(\frac{2}{\rho_{y2}} \right) \int_0^y \rho \, u \, dy \right]$

model 4, $\mu = K \rho_{CL} (u_e - u_{CL}) \delta'$

where $r_{1/2}$ is defined as that value of y where

$$\rho u = \frac{1}{2} (\rho_e u_e + \rho_{CL} u_{CL})$$

and where δ' is defined as that value of

$$\eta^2 = 2 \int \frac{\rho}{\rho_e} y \, dy$$

where $(u_e - u)/(u_e - u_{CL}) = 0.01$

In all of these assumptions a value for the constant K is required.

Model 1, is due to Zakkay, Krause and Woo (1964) used for jet-mixing problem.

Model 2, is due to Ferri, Libby and Zakkay (1962) who used to correlate a large number of hydrogen-air combustion experiments.

Model 2A, is due to Schlichting (1960) which is classical involving, only velocity difference.

Model 3, is due to Ting and Libby (1960) who applied a density transformation to model 1 resulting model 3.

Model 4, is due to Bloom and Steiger (1963) and Bloom (1964) who introduced density transformation through δ' [illegible] the velocity difference.

A comparison of the Mach number distributions along the wake centerline obtained by an analysis and experiment for length-diameter ratio of cylinder $(L/d)_1 = 50$ is shown in Fig.V.4. The effect of density transformation is slight as evidenced from the comparison of the results of models 1 and 3 and of models 2A and 4. Although the data is limited, it may be noted that any of the models with approximate constant K may fit the data over some range of x/d.

Nakkay and Fox (1967) concluded that the phenomena of mixing and the describing equations of the flow field with their transpot properties is analogous to the problem of the coaxial mixing. For blunt bodies, the Mach number recovers 95% of its value in a distance of L/d of 200. The velocity or velocity difference is not a good parameter to describe the far wake problem but rather the density and Mach number. The viscosity model successfully applied for a mixing problem with a chemical reaction can be also used for chemically reacting wakes provided that all of the initial species profiles are known before the shoulder expansion and at the base of the body.

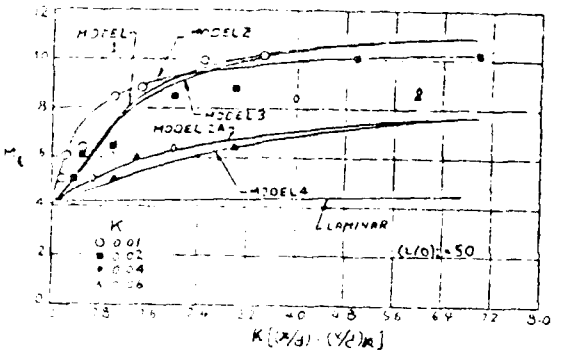

Fig. 7.6. A comparison of results of a theoretical calculation with experimentally measured distribution of the M number along the axis of a wake $(x/d)_K = 50$ [Zakkay and Fox (1967)]: A, B, C, D, E--Models of flows and streams; 1-- $K = 0.01$; 2-- $K = 0.02$; 3-- $K = 0.04$; 4-- $K = 0.06$; line 5 corresponds to laminar flow.

3. Experimental Investigation of Aerodynamic Heating at Reattachment Zone at High Speeds with or without Protruding Bodies.

Before describing the experimental investigation of aerodynamic heating at reattachment a theoretical solution of reattachment heat transfer is presented here

Telionis (1972) proposed a simplified model by a closed form approximation solution for engineering estimates of heat transfer in the neighborhood of reattachment for supersonic flow over a rearward-facing step with a suction slot.

Due to the difficulty of a base flow problem, it was necessary to treat separately the regions of separations, recirculating flow, free shear layer and outer flow and match the individual solutions along the relevent interfaces. The analysis becomes even more complex if the ratio

of the boundary layer thickness δ with respect to base height H, $\delta/H \sim 1$ because the whole recirculating flow is within the region of viscosity influence and inviscid core is eliminated, overlapping the region of separation and reattachment and the expansion of the compressible flow is immediately followed by recompression.

For simplified prediction of heat transfer at the reattachment, Telionis (1972), assumed that the flow properties in the neighborhood of reattachment are similar to the properties of stagnation flow and for $\delta/H \sim 1$ the heat transfer along the stagnation stream line is negligible. Therefore, the heat transfer at the reattachment is approximately equal to heat transfer at the stagnation point of a free stream with properties of those at the stagnation stream line before the expansion. A comparison of the predicted value with experimental data indicates that Telionis' method for no mass transfer predicts correctly the sharp decrease of the heat transfer rate with increasing δ/H for $\delta/H < 0.5$ and a mild increase for $\delta/H > 1$. It is expected that this method predicts also the effect of mass transfer in the case of suction.

In U.S.S.R., effects of a protruding body in the flow behaviors involving separation and reattachment, and shock interaction with a three-dimensional boundary layer are studied by the visualized limiting stream line pattern produced by the oil drop flow. On the other hand, the rates of heat transfer are evaluated by the degree of change of color or transparency of the temperature sensitive coating, independently to pressure, along the lines of reattachment and separation. The pertinent control techniques for elimination of the maximum heat flux

are also described.

The heat transfer rate in the reattachment zone is large exceeding by an order of magnitude compared to its surrounding area. Therefore, the parametric study of its heat transfer phenomena in M_∞, Re_∞, geometrical shape and the angle of attack as well as the proper control technique of reattachment zone heating are urgently needed. For these experimental investigations Borovoy (1968, 1968a), Borovoy and Ryzhkova (1969, 1971), Borovoy et al (1970) and Maykapar (1970) have selected simply shaped bodies such as a semi-cone with a flat surface, a circular cone, a wedge and a triangular plate.

The lines of separation and reattachment are determined by observing the limiting stream line (nearest stream line to the wall surface). If the limiting stream lines meet along a line tangentially, then such confluence line is considered the line of separation, and if the limiting stream lines spread along a line, then such a line is defined as the reattachment line. Although, these definitions are not an exhaustive one to obtain the complete understanding of the complex three-dimensional flow behavior.

3.1 Aerodynamic Heating with no Protuberance on the Surfaces of Semi-Cone, Cone and Triangular Plate.

3.1.1 Semi-Cone

On the flat surface of the semi-cone place downwind Borovoy (1969) photographed the change of color and its width in a function of time (Fig.V.7) and limiting stream lines (Fig.V.8). The length of these stream lines is propotional to the shear stress and spread

of these stream lines indicating reattachment is clearly shown in Fig.V.8.

3.1.1.1 Flat Side Downwind

From Fig.V.8, it is to be noted that if Re is reduced (c and e) the thermal flux peaks disappear. The measured heat transfer rate distribution over the cross-section of the flat side is shown in Fig.V.9. The maximum heat transfer of laminar flow is expressed in a function of $Re_\infty \cdot M_\infty^{-6}$ which is the parameter of viscous and inviscid flow interaction.

Borovoy et al (1968a) measured the complex heat transfer phenomena at angles of attack. As seen in Fig.V.10, at $\alpha = 15^\circ$, two maximum heat flux regions originating from the leading edge approach each other and merge into a single region at far downstream. At $\alpha = 25^\circ$ a single heat flux peak is formed on the front part while on the downstream part two peaks are formed on each side of the center line.

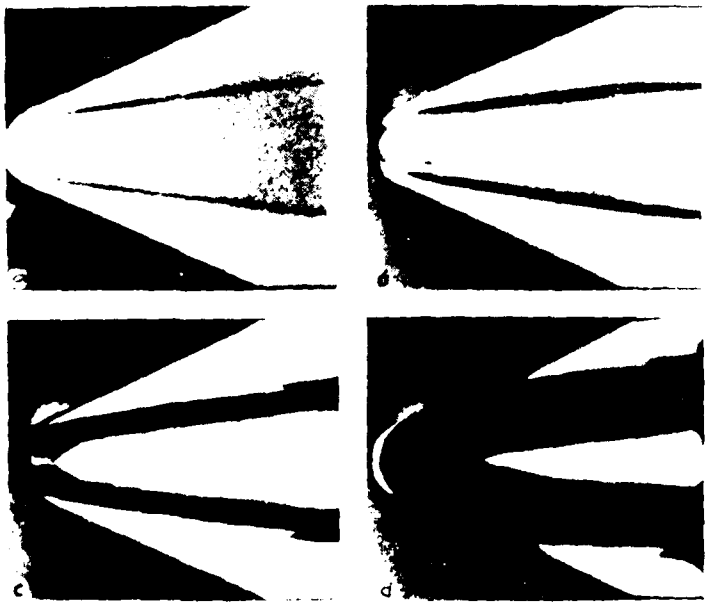

Fig.V.7. Semi-cone θ_x=24.30. Coated with temperature sensitive paint, angle of attack =0° (flat side facing downstream), M_∞ =5, $Re_{r\infty}$ =1.1·10^6, $Re_{L\infty} \cdot M_\infty^{-6}$=70. Borovoy et al, 1968a a-t = 0.8 S; b-t = 3 S; c-t = 12 S; d-t = 48 S.

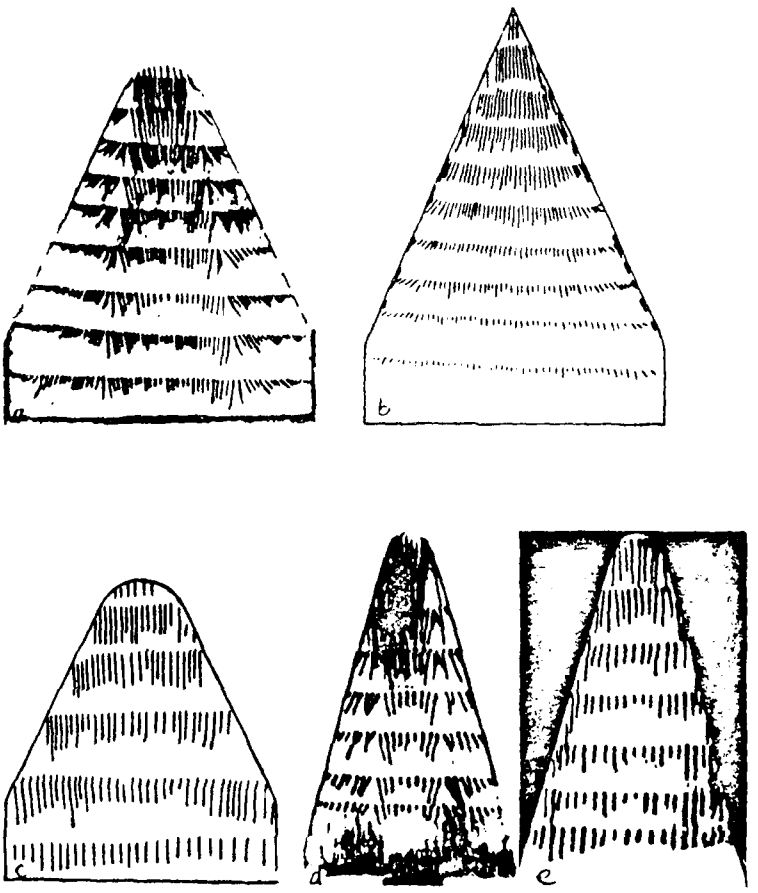

Fig.V.8. Limiting stream line patterns for semi-cone, $\alpha = 0^{\circ}$. [Boryvoy and Ryzhkova ,1969].

a) Blunt; b) Pointed; c) Blunt; d) Pointed

e) Blunt; L = Length.

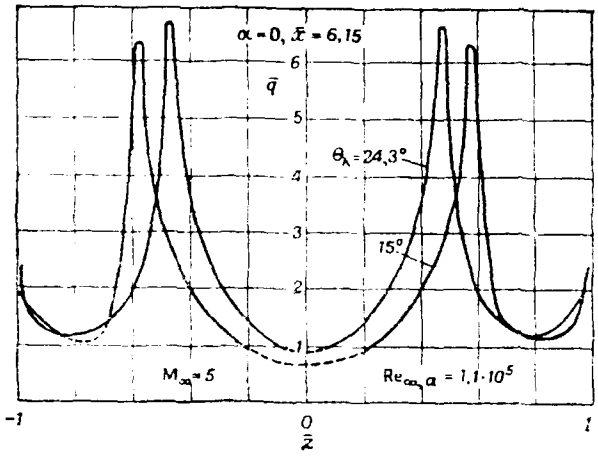

Fig.V.9. Thermal flux distribution over cross-section of flat side of blunt semi-cone. [Borovoy and Ryzhkova, 1969]. $\bar{x} = x/a$; a= tip radius, thermal flux $\bar{q}$ is referred to the thermal flux to the flat plate (laminar boundary layer).

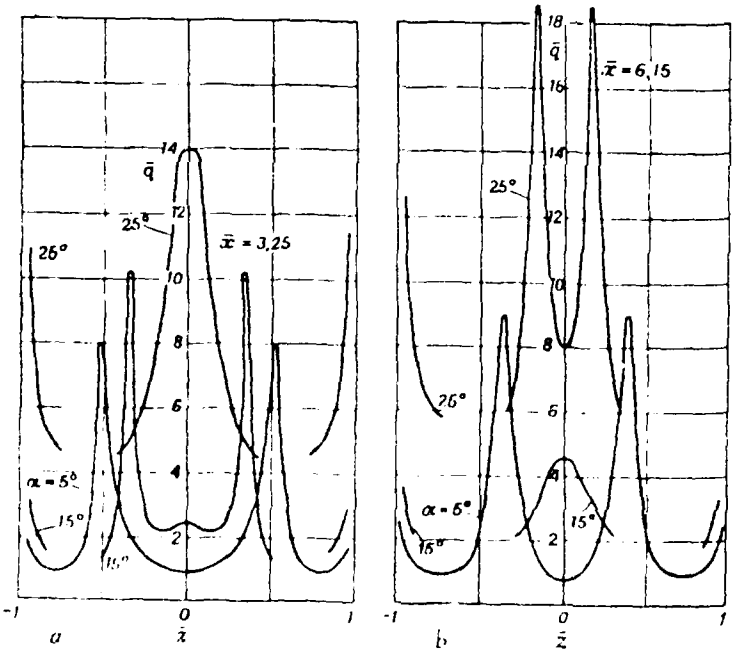

Fig.V.10. Thermal flux distribution along cross-section of flat side of blunt semi-cone as function of angle of attack ; $\theta_k = 24.3^\circ$; $M_\infty = 5$; $Re_{L\infty} = 1.1 \cdot 10^6$ [Borovoy et al, 1968b].

3.1.1.2 Flat Side Upwind

As shown in Fig.V.11 and V.12, regardless of the tip bluntness, a single line of reattachment is formed in the plane of symmetry. If Re is reduce, then the lines of flow spreading disappear reducing the axial heat flux as seen in Fig.V.12.

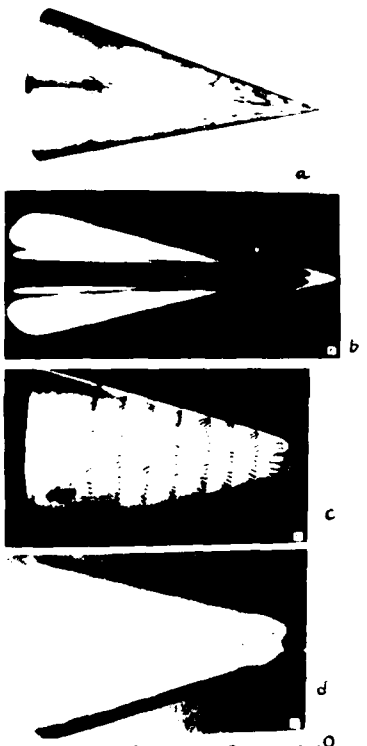

Fig.V.11. Semi-cone $\theta_k = 15^\circ$ with flat upwind side.
$M_\infty = 5$, $Re_{L\infty} = 10^6$ [Borovoy and Ryzhkova, 1971].
(a) Limiting stream lines $\alpha = 30^\circ$
(b) Model coated w/temp. sens. paint $\alpha = 25^\circ$, t = 50 c
(c) Limiting stream lines $\alpha = 25^\circ$
(d) Model coated s/temp. sens. paint $\alpha = 25^\circ$, t = 10 c

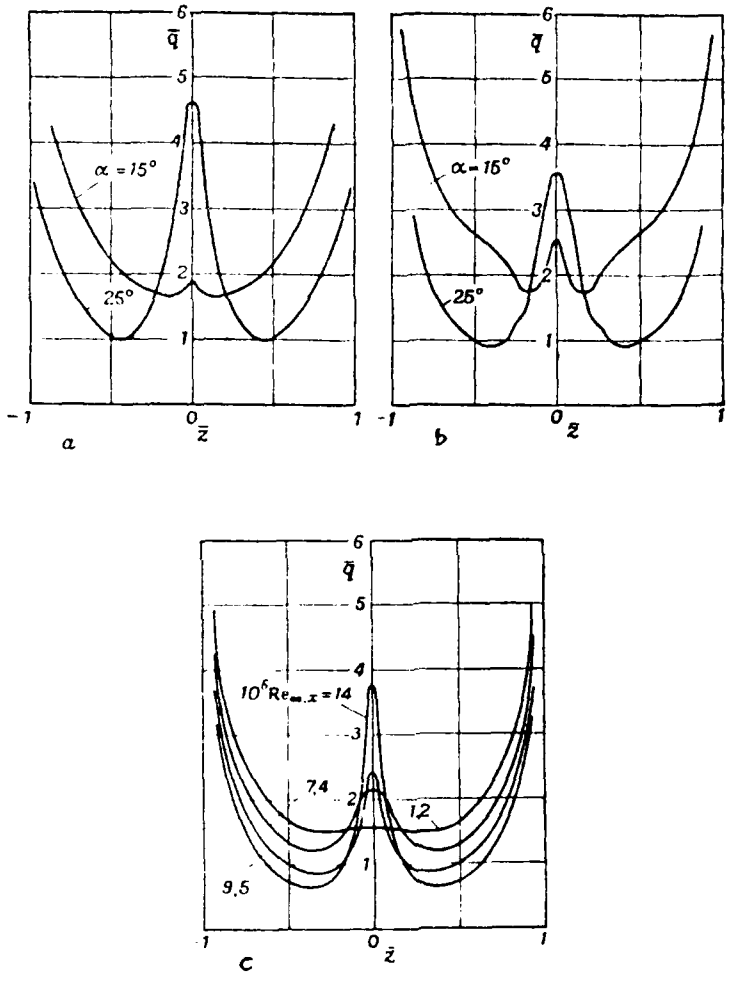

Fig.V.12. Thermal flux distribution along cross-section of downwind convex side of pointed semi-cone $\theta_k = 15^\circ$ [Borovoy and Ryzhkova, 1971].
(a) $M_\infty = 5$; $Re_{L\infty} = 0.4 \cdot 10^6$; $\bar{x} = 0.24$
(b) $M_\infty = 5$; $Re_{L\infty} = 0.77 \cdot 10^6$; $\bar{x} = 0.46$
(c) $M_\infty = 6$; $\alpha = 25^\circ$.

An interesting behavior of the heat flux peak on the plate side of the blunt semi-cone placed upwind, compared to that of the pointed one, is shown in Fig.V.13. The heat flux peak for the blunt model disappears on the front part of the model but appears only in the aft part in smaller magnitude than the pointed semi-cone.

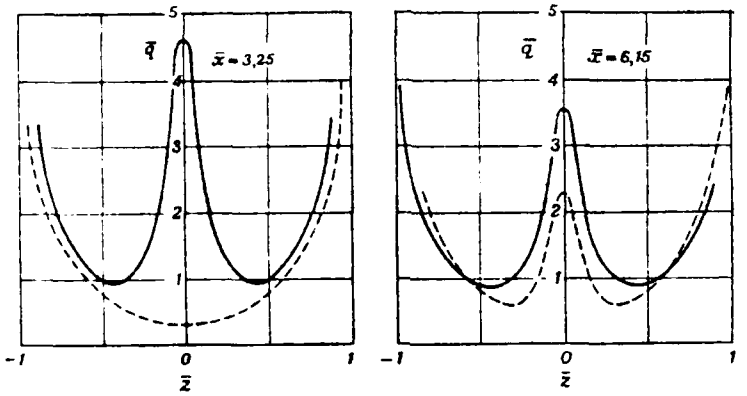

Fig.V.13. Thermal flux distribution along cross-section of downwind convex side of semi-cones. [Borovoy and Ryzhkova, 1971].
$\theta_k = 15$; $\alpha = 25^\circ$; $M_\infty = 5$; $Re_{L\infty} = 10^4$.
------- = Blunt semicones; ——— = Point semicones.

3.1.2 Circular Cone

The flow behavior on the downwind side of the circular cone, is as seen in Fig.V.14, similar to that of the over the downside convex side of the semi-cone. Based upon the observation of the limiting stream lines it appears that the secondary separation takes place along the second line of flow confluence.

3.1.3 Wedge

As seen in Fig.V.15 on the flat side, the heat flux peaks are observed in the reattachment zone and the blunting of the leading edge increases the heat transfer on the downwind side.

3.1.4 Triangular Flat Plate

Korovoy et al (1970) and Maykapar (1970) using a rounded apex triangular plate visualized the limiting stream lines and measured the heat transfer rate as shown in Fig.V.16.

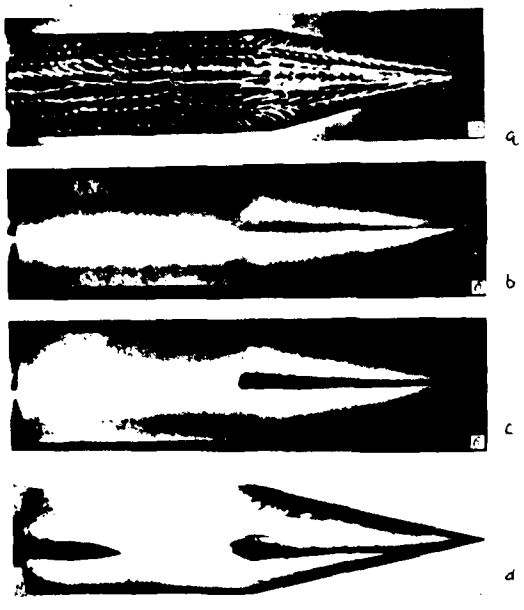

Fig.V.14. Cone $\theta_k = 135^\circ$, $M_\infty = 5$, $Re_{L\infty} = 10^6$, $\alpha = 20^\circ$ [Davlet-Kel'devev R. ., 1971].
a) Limiting stream lines on the downwind side;
b - t = 2S; c - t = 5S; d - t = 15S
Model with fusible temperature sensitive coating.

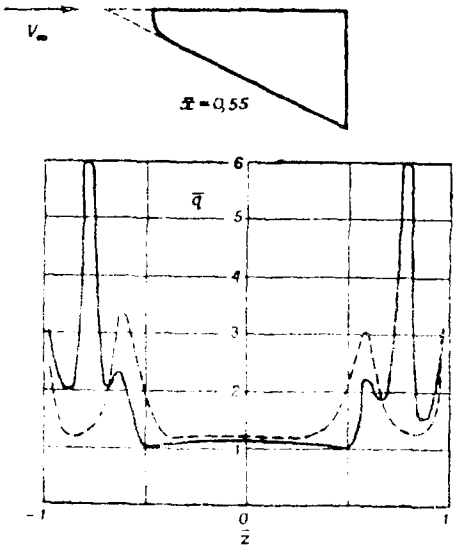

Fig.V.15. Thermal flux distribution along cross-section of downwind side of wedge; $M_\infty = 5$, $Re_{1\infty} = 9.5 \cdot 10^5$. [Borovoy et al, 1970].
——— = Blunt wedge; - - - - - - = Pointed wedge.

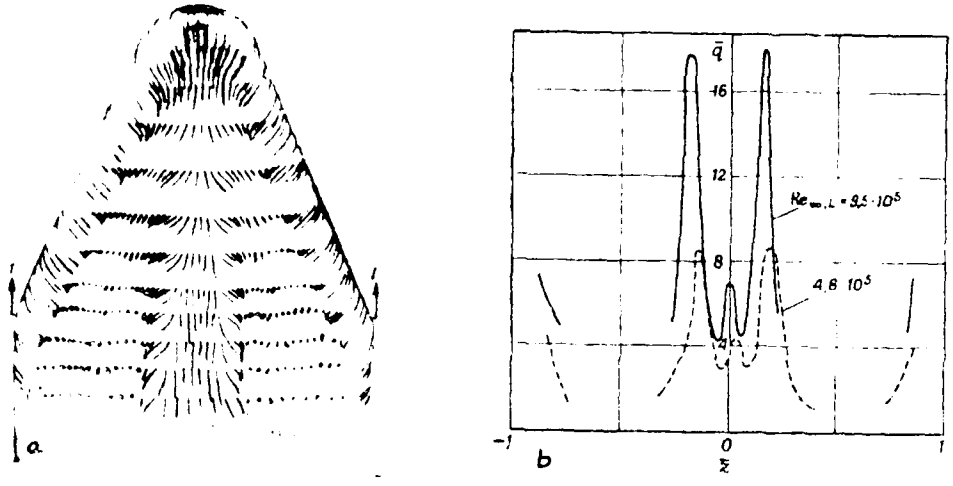

Fig.V.16. Limiting stream lines on downwind side of triangular flat plate with cylindrical edges and thermal flux distribution along its cross-section 1-1; $\alpha = 20°$; $M_\infty = 5$ [Borovoy et al, 1970].
a) Limiting stream lines
b) Thermal flux distribution.

The heat flux peak was observed on the downstream part along the single line of flow spreading similar to the case of a plate of blunt semi-cone placed upwind. It is also noticed, that the magnitude of this peak increases with the increase of Re. However, Whitehead and Bertram (1971) obtained different results. They found a line of flow spreading in the forward part which becomes two closely spaced lines of flow spreading wit a narrow region of separation free flow between them and two heat flux peaks symmetric with respect to the plane of symmetry.

For the triangular flat plate or delta wing with rounded apex, no overall information on the flow phenomena in leeward region was available. Therefore, Maykapar (Chang 1973) attempted to explain these two different experimental results of Borovoy et al (1970) and Maykapar (1970) compared to Whitehead and Bertram (1971), referring to the most complete investigations for sharp apex triangular plate of Witehead (1970) and Whitehead and Bertram (1971). Whitehead and Bertram (1971) visualized the viscous boundary over the leeward plate cross-section using a vapor screen technique showing the thin layer in the center area of the symmetry plane section extending sharply to thicker layer toward the plate edge. They conjecture that the paired vortices are formed within the thick viscous layer close to the symmetry plane with axis located near the maximum thickness of the viscous layer. This vortical motion induces a downwind flow toward the centerline which then turns outward, drawing a low energy fluid from the center area. The stagnation flow and the thinned viscous layer due to the departure

of the fluid cause the increased heating to the centerline. On the other hand Rao (1971) considered the formation of the embedded vortices within the boundary differing from the concept of flow impingement induced by free vortices following from the sharp leading edge causing the heat flux peak.

Maykapar (Chang 1973) realizes that the flow phenomena on the leeward side plate is affected by two vortices causing a heat flux peak. Nevertheless, he considers that the effect of the inner shock is important because this shock induces the flow toward the plate center line and removes the low energy gas from the middle of the plate causing thickening of the viscous layer and also the heat flux peak. Thus, together with the bow wave, the inner shocks determine separation and entire flow in the leeward region. Hence, the effect of vortices is regarded as a secondary phenomenon. The vapor screen visualization showing the thin viscous layer in the central part of the plate, is due to a transverse flow effected by the shocks and density increase. The two lines, instead of one, of reattachment and heat flux peak appeared in Borovoy et al's experiment (1970) and explaned by the change of flow pattern because of the increased distance between the shocks.

3.2. Aerodynamic Heating Involving Protuberance

Recently, in the USSR, by mounting the simply shaped bodies such as a straight and tilted cylinder, a triangular wing to flat plate, or by discharging the transverse jet into the supersonic flow from the hole in the plate or cone, the experimental program of aerodynamic heating in three-dimensional flow regions involving shock wave interaction with lami-

nar boundary layer has been carried out.

3.2.1 Cylinder Interference with a Flat Plate

In order to assess the upstream flow and heat transfer phenomena with the protuberance accurately, the height of the cylinder was selected sufficiently large and the surface stream line behavior and melting boundaries of the temperature sensitive points are investigated as seen in Fig. 7.17. The pressure distribution upstream, separation region and slope of a dividing stream line in the plane of symmetry are considered similar to those of a two-dimensional flow governed by the free-interaction law. For example, l_s at the beginning of separation is propotional to $\left[(M_\infty^2 - 1) \cdot Re_s\right]^{-1/4}$ where s refers to distance measured from the separation point and edge of the plate, the separated region length $Re_\infty^{-1/4} x_o$ and the dividing stream line slope $\theta \sim Re_\infty^{-1/4} x_o$ where x_o refers to distance to cylinder axis from plate edge as reported by Sorovoy and Ryzhkova (1972).

Tetervin's (1967) investigation shows that due to the interaction of shock emanating from the separated region with the shock wave, the heat flux and pressure peaks on the cylinder and in the region of separated layer reattachment appear. Measurements of upstream pressure distribution of the cylinder and the step mounted on a plate and jet discharged from a hole on a plate show that the pressure distribution along the symmetric line are initially similar to each other but differ significantly approaching the cylinder, step or jet, and for the jet it's upstream pressure distribution lies between those of cylinder and step as seen in Fig. 7.18. This writer notices that the in-

AD-A099 165 CATHOLIC UNIV OF AMERICA WASHINGTON D C DEPT OF MECH--ETC F/G 20/4
RECENT DEVELOPMENT IN FLOW SEPARATION.(U)
MAY 80 P K CHANG AFOSR-78-3636

UNCLASSIFIED AFOSR-TR-81-0451 NL

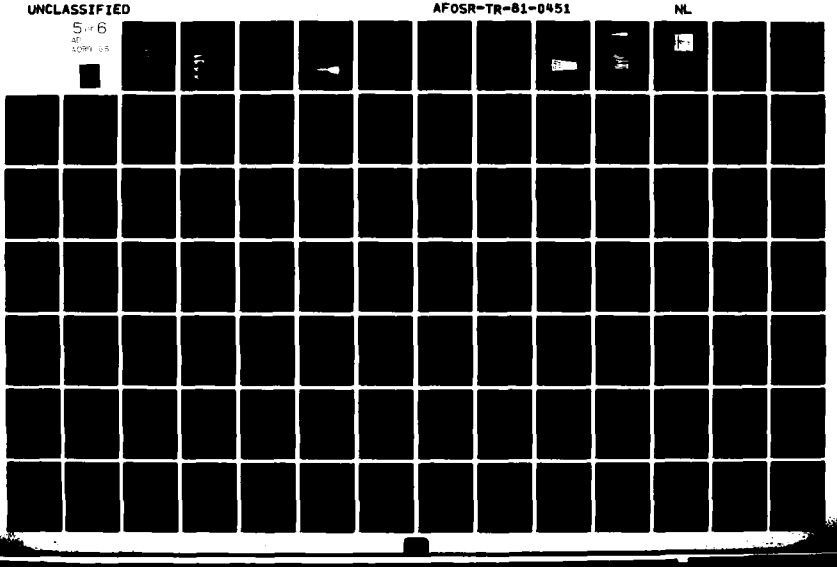

vestigations of Vogler (1963) and Werle et al (1970) are also useful to understand the upstream pressure distribution of protuberance.

Vogler (1963) measured the pressure distribution on the surface of a flat plate up- and downstream of a cylinder mounted on the plate

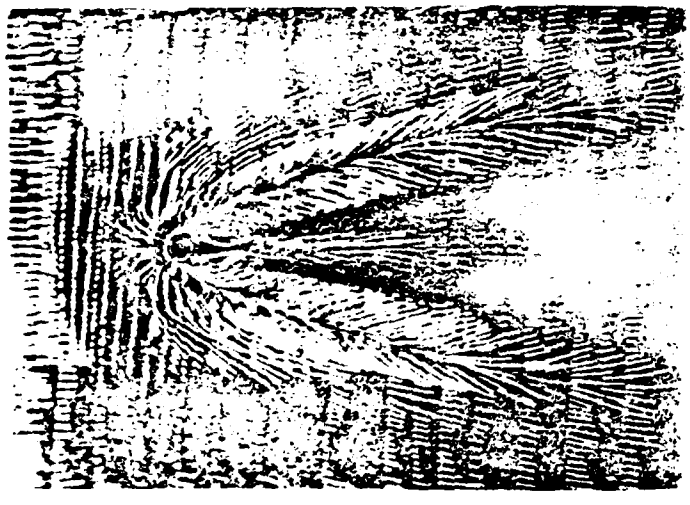

a

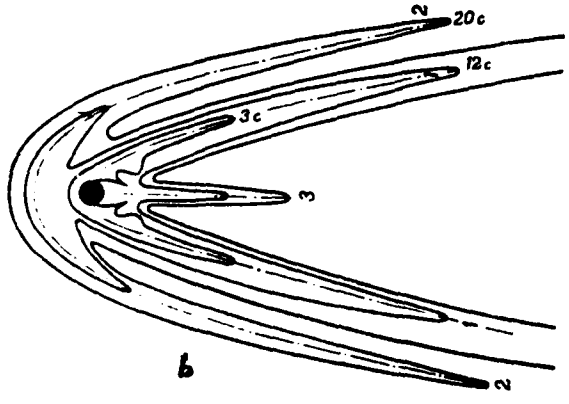

Fig.V.17. a) Limiting stream line pattern on plate with cylinder perpendicular to the plate surface (M_∞=5); b) Temperature-sensitive paint melting boundary(lines of constant surface temperature and thermal flux) for different times. [Borovoy and Ryzhkova,1972].

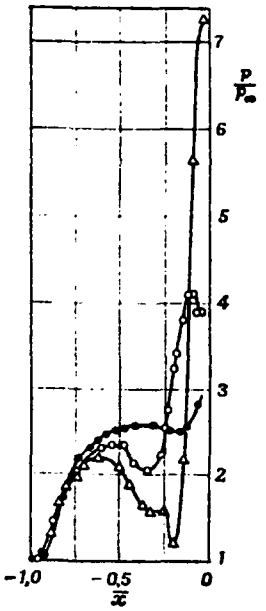

Fig.V.18. Pressure distribution over plate in the plan of symmetry ahead of forward-facing step, cylinder and jet, M = 3; ● = Step; 0 = Jet; P_{oj}/P = 40, Δ = Cylinder. [Glagolev, Zubkov and Panov, 1967].

Fig.V.19. Regions of fused temperature-sensitive coating. M_∞ = 6 [Borovoy and Ryzhkova, 1972]. a - t = 0.24 S; b - t = 1 S; c - t = 2 S; d - t = 4 S

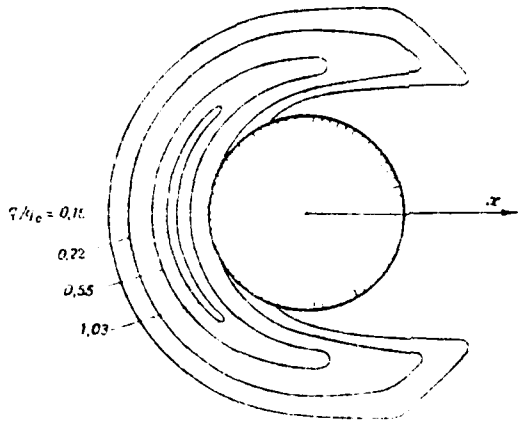

[illegible] ∞

ωx_c = [illegible] ; q/q_0 = 0.6 - 0.9

[illegible] heat flux to plate ;

[illegible] = heat flux to cylinder stagnation point ;

[illegible] Krovoy and Tyzhkova, 1972].

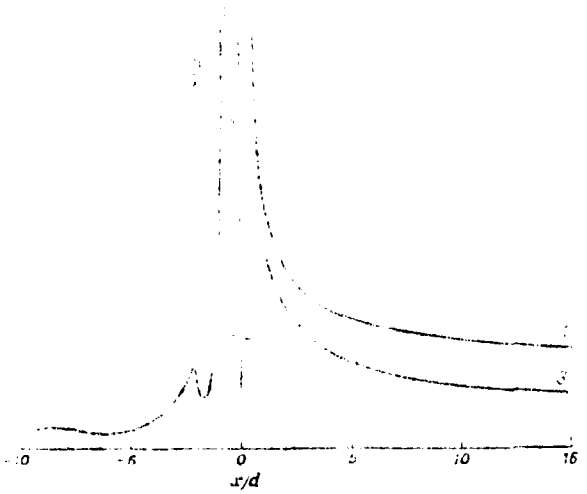

[illegible] late in symmetry plane
[illegible] nead of cylinder and on
[illegible] nes of flow spreadin
[illegible] of cylinder (2 nes

plate

[illegible] crovoy [illegible] Tyzhkova,

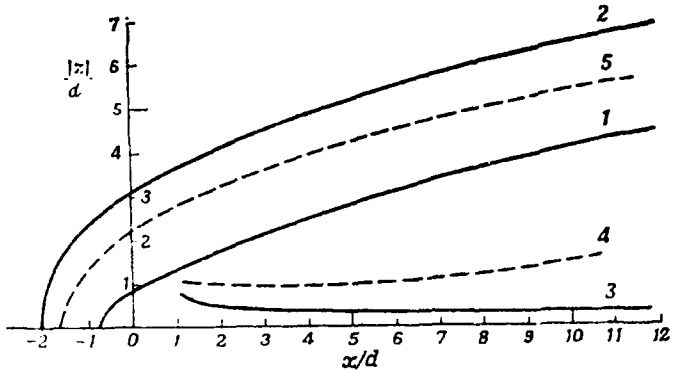

Fig.V.22. Cordinates of lines of flow spreading 1,3, line of second heat flux maximum 2 and lines of heat flux minimum 4.5, on plate; $M_\infty = 6$, $Re_\infty x_0 = 10^5$-10^6. [Borovoy and Ryzhkova, 1972].

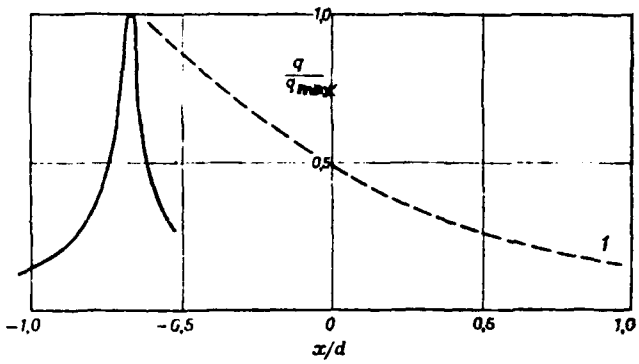

Fig.V.23. Heat flux distribution in plate symmetry plane and along line of flow spreading 1, $M_\infty = 6$. [Borovoy and Ryzhkova, 1972].

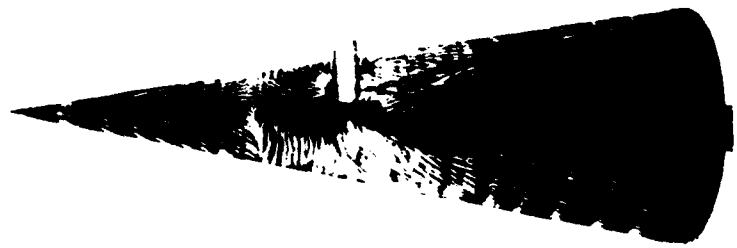

Fig.V.24. Pattern of limiting stream lines for cone $\theta_к = 10^\circ$ at angle of attack $\alpha = 20^\circ$ (upwind side) $M_\infty = 5$. [Borovoy and Ryzhkova, 1972].

and around a jet discharged vertically from a hole in the plate. The free stream velocity was subsonic corresoponding to transition flight speeds of VTOL aircraft. Werle et al (1970) obtained the pressure distribution with a supersonic turbulent free stream upstream of a forward facing step and jet issued vertically from a hole in the plate. In the three-dimensional separated flow zone, regions of supersonic flow, imbedded shock and secondary separation are formed, as well as the heat flux peak region as seen in Fig.V.19. This maximum heat transfer rate region is also determined by observing the limiting stream line spreading as sketched in Fig.V.20. The maximum heat transfer rate on the flat plate occurs in the narrow upstream of the cylinder and its magnitudeis comparable to that on the cylinder stagnation line. The fact that the interference of a protuberance increases the heat transfer rate on the plate up- and downstream of the protuberance compared to the plate alone is demonstrated in Fig.V.21 for a cylinder as a protuberance. Furthermore, on line 2 of Fig.V.17 and on Fig.V.18, a second small heat flux peak is observed upstream of the cylinder along which the pressure is highest. The coordination of these lines of the second maximum heat flux and the lines of minimum heat flux are plotted in Fig.V.22. The heat transfer rate distribution in the plane of symmetry upstream of a cylinder and along the line of the limiting stream line spreading are plotted by Borovoy and Ryzhkova (1972) in Fig.V.23.

3.2.2 Cylinder Interference with Cylinder and Cone

Flow and heat transfer phenomena over a cylinder mounted on a cone

and over a first cylinder mounted on a second cylinder are similar to those of a cylinder mounted on a flat plate as seen in Fig.V.24. Although, the latter case holds for $d/D < 0.1$ (where d and D refer to diameter of first and second cylinder respectively) and the second cylinder whose nose is hemisphere. Therefore, experimental results of aerodynamic heating due to interference of a cylinder mounted on a cone are presented with those of a plate in a good correlation as shown in Fig.V.25 and V.26. If the ratio of d/δ^* (where d is cylinder diameter and δ^* is displacement thickness of boundary layer) is reduced to 1 - 2, then the separation characteristics described thus far hold still, but if $d/\delta^* < 1$, then the separation region extends further upstream and the number of characteristic lines in the limiting stream lines decreases leaving only a single maximum heat flux

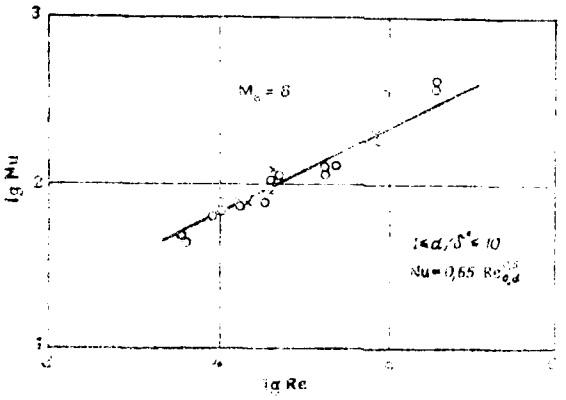

Fig.V.25. Maximal heat flux ahead of cylinder.

$Nu = \frac{q_{max}\, d}{\lambda_0 (T_0 - T_w)}$ $\qquad Re_{0,d} = \frac{\rho_0 v_0 d}{\mu_0}$ [Borovoy and Ryzhkova, 1972].

λ_0, μ_0 – Coefficients of thermal conduction and viscosity corresponding to stagnation temperature; ρ_0 = air density downstream of shock; 0 = plate; x = cone.

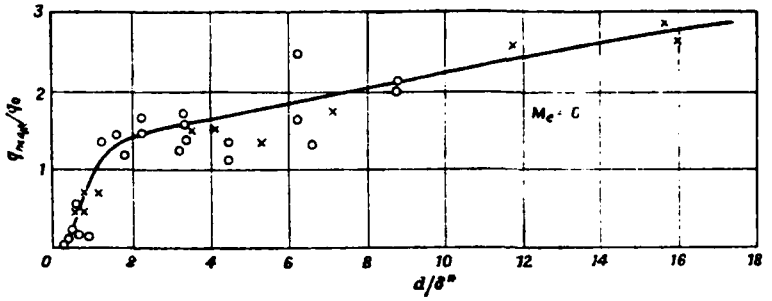

Fig.V.26. Maximal heat flux ahead of cylinder.
0 = plate; x = cone
[Borovoy, Ryzhkova and Sevast'yanova, 1972]

line (Fig.V.26) and the magnitude of maximum heat transfer rate upstream of the cylinder decreases sharply as indicated in Fig.V.26.

3.2.3 Interference of Tilted Cylinder

By tilting a protruding cylinder upstream, no fundamental differences of flow and heat transfer behaviors are noted compared to those of a straight cylinder. Although by tilting downstream, the separated flow region is reduced in the symmetry plane. The maximum heat flux upstream of a cylinder to a plate varies with the tilt angle similar to the heat transfer behavior to a yawed cylinder as reported by Borovoy and Ryzhkova (1972). The heat transfer rate on the downwind surface of the cone but upstream of the cylinder at an angle of attack $\alpha > \theta_k$ is considerably less compared to the case of $\alpha = 0^\circ$ but even in this case the pressure of the protruding

cylinder increases the maximum heat transfer rate [Borovoy, Ryzhkova and Sevast'yanova (1972)] .

3.2.4 Jet Interference

Borovoy and Ryzhkova (1972) presented Fig.V.27, V.28, and V.29 which indicate the similar upstream behavior of the flow separation compared to that of the protruding cylinder.

3.2.5 Interference of Sharp Edged Triangular Half-Wing

The flow behaviors of the separation and reattachment due to interference of a sharp edged triangular half-wing mounted on a plate at angle of attack are shown by the limiting stream line pattern. (Fig.V.30). These limiting stream lines indicate that the reattachment occurs at line 1, separation at line 2 and reattachment at line 3. The maximum heat transfer rate occurs on the reattachment line 3.

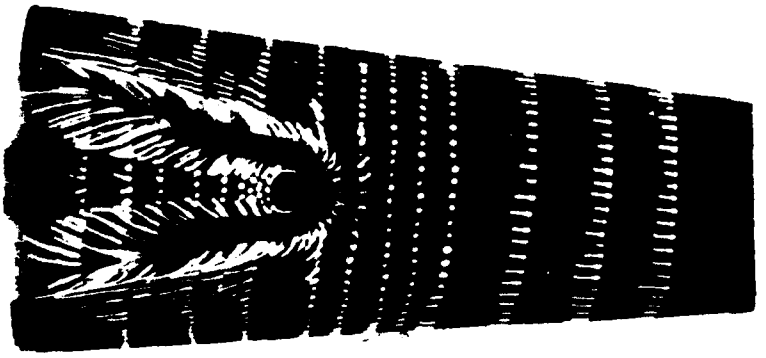

Fig.V.27. Pattern of limiting stream lines on cone with jet discharge. $\theta_k = 5^o$; $M_\infty = 5$; $\alpha = 0^o$; $P_{oj}/P_o = 1$. [Chang (1973)]

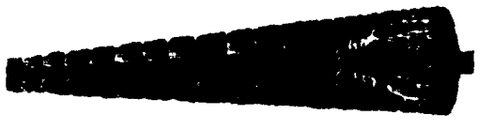

Fig.V.28. Pattern of limiting stream lines on downwind side of cone with jet discharge. $\theta_k = 5^\circ$, $M_\infty = 5$, $\alpha = 10^\circ$, $p_{oj}/p_o = 1$.
[Chang (1973)]

Fig.V.29. Boundaries of temperature-sensitive coating change. $\theta_k = 5^\circ$, $M_\infty = 5$.
a - t = 0.5 S, b - t = 1 S, c - t = 4 S, d - t = 16 S
[Chang (1973)]

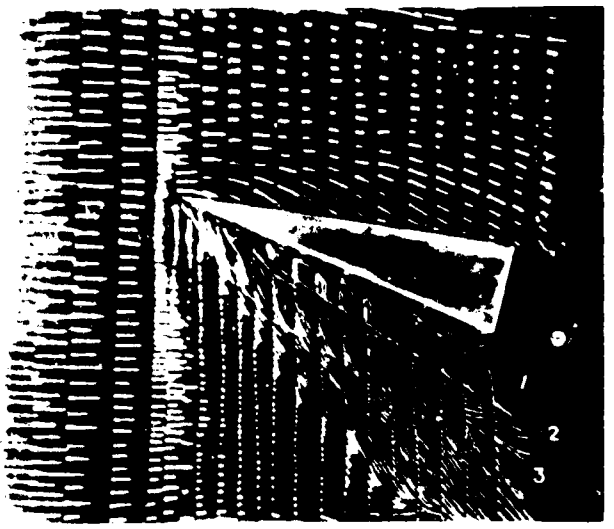

Fig.V.30. Pattern of limiting stream lines on flat plate with half-wing mounted on the plate, $M_\infty = 5$. [Borovoy and Sevast'yanova, 1972] [Borovoy, Ryzhkova and Sevast'yanova, 1972].

The maximum heat transfer rate occurs on the reattachment, line 1 and its magnitude increases linearly with increase of p_B/p_H (where p_B is pressure downstream of shock wave emanating from the half-wing leading edge and p_H is pressure on the plate outside the region of disturbance from half-wing) showing that for this case of shock interaction with the boundary layer this pressure ratio is the most important governing factor.

The writer notices that the experimental investigations for aerodynamic heating in the USSR described by Ma'lapar (Chang 1973) is for

[illegible] to the surfaces of plate, cylinder and cone only on which the various protruding bodies are mounted. But since the high rate of heat transfer also occurs on the reattachment line on the protruding body surfaces, the investigations for this aerodynamic heating is very desirable so that the disintegration of the mounted protruding body may be prevented.

References

Batt, R. and T. Kubota (1969). "Experimental Investigation of Laminar Wakes behind 20 Wedges at $M_\infty = 6$," AIAA J., vol. 6, No. 11.

Bloom, M. H. and M. H. Steiger (1963). "Diffusion and Chemical Relaxation in Free Mixing," IAS Paper 63-67.

Borovoy, V. Ya. Davlet-Kil'deyev, R. Z. and M. V. Ryzhkova (1968a). "Heat Transfer to the Surface of Some Lifting Bodies at High Supersonic Speeds," Izvestiya AN SSSR, MZhG, No. 1.

Borovoy, V. Ya. Davlet-Kil'deyev, R. Z. and M. V. Ryzhkova (1968b). "Nature of Heat Transfer to Semicone Surface in Supersonic Gas Flow," Trudy TsAGI, No. 1106.

Borovoy, V. Ya. and M. V. Ryzhkova (1969). "Heat Transfer to Semicone Surface at High Supersonic Speeds," Izvestiya AN SSSR, MZhG, No. 4.

Borovoy, V. Ya., Davlet-Kil'devev, R. Z. and M. V. Ryzhkova (1970). "Experimental Study of Heat Transfer on Wings and a Wedge," Trudy TsAGI, No. 1175.

Borovoy, V. Ya. M. V. Ryzhkova (1971). "Study of Heat Transfer on Downwind Convex Surface of a Semicone," Trudy TsAGI, No. 1315.

Borovoy, V. Ya and M. V. Ryzhkova (1972). "Heat Transfer on Flat Plate and Cone with 3-d Interaction of Boundary Layer with Shock Wave formed near a Cylindrical Obstacle," Trudy TsAGI, No. 1374.

Borovoy, V. Ya. Ryzhkova, N. V. and Ye. V. Sevast'yanova (1972). "Experimental Study of Gas Flow and Heat Transfer in Zones of 3-d Interaction of Laminar Boundary Layer and Shock Waves formed near a Cylindrical Obstacle and Semiwing," Fourth Conference on Heat and Mass Transfer, Minsk.

'hang, P. K. (1973). Separation of Flow, Russian translation and publication by MIR Publisher, Moscow. vol. III "New Results of Separated Flow Studies"

Cresci, R. J. and V. Zakkay (1965) "A Experimental Investigation of the Near Wake of a Slender Cone at $M_\infty = 8$ and 12" Aeronautical Research Lab. 65-87.

Lavlet-Kil'deyev, R. A. (1971). "Nature of Flow and Heat Transfer on Body of Revolution in Supersonic Gas Flow, Uchenye Zapiski TsAGI No. 6.

Ferri, A. Libby, P. A. and V. Zakkay (1962). Theoretical and Experimental Investigation of Supersonic Combustion in High Temperatures in Aeronautics, Pergamon Press.

Glagolev, A. I., A. I. Gubkov and Yu A. Panov (1967). "Supersonic Flow Around Gaseuns Jet Obstacle on Flat Plate," Izvestia AN SSSR MZhG No. 3.

Lees, L. (1964). "Hypersonic Wakes and Trails," AIAA J., vol. 2, No. 3.

Levensteins, Z. J. and M. V. Krumins (1967). "Aerodynamic Characteristics of Hypersonic Wakes," AIAA J. vol, 5. No. 9.

Lykoudis, P. S. (1960). "A Review of Hypersonic Wake Studies" AIAA J. vol. 6, No. 4.

Maykapar, G. I. (1970). "Aerodynamic Heating of Lifting Bodies," XIX Intern. Astron. Congress vol. 3, Pergamon Press, Polish Sci. Publ.

Muntz, E. P. and E. J. Softley (1966). "A Study of Laminar Near Wake," AIAA J., vol. 4, No. 6.

Rao, D. M. (1971). "Hypersonic Lee-Surface Heating Alleviation by Apex Drooping," AIAA J. vol. 9, p. 1875.

Schlichting, H. (1960). Boundary Layer Theory, McGraw Hill Book Co.

Stepanov, G. Yu. (1969). (Notes on an Article by G. I. Taganov "The Theory of Steady Separated Zones," AN SSSR MZhG 4.)

Telionis, D. P. (1972). "Heat Transfer at Reattachment of a Compressible Flow over a Backward Facing Step with a Suction Slot," AIAA J., vol. 10, No. 8.

Tetervin, M. P. (1967). "Study of Gas Flow in Region of Shock Incidence on Cylinder in High Supersonic Velocity Flow," Izvestiya AN SSSR, MZhG, No. 2, 1967. "Study of Gas Flow and Heat Transfer in Region of Shock Incidence on Cylinder in High Supersonic Velocity Flow", Izvestiya AN SSSR, MZhG, No. 3.

Ting, L. and P. A. Libby (1960). "Remarks on the Eddy Viscosity in Compressible Mixing Flows," J. Aerospace Sci., vol. 27, No. 10.

Todisco, A. and A. Pallone (1965). "Near Wake Flow Field Measurements" AIAA Paper 65 - 53. Jan.

Vogler, R. D. (1963). "Surface Pressure Distribution Induced on a Flat Plate by a Cold Air Jet Issuing Perpendicularly from the Plane and Normal to a Low-Speed Free-Stream Flow," NASA TN D-1629, March.

Werle, M. J. et al. (1970). "Jet-Interaction- Induced Separation of Supersonic Turbulent Boundary Layers. The Two-dimensional Problem," AIAA 3rd Fluid and Plasma Dynamic Conference. June 29-Jyly 1, Los Angeles, Calif.

Whitehead, A. H. (1970). "Effect of Vortices on Detta Wing Leeside Heating and Mach 6," AIAA J, vol. 8, p. 599.

Whitehead, A. H. and M. H. Bertram (1971). "Allevation of Vortex-Induced Heating to the Lee-Side of Slender Wings in Hypersonic Flow," AIAA J. vol. 9, No. 9. pp. 1870-72.

Wakkay, V. and H. Fox (1967). "An Experimental and Theoretical Investigation of the Turbulent Far Wake," AIAA J. vol. 5, No. 3.

CHAPTER VI

SYMBOLS

b	mixing coefficient
d_a	diameter of exhaust nozzle section
d_m	diameter of circle with center on the axis of nozzle passing through the joint point of flows
F	cross-sectional area of base between the nozzle
G	$G = \left\{ \gamma \left(\frac{2}{\gamma+1} \right)^{(\gamma+1)/(\gamma-1)} \right\}^{\frac{1}{2}} \quad \frac{1}{R}$
G_R	mass flow rate through all nozzle
g	coefficient of flow rate
H	$H = H^*/H^{**}$
H^*	$H^* = \delta^*/\delta$
H^{**}	$H^{**} = \left(\frac{\theta}{\delta} \right)^{j+1}$
Je & Ji	integral proportional to mass flow rate in the mixing zone between separation line and internal boundary respectively
k	coefficient of vortex convection at the boundary of the supersonic boundary layer and arbitrary constant
ℓ	distance from the base nozzle to effective radiation source of discrete tone
n	$n = p_a/p_\infty$
n^o	critical value of off-design ratio at which the instantaenous change from a decrease to an increase of pressure in a change of regime as n increases
p_a	pressure at nozzle exit

p_b	base pressure
R	radius
R_j	nozzle radius
Sa	area of exhaust nozzle section
S^*	area of critical nozzle section
T^*	total mean temperature
x	length of stream line along the boundary of the stream at the joint point of flow
x', y'	position of vortex
y_d	coordinate of stream line of a constant flow rate
y_j	coordinate of separation line at the nozzle exit section
β	interaction angle of stream line in a compressed layer inclined toward symmetry axis of form nozzle unit
θ	nozzle inclination or momentum thickness
ϵ_c	ratio of all clustered nozzle exit area to total area of throat
ϵ_N	ratio of all clustered nozzle exit area to throat area of single nozzle
φ	performance parameter
$\overline{\omega^2}$	spectral density of noise

subscript

a	exit section or boundary of nozzle section
e	mixing zone

CHAPTER VI.

Separated Flow Affected by Annular Outflow

For rocket technology, the problem of a rocket base flow is a particularly important one to be solved. The behavior of an exhaust gas flow from a number of nozzles closely located on the base surface is similar to that of an annular flow, but compared to the Laval nozzle flow less loss of thrust may be achieved and nozzles can be more conveniently laid out in the base of the body. In practice, it is advantageous to shorten the nozzle length. Therefore, an attention is given to study the thrust of such short nozzles involving the downstream flow separation parallel with an annular flow affected by pressure change in the external medium.

Recently, in the USSR, problems of the ring nozzle flow have been investigated. Numerical calculations of ring nozzle flows are presented by O. N. Katskova, V. A. Rubtsov, A. M. Ovsyannikov and Migdal et al. The flow in an annular nozzle with a central body was calculated by Ivanov and Kraiko (1972) using a finite difference scheme and by Vilensky et al (1972) using the method of characteristics. A review on the analysis of nozzles directed by G. I. Petrov is presented in the collection of papers of VTs MGU Computation Center, Moscow State University im. M. V. Lomonosov.

Approximate computational methods for an annular flow were developed by G. L. Grodzovisky, Yu Ye Kuznetsov and M. V. Tokarev et al.

Koshevoy and Kozlov (1971) introduced a model of flow interaction.

For incompressible annular flow, L. A. Gruzkov, L. A. Korobkov, Ye M. Levin, I. L. Povkh et al, presented an analysis and experiment of base pressure. V. I. Khanzhonkov, Kuzov, Moller and Elliott studied the thick annular flow of velocity suitable to an air cushion vehicle. Bondarev and Gushchin (1972) carried out the numerical calculations of outflow from a four nozzle block into a supersonic wake. Ginzburg, Prikhod'ko and Sizov (1970) evaluated test results of the flow effect to the base drag.

In western countries a number of investigations were made on the nozzle and annular flows. Robert (1965) computed a separated flow and a ring nozzle flow using quasi-uniform models and Lee (1966) studied the structure of jets from plug nozzles and the parameters of supersonic flow were determined by the method of characteristics and one-dimensional theory.

For multinozzle flows. the effect of the nozzle number and position of the nozzle on the base pressure and thrust characteristics are subjects to be investigated relating to flow parameters in separation zone, and shock wave interaction.

1. Calculation of Base Pressure

For convenience, analysis of the base flow is presented separately for subsonic, transonic and supersonic flows.

1.1 Subsonic Axisymmetric Flow

With an increase of an injected flow intensity, the dimensions of the

toroidal vortex located in the base region, first decreases due to boundary layer control by part of gas flow and the base drag coefficient increases as seen in Fig.VI.1a and Fig.VI.1b.

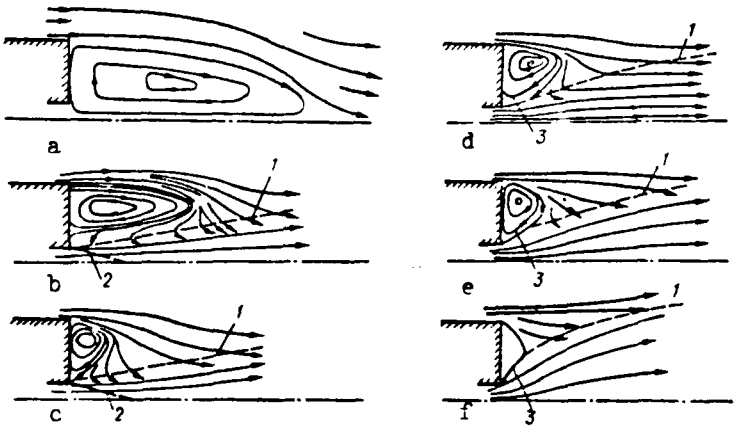

Fig.VI.1. Diagram of flow in the base region: [Craven (1960)]

a--Jet stream is absent; b--Velocity of the stream is subsonic; c--Velocity of the stream is sonic or calculated; d--Velocity of the stream somewhat exceeds the calculated; e--Stream strongly under-expanded; f--Compression due to strongly under-expanded stream (1--External boundary of the mixing region; 2--Boundary of a potential nucleus; 3--Pseudo-laminar field of mixing).

If the flow conditions are such that circulatory flow occurs, then the dimensions of the vortex become minimal (Fig.VI.1c) and the base drag coefficient reaches its maximum. A subsequent increase of intensity dimensions of the vortex increase (Fig.VI.d) and the base drag

coefficient decreases. However, further broadening of the flow boundary results again in a decrease of the vortex dimension (Fig.VI.e and Fig.VI.f) and in a monotonic increase of the base drag coefficient involving the alteration of stream line direction of expanding flow. An approximate analytical medel for the determination of pressure distribution in the base region of subsonic inviscid external flow with a small amount of injected fluid is shown in Fig.VI.2. External flow is givin by a continuously distributed source system of strength per unit length amounting $\int_{\infty} \rho_{\infty} u_{\infty} y d\theta$ along the radius, in a plane passing through the base region (outside the area of base region). It is postulated that no fluid flows in the radial direction from these sources. The entrained gas under the flow boundary is considered by a flow system of constant of per unit length continuously distributed along the x-axis. The flow circulation in the base region is presented by a vortex of intensity Γ , its center located at x' and y'. Its strength and center are determined from the boundary conditions. It is assumed that $y'/R = 0.7$ based upon the experimental data indicating that the minimum pressure location in the base at $y/R \approx 0.7$.

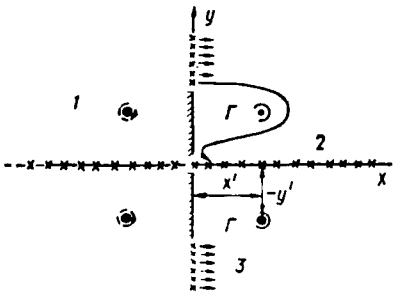

Fig.VI.2. Model of potential flow in a base region: [Craven (1960)]
1--Image system; 2--Intensity of flow; 3--Intensity of the source.

The comparison of analytical results with experimental data of pressure distribution along

y show that although both cases, the trend is similarly predicted absolute values are higher than that of experimental ones.

1.2 Transonic Axisymmetric Flow

For the solution of the problem of jet flow exhaused from the jet engine nozzle with the central body, existing analysis are usually based on the small perturbation method simulating a flow boundary by a cylindrical surface. However, such an approach may be considered as the first approximation because exhaust flow changes its shape during the flight of an aircraft.

Tagirov (1974) attempted to solve the ejection effect of the supersonic flow to the external transonic flow, by an iteration procedure assuming that the static pressure along the flow boundary is constant. At first, the external flow pressure distribution is assumed and computations are carried out for the flow field. Then, for a given flow boundary the external flow pressure distribution is computed precisely considering ejection flow effect, a boundary layer on the body, and the body shape etc. The results show that at external transonic flow speeds, the ejection effect is weak.

Kurn (1968) found that predicted pressure distribution on the circular arc shaped trailing section agrees with the experimental data. A satisfactory agreement on pressure distribution on the thin parabolic body with experimental data is reported by Spreiter and Stahara (1971).

1.3 Supersonic Axisymmetric Flow

Yurchenok (1974), using Korst theory, computed the base pressure and

the base temperature behind an axisymmetric body at supersonic speed affected by a single jet flow in the base region.

Numerous studies indicate that the base pressure affected by the jet flow depends on various parameters whose effects may not be ignored even in approximation computations. Therefore, it is desirable to establish the generalized criteria relating them so that it may be possible by simple formulas to compute the base pressure in a broad range of parameteric variations of trailing edge sections and jet nozzles.

Shvets and Isayev (1969) developed an approximate computational method of the base pressure affected by the jet flow involving two generalized parameters for axisymmetric trailing sections with a central jet flow. Statistical study of experimental data indicates that parameters to be used for analysis are the angle between the mean flow direction at the trailing section and the straight line joining the trailing section and the point of maximum expansion (or point of minimum contraction for an over expanded nozzle) of jet flow.

2. Flow System

2.1 Separation Stream Line Method

The flow characteristics in the interal and peripheral (with an external flow) zone of base involving the outflow system depend to a significant degree on the mixing process at the external flow boundaries and on the interaction of separated flow.

For the approximate computation of the mean base pressure and base region configuration involving the closed base area, one usually uses the modified separation line method of Goethert (1961). Instead of the actual space interaction of supersonic streams discharged from the neighboring nozzles, one considers a hypothetical two-dimensional flow in a certain plane of interaction where the inviscid external flow is determined for a given base pressure by the contour of an axisymmetric supersonic flow.

Since the flow mixing phenomena is three-dimensional, it is proposed that there is a certain characteristic point on the line of flow interaction in the center which determines all interactions if one starts from the simple mixing principle given by $u/u_e = (1 + \text{erf}\ \eta)/2$ and by Korst flow distribution; total pressure on the separation stream line (when $M_j \leq 1$) or total pressure behind a normal shock on this stream line (when $M_j > 1$) must be balanced by static pressure downstream of an oblique shock at the joining point of the streams. For such a point, one may select the point where the boundaries of the neighboring flow first touch each other (joint angle at this point is maximum). In order to approximately compute the formation of a boundary layer on the internal surface of the nozzle, the mixing length is increased by $\Delta x/d_a = 1.4\ (1 - 1/\sqrt{s_a/s^*}\ )$ where d_a and s_a are diameter and area of the exhaust nozzle section, s^* is the area of the critical nozzle cross-section. The mass flow rate returned to the base region by a four-nozzle unit is given by

$$\frac{\Delta G}{G_R} = (J_e - J_i)\ \frac{1 - (u/u_e)^2}{6}\ \frac{\rho_e\, u_e}{\rho_a\, u_a}\ \frac{d_m}{d_a}\ \frac{x + \Delta x}{d_a}$$

where G_R is the mass flow rate through all nozzles, J_e and J_i are integrals proportional to the mass flow rate in the mixing zone between the separation line and internal boundary respectively, d_m is diameter of circle with the center on the axis of the nozzle passing through the joint point of flows, x is the length of the stream line along the boundary of the stream at the joint point of flows, subscript e and a refer to boundary of the mixing zone and the nozzle section respectively. All gases returning to the base region flowing between the nozzles to the ambient atmosphere are considered to take place at the the speed of sound. The total pressure of the exhaust flow is equal to the base pressure. Total mean temperature of any section of the boundary layer in the exit section of nozzle formed in the near wake is given by

$$T^* = \int_0^{y_o} \rho u T^* dy \Big/ \int_0^{y_j} \rho u dy$$

where y_j is the coordinate of the separation line at the nozzle exit section used only for the denominator.

For a closed base area, the flow rate going into the external gas medium is

$$\int_{y_d}^{y_j} \rho u dy = g G p_b F / \sqrt{T_b}$$

where

$$G = \sqrt{\gamma \left(\frac{2}{\gamma + 1} \right)^{\frac{\gamma+1}{\gamma-1}}} \cdot \frac{1}{R}$$

y_d is the coordinate of the stream line of a constant flow rate, F is the crossectional area of the base between the nozzles and g is a coefficient of the flow rate. For a four-nozzle unit by taking g = 0.5,

an agreement between the analysis and experiment may be obtained.

If the external flow effect is ignored, the flight attitude at which the regime of the internal zone flow chocking begins can be determined. Fig.VI.3 indicates the computed data by the modified separation line method, characterizing the effect of parameter of s/s* on the base pressure in chocking conditions. In Bn TI IsAGI (1969) "Research on Flows with Gas Streams (foreign references 1953 - 1968)" 290, Moscow, an analysis is reported which employs the separation stream line method to compute approximately the pressure in the base region and the heat flow at the critical point for different nozzle units and variable external conditions.

If the base region condition is such that the gas outflow from the internal zone to periphery is impossible for example for a ring nozzle, the computation system is almost identical with that of a closed base region. The predicted external flow pressure is not equal to the free stream static pressure in the peripheral annular zone of base region. Thus, the analysis is to be improved.

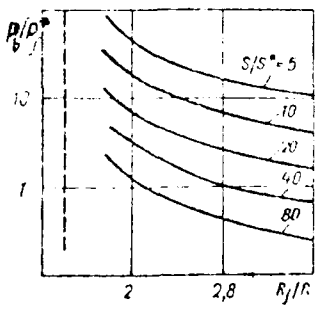

Fig.VI.3. Dependence of base pressure on the ratio of the area of the nozzles and the distance between the nozzles for a four-nozzle unit in chocking conditions for the base region [Goethert(1961)] (dashed line corresponds to contact of the nozzle walls; R_j/R--is the ratio of nozzle radius to the radius of the unit; p_b/p^*_j-- is the ratio of base pressure of the stream; S/S*-- is the ratio of the exit section of the nozzle to the critical section).

For this purpose, a closed nozzle unit is considered as an equivalent single ring nozzle whose internal diameter is equal to the diameter of a circle passing through the nozzle axis and the external diameter is determined assuming that the exit section of the ring nozzle equals half the total of the exit sections of all nozzles in the actual unit. The parameters in the peripheral annular zone of the base region may be computed similarly by taking into account a certain additional gas quantity coming into the internal zone compared to the case of single nozzle. For the completion of the solution, mass balance of both zones in the base region must be considered (steady flow). After achieving flight conditions at which the gas flow rate between the regimes corresponds to the speed of sound, the pressure change in the internal zone may not occur by further increasing the altitude and in the peripheral zone after this, the pressure decreases continuously. Dixon and Page (1966) compared some of the predicted base pressure for SA - 1 rocket with data of the flight and model testing in two zones of a first stage as shown in Fig. VI.4.

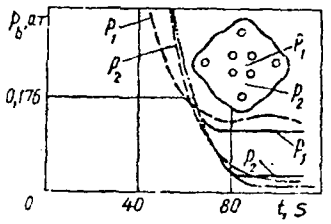

Fig.VI.4. A comparison of calculated values of base pressure for the SA-1 Saturn first-stage rocket and the results of flight tests of the rocket [Dixon and Page(1966)] (dashed lines--results of flight testing, solid line--calculation, dashed-dotted line--external pressure).

When the flows join a shock wave occurs and causes pressure rise of cold gas in the boundary layer and its reverse flow. Sizov (1970) predicted the base pressure not only in the chocking regime of the base

region but also for the weak reversed flow considering the constancy of mass circulating in the region $G_+ = G_-$ where G_+ is mass inflow rate in the base region due to interacting stream and G_- is outflow rate from the base region.

Hall and Mueller (1971) by using a model of a near wake behind a body studied the irregularity of the flow and effect of the base injection on the base pressure and thrust for separated annular flow. Analytically and experimentally the flow rate for nozzles with different central bodies and the effect of parameters of external medium were determined.

2.2 Integral Method

Gogish and Stepanov (1971) analyzed the problem of flow interaction of two-dimensional ($j = 0$) and axisymmetric ($j = 1$) quasi-uniform stream and uniparameter wake by the following system of six inviscid flow equations.

$$dy_o/dx = v_o/u \; ; \tag{1}$$

$$dy_1/dx = v_1/u \; ; \tag{2}$$

$$\frac{dy_o}{dx} = (j+1)\,\frac{v_1\left(1+\frac{1}{\gamma-1}\,\frac{\pi_1}{\pi}\right)v_1^j - v_o\left(1+\frac{1}{\gamma-1}\,\frac{\pi_o}{\pi}\right)y_o^j}{\frac{\gamma}{\gamma-1}(M^2-1)(y_1^{j+1}-y_o^{j+1})} \tag{3}$$

$$\frac{da}{dx} = (j+1)\,\frac{v_o\left[\gamma M^2-\left(1-\frac{\pi_o}{\pi}\right)\right]y_o^j - v_1\left[\gamma M^2-\left(1-\frac{\pi_1}{\pi}\right)\right]y_1^j}{\frac{2\gamma}{\gamma-1}(M^2-1)(y_1^{j+1}-y_o^{j+1})} \tag{4}$$

$$\frac{dv_o}{dx} = -(j+1)\frac{1}{a_o}\frac{a}{\gamma}\frac{(1-\frac{\pi_1}{\pi})\, y_o^j}{M(y_1^{j+1}-y_o^{j+1})} \tag{5}$$

$$\frac{dv_1}{dx} = (j+1)\frac{1}{a_1}\frac{a}{\gamma}\frac{(1-\frac{\pi_1}{\pi})\, y_1^j}{M(y_1^{j+1}-y_o^{j+1})} \tag{6}$$

and two equations for a wake

$$\frac{\partial \ln H}{\partial m}\frac{dm}{dx} + \left[\frac{\partial \ln H}{\partial \ln C} - (2 + H - M^2)\right]\frac{d\ln C}{dx} = (j+1)\frac{d\ln \delta^*}{dx} \tag{7}$$

$$\frac{dm}{dx} + \frac{m(2-m)}{(1-m)(1-C2)}\frac{d\ln C}{dx} = -(j+1)(-ak)\frac{m^2}{1-m}\frac{(H^*)^{\frac{2-j}{2}}}{\delta^*} \tag{8}$$

where

$$H = H^*/H^{**}\ ,\ H^* = \left(\frac{\delta^*}{\delta}\right) = (j+1)\int_o^1 \left(1 - \frac{\rho u}{\rho_\delta u_\delta}\right)\eta^j d\eta$$

is ratio of thickness of displacement,

$$H^{**} = \left(\frac{\theta}{\delta}\right)^{j+1} = (j+1)\int_o^1 \frac{\rho u}{\rho_\delta u_\delta}\left(1 - \frac{u}{u_\delta}\right)\eta^j d\eta$$

is ratio of momentum thickness

$$m = (u_\delta - u_o)\ /\ u_\delta\ ,\quad \eta = \frac{Y}{\delta}$$

u and v are longitudinal and lateral components of velocity; indices o and 1 apply to the parameter on the axis and on the boundary of the stream. In equation(7) and (8) one must assume $\delta^* = y_o$ and $\frac{d\delta^*}{dx} = \frac{dy_o}{dx} = \frac{v_o}{u}$; $C = u/u_{max} = M\left(\frac{2}{\gamma-1} + M^2\right)^{-1/2}$ is the ratio of velocity of the external flow on the boundary layer of the wake;

$$\pi = (1 - C^2)^{\gamma/\gamma-1} = \left[1 + M^2(\gamma-1)/2\right]^{-\gamma/(\gamma-1)}; \quad v = \alpha_1 v_1 + \alpha_2 v_2;$$

for an annular stream $\alpha_o = (y_1+2y_o)/3(y_1+y_o) = 1/3-1/2$; $\alpha_1 = (2y_1+y_o)/3(y_1+y_o) = 2/3 - 1/2$; for a two-dimensional stream $\alpha_o = \alpha_1 = 1/2$. The initial conditions are known in the x = o cross section.

One must add additional equations to the system of equations for an inviscid stream in order to determine length (surface) of external and internal boundaries of an inviscid stream:

$$\frac{dS_i}{dx} = (j+1)\, y_i^j \sqrt{1+\left(\frac{v_o}{u}\right)^2} \simeq (j+1)\, y_i^j, \quad i = 0,1, \qquad (9)$$

necessary for calculating the thickness of a stream of a turbulent mixing layer.

The initial conditions of a near wake are defined from conditions of attachment of an isobaric flow of mixing in the base region with the flow of interaction in the wake. When calculating a turbulent layer of mixing behind an axisymmetric face, one must begin from these same approximate relationships which in a two-dimensional flow, are: profile of velocity in the mixing layer is universal; $\frac{df}{dS} = b(C)$, where $f = (j+1)y_o^j \delta$ -- is the area (thickness) of the cross section of the mixing zone; b -- is the mixing coefficient.

Conditions of continuity δ and δ^* in the attachment section and conservation of mass in the stagnant area are described in the form

$$y_o^{j+1}(x) + b^o S_o(x) \left[1 - H^*(1,C,0) \right] = \delta^{j+1} \qquad (10)$$

$$y_o^{j+1}(x) = \delta^{j+1} H^*(m,C,j) \qquad (11)$$

$$\delta^{j+1}(m,C,j) = (1-B) b^o H^{**}(1,C^o,0) S_o(x) \qquad (12)$$

where

$$B = (\rho u)_i / (\rho u)^o b^o H^{**}(1,C^o,0) S_o(x)$$

$$(m,C,j) = -(j+1) \int_0^{\eta_*(m)} \frac{\rho u}{\rho_\delta u_\delta} \eta^j d\eta \,, \quad f(\eta_*) = m^{-1}$$

$$S_o(j+1) \int_0^x y_o^j \sqrt{1 + \left(\frac{v_o}{u} \right)^2} \, dx \simeq (j+1) \int_0^x y_o^j \, dx$$

is the area (length) of the ejected surface of the stream.

Relative integral thicknesses are expressed as a function of three arguments: form-parameter m derived, velocity C and parameter j.

From equations (10)--(12), it follows that the initial value of the form parameter m^o is defined depending on the magnitude of C^o from equation.

$$\frac{1 - H^*(m,C^o,1)}{(m,C^o,1)} = \frac{1 - H^*(1,C^o,0)}{H^{**}(1,C^o,0)(1-B)}$$

and coordinate $x = x^o$ of the cross section of adhesion from equation

$$\frac{y_o^{j+1}}{S_o} - b(C^o) H^*(m,C^o,1) \frac{1 - H^*(1,C^o,0)}{1 - H^*(m,C^o,0)} = 0 \qquad (13)$$

Calculation of flows of interaction is carried out in two parts. First, for a given magnitude of base pressure p_b, integrating of the

equation (1) - (6) for inviscid flow, the flow on the isobaric section downstream of the body up to the attachment section is determined by eq.(13). Then, by integration of the same equations, the flow in the interaction region is computed. The actual value of the base pressure p_b and the actual flow in the interaction region are determined by the condition of passage of integral curve through a particular point (wake neck).

It is well-known that the numerical particular solution of equations for the neighborhood of the saddle of a particular point whose position is to be fixed during the calculation is difficult. However, in practice it is adequate to set up two non-specific solutions relating to different families; the difference of their base pressure values is smaller than the prescribed value of $(p_b/p_\infty)_1 = (p_b/p_\infty)_2 < 10^{-2}$. Fig.VI.5 shows integration using the Runge - Kutta method for two dimensional flow of $M = 3$, $y_o = 1$, $y_1 = 2$, $\theta_o = -0.1$, $\theta_1 = 0.1$, $p_a/p_\infty = 0.8$ (p_a is pressure at nozzle exit) for various p_b values.

Commas in Figure VI.5 are equivalent to decimal points .

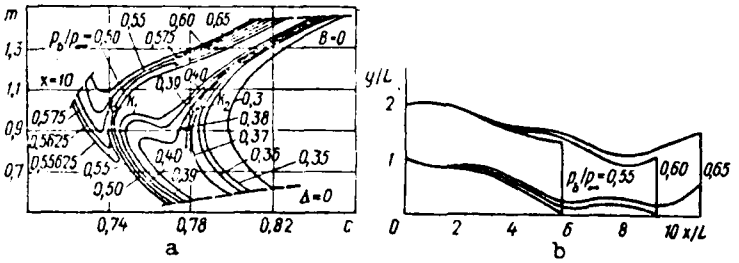

Fig.VI.5. Change in the parameters of a viscous layer (a) and contours of inviscid streams (b). [Shvets and Shvets (1976)]

The lower flow boundary $y_o(x)$ in the interaction region corresponds to the displacement thickness $\delta^*(x)$.

Non - specific integral curves in Fig.VI.a do not correspond to any kind of actual flow and all curves begin on a line of initial data. (with absence of injection B=0). The right branches end on a maximum - line determined by condition of $\Delta(m,C) = 0$; the left branches are limited conditionally and adequately by elongated section x = 10 ; for this the solution has physically unrealistic peculiarities. From Fig.VI.5, it is seen that there are two prescribed initial conditions for particular curves. These two special curves are drawn as the average between the non specific relating to two different families and these non specific curves have been close to each other. Corresponding to them two specific flows of interaction are sketched in Fig.VI.6.

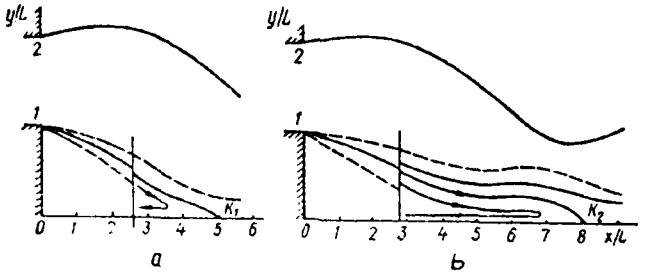

Fig.VI.6. Two steady flows of interaction: [Stepanov and Gogish (1973)]
a--$p_b/p_\infty = 0.375$; b--$p_b/p_\infty = 0.55$.

The existence of two values in the interaction flow in a given case indicates the possibility of quasi-steady oscillation with amplitude

$$2\left[(p_b/p_\infty)_2 - (p_b/p_\infty)_1\right] / \left[(p_b/p_\infty)_2 + (p_b/p_\infty)_1\right] \approx 0.4.$$

2.3 Computation of Flowfield with Mass Addition

Numerical evaluations of performance characteristics of a plug nozzle jet flow with an additional secondary jet injection in the base were intensively investigated recently, but this complex flow phenomena is not well understood.

It is known that the viscous effects play a major role in these plug nozzle jet flowfields interacted by the secondary injected jet. However, if the mixing effect does not modify the inviscid flowfield extensively, the dissipative region can be simply superimposed on the inviscid flow pattern. Lee (1966) analyzed, using the aerodynamic plug nozzle flow schematic shown in Fig.VI.7, the gas dynamic structure of jets from plug nozzles.

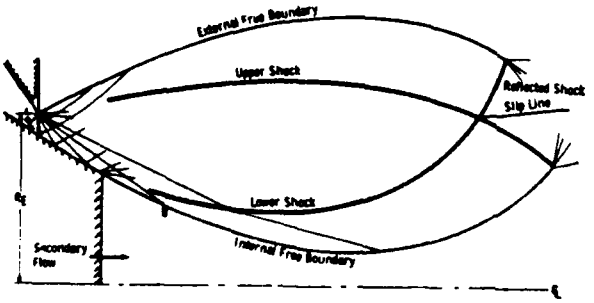

Fig.VI.7. Aerodynamic plug nozzle flow schematic. [Lee (1966)]

The aerodynamic plug nozzle flowfield is characterized by two sets of a boundary, external and internal and shocks, upper and lower downstream of the nozzle. Behind the intersection of upper and lower shocks, two reflected shocks and a slip stream occur. A numerical scheme for solving this part of the flow field has been presented by Der et al (1963).

As a first approach [Lee (1966)] an inviscid solution for the primary and secondary flow is obtained. The computer program starts at the

nozzle throat, where that flow is assumed to be uniform, using Prandtl Meyer equations at slightly supersonic M = 1.05. The primary supersonic properties are determined by using the characteristic method. The gas properties at the lip of the shroud and at the corner of the plug are evaluated by the Prandtl-Meyer relations and the secondary flow properties are determined by one-dimensional isentropic equations. The flowfield points are coupled along right running characteristics until the last one originating from the nozzle lip is completed or the flow behind the lower shock becomes subsonic. Then, the upper field points are computed along the left running characteristics until the upper shock meets the lower one.

If a secondary flow is injected in the plug base, the solution for boundary points between the primary and the secondary flow must be iterated in order to determine a common static pressure. The procedure starts by computing the secondary sonic area A* based on the given total pressure, total temperature, ratio of specific heats and the mass flow rate of the secondary flow. By knowing the initial value for the boundary coordinate at point B (Fig.VI.7), the cross-sectional area can be determined by the characteristic method. The Mach number of the secondary flow can be evaluated by successive approximation using the following equation ;

$$A/A^* = \frac{1}{M}\left[\left(\frac{2}{\gamma+1}\right)\left(1+\frac{\gamma-1}{2}M^2\right)\right]^{(\gamma+1)/2(\gamma-1)}$$

The static pressure of the secondary flow is determined by isentropic relations and the flow properties of the primary flow at the boundary are computed based on the given boundary static pressure. All these

flow properties are considered as the second approximations for the computations.

Lee (1966) used for simplicity, a nozzle of arbitrary design with expansion ratio R_E^2/A_T of 25, where R_E and A_T are the radius of a nozzle shroud and a nozzle throat area respectively. The throat inclination angle of 45^o, and the nozzle wall is made up of a 45^o straight line to investigate the variation of a plume shape affected by an ambient pressure and a secondary total pressure as shown in FigVI.8a and Fig.VI.8b.

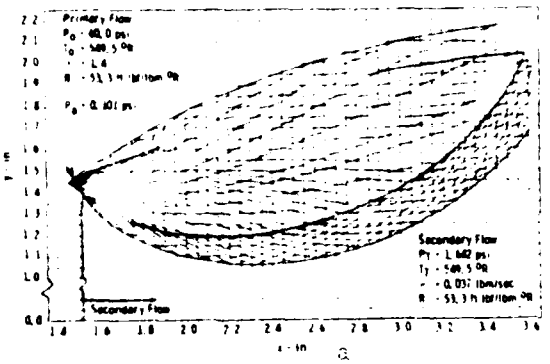

a

Fig.VI.8a. [illegible] plug nozzle. [illegible].

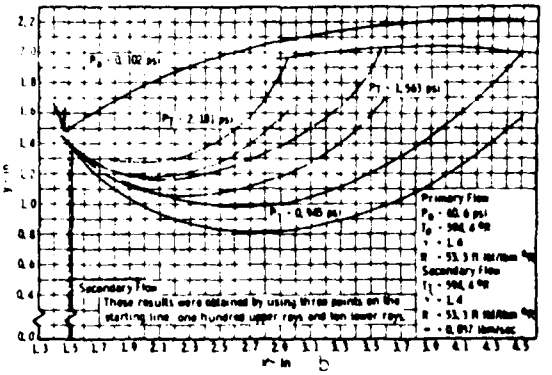

b

Fig.VI.8b. Variations of plume shapes for various secondary total pressures. [illegible].

The jet exhaust from a plug nozzle exhibits a periodic structure similar to that from a converging-diverging nozzle. If the ambient pressure decreases, the jet boundary expands farther from the axis and the jet wave length decreases. The result indicates that the ambient pres-

sure has very little effect on the secondary flow as long as the nozzle is an overexpanded one. As shown in Fig.VI.8b, if the secondary flow total pressure increases the jet flow is pushed outward, the wave length of the jet decreases, but the jet external boundary remains the same. When the total pressure of the secondary flow is about doubled, the length from the nozzle tip to the shock intersection is about half, indicating that the total pressure is a dominant parameter in the jet feature.

3. Experimental Study of Annular Jet

If a set of jet nozzles is closely arranged round the circumference of body base, then at certain operating modes the flow behavior is similar to an annular jet. Annular nozzles have advantages compared to Laval nozzles. For example, thrust loss is smaller at over expansion operating modes and it is more convenient to lay out in the body base. Greatly shortened annular nozzles are very useful in various practical applications and for the determination of the thrust of such nozzles, it is necessary to study the separated flow at the base of the centerbody. A number of experimental investigations of an annular flow involving separation, a shock interaction as well as mass addition etc. are available.

3.1 Separated Flow

The annular jets discharged from axisymmetric nozzles at the Mach numbers [illegible], 3.1 and 3.7 are described. The ratio of the annular nozzle area to the overall base was 36.5%.

The radial pressure distribution over the central part of the nozzle

was nearly constant. The relative base pressure p_b/p_∞ measured at the central point of the nozzle base, in a function of the jet off-design flow ratio $n = p_a/p_\infty$ (p_a is static pressure at the nozzle

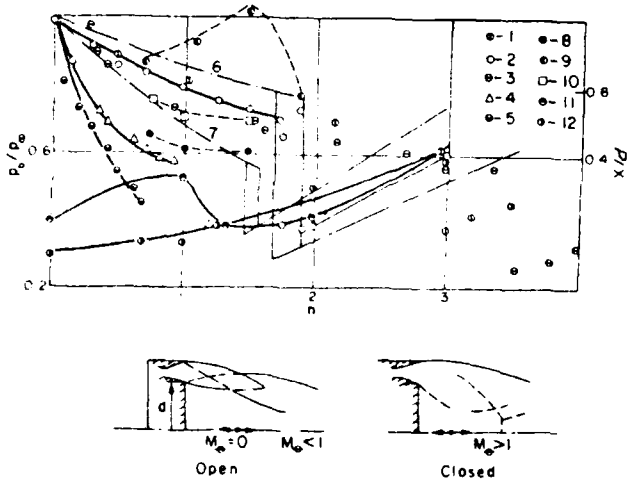

Fig.VI.9. Base pressure and flow parameters on the wake axis. (1) $M_1 = 1.35$, (2) 2, (3) 2.5, (4) 3.1, (5) 3.6, (6) calculated, $M_1 = 2$, [Stepanov and Gogish (1973)], (7) $M_1 = 3$, [Stepanov and Gogish (1973)], (8) positions of the point p_{min}, $M_1 = 2$, (9) positions of the point $p_{\theta\ max}$, $M_1=2$. (10) position of the stagnation point, (11) $M_1 = 2$, $M = 2$, (12) $M_1 = 2$, $M = 3$. [Shvets (1978)].

exit) is shown in Fig.VI.9. With the increase of an off design ratio, the base pressure decreases initially and at larger M_j the pressure curve becomes lower. For each M_j, there exists a critical value of n^o or the off-design ratio at which the instantaneous change from a decrease to an increase of pressure in a change of regime as n increases (M_j = 1.35, 2, 2.5, 3.1, 3.6, n^o = 3, 1.8, 3.5, 1, 0.9 respectively).

The reduction of the pressure corresponds to an "open" base region while the increase to a "closed" one.

The base pressure reaches its minimum value just after closing which takes place if the supersonic jet regions mutually interact. After closing, the base region is entirely surrounded by the supersonic flow, and the jet pressure is proportional to the pressure in the injection settling chamber and does not depend on the surrounding pressure.

Fig.VI.9 shows the base pressure in a function of an off-design ratio and the Mach number at the nozzle exit (where flow is assumed uniform and parallel to the center line) computed by Stepanov and Gogish (1973) compared with experimental data. For the nozzle $M_j = 2$ in the open base, the computed values are larger than experimental data whereas in the closed base smaller.

Intense oscillations of the jet structure were observed from the photographs taken by a high speed camera as the mass flow rate was changed. The values of pressure and n^o vary by 10 - 20% when approaching n^o from above or from below the critical value. The hysteresis is related to the history of the flow state change when passing from one stable state to other. The possible existence of quasi-stationary oscillations and an approximation of the hysteresis region was indicated by Stepanov and Gogish (1973). Intense pressure pulsations during the changes of the flow regime were also observed on multinozzle arrangements and with a disk-shaped nozzle by Gogish (1969).

The measurements of the static and the pitot pressure of the reverse flow indicate that the stagnation point approaches the nozzle base as

the off-design ratio is increased.

The dimensions of the jet and separated zone were determined by an optical flow visualization and shown in Fig.VI.10. In the zone of an annular jet, a toroidal circulatory flow is formed which ends with a contraction recalling the wake neck. The contraction or necking formed by the first cell (d_2', ℓ_2') at small deviations from the design flow ratio has a diameter close to that of the centerbody. By increasing the off-design ratio about n = 0.4, the first contraction and its downstream distance decrease and this process is very intense close to n°. The effect of the off-design ratio on the second contraction (d_3', ℓ_3') is similar, although at n ≈ 0.8 flowfield changes and the second contraction cell disappears. As the off-sign ratio increases, the throat of the complete jet (d_4', ℓ_4') becomes large and moves away from the base. Therefore, it may be said that the behavior of the inner and onter boundaries of the annular jet with an off-design ratio change is different. If for the inner boundary the state of flow, in particular

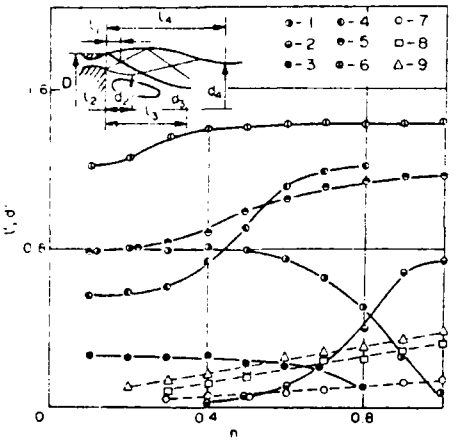

Fig.VI.10. Relative dimensions of the jet and the separation zone, M_1=3.6 ($\ell'=\ell/D$, $d'=d/D$). (1) d_2', M_1= 3.6, (2) ℓ_2', M_1=3.6, (3) d_3', M_1=3.6, (4) ℓ_3', M_1=3.6, (5) d_4', M_1=3.6, (6) ℓ_4', M_1=3.6, (7) ℓ_1', M_1=2, (8) ℓ_1', M_1= 3.1, (9) ℓ_1', M_1=3.6.
[Shvets (1978)]

whether the base is open or closed, is the determining factor, the outer boundary varies like a jet exhausting from a Laval nozzle as the outer pressure decreases the boundary moves from the axis and increases the cell length.

3.2 Shock-Wave Interactions

The main difference between the supersonic annular jet and the continuous circular is found in the existence of two states of flow, with open and closed regions. The distinct feature of the annular jet is the existence of different pressures on its inner and outer boundaries. Due to these factors, the field is considered with a system of compression and rarefaction waves, differing for the inner and the outer part of the jet flow. From the relationship of off-design ratio and outer pressure, it is seen that the flow states for which the jet will be expanded relative to the outer flow and underexpanded relative to the inner flow are possible.

The geometrical configuration of the jet and shock changes abruptly when the regimes change and outer barrel shocks form the Mach wave configuration. With increase of off-design ratio, the Mach disk so formed moves away from the nozzle and for $M_j = 2$ and $n = 2.5$ the outer and inner shocks intersect regularly at first while at higher values a Mach interaction of reflected outer shock waves occurs. For jet flows of $M_j = 3.1$ and 3.6 at $n^o = 1.0$ and 0.9, the outer and inner barrel shocks interact regularly after the change of the regime. Approaching to n^o the expansion wave leads to a sharp decrease of the recirculating zone pressure. For all nozzles tested, in the over critical flow

wake is surrounded only by the first jet cell.

3.3 Injection into Base Region of an Annular Nozzle

The thrust loss reduction of an annular nozzle flow can be achieved by injecting gas into the stagnation zone surrounded by the jet. Experimental results indicate that as in the case of the distributed base injection with an outer flow, the maximum value of p_b/p_∞ , may be achieved at a definite value of the injection parameter. If the gas is added at the central part of the annular nozzle, the total pressure of the injected gas has a dominant influence on the jet shape as Lee (1966) shows.

3.4 Outflow into a Parallel Co-Current Stream

Shvets, Kravets and Kazakov (1974) studied the base pressure on the external Mach number by mounting annular nozzles of M_j = 2, 3.1 and 3.6 inside the rear part of the nozzle ; indicating the general regularities in the base pressure variation and the way in which the flow regime changes as shown in Fig.VI.a.

The three types of flow may be classified by the wake flow Mach number. The first type of flow corresponds to small off-design ratios ($n < 0.5$).

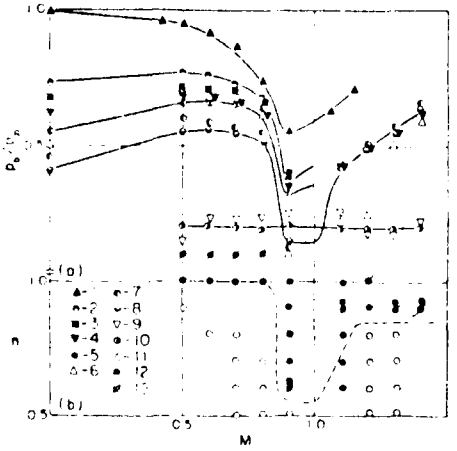

Fig.VI.11. Base pressure (a) and flow regimes (b) for an annular jet (M_1=3.6). (1) n=0, (2) n=0.2, (3) n=0.3, (4) n=0.4, (5) n=0.5, (6) n=0.6, (7) n=0.7, (8) n=0.8, (9) n=0.9, (10) n=1.0, (11, 12) open and closed base regions, optical measurements, (13) closed base region, pressure measurements. [Shvets (1978)]

An increase of the Mach number up to 0.9 is accompanied by a pressure drop while by further increasing velocity, the pressure is also increased.

The base pressure within the nozzle varies similar to the case of no bleed (n = 0), an increase of the off-design ratio, producing a general pressure reduction. For this type of flow, no change of the flowfield is noticed. The second type of flow corresponds to an over expanded jet with a pressure recovery by means of a system of Mach waves or regular waves (n = 0.6 - 0.8). A change of the external flow velocity from M = 0.8 - 0.9 caused a sharp drop of the base pressure accompanying a change from an open to a closed type of base flowfield. The base flow remains closed up to M = 1.1 and a further velocity increase leads to a second change of the jet flowfield, from the closed base pattern to the open one, with a rapid increase of the base pressure. The third type of flow close to the design condition (n = 0.9 - 1.0) is characterized by small base pressure changes for the whole range of external flow velocities investigated. This can be explained by the closing of the base flow at $n \geqslant 0.9$ for an $M_j = 3.6$ nozzles, as a result of which the base pressure is completely determined by the parameters of the out flowing jet.

The limiting conditions between the open and closed base flow regimes were determined from the optical study and pressure measurements shown in Fig.VI.b.

The closure of the base flow region in the transonic flow range of off-design ratios close to the critical value may be reasoned as follows :

At transonic external flow velocities a local supersonic zone, limited at the jet neck by a compression shock, appears close to the nozzle exit. The pressure in this region is lower compared to that of surrounding flow. Therefore, a local off-design ratio larger than the specified one is induced and so reaches n^o, which in turn leads to the closure of the base region at lower values of n^o than for outflow into an open space. An increase of the outflow velocity is accompanied by a transition to a fully supersonic flow pattern with a supersonic velocity behind the closing shock. A compression shock occurs upstream of the first jet cell and the pressure on the separation surface increases. Therefore, for a given off-design condition the actual local value on n will be smaller than n^o and the base flow opens up.

Let up consider now the flow in a jet discharged into a supersonic flow. Similar to the case of the outflow into the infinite space the pressure distribution over the nozzle base is nearly constant as shown in Fig.VI.9. The relation $p_b/p_a = f\ (p_\infty/p_a)$ where p_a is static pressure at the nozzle exit from experiments and Stepanov and Gogish's (1973) predictions for outflow into an infinite space and a parallel flow are given in Fig.VI.12.

In the open base flow region p_b/p_a is nearly linearly dependent to p_∞/p_a. Approaching to the regime change, the slope of curves increases sharply and in the case of closed flow regimes the ratio of p_b/p_a remains constant. Pitot pressures and flow patterns determined from the schlieren photographs are shown in Fig.VI.13.

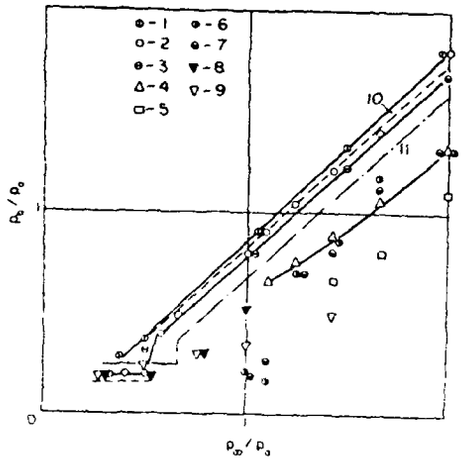

Fig.VI.12. The relation $p_b/p_a=f(p_\infty/p_a)$ (1) $M_1=1.35$, M=0. (2) $M_1=2$, M=0. (3) $M_1=2.5$, M=0, (4) $M_1=3.1$, M=0, (5) $M_1=3.6$ M=0, (6) $M_1=3.6$, M=0.5, (7) $M_1=3.6$, M=0.7, (8) $M_1=2$, M=2, (9) $M_1=2$, M=3, (10) calculated values, $M_1=2$ [Stepanov and Gogish,(1973)] . (11) $M_1=3$ [Stepanov and Gogish,(1973)] . [Shvets (1978)]

The region of constant pressure in the jet center corresponds to the reversed flow zone. With increase of the off-design ratio, the maximum pressure region in the jet appraches the axis. The rearrangement of the flow is accomplished by a substantial decrease of the reverse flow region and in the closed base flow regime, the pitot pressure in the flow near the axis increases and the jet boundaries expand.

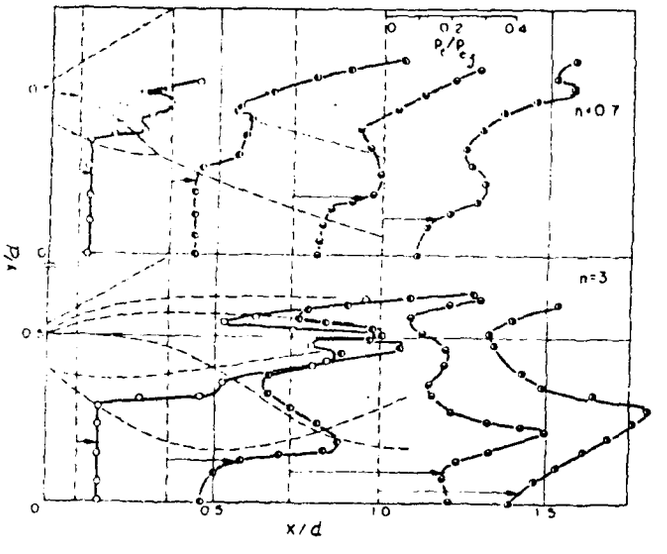

Fig.VI.13. Pitot pressure measured in the base region behind an annular jet (M_1 = 2, M=3). ----, flow features from Schlieren photographs. p_1 —Pitot pressure in free jet for n=1 (calculated). [Shvets (1978)]

4. Fluctuations in the Separation Zone

Base pressure fluctuations depend on a number of factors such as quasi-steady changes of the flow regime in multinozzle arrangements or annular jets, the acoustic jet radiation and non-stationary flow in the base region etc. In this section only the base pressure oscillations affected by non-stationary base flow are described.

4.1 Plug Nozzle

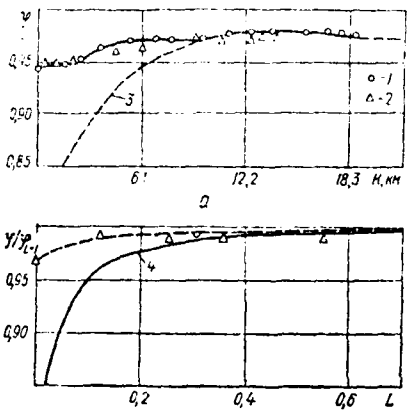

Fig.VI.14. Dependence of the coefficient of thrust of a 24-nozzle model on its height (a) and relative thrust on the degree of shortening of the central body $L = \ell/d$ (b)[Migdal et al (1964)] : 1--ring nozzle, L = 0.3; 2--annular binding L = 0.55; 3--Laval nozzle; 4--p_b = 0.

A comprehensive presentation for a plug-nozzle is given by John(1973) as follows:

The plug nozzle, a relatively new development in jet propulsion system which essentially replaces the diverging portion of a conventional supersonic nozzle with a Prandtl-Meyer expansion so as to increase the off-design performance of the nozzle. The plug nozzle is a device which is intended to allow the flow to be directed or controlled by the ambient pressure rather than by the nozzle walls, and in this nozzle supersonic flow is not confined within solid walls but is exposed to the ambient pressure. Thus, the expansion along the plug is controlled by the back pressure whereas the converging-diverging nozzle expansion

is controlled by nozzle geometry.

The design condition of a plug nozzle is to ensure the final expansion wave intersects the plug axis at the design pressure ratio. Therefore, under this operating condition, the pressure at the plug wall decreases continuously from the throat pressure to ambient pressure just as with the converging-diverging perfectly expanded nozzle. For the under expanded case, the operation of the plug nozzle is similar to that of the converging-diverging nozzle.

The major advantage of the plug-nozzle is expected for the over expanded operation. This fact is significant because for a rocket nozzle, for example, accelerating from a sea level up to design speed and altitude must pass through the over expanded regime.

The pressure along the plug surface does not decrease below ambient, so there is no negative thrust due to pressure difference. Thus, the plug nozzle provides an improved thrust over the converging-diverging nozzle for the over expanded case. A simple cone of up to 40° half angle can be used without undue loss in thrust performance. Thus, the plug nozzle has the further advantage of being short and compact. However, one major problem with the plug nozzle is that of design to withstand the high temperature. For example, in the exhaust gases of rocket engine.

The plug cluster nozzle designed with closely spaced units has performance levels and characteristics identical to the annular plug nozzle. Severe truncation of the plug causes little or no less in performance. The cluster arrangement is more than 12 units. Migdal, Horgan and Chamay (1964) found that a simple geometric relationship combined with a

well-known isentropic relationship connecting the Prandtl-Meyer angle to increase in the area ratio from ϵ_N to ϵ_c is quite useful to indicate the practical range for a cluster arrangement. The symbol ϵ_c refers ratio of all clustered nozzle exit areas to total area of throat and ϵ_N refers to throat area of a single nozzle. Then, in general, it may be assumed that

$$\epsilon_c/\epsilon_N = \left(\frac{\pi}{N} + \cos\theta \right)^2 / N$$

where N is the number of the unit and θ is the unit nozzle inclination. For example, a typical rocket motor with $\epsilon_c = 40$ and $\epsilon_N = 75$ requires 44 units and a 27° inclination angle if axial flow at ϵ_c is desired. If the number of units is smaller, the difference between ϵ_N and ϵ_c is small and the individual nozzles are directed almost axially resulting the total thrust essentially as the sum of the individual nozzle thrust. Migdal et al (1964) experimental data was obtained with high-pressure cold dry air. The contours of the plug were designed by the axisymmetric method of characteristics assuming the annular flow and the individual units were truncated perfect nozzles.

Axial and lateral forces were measured directly and the weight flow computed with a calibrated bell-month.

A comparison of the off-design characteristics of the cluster and annular plug nozzle is shown in Fig.VI.14, demonstrating the ability of the plug nozzle to adjust to the back pressure and similar performance of an annular-and clustered plug nozzle.

The performance parameter φ (Migdal et al denotes by C_v) is the ratio of measured to an ideal thrust calculated from the measured weight flow and isentropic expansion to ambient pressure. The nozzle were tested

with several plug lengths obtained by truncating the full-length design contour. The drastic reductions in the plug length have little or no effect on performance as shown in Fig.VI.14b.

The effect of spacing between the units of the cluster were evaluated by blocking the flow through several nozzles but providing symmetric configurations of 12 and 8 operating units. The results indicate that a large gap between nozzles causes an appreciable performance loss and this loss is due to the depressurization of the base area between units. A change in plug contour eliminated this loss.

Test results of vectoring by throttling units show that by increasing the plug length the effectiveness of vectoring decreases. Thus, the longer the plug acts as a flow diverter rearranging the initial asymmetric flow back to an almost uniform flow in the axial direction. The test of gimballing indicates that large angular movements are required to obtain the significant side forces but gimballing a portion of the plug appears to be relatively inefficient. Particularly since that portion of the plug which is gimballed can be removed with no loss in performance.

Shock vector control via secondary injection through the plug wall yields results equivalent to the same technique in a conventional nozzle.

The most promising methods of vectoring appear to be throttling or gimballing the individual nozzles with the shortest plug length consistent with satisfactory unvectored performance.

Experimental studies for thrust performance, distribution of pressure

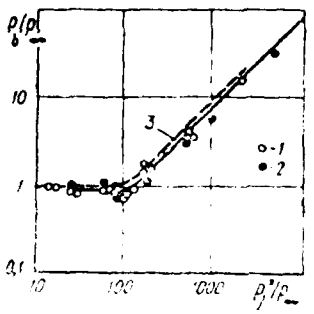

Fig. VI.14. Base pressure for a model of a 24-nozzle unit [Hendershot et al (1967)]: 1--L = 0; 2--L = 9.46; 3--cold air.

and heat transfer on the centerbody using a momentum method for cold air injection and hot gaseous hydrogen and oxygen are reported by Hendershot et al (1967). The measured base pressure is shown in Fig.VI.15. In a flow regime with a closed base region, the pressure affected by a short centerbody is almost the same compared to the pressure with the zero length of the centerbody.

If the base region is open, the base pressure appears to be almost equal to the pressure on the external flow. If the initial expansion of the individual nozzle is decreased while the inclination angle is appropriately increased, the base pressure with a closed base region may become larger than the external pressure. In the opposite case, a significant low pressure may occur in the base region. In order to evaluate the heat transfer to the base of the rocket, it is necessary to understand the base flow structure thoroughly accompanied by analysis of the reverse flow occurring in the near wake.

Leytes (1974) studied the interaction of two and four underexpanded streams. At first, the neighboring streams interact and part of the gas flows toward the symmetry axis of the system.

Because of the flow turning compression occuring in the neighborhood of the symmetry axis and the pressure increase is given approximately by

Newton's formula ;

$$p_4 = \rho_2 v_2^2 \sin^2 \beta$$

where p_4 is the static pressure in the area of interaction of four streams, ρ_2 and v_2 are density and velocity during the interaction of the two streams and β is an interaction angle of the stream line in a compressed layer inclined toward the symmetry axis of a four nozzle unit. Approximate calculations show that the static pressure in the four streams interaction region is invesely proportional to the square of the distance between nozzles. The formula for pressure changes along the axis of stream from the four nozzles has the same form as for a two nozzle unit and the distance between its axes is equal to the distance between the axes of an opposite nozzle in a four nozzle unit. Therefore, the position of the maximum static pressure in this unit system coincides. The Mach number in the four streams interaction region is approximately $\sqrt{2}$ times smaller than in a field of two streams interaction. The tests show that in the interaction zone the viscous effect is small for static pressure, and it can significantly influence the dynamic pressure.

Goethert (1961) formulated the similarity of base pressure of test model and prototype by

$$\left(\frac{p_a}{p_\infty}\right)_M = \left(\frac{p_a}{p_\infty}\right)_P \quad , \quad \left(\frac{1}{p}\frac{dp}{d\nu}\right)_M = \left(\frac{1}{p}\frac{dp}{d\nu}\right)_P$$

where ν is turning angle of Prandtl-Meyer flow.

In order to satisfy this similarity, the turning angle of the stream at the exit of the model and the actual motor must be the same and the following approximation equation holds, relating to Mach number Ma at the exit of actual nozzle.

$$\left(\frac{\gamma Ma^2}{\sqrt{Ma^2-1}}\right)_M = \left(\frac{\gamma Ma^2}{\sqrt{Ma^2-1}}\right)_1$$

Using these similarity relations and based upon the characteristic Mach number at the exit of the actual nozzle and the adiabatic combustion products of the working medium (ordinary air), it is possible to determine the Mach number of the model nozzle.

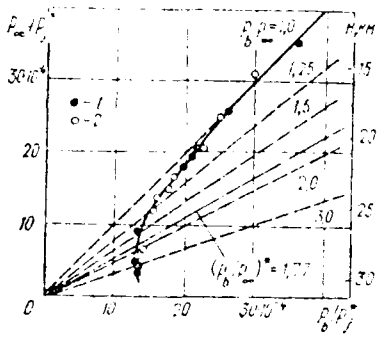

Fig.VI.16. Dependence of maximum relative base pressure on relative pressure in the ambient atmosphere for models with hot and cold jet streams [Goethert (1961)]:

1--hot jet streams;
2--cold jet streams;
3--dashed-dotted line--critical ratio)

Fig.VI.16 shows the base pressure at the center of the base shield of a four nozzle unit obtained for equivalent medels referring to the working medium involving cold air and combustion products of jet fuel:

During the flight, if the nozzle units are closed, then an existence of flow regime should be considered within which part of the hot gases of jet streams returns. Therefore, it is necessary to provide a thermal shield in the base region in order to protect the base from the radiant heat from the reactive streams but also from the con-

vective heat from the returning hot gas.

Tufts and Smoot (1971) computed and compared with the experimental data of mixing coaxial streams, free and bounded, of regulated and non-regulated gases with presence of solid particles and secondary flows referring to the velocity and gas concentrations along the stream axis. The coefficients of correlation between the cell length of the stream, the velocity, the concentrations, the coefficients of mixing and the vortex diffusion were also investigated.

4.) Oscillation of the Base Pressure Affected by Annular Jet Outflow

The pressure oscillations in the base region depend on many factors, such as, quasi-steady changes of the flow field in annular jets, acoustic radiation of jets and non-steady flow behavior etc. For multinozzle lay out, non-stationary influence on the base flow caused by relaxation oscillation and discrete acoustic radiation is of the greatest importance.

Some investigations on the acoustic jet radiation are described here. Lighthill (1963) investigated subsonic jet noise by relating the acoustic pressure generated by turbulence to a system of quadrapolar sources fixed in a quiescent medium. Corcos (1959) studied the structure and noise of a low velocity jet and Ginevskiy (1969) studied the influence of the acoustic interference on the initial part of the turbulent jet. The results of theoretical and experimental investigations of aerodynamic noise are all described in the book Aerodynamic Acoustics . (Ed. Munina and Kvitki 1973)

Rimsky-Korsakov and Munin (1974) report a large number of papers on noise in supersonic jets. One of the research trends is concerned with investigations of the discrete components of the noise spectrum. Powell (1953) proposed a self-exited oscillation cycle to investigate the jet whistle and Hammit (1961) and Merle (1965) proposed the positions of discrete tone sources. Some papers indicate that this radiation is nearly isentropic but Powell (1953) and Rimsky-Kovsakov (1970) showed that for the basic and first harmonic frequencies, there exist preferred directions.

Sedelnikov (1971) developed an instability theory applicable to free jets and ejectors and Lebedev and Telenin (1970, 1974) solved the problem of the jet interaction with an external acoustic field case and in non-linear approximation for a plane case.

The high frequency portion of the noise generating jet spectrum is studied by Krasilnikov and Shihlinskaya (1964). The acoustic interaction of a supersonic jet in the nozzle base by Belenkov (1970). Poldervaart et al (1968) investigated the discrete tone for the supersonic jet outflow from a slotted nozzle and Hay and Rose (1970) the noise spectrum of a jet engine of an airplane in flight.

For a large class of supersonic jets, Anufriev et al (1969) established general laws for the frequency characteristics of the discrete components of noise spectra. Data on the influence of an ejector on the noise radiation spectrum of a jet is available in the publications of Middleton (1956) and Pychov (1968).

4.3 The Level of Fluctuations.

Since the structures of annular jets differ from those of cylinder jets involving, open and base flow regimes, it may be conjectured that pressure fluctuations due to acoustic radiation of the annular jet would be a distinct phenomena. The pressure fluctuations at the case of the annular nozzle depend indeed on the flow regime of the jet and substantial differences in the discrete components of the fluctuation spectrum were found by Ljutev et al (1973).

The supersonic jet is a source of three types of acoustical radiation; boundary perturbations, turbulent noise and discrete tones. One of the main sources of supersonic jet noise is the boundary perturbation as Crandall and Mark (1963) indicate. The instability of the jet boundary, which amplifies small perturbations starting at the jet exit is the case of turbulent noise.

[Chvets and Chvets (1976)]

The relation between the integrated level of pressure fluctuations L at the central point of the nozzle and the off-design ratio n is given in Fig.V.17 for nozzles of $F_2 = 1$, 3.1 and 5.1. An increase of acoustic radiation of the outflowing jet up to $n \approx 0.8$ is accompanied by an increase of fluctuations. A further increase of the off-design

ratio for the last two nozzles produced a decrease of fluctuation level but for $M_j = 2$ nozzle the transition to the underexpanded nozzle flow case is accompanied by an increase of L_{Σ}.

A characteristic feature of the annular jet is the sharp reduction of the pressure fluctuation level when the flow regime changes. At the same time also an appreciable reduction of an acoustic pressure level in the far field occurs. Therefore, this feature can be used to determine the transition from the open to the closed base flow regime using acoustic measurements only. The value of the pressure fluctuation characterized the additional pressure variation because of the passage of a shock wave.

The pressure in the separated zone inside the jet differs greatly from the pressure in the surrounding space. Therefore, the flow parameters in this zone affect the displacement of shocks toward the base. The value of $\zeta = K(\bar{p}^2/\rho_b a_b)$ (where K is an arbitrary coefficient) was used for a qualitative analysis of the intensity of fluctration source. The magnitude of ζ is similar to the mean flow of acoustic energy passing through a unit area of a plane acoustic wave under the assumption of uniform distribution of fluctuation at the base (Fig.VI.17). Thus, it may be noted that the behavior of the curve $\zeta = f(n)$ is similar to the ones of $L_{\Sigma} = f(n)$. Rimsky and Korsakov (1970) indicate that in the rear of the hemisphere a broad maximum of noise spectrum exits. The formation of a broad maximum in the pressure fluctuation spectrum is in some cases more pronounced and appears over a wide range of off-design ratios and in other case less pronounced. No clear re-

lations between the flow regime and the positioning of the broad maximum was found.

The acoustic noise resulting from turbulent fluctuations in the jet and the boundary perturbations at supersonic speed is a stationary stochastic process and the characteristic parameters of such a process are: the mean value and the second order statistics which can be given either by the correlation function or the spectral density function.

The generalized spectral density of the annular jet noise is compared with experimental results of model rocket engines by Humphrey (1957) as shown in Fig.VI.18. The Strouhal number is defined by $Sh_o = f\, da/a_j$ where da is diameter of the nozzle exit (for annular jets the equivalent diameter of a circular jet based on exit section area) and a_j is the velocity of the sound in the jet. The ordinate shows the value of the generalized spectral density

$$S = 10 \log \frac{a_j \overline{\omega^2(f)}}{d\int \overline{\omega^2(f)}\, df}$$

where $\overline{\omega^2(f)}$ is the spectral density of noise.

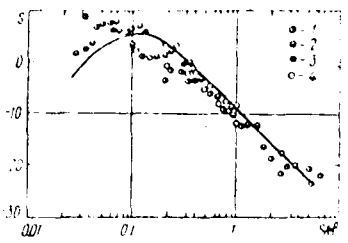

Fig.VI.18. Comparison of generalized spectral densities of jet noise. (1) Rocket engine of 40-50 tons thrust, (2) 1-15 t, (3) 0.4 t [Humphrey (1957)] (4) annular jet of 0.15-0.3 t thrust. [Shvets (1978)]

It is apparent that the distributions of generalized spectral densities of the noise of the annular nozzle models are similar to the experimental results from the full-scale rockets and turbojet engines.

Let us consider briefly the influence of the jet shape on the radiated noise. There are three methods to reduce the noise of supersonic jets. The first one is based on the reduction of the effective outflow velocity, the second on increasing the width of the frequency range and the third on the fact that the maximum noise of a nozzle system is lower than the sum of the maxima of each nozzle taken separately. The last one is due to the difference in the directions of the maximum noise for each nozzle. To the first approximation the length of the acoustic wave is determined by the width of the displacement region in any jet section and the value of the average velocity in this region. As, for the same mass output and neck diameter, the perimeter of an annular jet is larger than that of a circular one, the distance along the axis required for entrainment of a given quantity of air is diminished, i.e. the linear scales of the mixing process change. If the exit area shape of the nozzle is changed without increasing its area in such a way that the jet flows out in the thin annular jet shape, then the radiated noise frequency increases approximately proportionally to the ratio of the initial diameter over the slot width. The reduction of the intensity of the low frequency noise when the nozzle shape is changed, is not accompanied by an increase of the high frequency noise. This is another interesting feature noted in the experiments of an underexpanded annular jet of $M_j = 1.13$ by Richard (1958).

4.4 Discrete Components

For supersonic jet flow, a discrete tone is emitted. Merle (1965) observed the most intensive acoustic radiation in a cylindrical jet from

the sixth to eighth cell and Hammit (1961) from the third cell of a plane jet. Predictions of Lebedev and Telenin (1970), using the linear approximation of plane jet, agree with these results. The first discrete tone harmonic is directed upstream at 30° to the jet axis while the second is propagated perpendicular to the jet. When the acoustic perturbation reaches the nozzle base, a cyclic process of acoustic resonance develops.

From the fluctuation spectra, the discrete tone part of the fluctuation energy observed at the central point of the nozzle base may be determined. It is estimated that the discrete component contains about 30% of the total energy spectrum. In the continuous jets radiating into the rear hemisphere, the energy of the discrete tone is sometimes comparable to the background noise energy as Rimsky-Korsakov (1970) noted. In the over expanded regime, an overshoot of the level ΔL_o of the discrete component (for 7 Hz band width) over the average level of the continum spectrum for nozzles of M_j = 3.1 and 3.6 is observed as shown in Fig.VI.19. The discrete components of plane jets of M_j = 2 begin at off-design ratio n = 0.9 and reach a maximum value at n = 1.3. Hence, exist also at n = 1, whereas for cylindrecal jets the acoustic resonance disappears at the design flow output.

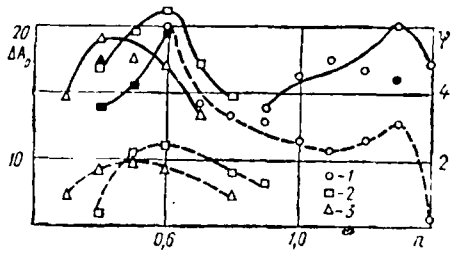

Fig.VI.19. Amplitude and power of the discrete component, ——, ΔL_o[dB], ---, ψ, (1) M_1=2, (2) M_1= 3.1, (3) M_1=3.6, open symbols - amplitude of the fundamental tone; filled symbols-amplitude of the first harmonic. [Shvets (1978)].

The discrete tone of an axisymmetric jet of $M_j = 2$ detected for $n = 1$ by Belenkov (1970) is considered as an exception. The existence of a discrete radiation in the design flow of an annular jet can be explained by the determination of the off-design regime on the basis of the external pressure, whereas at $n = 1$, so determined, the jet will be in an off-design regime when related to the internal pressure and this leads to a flow with a system of compression and expansion waves which will be different inside and outside the jet.

One of the main experimental results to be noted, is the reduction of the discrete component of the fluctuation spectrum when the flow regime changes. Measurements in the rear and far acoustic fields also exhibit a disappearing discrete tone at or about $n = n^{o}$.

The acoustic radiation of a supersonic annular jet propagates into the external space as well as into the internal region downstream of the nozzle central body. A qualitative estimate of the influence of the off-design ratio on the ratio of the power content of the fluctuating pressure at the nozzle base to the full jet power can be made assuming that the fluctuation distribution over the base is uniform (see Fig.VI.19 $\psi = \frac{\kappa \overline{\omega^2}^{as} \pi d_b^2}{4N}$ where κ is an arbitrary coefficient, d_b is a base diameter and N is the full jet power). For a nozzle of $M_j = 2$ in the underexpanded flow case, when the discrete component is at a maximum ψ becomes also maximum.

A comparatively large ψ -value in the overexpanded regime may be explained as the pressure in the separation zone is not much lower than the pressure in the surrounding space. Therefore, the fluctuation

energy is transmitted to the base with no substantial losses. For jets of M_j = 3.1 and 3.6, the variation of ψ agrees well with that of ΔL_o, indicating that the discrete tone is one of the most effective sources generating the pressure fluctuations. The range in which the discrete components appear were determined by spectrogram and analyzing an expanded frequency scale. This enables one (using a narrow band analyser) to evaluate the Strouhal number corresponding to the discrete component $Sh_o = f_o d/a$ (where d is the outside diameter of the annular nozzle and a is velocity of sound in the surrounding space) accurately as shown in Fig.VI.20.

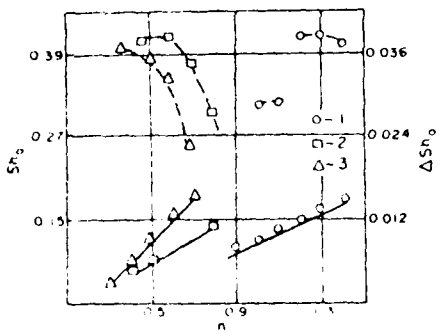

Fig.VI.20. Strouhal number and band width of the discrete component -- Sh_o, —— ΔSh_o. (1) M_1 = 2, (2) M_1 = 3.1, (3) M_1 = 3.6. [Shvets (1978)]

The discrete component of M_j = 2 nozzle shows a frequency discontinuity close to the design flow regime. Nozzles radiating a discrete component in the overexpanded regime exhibit a monotonic decrease of frequency if the Mach number or off-design ratio increase.

A similar relation is obtained for the continuous jets discharged from the supersonic nozzles by Rimsky-Korsakov (1970) while for the circular sonic nozzles and ejectors Powell (1953) and Hammitt (1961) note the relation fo = f(n) has a discontinuity.

If it is assumed that the parameter Δ Sho remains constant when the

characteristic dimension is changed, then the width of the frequency band must increase as the nozzle diameter increases. It is possible that in some cases the widening of the diserete component frequency band causes the absence of the reasonance process on full scale engines. Let us compare the non-dimensional frequency of the discrete components of pressure fluctuation spectrum with the data on radiation of discrete tone by continuous jets. The Strouhal number $Sh_1 = f_o d_1/a$ (where d_1 is the sonic diameter of circular nozzles or the equivalent diameter of circular nozzle with the same area as the sonic section of annular jet) is given in a function of relative pressure in the settling chamber p_o/p_∞ in Fig.VI.21a. In Fig.VI.21b data of annular jets and experimental results of continuous jets are shown.

The curve I give a relation $Sh_1 = 0.567(p_o/p_\infty - 1)^{\frac{1}{2}}$ based on the experimental data of cylindrical jets by Rimsky-Korsakov (1970) in an agreement with Powell's (1953) formula for circular jets at low values of p_o/p_∞. If the Strouhal number of annular jets Sh_1 were to be based on the width of the gap of the sonic section of the nozzle, then the value of Sh would be several times smaller. At the same time the values of Sh_1 for annular jets obtained for a wide range of n, coincide satisfactorily with cylindrical jet data. Hence, the characteristic length for the formulation of Sh_1 for the annular jet may be taken as the diameter of the circular jet having an area equal to the sonic section. Anufriev et al (1969) analysing data of discrete frequency measurements of cylindrical and rectangular jets found that all data fall on a single curve if the experimental data are given as a depen-

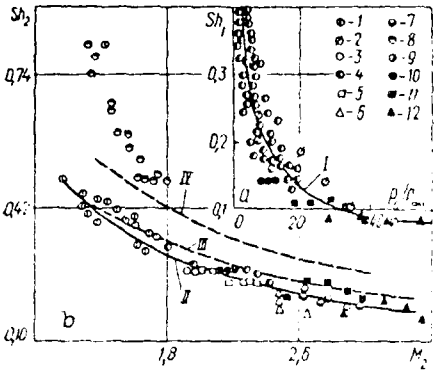

Fig.VI.21. Strouhal number dependences for annular (10-12), cylindrical, (1-7) and flat (8,9) jets, calculated according to the equivalent critical sectional area, on the relative pressure in the injection settling chamber (a) and on the average Mach number in the jet, assuming isentropic expansion. I— [Mamin and Rimsky-Korsakov (1969)]; II—[Anufriev (1969)]; III,IV—calculation for flat and cylindrical jets [Lebedev and Telenin(1974)]. (1) M_1=1 [Powell (1953)], (2) M_1=2 [Belenkov (1970)] (3) M_1=2 [Merle (1965)] (4) M_1=2.17 [Mamin and Rimsky-Korsakov (1969)]. (5) M_1=3 [Merle (1965)], (6) M_1=3 [Anufriev (1969)], (7) M_1=3.7 [Anufriev (1969)], (8) M_1=1 [Hamitt (1961)], (9) M_1=1[Poldervaart(1968)](10) M_1=2 [Ljutey et al. (1973)], (11) M_1=3.1 [Ljutey et al.] (1973), (12) M_1=3.6 [Ljutey et al. (1973)]. [Shvets (1978)]

dence of the Strouhal number Sh_2 on the average Mach number in the jet M_2.

Anufriev et al (1969) approximated the curve II in Fig.VI.21 by

$$Sh_2 = 0.85 \left[\sqrt{(M_2^2 - 1)} + \frac{a}{a_1} \right]^{-1}$$

where $d_2 = 1.78 \left(\frac{G\,T_0^{\frac{1}{2}}}{qM_2 p_0} \right)^{\frac{1}{2}}$ is the reduced diameter

of an annular jet based on the output, G is the output of air through the nozzle per second and T_o and p_o are the temperature and the pressure in the settling chamber respectively.

From this figure, it can be seen that experimental data of circular and annular jets form a single curve. Hence, for an annular jet, the characteristic parameter for Sh_2 is jet the Mach number determined on the assumption of isentropic expansion in the nozzle.

Lebedev and Telenin (1970) formulated the following equation of frequencies of external acoustic waves at which jet perturbations in the design flow conditions are most strongly amplified,

$$Sh = \frac{f_o d}{a} = \frac{h(n)}{\sqrt{\left(\frac{a}{a_1} + M_1\right)^2 - 1}}$$

where d is cylindrical jet diameter or the width of plane jet.

The function h(n) is ;

$$h(n) = \begin{cases} n - \frac{1}{2} & (m=0,\ j=0) \\ n & (m=0,\ j=1) \\ \mu^0/\pi & (m=1,\ j=0) \\ \mu^1/\pi & (m=1,\ j=1) \end{cases}$$

where m = 0 in the plane and m = 1 in the cylindrical case;

j=0 for symmetric and j=1 for axisymmetric perturbation of the external wave and μ^o and μ^1 are n the roots of the Bessel function I_o and I_1.

The first two values of the function h(n) for the cylindrical case are : for j=0, h(n)=0.76 and 1.66; for j=1, h(n)=1.22 and 2.23.

The computed curves for plane III and cylindrical (IV) jets in an an-

tisymmetric acoustic field are shown in Fig.VI.21b.

Sedel'nikov's (1971) investigations of the low frequency approximations of the dispersion equation of a double layered cylindrical jet have shown that an annular jet tends to oscilliate as a single unit. Oscillations of plane jets are in the bending mode and this is essentially true also for circular jets, but the latter, at certain flow regimes, oscillate with symmetric modes. Lebedev and Telenin (1970) indicate that by computing the plane jet frequancies, the jet is more stable in the symmetric external acoustic field than in the antisymmetric one.

If the base flow region is open, coupling is due to wave radiation of a few periodic jet cells. As the flow regime change is approached but before the jet closes there exists only one, fast growing annular cell after the jet becomes a continuous Mach or regular wave interactions are realized. In this case the whole jet does not have a definite periodic structure and does not oscillate as a single entity, therefore there is no resonance process.

4.5 Co-Current Flow

Tests on a jet aligned with free stream in a wind tunnel show that due to deflections, the tunnel walls have a great influence on the jet stability. The tunnel wall influence is particularly important for discrete components in noise spectrum patterns. Therefore, results obtained in a co-current flow in tunnels may not be compared directly with those of a free jet in an infinite outer space. On the other hand, there exist common characteristics in both flows

Subsonic flow data may be used to plot the quantitative curves while values of transonic flow are applied only for a qualitative presentation. The dependence of level of pressure fluctuation on the Mach number of the co-current flow is distinguished by three groups of curves of different values of off-design ratios as shown in Fig.VI.22.

Fig.VI.22. Dependence of the pressure fluctuation level on Mach number of a co-current stream. (1) n=0.4, M_1=3.1, (2) n=0.6, M_1=3.1, (3) n=0.7, M_1=3.1, (4) n=0.8, M_1=3.1 (5) n=0.4, M_1=3.6, (6) n=0.6, M_1=3.6, (7) n=0.7, M_1=3.6, (8) n=0.8, M_1=3.6, (9) n=0.9, M_1=3.6, (10) n=1.0, M_1=3.6. [Shvets (1978)]

At $n < 0.5$, the level of pressure fluctuation up to M=0.8 is nearly constant and then decreases slightly. For n = 0.6-0.8 the value of L decreases sharply while passing from M=0.8 to 0.9 and then increases sharply when the Mach number increases from M=1.1 to 1.2. At M=0.9-1.1, the base region is closed and surrounded by a supersonic annular jet and only the radiation from the part of the jet below the sonic point penetrate up to the base of the nozzle. After the change of regime, the area of the inner surface of the jet which is the main source of radiation toward the base, decreases sharply. In this case, as during the outflow into an open space, the pressure fluctuations in the closed base region are smaller than in the open one. Close to the design outflow n=0.9-1.0, the accustic pressure is relatively small as the base region remains closed for the entire investigated range of velocity of the external flow.

reduction of jet turbulence is an effective method of noise reduction. The largest turbulence is attained in the zone of tangential longitudinal discontinuity of velocity between the jet and the outside flow. As the co-current flow velocity increases, the outflow jet velocity relative to the surrounding flow is reduced, leading to a reduction of the intensity of turbulence in the viscous layer and to a reduction of noise. Dorcos (1959) reduced the noise of a low velocity jet in a co-current flow.

In experiments of annular jets, an increase of the outer flow velocity up to the sonic value, is accompanied by a reduction of the broad maximum and also by its displacement towards low frequencies. One of the main noise sources of supersonic jets are waves radiated by supersonic boundary vortices as Crandall and Mark (1963) note. For high frequency jets, it is necessary to take into account the Doppler coefficient (1-Me cos θ) and in the case of the upstream transmission of perturbation (1 + Me), where Me is the Mach number of the boundary perturbations and θ is the angle between the direction of radiation and jet axis. For the subsonic co-current flow, frequencies change proportionally to (1 - M) as this coefficient determines the change of the wave velocity relative to the nozzles. The experiments using a closed type tunnel, the flow velocity reaching 0.5 M, in the measuring section due to the ejector effect of the jet with no forced external flow, show that there exist two types of discrete components; one due to an induced acoustic coupling and the other to the resonant excitation of the ejector. For narrow gap nozzle (M_j = 2.5) a discrete

[illegible] the value of Δf_o to grow rapidly at n = 1.1-1.3 then remains nearly constant equal to 25-27 dB. The frequency f_o remains constant and the band width Δf_o is approximately equal to 14 Hz for the base component and the harmonics. If the frequency of the discrete jet tone is close to the resonant frequency of the ejector ($0.75\, f^o < f_o < 0.95\, f^o$, where f^o resonant frequency of the ejector), then an excitation of the resonance process in the ejector can occur and the value f_o changes into f^o as Brown (1966) indicates.

The excitation frequency for ejectors of the square cross-section is $f^o = (2n + 1)a/2H$ where H is length of square edge. The relation $f_o = f(n)$ for the ejector has a discontinuity and a locking in of the oscillations to the frequency f^o past the discontinuity is noticed. The discrete frequency component of a nozzle of M=2.5 remains constant despite the variation of the off-design flow ratio in a wide range of (n=0-4) and at a velocity of the ejected stream up to M=0.5. The non-dimensional frequency of the discrete component is close to the excitation frequency of the ejector $Sh^o = [(2n+1)\, d/2H] \approx 0.27$ (Sh^o of the ejector excitation defined by characteristic dimensions d and H of the nozzle and the constancy of the band width Δf_o shows the [illegible] of the excitation mechanism. In this case the excitation [illegible] oscillation is expected. Experiments with nozzles [illegible] show that the variation of the off-design ratio [illegible] as well as the variationof the velocity of the latter with no change of off-design ratio, lead to a continuous variation of frequency of the discrete component. Therefore, it

may be concluded that the investigated processes are not determined by the resonant excitation of the ejector, for which a sudden frequency change, from one resonant value to another, is characteristic.

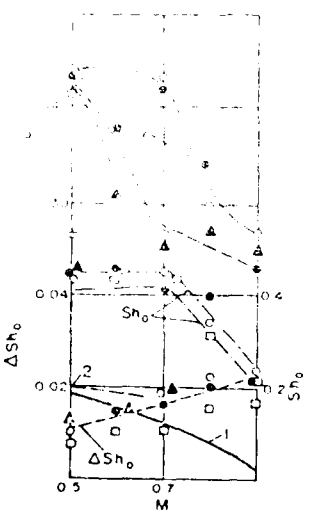

Fig.VI.23. Discrete component when exhausting into a co-current stream (1) Cylindrical jet, M_1=?%, calculation [Lebedev and Telenin (1974)], (2) experiment, [Lebedev and Telenin (1974)] (notation as in Fig.VI.22). [Shvets (1978)].

As M increases, L_0 initially grows, while above M=0.6-0.7, it decreases and maintains approaching to the velocity of sound as Fig.VI.23 shows. Lebedev and Telenin (1974) observed a similar behavior of the relation $L_0=f(M)$ in experiments of cylindrical jets exhausting into a co-current flow with free surfaces. The computation of Shvets (1978) indicates that the existence of a co-current flow exerts a stabilizing influence on the jet for antisymmetric excitations in the external acoustic field and causes a "symmetrization" of excitation. Further investigation is needed because the level of the discrete tone of a circular and annular jet with M is initially increased, and not decreased as would be expected considering the feed-back coupling scheme.

In a number of cases another discrete component of much lower level, with a frequency of a few tens to a few hundred Hz different from the

frequency of the main component is noticed in the fluctuation spectrum together with the main discrete component and its harmonics.

In the open base region flow regime the discrete tone radiation, propagating upstream, interacts with the jet close to the base of the nozzle at both the external and internal boundaries of the annular jet. Therefore, the existence of two feed-back coupling loops, an external and an internal one, can be expected. As a result of differences existing in the flow surrounding the jet on the outside and the inside, the frequencies connected with the external and interal couplings can be different.

If the outflow into a co-current stream occurs, the sound waves propagated upstream are carried down by the stream. As the velocity of the co-current flow increases, the upstream propagation velocity of perturbations decreases, and when the velocity of sound is approached, the external coupling loop is interrupted. The cyclic process is disturbed and the jet-acoustic system, acting as a filter and amplifier of the oscillation becomes imperative.

Hence, for annular jets the external coupling loop is of primary importance. The Strouhal numbers are determined from the frequencies corresponding to the maximum level of the discrete components.

As shown experimentally, after reaching a determined velocity of co-current flow, the frequencies remain nearly constant. However, the value of Sh_o increases slightly as the velocity of sound of the co-current flow decreases with increase of the Mach number.

The frequency band-width of the discrete component ΔSh_o increases almost two times when the co-current flow velocity changes from M=

Comparing this fact with the increase of ΔSh_o as the off-design ratio increases for the outflow into a submerged space, it may be noted that in the case of maximum level of the discrete component, the width of the band ΔSh_o is minimum. Hence the best performance of the oscillation system with an acoustic coupling may be obtained with a minimum band width. For the solution of supersonic jet interaction with an external acoustic field of subsonic co-current flow, Lebedev and Telenin (1974) determined the frequencies of external acoustic waves for antisymmetric perturbation from the following equation:

$$Sh = \frac{h(n)}{\left[\left(\frac{a}{a_1} + \frac{M_j - 1}{1 - M}\right)\left(\frac{a}{a_1} + \frac{M_j + 1}{1 - M}\right)\right]^{\frac{1}{2}}}$$

The relation between the frequencies and the Mach number of the co-current flow for a cold cylindrical jet is shown by curve 1 of Fig.VI.23. On the same figure experimental data for a cold cylindrical jet [Lebedev and Telenin (1974)] where the discrete component was recorded at two close frequencies are shown in curve 2.

In these experiments the frequencies f_o did not change when the ratio of the jet cross-section to the stream cross-section was below 7% while any further increase in this ratio reduced an increase of f_o. The ratio of the cross-section areas did not affect Lo.

The period of the resonance system is determined by the time necessary for the perturbation to cross the distance from the nozzle to the effective source and the time the sound wave needs to get back to the nozzle. In the case of outflow into an infinite space, Hay and Rose (1970) formulated

$$t_o = \frac{\ell}{k u_j} + \frac{\ell}{a}$$

... of the co-current flow $t'_o = \frac{\ell}{u + k(u_j - u)} + \frac{\ell}{a - u'}$

where k is the coefficient of vortex convection at the boundary of the supersonic boundary layer, (k = 0.625), ℓ is the distance from the base of the nozzle to the effective radiation source of discrete tone and u_j and u are the velocities of the jet and the co-current flow respectively. The ratio of the discrete tone frequencies for the outflow into a co-current flow to the corresponding frequency for the zero co-current flow velocity is ;

$$\frac{f'_o}{f_o} = \frac{t_o}{t'_o} = \frac{[u+k(u_j-u)]\,[(a-u)(a+ku_j)]}{ku_j a\,[a+k(u_j-u)]}$$

Using Powell's (1953) empirical formula, $f_o = \frac{a}{k_1 d_1}\left(\frac{p_o}{p} - 1.89\right)^{-\frac{1}{2}}$

where k_1=const. and d_1 is the diameter of the sonic section of the nozzle,

$$\frac{f'_o d_1}{a} = \frac{F}{k_1} = \frac{[M+k(M'-M)](1-M)(1+kM')}{kk_1M'\,[1+k(M'-M)]}$$

$$x\left(\frac{p_o}{p} - 1.89\right)^{-\frac{1}{2}} \quad \text{where} \quad M' = u_j/a.$$

Experimental values for the two values of n are shown in Fig.VI.24.

Where $St_1 = \frac{f_o \cdot d_1}{a}$

$$F = \frac{[M+0.625\,(M'-M)](1-M)(1+0.625M')}{0.625M'\,[1+0.625(M'-M)]} \quad x \quad \left(\frac{p_o}{p_-} - 1.89\right)^{-\frac{1}{2}}.$$

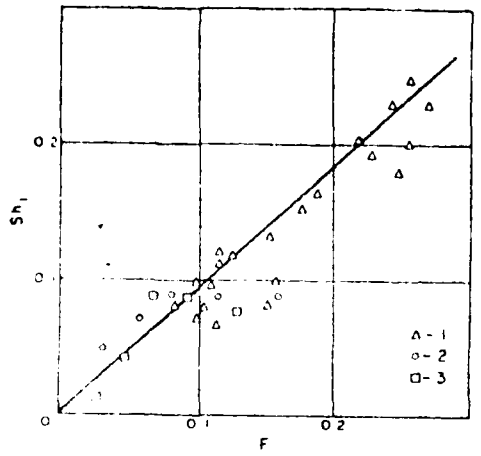

Fig.VI.24. Dependence of the Strouhal number Sh_1 on the parameter F. (1) Flight experiments, [Hay and Rose (1970)], (2) annular jets M_j=3.6, n=0.4, (3) annular jets M_j=3.6, n-0.6. [Shvets (1978)]

Also shown are results from the free flight test of Hay and Rose (1970) who measured the second harmonics. The Sh_1 values given here are therefore obtained by halving the orginal recorded frequencies. The linear variation shown is a good fit if k is taken as 1.1, which however is markedly different from that k_1 = 3, which fits the data of Powell (1953). The results for the annular jets lie close to this linear dependence only in the range of M=0.6-0.9 corresponding to a falling frequency.

References

Anufriev, V. M. Komarov, V. V. Kuptsov, V. M, Melnikov, D. A, and A. A. Sergienko (1969). "Discrete Components in the Noise spectrum of Supersonic Jets," Izv. AN SSSR MZhG. 5.

Belenkov, V. D. (1970). "Acoustic Radiation of a Supersonic Jet Towards the Nozzle Base at Different off-design States," Uch. Zap. Leningradskogo Universiteta, Gazod. i. Teplo. p.2.

Bondarev, Ye. N. and G. A. Gushchin (1972). "Spatial Interaction of Streams Propagated into a Wake Supersonic Flow," AN SSSR MZhG 6.

Corcos, G. M. (1959). "Some Effects of Sound-Reducing Devices on a Turbulent Jet," J. Aerospace Sci. vol.26, No. 10.

Craven, A. (1960). "Base Pressure at Subsonic Speeds in the Presence of a Supersonic Jet," Dept. N. 129. The College of Aeronautics, Cranfield.

Crandall, S. H. and W. D. Mark (1963). Random vibration in Mechanical Systems, Academic Press.

Der, J. Jr. Mullingt, B. N, Hoffman, G. H. and B. N. P. Brown (1963)."Numerical Analysis of Supersonic Flow Through Curved Channels," Northrop Norair, Hawthorne, Calif. Aerospace Res. Lab. 63-117.July.

Dixon, R. I. and R. H. Page (1966). "Theoretical Analysis of Launch Vehicle Base Flow," Separated Flows. part 2 Rutgers University. New Brunswick, N. J.

Ginevskiy, A. S. (1969). "Theory of Turbulent Jets and Wakes," Mashinostroenie. Moscow.

Ginzburg, I. P. Prikhod'ko, V. D. and A. M. Sizov (1970). "Study of Component Streams," Uchyenyye zapiski, LGU Gazodinamika i teploombmen 357.

Love, E. H. (1961). "Base Flow Characteristics of Missiles with Cluster Rocket Exhausts," Aerospace Eng. 20/3.

Gogish, L. V. (1969). "Relaxation Oscillations in a Turbulent Near Wake," Izv. AN SSSR MZhG 6.

Gogish, L. V. and G. Yu. Stepanov (1971). "Quasi-Unidimensional Theory of Interaction of a Turbulent Wake with a Supersonic Flow in a Channel and a Stream," Trudy Instituta Mekhaniki, Works of the Institute of Mechanics, vol. 11, MGU Publishers, Moscow.

Hall, G. T. and J. J. Mueller (1971). "An Analytical and Experimental Study of Nonuniform Plug Nozzles Flow Fields," AIAA Paper 71-41.

Hamitt, A. S. (1961). "The Oscillation and Noise of an Over Pressure Sonic Jet," J. Aerospace Sci. vol. 28, No. 9.

Hay, J. A. and E. C. Rose (1970). "In-Flight Shock Cell Noise," J. Sound Vibr. 11(4).

Hendershot, K. C. et al. (1967). "A New Approach for Evaluating the Performance and Base Environment Characteristics of Nonconventional Rocket Propulsion Systems," AIAA Paper 67-256.

Humphrey, A. J. (1957). "Noise Radiation from Fourteen Types of Rockets in the 100 to 130,000 Pounds Thrust Range," WADC Rept. UTR 57-354.

Ivanov, M. Ya and A. N. Krayko (1972). "Method of Start-to Finish Calculation for Two-dimensional and Spatial Supersonic Flows," ZhVM i MF 3.

John, J. E. A. (1973). "Gas Dynamics," Allyn and Bacon, Boston.

... the Effects of the ... Stream on Flow in the Region of the Base Section," Trudy II Respublikanskoy konferentsii po aerogidrodinamika, (Works of the II Republic Conference on Aerodynamics), KGU Publishers, Kiev.

Krasilnikov, V. and R. Shinlinskaya (1964). The High Frequency Region of the Jet Noise Spectrum, Physics, Series. No. 3 Moscow University Press.

Korst, H. H. (1968). "Drag Measurements on a Series of Afterbodies at Transonic Speeds Showing the Effect of Sting Interference," Aeron. Res. Council Current Paper 384.

Lebedev, M. G. and G. F. Telenin (1970). "Investigation of the Interaction of a Supersonic Jet with an Acoustic Field," Izv. AN SSSR MZhG 4.

Lebedev, M. G. and G. F. Telenin (1974). "Supersonic Jet in an External Acoustic Field," Izv. AN SSSR MZhG. 2.

Lee, C. C. (1966). "Gasdynamic Structure of Jets from Plug Nozzles," AIAA J. vol.4, No.6.

Leytes, Ye. A. (1974). "Study of Flow in the Field of Interaction of Two and Four Streams," Trudy TsAGI, (works of TsAGI) 1575 TsAGI Publishers, Moscow.

Lighthill, M. J. (1963). "Jet Noise," AIAA J. vol.1, No.7.

Lyutei, V. A. Novikov, I. V. and A. I. Shvets (1973). "Pressure Pulsations in Annular Nozzles," Izv. AN SSSR MZhG 5.

Manin, V. N. and A. B. Rimskiy Korsakov (1969). "Certain Experimental Studies of Whistle Noise of a Supersonic Air Stream," Trudy Akusticheskogo in-ta AN SSSR, Works of the Acoustic Institute of AN SSSR vol. , Nauka Press, Moscow.

Merle, M. (1965). "Emissions acoustigues associes aux jets supersoniques," J. Mechanique, vol.4, No.3.

Middleton, D. (1965). "The Noise of Ejections," ARC and M. 3389.

Migdal, D, Horgan, J. J. and A. Chamay (1964). "An Experimental Evaluation of Plug Cluster Nozzles," AIAA J. vol.2, No.7.

Poldervaart, L. S. Vink, A. T. and A. P. Wijnands (1968). "The Photographic Evidence of the Feedback Loop of a Two-Dimensional Screeching Supersonic Jet of Air," 6th Internat. Congress. Acoust. Tokyo.

Powell, Y. A. (1953). "On the Mechanics of Choked Jet Noise," Proc. Phys. Soc. B 66, (408).

Pychov, L. S. (1968). "On the Oscillation Mode of a Supersonic Jet in a Ejector," 6th All Union Acoustics Conference, Nauka Moscow 4.

Richards, E. J. (1956). "A New Types of Tip Jet to reduce Noise," J. Helicopter Gt Br. 9,404.

Rimskiy-Korsakov, A. V. (1970). "Investigations of Aerodynamic Noise," Reports of the Acoustical Institute, AN SSSR. Issue, X.

Rimsky-Korsakov. A. V. and A. G. Munin (1974). "The Noise of Gas Jets," TsAGI, Rept. No.1539, Moscow.

Roberts, J. B. (1963). "Coherence Measurements in Axisymmetric Wake," AIAA J. vol.11, No.11.

Sedelnikov, T. H. (1971). "Self Exited Noise Generation during the outflow of Supersonic Jets," Nauka. Moscow.

Shvets, A. I. and S. P. Isayev (1969). "Structure of Flow in a Base Region," Trudy 1 Respublikanskoy konferentsii po aeromekhanike, (Works on the I Republic Conference on Aeromechanics) KGU Publishers. Kiev.

Shvets, A. I. V. V. Kravets and M. N. Kazakov (1974). "The Aerodynamic Coefficient of a Conical Body with a Star-like Cross-section," Izv. AN SSSR MZhG. 6.

Shvets, A. I. and I. T. Shvets (1976). Gas Dynamics of Near Wakes, Naukova Dumka Press, Kiev.

Shvets A. I. (1978). "Base Flow" Prog. Aerospace Sci. vol.18, pp. 177-208, Pergamon Press.

Sizov, A. M. (1970). "Calculation of Base Pressure with Flow of a Number of Streams," Gazodinamika i teploobmen 2/357.

Spreiter, J. R. and S. S. Straha (1971). "Aerodynamics of Slender Bodies and Wing-Body combinations at $M_\infty = 1$," AIAA J. vol.9, No.9.

Stepanov, G. Yu. and L. V. Gogish (1973). "Quasi-stationary Gasdynamics of Rocket Engine Nozzles," Mashinostroenie Moscow.

Tagirov, R. K. (1974). "Transonic Flow Past a Rotational Body with Flow of Jet Stream from Rear Section," AN SSSR MZhG 2.

Tufts, L. W. and L. D. Smoot (1971). "A Turbulent Mixing Coefficient Correlation for Coaxial Jets with and Without Secondary Flows," AIAA Paper 3.

Vilenskiy, F. A. et al. (1972). "Study of off-design Regimes of an Axisymmetric Annular Nozzle with a Central Body," AN SSSR MZhG 4.

Yurchenok, K. Ye. (1974). "Base Pressure and Temperature Behind Axisymmetric Bodies with Interaction of the Stream with Supersonic Flow," AN SSSR MZhG 2.

	[illegible]
	mass flow rate
	width of wake
	injection parameter
	ejected gas flow parameter
$_g$	injection parameter
$_M$	mass flow rate
$_u$	injection parameter
$_\lambda$	non-dimensional flow rate
	ratio of base pressure with a mass addition to base pressure with no mass addition
	momentum coefficient
	body length
	Mach number or molecular weight
	mass flow rate
	mass flow rate of separate component of ejected gas
	mass flow rate
	suction mass flow rate

S	base area
S'	area ratio of perforation to base area
U_B	constant
u_i	velocity of injected gas
u_θ	velocity along the axis
ε	boat-tail angle
Γ	dimensionless bleed number
θ_i	initial momentum thickness
κ	constant
λ	initial boundary layer thickness

subscripts

B	base injection quantity
m	mixing region

CHAPTER VII

Control of Separated Flow

Among the available various control techniques, the separation controls by injection of fluid and energy and by combustion are presented in this chapter.

The drag of a body with a blunt trailing edge at supersonic speed can be considerably reduced by injecting mass and energy (heat) into the downstream of the trailing edge. Because the drag reduction can be achieved with a relatively low velocity and a small quantity of mass of the injected fluid, an effective flow control may be accomplished by injecting gas from a compressor. The fuel burning in the near wake is also effective to decrease the base drag. Due to the addition of mass and energy into the complex near wake region, the problem of the near wake with mass and energy injection becomes more complex depending on a number of parameters such as the Mach number, the Reynolds number, the shape of the body thickness of the boundary layer and the characteristics of the boundary layer etc.

The control of the base drag can be more effectively accomplished by the burning of hydrogen in the base region compared to that of an addition of hydrogen in combustion chamber of an engine. Davis (1968), confirmed this control technique by analysis, using a two-dimensional Chapman-Korst flow model with the addition of a reaction region along the free shear boundary and the recirculation of combustion products

[illegible] drag reductions [illegible]

The problems of gas injection into the base region are presented first followed by the problems of energy injection and addinal information on combustion.

1. Injection of Gas in the Base Region

For convenience, the problems of gas injection are presented separately for subsonic, transonic and supersonic speeds of external flow.

1.1 Subsonic External Flow

[illegible] and [illegible] ([illegible]), studied analytically the effect of the base [illegible] the near wake for a very low Reynolds number to the [illegible] and [illegible] of the base [illegible] [illegible] parameter that determines the importance and [illegible] of viscous [illegible] in the base region is the ratio $\delta = \delta_i/H$ where δ_i is the initial boundary layer thickness and H is the base

[illegible] small [illegible] Reynolds number) viscous [illegible] lying layer made up of [illegible] layer and [illegible] the recirculating [illegible] δ so that the greater [illegible] as δ increases until [illegible] enough δ [illegible] δ [illegible] proportional [illegible] where L is the body length, [illegible] the more slender the body, the more important are viscous effects in the base flow. For the slender body at a low Reynolds number and the large value of δ, the incompressible base is entirely viscous. In the base region, it may be assumed that viscous forces are dominant over the inertia forces. Conditions for the Stoke's approximation are applicable at least locally. By solving the incompressible Stoke's approximation equations at $x > 0$ with boundary conditions on the base plane ($x = 0$) with a far way uniform flow, the effect of the base bleeding on the near wake may be analyzed.

The governing equation is

$$\nabla^4 \psi = 0$$

and the boundary conditions are

$$\psi(0, y) = \psi_i(y), \quad \left(\frac{\partial \psi}{\partial x}\right)(0,y) = -v_i(y)$$

where ψ and [illegible] are normalized by $u_\infty H$ and the free stream velocity u_∞ and the subscript i refers to the base plane $x = 0$.

Because of the linearity of the problem, the solution of the near wake problem with a fluid injection in the base can be obtained by superposition of solutions without and with a injection.

First with no injection, Stokes two-dimensional stream line patterns are determined.

With the injection, since the base flow structure is modified for simplicity, the initial velocity profile with the injection is given by

$$u_{Bi}(y) = U_B (y^2 - 1)^2 \qquad v_{Bi} = 0 \qquad |y| \leq 1$$

where B denotes the base injection quantity, and U_B is a constant. This symmetric profile has the maximum injection at the base center and zero at the edges. The stream function obtained for this case is simply added to that of a two-dimensional Stokes flow. The resulting flow fields for two different values of U_B are shown in Fig.VII.1a and Fig. VII.2b.

For a small value of $U_B = 10^{-4}$, Fig.VII.1a, shows that the recirculating flow region is separated from the wall by the injected fluid and there are two dividing stream lines, $\Psi = 0$ which surround the recirculating flow and $\Psi = (8/15)\, U_B$ which separated injected fluid from the external flow. For a large value of $U_B = 10^{-2}$, Fig.VII.1b indicates that the recirculating zone shrinks and disappears.

The base bleed contributes an additional term to the pressure and the pressure change caused by the base bleed is shown in Fig.VII.1c. The pressure is increased near the x-axis but decreases at some distance away. The net effect is an increase in the mean base pressure. Hence, a decrease in the base drag. In order to be effective, U_B should be at least of order of 0.1.

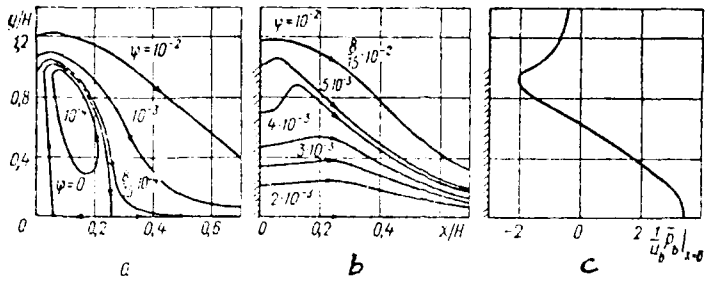

Fig. VII.1. Stream lines (a, b) and change in pressure (c) during injection of a fluid in the base region [Berger and Viviand, (1965)]

The drag coefficient C_D depends on the momentum coefficient defined by

$$k_j = \frac{G\, u_j}{0.5 \cdot \rho_\infty u_\infty^2 S}$$

where $G\, u_j$ is the mass flow rate, u_j is the isentropic expansion velocity from the total pressure to the static pressure in the free stream flow, and S is the base area. This relation is shown in Fig. VII.2 by Graven (1960) for a supersonic jet in a parameter of u_∞.

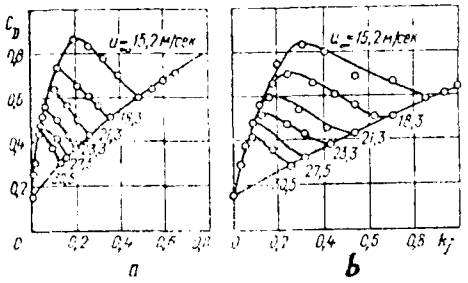

Fig. VII.2. Dependence of the coefficient of the base pressure on the coefficient of the quantity of motion of a stream when u_∞ =15.2 m/s [Graven (1960)]: a- sonic stream; b--M_j = 1 41

For various free stream velocities C_D increases montonically with an increase of the injection, and C_D is given by a single curve in a function of k_j. Although the injection affects not only in the wake but also upstream, its effect is damped rapidly and basically (about 90%) drag reduction

is achieved by the base pressure change.

For in the compressible flow, the base pressure depends also on the injection parameter

$$\frac{}{} = \frac{u_j}{u_\infty} S'$$

where u_j and u_∞ are velocities of the injected fluid and the free stream respectively and S' is area ratio of perforation to the base area as seen Fig.VII.3.

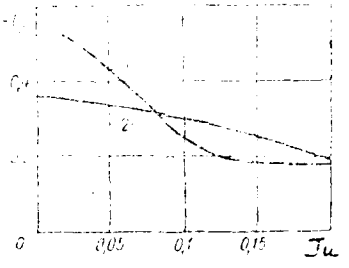

Fig.VII.3. Dependence of the base pressure on the parameter of the injection 1--injection and porous base [Bearman,(1969)]; 2--injection from a base cavity [Townend and Reid, (1963)].

1.2 Transonic External Flow

Sykes (1970), investigated the base pressure and the base drag of the cylindrical and boat-tailed after bodies with a gas ejection in the transonic flow (M_∞ = 0.8 - 1.1) Re = $4 \cdot 10^6$/ ft , at atmospheric stagnation pressure. The combined effects of the gas ejection and the boat-tail were presented at M_∞ = 0.95. The model consisted of a 1 in. diameter 4 caliber centerbody and interchangeable 2 caliber afterbodies. The afterbodies consisted of a cylinder and six conical boat-tails with angles of 3°, 6° and 9° and of lengths amounting $\frac{1}{2}$ and 1 caliber.

[illegible] boundary layer thickness δ was close to that predicted [illegible] turbulent boundary layer of a 1/7 power law and $\delta/d = \frac{1}{8}$ (d is body diameter) measured was a typical one for a conventional profile.

The pressure distribution on the boat-tailed bodies was measured at [illegible] this condition, the flow became supersonic over the [illegible] the start of the boat-tail and underwent a rapid compression [illegible] flow downstream of this shoulder followed by a slow [illegible] compression and the flow remained attached to the boat-tail surface throughout.

The pressures on the boat-tail and cylendrical after body were independent of ejected mass flow rate and at $M_\infty = 0.95$,

$$C_p = C_{pb}(\Sigma, \ell)_{J=0} + C_{pb}(J)$$

and

$$C_{pb}(J) = -2.4\,J + 60\,J^2$$

for

$$J = \dot{m}/\rho_\infty u_\infty S \leq 0.03$$

J is an ejected gas flow parameter, $\dot{m}$ is mass flow rate, S is a cross-sectional area of the body, Σ is a boat-tail angle, ℓ is a body length and the subscript b refers to the base. $(C_{pb})_{J=0}$ has been evaluated by Sykes (1970) and given in a function of Σ and a boat-tail caliber. The after body drag C_D is evaluated by the integration of the body pressure, and then combined with the base pressure, assuming that its value is constant over the base and the exit of the nozzle. The results of C_D for the boat-tail and the after body are

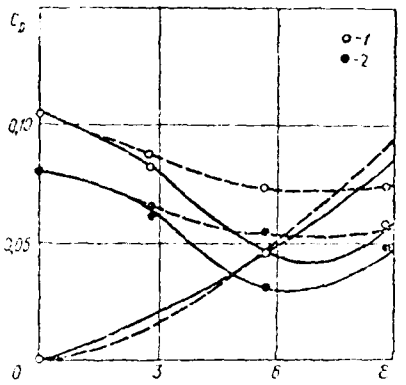

Fig.VII.4. Coefficient of the drag of various trailing-edge sections [Sykes,(1970)] (solid line--1 diameter, dashed line --1/2 diameter): 1--J=0; 2--J=0.02.

shown in Fig.VII.4, indicating that J = 0.02 as the optimum rate, for the drag reduction. Since the effect of the thrust from the ejected gas momentum has not been included, this could amount to about 0.02 change in C_D at J=0.03.

The results also show that the optimum boat-tail angle (of about 7^o) is relatively insensitive to the gas ejection rate or the boat-tail length. The same optimum condition and behavior are also reported by Bowman and Clayden (1968) at M_∞ = 2,0.

Experiment of Bowman and Clayden (1967), for cylindrical after bodies at M_∞ = 1.5 - 3.0 shows that the peak in the base pressure occurs at a comparatively low rate of gas ejection of $J = \dot{m}/\rho_\infty u_\infty S$ amounting to about 0.01. Test air was ejected at the room temperature through a nozzle. The base pressure is independent of the nozzle geometry for values of J less than 0.01. Thus, the choice of the nozzle is comparatively unimportant for the region of practical interest.

1.3 Supersonic External Flow

The base flow region, where fluid injection takes place, may be characterized by two stream line; dividing and critical stream lines as

shown in Fig.VII.5.

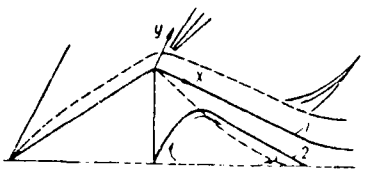

Fig.VII.5. Flow in the base region [Baum, King and Denison (1964)]: 1--Dividing stream line; 2--Critical stream line.

The critical stream line devides the flow downstream through the neck from the flow circulating in the base region.

If no injection takes place, then these two lines coincide, and with an injection, the flow rate of the injected fluid is equal to that between these two lines.

Fuller and Reid (1958), studied the problem of gas injection to the supersonic external flow and the pressure distribution in the two-dimensional wake as seen in Fig.VII.6, VII.7 and VII.8.

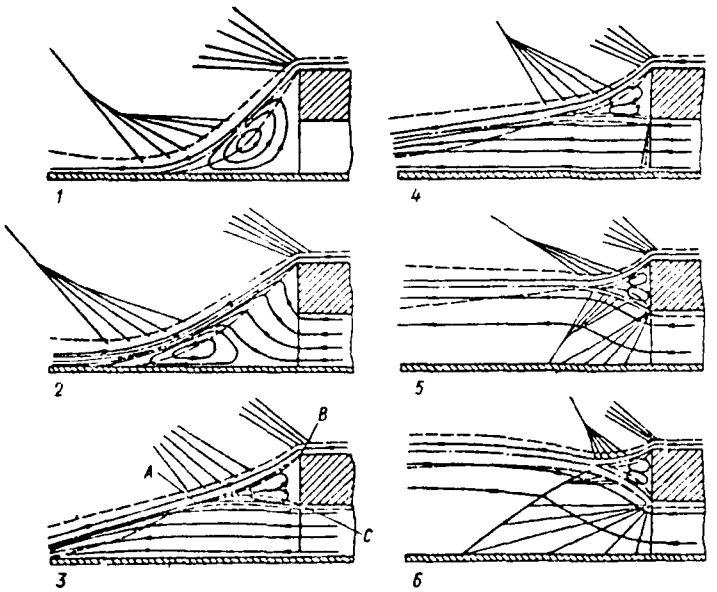

Fig.VII.6. The effect of streams on the flow in the base region [Fuller and Reid (1958)] (Dashed-dotted lines indicate the dividing stream line, dashed lines indicate the boundaries of viscous flow, the arrows indicate stream line).

[illegible], shows the wake flow depending on the ratio of the total pressure of the injected stream p_{t_j} to the static pressure in the free stream p_∞ behind a body with a sonic nozzle. The ratio of heights of the base section to the nozzle was 2 and the free stream Mach number was 2.3.

[illegible] show the p_b/p_∞ in a function of p_{t_j}/p_∞ and [illegible] presents the static pressure distribution along the axis. These three figures are interrelated to each other.

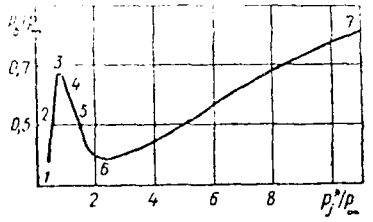

Fig.VII.7. The effect of a stream on the base pressure (M=2.3) [Fuller and Reid (1958)]

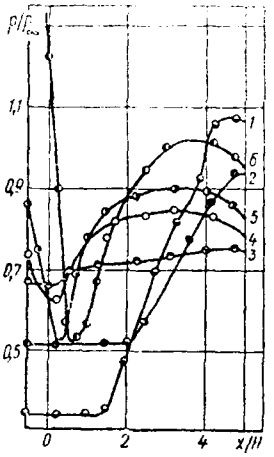

Fig.VII.8. Distribution of the static pressure along a plate (M=2.3)[Fuller and Reid (1958)]

Neverthless, it is possible to differentiate the various flow regimes in the base region, (between points 1 - 3, 3 - 6, and 6 - 7, in Fig.VII.7. Point 1, corresponds to no injection and with a gradual increase of the total pressure (point 2) a part of the gas sucked into the external flow from the base region is supplied from the internal stream. The dimension of the vortex and tendency of movement of the vortex toward

the external flow decreases. Inclination of the external flow also decreases, but the base pressure increases. Static pressure along the axis remains constant up to the point where with supersonic flow takes place. When the gas flow rate approaches to the maximum amount [illegible] to be sucked in the external flow, the pressure in the base [illegible] reaches the maximum (point 3).

[illegible] case, the pressure along the axis is approximately constant and its stream velocity is subsonic. Even at this stage, a pair of vortices develop between two flows close to base section, but their strength is low having practically no effect on the pressure distribution in the base. With a further increase of the pressure beyond point 3, the velocity increases and reaches to the speed of sound between points 4 and 5.

After this, on the nozzle section c (Fig.VII.6), expansion waves occur and the velocity downstream of the base becomes supersonic. Beyond point 3, the velocity along the dividing stream line CA increases with the increase of the pressure, increasing the strength of the pair of vortices, but the pressure drops between points C and A. Thus, the base pressure p_b decreases compared to the pressure at point A. Along the curve 3-6, p_b/p_∞ decreases but beyond point 6, p_b/p_∞ increases monotonically. For axisymmetric flow, this trend is similar to the two-dimensional flow.

1.4 Analysis of Fluid Injection

Shvets and Chvets in their book (Chapter II), treated the analysis of the fluid injection. Thus, here only briefly a presentation is made

by combining parameters of the injection and the effect of supplying the reacting gases.

Korst et al (1956), were the first who attempted to analyze the mass injection into the stagnant zone by introducing a semi-empirical coefficient. Chow (1959), analyzed the base pressure effected by the fluid injection into the stagnant zone involving interaction between the supersonic external flow with the jet engine stream. It is assumed that the flow is turbulent and an isoenergetic mixing takes place between the external flow and the fluid in the stagnant zone at a constant pressure achieving an agreement with experimental results.
Korst et al (1959) and Nash (1962), found that both the injection of gas into the base region and the initial boundary layer thickness increase the base pressure.
Golik (1962) and Tang and Barnes (1967), introduced a combined parameter of the base bleed and the initial boundary layer thickness as

$$\lambda = \frac{\theta_i}{H} + \frac{G}{(\rho u)_e H}$$

where θ_i is the initial momentum thickness, H height of the base and G the base bleeding rate per unit width of the base and the predicted base pressure in an agreement with the laminar and turbulent flow experiment as shown in Fig.VII.9.

Kurchenok (1971), investigated effect of reacting gas injection on the parameters in the base region, by presenting a burning gas diffusion model and computing base pressure by Korst's method.

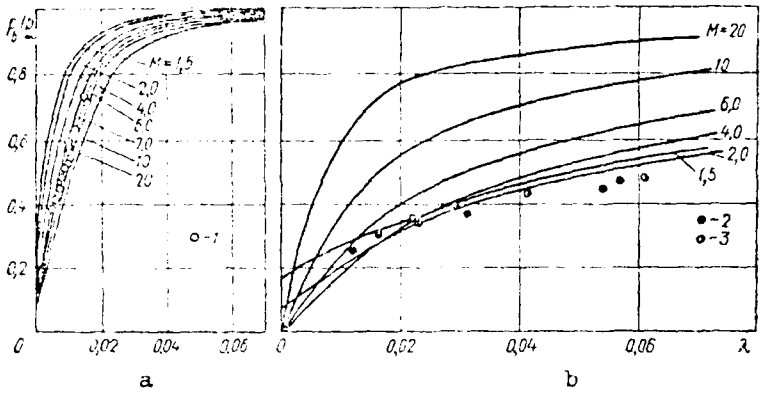

Fig. VII.9. Theoretical and experimental values of the base pressure in relation to the combined parameter for laminar (a) and turbulent (b) flows [Tong and Barnes (1967)] 1--the effect of thickness of the boundary layer M = 7 [White, (1965)]; 2--the effect of the thickness of boundary layer [Nash, (1962)]; 3--the effect of injection in the base region, M = 2 [Korst, Chow and Zumwalt, (1959)]

The turbulent eddy viscosity ϵ is given by Prandtl's hypothesis,

$$\rho \epsilon = f(x) = \kappa c k \rho_m u_m$$

where κ and c are constants to be determined empirically and subscript m refers to the mixing zone. If a reacting gas is injected into the base region, under the pertinent conditions, a chemical reaction occurs with the components of the external flow. It may be conjectured that the rate of chemical reaction is infinitely large in comparison with the rate of diffusion. Concentration of the oxidizing agents and flames burning, is reduced to zero and the diffusion flows of these components are determined by stoichiometric relationships. Conservation of the mass in the base region is given by

$G = \Psi_j$ where G is the flow rate of ejected gas per unit length, Ψ_j is the stream function determining the position of the dividing stream line. The mass flow rate of separate components of the injected gas is

$$m_j = G + \int_{\Psi_j}^{\Psi_m} c_j d\Psi , \qquad j = A, I,$$

where Ψ_m is the stream function corresponding to the boundary position between mixing zone and the base region; c_j is the concentration of j component, A is the fuel and I is an inert gas.

For other components,

$$m_i = \int_{\Psi_j}^{\Psi_m} c_i d\Psi , \qquad i = R, P.$$

where R is oxidizing agent, P is a product of reaction.

Summarizing the mass flow rates of all components, the mass flow rate of gas entering into the base region,

$$m = \sum_i m_i = G + \Psi_m - \Psi_j = \Psi_m$$

It is assumed that the rate of chemical reaction between components A and R somewhat exceeds the rate of transfer process. In this case, depending upon the ratio m_R/m_A a chemical interaction between the reacting components takes place either in the base region or in the mixing zone. If $m_R/m_A > L$ where $L = \nu_R M_R/\nu_A M_A$ where M is the molecular weight, then the injection component A burns out completely in the base region. Burning in the mixing zone does not take place and in the base region, only components R, N, P are present.

The results of the computation of the base pressure,

$p = p_b/p_{b(G=0)}$ downstream of the axi-symmetric body effected

[illegible] injection in the base region agree with the experimental of Clayden and Bowman (1968).

The base pressure varies also in the vertical direction or the radial direction. The base pressure distribution along the base radius is shown in a function of J in Fig.VII.10. In the range of an injection [illegible] circulation of flow, the pressure along the radius of the base is approximately uniform but for a large flow rate corresponding to a monotonic increase of base pressure, the pressure increase from y/d = 0.[illegible] to the edge.

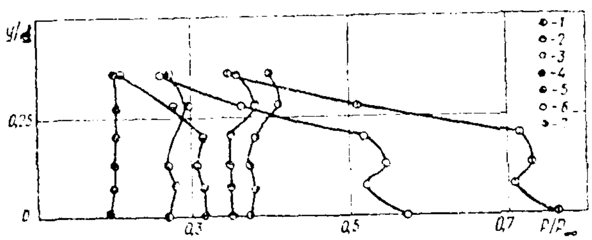

Fig.VII.10. Change in the pressure along the radius of the base section (model 1, M=3); [Shvets and Shvets (1976)]
1--J = 0; 2--J = 0.005; 3--J = 0.009; 4--J = 0.04; 5--J = [illegible]; 6--J = [illegible]; 7--J = 0.226.

The base pressure distributions in functions of J and Re_∞ in parameters of a free stream Mach number and an injection Mach number are shown in Fig.VII.11.

With the increase of a free stream Mach number, the maximum base pressure decreases at same J. Although the trend of dependence of the

base pressure on Re_∞ is different, Re_∞ at which the base pressure becomes practically independent of Re_∞ are close to each other. ($Re_\infty \simeq$ [illegible]$.5 \cdot 10^6$)

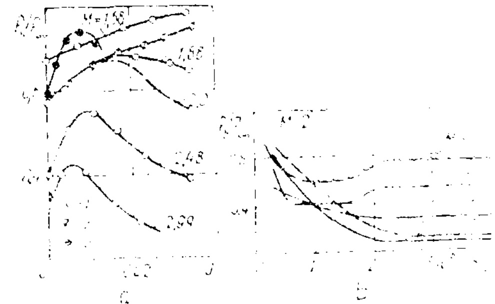

[illegible] Dependence of the base pressure on the parameter of the injection [illegible] and on the [illegible] of [illegible] [illegible] [illegible] [illegible] [illegible] (197[illegible])]
[illegible]--[illegible] [Bowman and Clayden (19[illegible])]; --porous [illegible] [Bowman and Clayden (196[illegible])]; [illegible]--helium [Craven et al (19[illegible])]; dashed line--nozzle of different deameters [Reid and Hastings (19[illegible])]

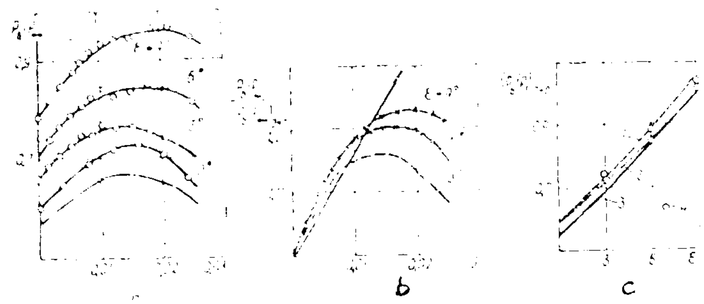

[illegible] base pressure (a), dimensionless ratio [illegible] [illegible] [illegible]-tail angle and base [illegible] [illegible] 1.98, [illegible] [illegible] 10^6 [Bowman [illegible]] [illegible] [illegible] [illegible] [illegible]; [illegible] [illegible] [illegible] [illegible]; [illegible] [illegible]; --- [illegible] [Bowman and Clayden ([illegible])]

AD-A099 165 CATHOLIC UNIV OF AMERICA WASHINGTON D C DEPT OF MECH--ETC F/G 20/4
RECENT DEVELOPMENT IN FLOW SEPARATION.(U)
MAY 80 P K CHANG AFOSR-78-3636

UNCLASSIFIED AFOSR-TR-81-0451 NL

6 of 6

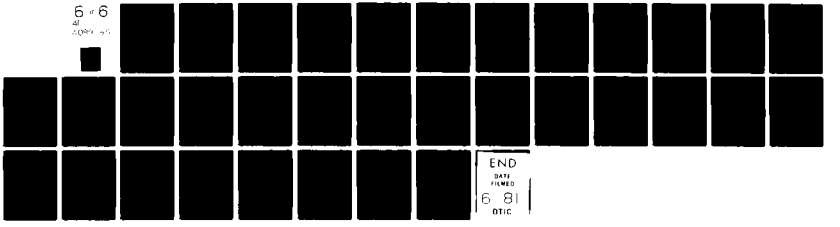

The base drag of axisymmetric bodies may be significantly reduced by the combined effect of gas ejection of a small amount with a low velocity into the base region immediately downstream of the base and of the boat-tailing. Bowman and Clayden (1968), measured the base pressure at $M_\infty = 2$, $Re = 5 \cdot 10^6/\text{ft}$, stagnation pressure about 1 atm. ejecting air through a nozzle at room temperature. The afterbodies of the model consisted of a cylinder and 6 boat-tails of length $\frac{1}{2}$ and 1 caliber with boat-tail angles of 3°, 6° and 9°. The nozzle geometry is comparatively unimportant for the value of an ejection parameter defined by $J = \dot{m}/\rho_\infty u_\infty S$ (where $\dot{m}$ is the rate of ejection, S is maximum cross-sectional area of the body) sufficiently small to insure that the velocity of ejected gas is too low to cause entrainment. The boundary layer thickness δ just upstream of the after end of the cylinder was in close agreement with a theoretical flat plate turbulent boundary layer and $\delta/d = 0.07$ (d is body diameter) was the same order as on a typical projectile. The measured base pressure for various boat-tail angles Σ , are shown in Fig.VII.12 a with data obtained by Reid and Hasting (1961), for $\delta/d = 0.05$ in a function of J and in agreement within about 5%. In Fig.VII.12a, the parameter J is based on the fuel diameter of the center body.

From Fig.VII.12b, it is seen that for the ejection parameter $J < 0.01$, the base pressure values tend to from a straight line from which the base pressure may be predicted to within 3% by

$$p_b/p_\infty = (p_b/p_\infty)_{J=0} \quad (1 + 16\, J)$$

The values of $(p_b/p_\infty)_{J=0}$ may be obtained from Fig.VII.12c in which p_b/p_1 is plotted in a function of the boat tail angle ε The symbol p_1 refers to the pressure on the conical surface of the boat-tail just upstream of the base evaluated by a characteristic solution. In this figure, an experimental curve of parabolic and conical boat-tails and two theoretical curves obtained by semi-empirical methods of carrelation are also shown. The slight differences among the results are attributable to a boundary layer thickness difference. Pressures measured along the conical surfaces of the boat-tails were found to be independent of the gas ejection rate over the whole range of the ejection. For both 6^o and 9^o boat-tails, the base pressure may be significantly higher than the pressure on the conical surface just upstream of the base, with the consequent development of a shock from the rim of the base. The optimum boat-tail angle is relatively insensitive to the gas ejection rate and the drag reduction produced by a given rate of gas ejection is insensitive to the boat-tail angle.

1.5 Flow Regimes and Injection Parameter

The injection effect of the pressure in the base section can be classified in three significantly different regimes, if an emphasis is made for the greatest effect on the change in the flow field with respect to the mass flow rate of injected components, intensity of motion or volumetric flow rate.

For the negligibly small injection flow rate, Chapman (1956) and Korst et at (1956), introduced a flow model.

The change in the base pressure, consequently the characteristics of near wake is considered to depend on the normalized mass flow rate. This idea is supported by the experimental evidence of injected air. Lewis and Behrens (1969), through the experiment of the base region behind a wedge of 6^{o} half-angle at M = 4, in the range of Re_H = 2.7 x 10^4 - $3.0 \cdot 10^5$ where H is the base height, found that the base injection stabilizes not only the near wake and delays the wake transition, but also alters it, thus, affecting the base pressure. The instability process becomes like that of a parallel wake flow without a pressure gradient. The flow field is significantly changed by a helium injection. The wake neck opens up and a steady laminar region presumably coincident with the injectant gas persists for several base heights. As the injection rate of the gas is increased, the laminar steady region about the wake axis which is associated with the injectant flow is widened, but the inner shear layers merge with the turbulent remnant of the boundary layer and their fluctuations intensities are increased. Thus, there appears to be an optimum amount of injection to achieve a minimum fluctuation level in the near wake. Helium is more stabilizing than nitrogen even when the mass flow rates are adjusted to cause initially the same effect on the pressure gradient and the wake thickness. A small amount of base injection has a profound effect on the near wake field, however, for x/H = 8.0 the wake turbulence is relatively unaffected.

The following three injection parameters may be noted.

Korst (1956) and Chapman (1956) proposed a parameter

$$J_g = \left(\frac{Gi}{G\infty} \right) G(M)$$

where

$$G(M) = \frac{p_t}{p_\infty} \frac{1}{M} \left(\frac{T_\infty}{T^*} \right)^{\frac{1}{2}}$$

Golik (1962) and Tang and Barnes (1967), used the combined parameter taking account of initial boundary layer thickness and fluid injection in λ ,

$$\lambda = \frac{\delta_i^*}{H} + \left[\frac{G}{(\rho u)_e H} \right]$$

Collins, Lees and Roshko (1970), carried out the experiment of a laminar near wake flow field of a two-dimensional adiabatic circular cylinder with a surface mass transfer at M = 6 and Re_d = 0.9 and 3.0 x 10^4. Results show that the mass addition from the forward stagnation region has no measurable effect on the near wake pressure field for a moderate mass transfer rate. But, for mass addition from the base, under the condition of a non-vanishing recirculating flow in the near wake, the following injection parameter I correlates the base pressure and the entire near wake pressure field,

$$I = \left(\frac{\dot{m}i}{2\dot{m}_{BL}} \right) \left(\frac{M\,air}{Mi} \right)^{\frac{1}{2}} = \frac{const \cdot \dot{m}i}{(Re_{\infty d})^{\frac{1}{2}}} \left(\frac{M\,air}{Mi} \right)^{\frac{1}{2}}$$

where $\dot{m}_{BL} = \int_0^\delta \rho\, u\, dy = \rho_e u_e (\delta - \delta^*)$ is a mass flux per unit span in the cylinder boundary layer upstream of separation, $\dot{m}_i$ is the mass flux per unit span of injectant, M_{air} and M_i are a molecular weight of air and injected fluid respectively. Thus, this parameter I is based upon the momentum flux of injected fluid and not based upon the mass flux proposed by Korst for example. The effect of the molecular weight

is crucial to distinguish the roles of the mass flux, momentum flux and volume flux.

This flow model is for the interaction between the injected fluid and the reverse flow. The mechanism determining the behavior of the base pressure with the mass addition is the establishment of a stagnation point off the base, formed by the balance of momentum between the injected fluid and reverse flow and consequent impression of the injected gas on the free shear layer near the separation. If the momentum flux of the injected gas is increased, the reverse flow is reduced as a consequence of a reduction of the flow velocity along the dividing stream line. Therefore, the base pressure increases with the increase of the mass addition.

When the total pressure of the injected fluid exceeds the maximum available total pressure in the reversed flow, the entrainment required by the shear layer is satisfied by the injected gas and the reversed flow disappears.

1.6 Fluid Injected Flow Field

The mixing layer angle may be correlated in a good agreement with Prandtl-Meyer flow angle, expanding from the static pressure on the body surface close to the trailing edge to the base pressure as shown by Bowman and Clayden (1967), in Fig.VII.13. The measured angles are less than would be expected from Love's (1957), empirical method assuming that the effective two-dimensional expanion angle is 0.85 of the shear layer angle.

Downstream of a body, the position, with and inclination angle of shock are shown in a function of J in Fig.VII.14.

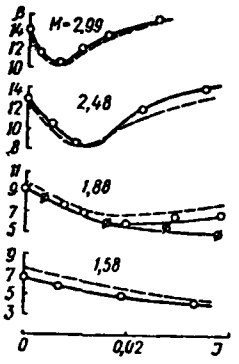

Fig.VII.13. Angle of inclination of the mixing layer [Bowman and Clayden (1967)] (dashed line--Prandtl-Meyer flow, crossed circles--Porous bottom).

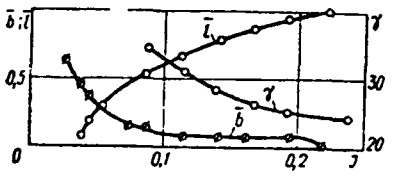

Fig.VII.14. Dependencies of the relative distance from the base to discontinuity $\bar{l}_*$ the width of the central section $\bar{b}$ and angle of inclination of leading discontinuities with undulating configuration of waves γ on the parameter of injection (M=3) [Shvets and Shvets (1976)] $\bar{l}$ and $\bar{b}$ are normalized with respect to diameter of base.

At a certain value of J (for example J = 0.22) the wave-like shock configuration transfers to a regular wave interaction and at this moment all flows in the wake become supersonic.

Bauer (1967), investigated experimentally the variation of the base pressure with a Re, cone angle and the movement of the rear most stagnation with a base injection rate at $M_\infty = 3$ and Re = 113000 - 170000, using three cone models of 8°, 12° and 16° cone half angles. At first, the pressure map of the flow field behind the cone, with no injection, was drawn locating the recirculation zone and the wake neck. Measurements by a hot-wire and pitot show that the boundary layer on 12° cone was laminar at R_{ed} = 113.000, transitional at 130.000 and fully turbulent near 170.000. In the laminar range of Re_d, p_b/p_∞ decreased like $Re_d^{-0.6}$ while in the turbulent range, p_b/p_∞ remained

almost constant with Re_d.

The effect of nitrogen from the base of a 12° cone was to widen the wake picture of no injection, for example, the edge of the shear layer located 1.5 diameters downstream distance moved upward. The rear stagnation point of the recirculation zone was located at the point at which the pressures were equal. In the recirculation zone, the pitot pressure is smaller than the static pressure in as much as the flow past the pitot head was reversed from its usual direction and this reverse flow phenomena persisted as the injection flow rate $J = \dot{m}/\rho_\infty u_\infty S$ where S is base area was increased from 0 to 0.03. When J was increased to 0.036, the reverse flow region has just disappeared and the flow fluctuated.

Berger and Viviand (1965), predicted such disappearance of the recirculation zone and Zakkay and Fox (1966), found that their recirculation zone was blown away at J = 0.02. Fig.VII.15, shows the position of rear stagnation affected by an injection with Herzog's (1964) data obtained using a circular cylinder placed its axis perpendicular to the free stream of M = 6 with a laminar boundary layer. His recirculation zone was blown away at J = 0.015. The position of stagnation is much more sensitive at a small injection rate than at a large injection rate. It may also be noted from Fig.VII.15 that the recirculation zone does not move bodily downstream with an increasing injection rate, but apparently shrinks until some critically small size is attained, below which it can not be maintained in its closed stream line form.

The constant Mach lines in the base region of a blunt cone moving at M = 3.035, $R_{ed} = 1.13 \cdot 10^5$, with a nitrogen injection, are shown by

Bauer (1968), in Fig.VII.16.

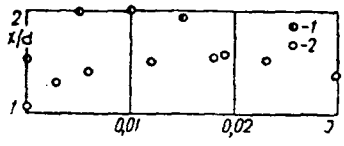

Fig.VII.15. Dependence of distance from the base of the model to the rear stagnation point on the parameter of injection (Bauer (1967)) :

1--Two-dimensional flow, M = 6 (Herzog, (1964)) ; 2--Axisymmetric flow, M = 3 (Bauer, (1967)) .

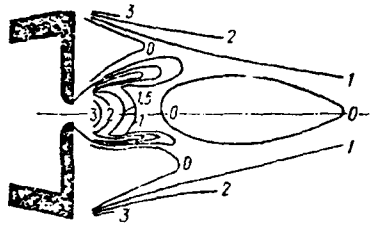

Fig.VII.16. Lines of constant M numbers with injection of nitrogen (M = 3.03, Re = $1.1 \cdot 10^5$, J_M = 0.012 (Bauer,(1968)) .

The boundary layer on the model was laminar and its displacement thickness amounted to 17% of the base diameter.

The nitrogen was discharged at a flow rate of $J_M = \frac{M_i}{M_\infty} \frac{G}{\rho_\infty u_\infty S} = 0.012$

where M_∞ is the molecular weight of the free stream and M_i is molecular weight of the nitrogen. The experiment was repeated with a helium injection of $J_M = 0.05$ and the stagnation zone configuration was similar to that in Fig.VII.16. The mass injection rate was always more than sufficient for the nozzle throat to be sonic. Therefore, the injected flows were underexpanded at the nozzle exits and the stream became supersonic.

It is to be noted that in spite of the fact that the injected gas reached Mach number 3, at a distance of 0.1 d, the gas flow slows down to the zero velocity at a distance of 0.6 d. Such an injection does not blow away the usual recirculation bubble. Instead, the stream di-

vides and goes around the recirculation bubble which is identified by the line of a zero Mach number.

The interaction phenomena of an injected gas with the reversed flow may lead to the understanding of the pressure in a near wake. Namely, the change of the pressure in the near wake is caused by the balance between momentum flux of the injected gas and the reversed flow with a high degree of dissipation at the base point of deceleration.

1.7 Injection of Different Gases

Since no theoretical model exists to formulate the similarity of behaviors of various different injected gas, parameters such as the Mach number, flow rate, momentum and velocity proportional to volumetric flow rate and total enthalpy of flow etc. are to be investigated.

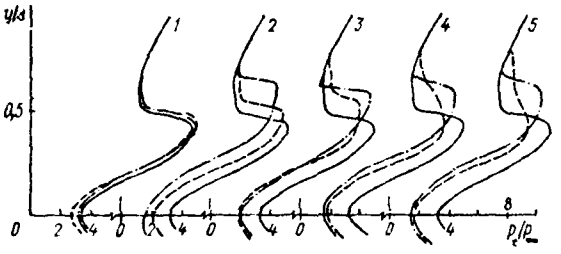

Fig.VII.17. Ratio of pressure, measured by a pitot tube, to static pressure of free-stream flow (M = 3, J_M = 0.018) [Bauer (1968)] (Solid line--without injection, dashed-dotted line--injection of nitrogen, dashed--injection of helium; the figures designate the model numbers).

Bauer (1968), measured the ratio of pitot pressure to the free stream static pressure at 3 diameters behind the model base and showed the change in the pitot profile effected by a helium and nitrogen injection in Fig.VII.17.

The location and size of injection ports are :

model	number of holes	ratio of total hole area to base area	hole locations
1	63	0.053	spaced to cover inner 70% of the base radius
2	1	0.0088	at base center
3	1	0.052	at base center
4	8	0.0098	on a circle of radius equal to 62% of the base radius
5	8	0.054	on a circle of radius equal to 62% of the base radius
6	8	0.0156	hole was in the inner radius of a tube that extended a distance of 156% of the base radius outward normal to the base

Fig.VII.17, shows the coordinate y, the distance from the model symmetry axis, normalized by base diameter d. Near y/d = 0, the pitot pressure "bucket" exists which corresponds to a viscous wake. At y/d= 0.5 with zero injection the wake recompression shock appears as a sharp negative gradient in the pitot pressure. The pitot pressure increase again beyond the shock where the Mach number is decreasing with increasing y/d.

For model 6, helium on the nitrogen injection of J_M = 1.8 %, has little

effect on the pitot profile, while for model 2 and 3, with a central injection, a viscous bucket deepens and pushes the wake recompression shock farther from the axis in opposition to the intuitive idea that the injection along the axis should fill the wake bucket.

When the injection ports are moved outward toward the base periphery for the cases of model 4 and 5, the viscous wake bucket and recompression shock are affected to a larger degree by the injection of J_M=18%. The helium is almost as effective as the nitrogen in deepening the wake bucket despite of the fact that the helium mass flow rate was seven times smaller than that of the nitrogen, since the number of molecules injected was same in both cases. The helium injection causes the large pressure gradient representing the wake recompression shock to disappear for models 4 and 5, whereas a nitrogen injection does not do this. A cause of this phenomena may be the much larger sonic speed in helium which may result in a subsonic type of recompression at the wake neck. The model 1 was tested with a nitrogen injection only and its injection effects were intermediate between those obtained with models 3 and 5.

1.9 Boundaries of a Wake

Lewis and Chapkis (1969), measured the wake growth and the wake boundary behind an adiabatic two-dimensional wedge at Mach 4 with tripped turbulent boundary layers and base mass addition.

It is noted that the injectant velocities are considerably larger fractions of the free stream velocity than would be the case for the

flight conditions even though the mass addition rates are comparable.

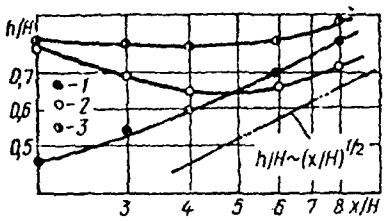

Fig.VII.18. Growth of the lateral dimensions of a wake [Lewis and Chapkis (1969)]
1-- J=0; 2--Helium u_i/u =0.47; 3--Nitrogen u_i/u = 0.5.

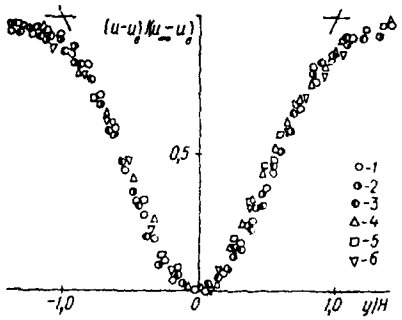

Fig.VII.19. Similarity of velocity profiles in a wake without an injection and with injection of nitrogen [Lewis and Chapkis (1967)]:
1--x/H=8, J=0; 2--x/H=6, J=0; 3--x/H=4, J=0; 4--x/H=8, J=0.03; 5--x/H=6, J=0.03; 6--x/H=4, J=0.03.

The wake width was altered (thinner for helium injection) but the differences are small amounting 15%. The no-injection wake growth is close to that predicted for a self-similar incompressible wake. Apparently effects of compressibility and nonsimilanty are negligible. The range of investigation up to $x/H \lesssim 8$ does not allow one to express an opionion for the relative asymptotic growth of the injected wake, but it seems to indicate that their growth rate is close to that of a noninjected wake. A similarity of a mean velocity profile in a wake with and without a nitrogen injection in Fig.VII.19 may be he approximated by the Gaussian profile given by

$$\frac{u - u_\theta}{u_\infty - u_\theta} = 1 - e^{-s(\frac{2y}{h})^2} \qquad \text{and} \qquad s = 2.06$$

where u_θ is the velocity along the axis, s is the base area and h is the width of the wake.

The mean velocity profiles for both wakes are seen to exhibit a remarkable similarity and as close as $x/H = 4$, no significant distortion of the velocity profile is perceptible.

Lewis and Chapkis (1969), found that the base pressure increased with increasing ı mass addition when the injection was subsonic, whereas the supersonic injection (which occurred for a nitrogen injection when $\dot{m}/\rho_\infty u_\infty S > 2.5\%$) resulted in a decrease in base pressure.

The static pressure gradients in the wake were greatly reduced by small amounts of a base mass addition. The recirculation zone was slightly displaced with the base injection and to decrease in size with the increasing mass addition until it vanished.

1.9 Field of Concentration

The dominant feature of the near-wake mass-concentration field is the axial decay of the mass concentration from the base toward the rear stagnation point due to the counter-flow diffusion of the injected species into the reverse flow. Another important aspect of the mass-concentration field is the existance of an outer transport layer shown in Fig.VII.20 which is an isometric plot of the argon mass-concentration field. This outer layer occurs in the vicinity of the shear layers and governs the transport of mass between the recirculating vortex and the outer flow by diffusion across the shear layers, thus, establishing the outer boundary condition on the inner recirculating flow.

For $Re_{\infty d} = 3 \times 10^4$, the transverse mass-concentration profiles in Fig.VII.20 are characterized by an off-axis maximum in the vicinity of the u = 0 locus as a result of the convection of the high mass-concentration layer near the base into the shear layer by the recirculating flow. For $Re_{\infty d} = 0.9 \times 10^4$, the mass-concentration field is diffusion dominated within the recirculating zone. At this lower Reynolds number, there is no local maximum and the outer transport layer is no longer distinct.

Scott and Eckert (1966), postulated the existance of two thin layers to describe the transport of heat between the body and the outer flow. The first layer in their model, a boundary layer at the base governs the transport of heat or mass at the body surface. This layer corresponds to the base boundary layer for low Reynolds number of the Collins et al (1970) experiment. The second layer of Scott and Eckert's (1966) model corresponds closely with transport layer observed by Collins et al and governs the transport of heat or mass between the recirculating vortex and the outer flow.

The presence of the rear stagnation point imposes as the solution to the species equation for the linear superposition of a positive and a negative exponential function. This negative exponential corresponds to the decay from a source at the base stagnation point into a uniform flow of finite extent with lateral diffusion, whereas the positive exponential represents the decay toward the base of the mass concentration supplied by a source at the rear stagnation, whose strength is determined by the outer flow.

The presence of the rear stagnation point and the finite width of the mass-concentration profiles at the neck, require that there be an intermediate-wake region. In this region, the mass-concentration and velocity fields experience a transition from those imposed at the rear stagnation point by the near-wake flow to their respective asymptolic far-wake distribution.

In the intermediate-wake region, the mass-concentration field has been examined by an approximate theoretical model, assuming the mass-concentration distribution is Gaussian in the incompressible plane.

For the argon addition, the axial diffusion terms are negligible and the species conservation equation on the axis gives a representation for the axial decay.

1.10 Injection into a Boundary Layer

By injecting fluid over the surface of a body, the velocity profile is changed, especially within the boundary layer, increasing the velocity if the injection fluid velocity is tangential to the body surface. For the analysis of self-similar injection, Baum, King and Denison (1964), used profiles of Emmons and Leigh (1953) and for enthalpy profile the Crocco integral. With the increase of an injection on the body surface the velocity ratio u_j/u_e along the dividing line increases slowly causing longer wake.

Cassanto and Mendelson (1968), after a brief survey of turbulent ground test base pressure data and full-scale flight data, have hypothesized that the following two mechanisms may account for the increase of the

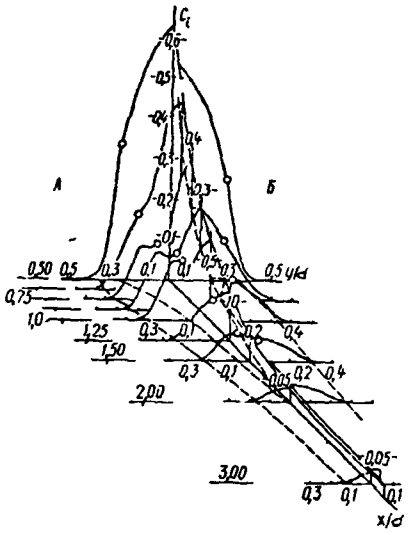

Fig.VII.20. Field of concentration of argon in a near wake with injection through the base section (dashed lines --boundary of the wake) [Collins, Lees and Roshko(1970)]
A--$Re_{\infty,d}=2.95 \cdot 10^4$, $J=4.28 \cdot 10^{-2}$;
B--$Re_{\infty,d}=0.90 \cdot 10^4$, $J=4.15 \cdot 10^{-2}$.

base pressure level and the gradient with an increasing mass addition rate.

First, the mass addition tends to thicken the boundary layer, especially the laminar sublayer, and the large laminar sublayer may become a pseudo-laminar in the base region. The thicker boundary layer which includes the mass flow due to ablation, flows into the wake region and enlarges the wake neck and changes the wake expansion angle. Such larger expansion angle is similar to what would be expected in laminar flow causing higher base pressure.

Secondly, the thicker boundary layer may cause a greater adjustment of the inveiscid flow field to the boundary layer flow. The effect of increasing the boundary layer by a mass addition is to increase the shock angle. Consequently, to decrease the local edge Mach number and to increase the edge pressure.

Bulmer (1972), presented the flight test data on the base pressure for two re-entry vehicles with a very low ablation mass flow rate J =

0.001 - 0.002 in the turbulent flow at $14 < M < 16.5$, angle of attack, less than 0.3 and compared with the low ablation rates.

The flight vehicles were a relatively sharp cone of a half angle 9° and bluntness 0.05.

The heat-shield ablation rates were determined by a coupled solution between the detailed ablating boundary layer and the transient heat conduction calculations.

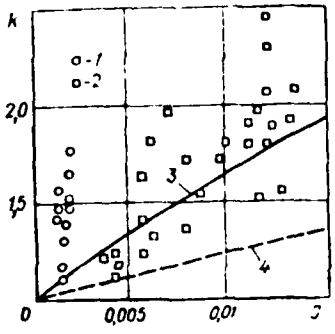

Fig.VII.21. The effect of intake of mass on base pressure with turbulent flow [Bulmer (1972)]; 1--r/R_b = 0.1 [Bulmer(1972)]; 2--r/R_b = 0.5, flight tests [Cassanto and Hoyt (1970)]; 3--r/R_b = 0 [Cassanto and Storer (1968)] (correlation); 4--r/R_b = 0.3 [Cassanto and Storer (1968)] (correlation).

Fig.VII.21 shows a comparison of Bulmer's (1972) data with others and correlations in terms of the k, the ratio of the base pressure with a mass addition to the base pressure with no mass addition. It is apparent from this figure that even a very low J-values may have a substantial effect on turbulent base pressure. Cassanto (1972), provided further evidance that the base pressure may be increased significantly by a small ablation mass addition amounting $J < 0.0005$. This flight data measured with bluntness $r/R_b = 0.3$, corresponds approximately to $1.2 < k = 1.4$ for $Re_L = 1.0 - 2.4 \times 10^8$ where k is the ratio of the base pressure with

a mass addition to the base pressure with no mass addition and reveals a much higher pressure than predicted by correlation in VII.21 ($k \approx 1.1$). This data representing the lowest ablation rates reported are additional evidence that even a very low mass addition may produce substantial increase in the turbulent base pressure.

c. Injection of Energy

Page and Korst (1955), indicated theoretically and experimentally that for a two-dimensional system, a further but relatively smaller decrease in the base drag may be achieved by heating the ejected gas. In practice, Clayden and Bowman's (1968) experiment for the base drag reduction by a hot gas ejection behind the cylindrical after bodies at M = 2.0 is applicable to external ballistics. Clayden and Bowman (1968), used a model of an axisymmetric open jet nozzle concentric with a cylindrical body ejecting heated argon from the cylindrical base. Although the tunnel was operated continuously, the argon concentration in the main stream did not rise more than about 1%, because the tunnel circuit was continuously evacuated and simultaenously replenished with dry air. The argon was ejected through either of two nozzles, nozzle 1 of exit diameter 3/4 in. and nozzle 2 of exit diameter 0.2 in.. These are considered to be typical of the nozzles used in the rocket-assisted shells. Nozzle 1 was used for all tests up to values of an ejected gas flow rate for which a peak in the base pressure occurred (for hot gas $J \sim 0.003$). The ratio of turbulent boundary layer thickness, just upstream of the base to body diameter, was ~ 0.007 and is of the same order as on a

typical projectile. The measured base pressure in functions of J and an enthalpy increase of ejected gas Δ i/Gi (joule/g) are shown in Fig.VII.22.

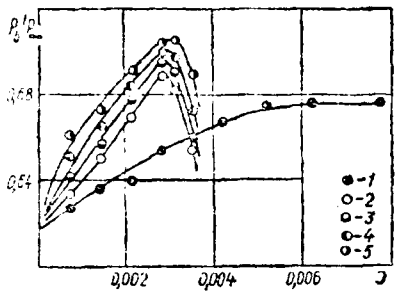

Fig.VII.22. Dependence of the relative base pressure on the flow rate of the ejected gas [Clayden and Bowman (1968)] : 1--$\Delta i/G_i = 0$, $T_i = 290$; 2--$\Delta i/G_i = 1000$, $T_i = 2200$; 3--$\Delta i/G_i = 1500$, $T_i = 3160$; 4--$\Delta i/G_i = 2000$, $T_i = 4100$; 5--$\Delta i/G_i = 2500$, $T_i = 5070$.

For the temperature evaluation it was assumed that the gas was in equilibrium. In a practical case it is possible that the ejected gas may consist of combustion products which would be significantly ionized.

In this figure, it is shown qualitatively that at low flow rates, the increase in base pressure is approximately proportional to the increase in ejected gas enthalpy, but at higher flow rates this trend does not persist for high enthalpies. It is noted that for a given ejected gas flow rate, by heating the gas from the air stream stagnation temperature to a typical rocket propellant the gas temperature ($\sim 2500^{\circ}$k), approximately doubles the increase in the base pressure due to an ejection and the peak in the base pressure occurs at roughly half the mass flow rate corresponding to the cold gas peak. For the region of practical application, i. e. for values of J, below to the peak in the curve of p_b/p_∞ vs J, and for ejected gas temperature $T_i < 3000^{\circ}$K, data of Fig.VII.22 are correlated by

$$p_b/p_\infty = (p_b/p_\infty)_{J=0} + [k_1 + k_2 (T_i - T^*)] \cdot J$$

where $k_1 = 12.25$, $k_2 = 0.005$ and T_i is the temperature of ejected gas and T^* is the temperature of decleration of the gas of external flow.

An unexpected finding was obtained by using nozzle 2, because for a given flow rate and ejected gas temperature, measured value of p_b with nozzle 2 (smaller exit diameter) was almost twice as large as nozzle 1 (larger exit diameter) contrary to the previous conclusions of Reid and Hastings (1961) and Bowman and Clayden (1967) that the method of ejecting gas appears to be important even at very low mass flow rate. It is not clear why the smaller nozzle should be more effective, but it may be possible that the high-speed jet from the nozzle impedes the formation of stable vortex ring in the separated flow region and hence reduces entrainment by the shear layer.

Beyond the peak of p_b/p_∞ vs. J for the heated gas, the base pressure drops rapidly with an increasing flow rate and the reduction in the base pressure is so rapid that the increase in the base drag more than offsets the increased thrust due to ejection. Therefore, if a small rocket motor were operated in this region, an increase in flow and thrust could result in an over-all loss of performance.

If the increase in the base pressure is converted to an equivalent thrust, the efficiency of the gas ejection process may be expressed in terms of specific impulse and in the following table specific impulses of nozzle 1 and 2 are compared.

Table ; specific impulse due to increased base pressure and thrust

nozzle	J	ejected enthalpy increase(joule/g) i/G	Effective S.I. due to increase in base pressure sec	Estimated S.I. due to thrust
1	0.002	0	113	—
	0.002	1000	226	—
	0.002	1500	260	—
2	0.002	0	207	40
	0.001	1350	377	140

Jakubowski and Lewis (1973), measured the heat transfer and the pressure distribution in laminar supersonic flows downstream of a rearward facing step without and with a mass suction from the separated region. Flow and test conditions were $M \approx 4$, $40 < Re_{\infty h} < 2200$, $0.1 < h/\delta < 2.4$, $0.055 < Tw/To < 0.11$ and $0.1 < w < 0.8$ where h is the step height, subscript w and o, refer to wall and stagnation, symbol $w = \dot{m}_s/\rho_\infty u_\infty bh$ the nondimensional mass suction rate, $\dot{m}_s$ is suction mass flow rate and b is model width.

The following results were obtained ;

For both suction and no-suction cases, an increase in the step height caused a sharp drop in the initial heating rates at the step base which then generally recovered to less or near the attached flow rates. The height of the step controlled the heating rates at the step base, clearly dominating the effects of stagnation temperature and pressure.

The ratio of the maximum heat transfer in the recompression zone to the attached flow rate at the step ($\dot{q}_{max} / \dot{q}_{step}$) was less than unity and decreased slowly with h/δ or $Re_{\infty h}$.

The mass suction from the separated area increased the local heating rates. The relative increase being most significant immediately behind the step. However the effect of the mass suction on the heat transfer at all-laminar flows was relatively weak and a mass suction rate exceeding the mass flow rate of the entire boundary layer upstream of step was needed to reach the post-step heating rates above the flat-plate value. Pressure distribution downstream of the step depends on the entrainment at separation. Without suction, the base pressure correlated reasonably well with parameters $Re_{\infty h}$ and h/δ and the length of the pressure plateau behind the step was very small. With the suction, pressure distribution downstream of step resembled those of no-suction solid step.

3. Combustion

Because the combustion process in a wake is complex, the solutions of the combustion problems are rather approximate. Libbi (1962) and Abramovich (1963), considering the chemical reactions in the mixing zone of two free streams, consider that the reactions occur in the very narrow diffused zone or within a flame front. Based upon the concept of a flame front of the flow in a base region, the parameters of a near wake flow may be formulated.

Libbi (1962), proposes for the analysis of the turbulent mixing of reacting gases, applicable to a supersonic hydrogen combustion that

the flow is assumed to be either frozen or in chemical equilibrium. The analytical results based upon chemical equilibrium agree very well with experimental data obtained for hydrogen flames with a low flow velocity.

Bowyer and Carter (1965), investigated experimentally the base pressure affected by hydrogen burning in the separated zone downstream of a protuberance as shown in Fig. VII.23 in a function of non-dimensional flow rate J_λ of hydrogen injected and burned, where

$$J_\lambda = \frac{\dot{w}_{H2} R_M (T_{oa})^{\frac{1}{2}}}{g A_b R_A P_{oa}} \left(\frac{\gamma - 1}{\gamma} R_A \right)^{\frac{1}{2}}$$

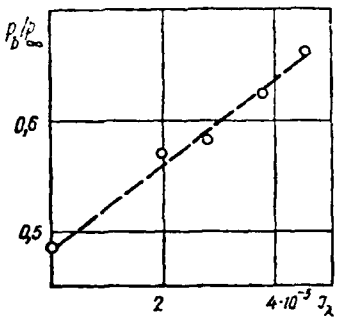

Fig.VII.23. Dependence of relative base pressure on dimensionless flow rate of the mass injected in the base region (M = 1.54) [Bowyer and Carter, (1969)] (Dashed line -- is linear approximation of experimental data).

$\dot{w}$ is weight rate of hydrogen bleed, p_{oa} is supply stagnatric pressure, T_{oa} is supply stagnatric temperature, g and R are gravitational and gas constant, respectively and A is area.

Davis (1968), presented the analysis and experiment of turbulent near the wake flow downstream of blunt based bodies with a chemical reaction occurring along the free shear layer. Analytically, the bulk properties of wake, temperature, density and species concentration profiles through the reaction region were determined by an iterative process, employing conservation equations of mass, species and energy.

An experiment was carried out for a free stream Reynolds number per foot

1.3×10^7 affected by turbulent shear at the Mach number of 1.98. Gaseous hydrogen was bled into the near wake and was ignited by a spark. Davis (1968), attempted to employ a modified Chapman-Korst flow model as seen in Fig.VII.24, including a nonisentropic recompression coefficient and a flame-sheet reaction concept assuming unity of Prandtl and Lewis number so that Crocco integrals are applied yielding element mass fractions and total enthalpy functions which are linearly dependent on velocity.

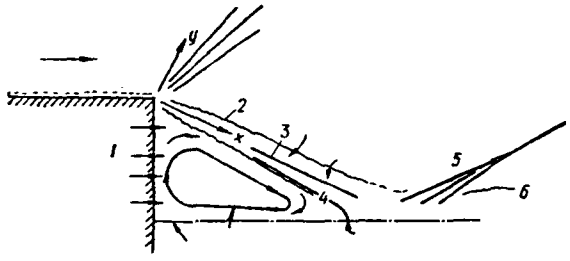

Fig.VII.24. Simplified model of flow [Davis (1968)]

1--Injection of hydrogen; 2--Mixing zone -- combustion in a free shear layer; 3--Separation stream line; 4--Zero stream line; 5--Field in front of the discontinuity; 6--Field behind the discontinuity.

Furthermore, the following assumptions are made for analysis ;

Constant pressure mixing along the free shear layer, fuel and oxidizer diffuse towards the reaction region from opposite sides in stoichiometric amounts and are completely consumed at a thin flame sheet, recompression between 5 and 6 is such that $p_{05d}/p_5 = N\ (p_6/p_5)$ where subscripts 0 and d are stagnation and dividing stream line, N is an empirically determined recompression coefficient (David(1968), found that N = 0.78 - 0.80 in his experiment) and p_6/p_5 is oblique shock pressure ratio and properties within the recirculation regions are homogeneous.

The measured and computed properties are given in a function of the

dimensionless bleed number Γ defined by

$$\Gamma = (G_B/p_{oa}.H) \left\{ T_{oa} R_a \left[(\gamma_a - 1)/2\gamma_a \right] \right\}^{\frac{1}{2}}$$

where G_B is the bleed mass flow rate per unit length, H the base height, R the base constant, γ the ratio of spectific heats of gas mixture and subscripts o and a are stagnation and free stream conditions respectively.

The agreement, between the data of experiment and analysis for density ratio through the mixing-reaction region and concentrations of hydrogen and nitrogen, is obtained. However, the observed concentrations of water vapor were considerably less than that predicted by the theory and definite amounts of oxygen were observed within the wake. As shown in Fig.VII.25a, at a bleed number above about 5.0×10^{-5} the effect of the combustion remains nearly constant indicating that a maximum energy release has been reached. Thus, any additional increase in the base pressure was due to mainly to a mass addition.

The question whether it is more effective to reduce the drag by external burning in the base region or to overcome the drag by supplying more power to the main propulsion system is answered by an effective specific impulse of base burning based on the bleed rate of hydrogen shown in Fig.VII.25b, where S. I. is the effective specific impulse-reduction in base drag/fuel flow rate - for base burning of the order of 10,000 sec.

Fig.VII.25c, indicates the mean wake temperature. The higher temperatures measured at lower bleed rates are due to the theoretical shift in the location of the flame as the hydrogen concentration in the wake

decreased. At lower bleed rates, the theoretical location of the flame was inside the dividing stream line, causing oxygen to recirculate into the near wake and combustion to take place inside the mixing region, failing the concept of flame sheet.

Fig.VII.25d, shows the locations of the flame and the dividing stream line as affected by the base bleed rate.

The turbulent diffusion gas torches for burning gas or any fuels are to be considered for analysis. The distribution of a flame front in a wake flow with low velocity can be obtained by solving equations of

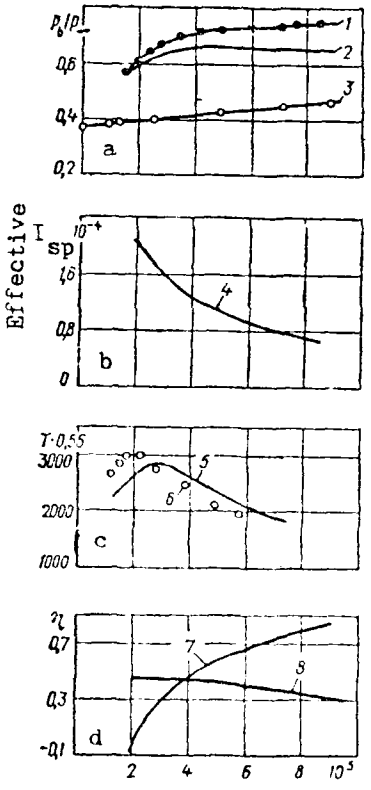

Fig.VII.25. Influence of wake burning as base pressure (a) the effective specific pulse for base burning (b) Bulk wake temperature with base burning x/L = 0.4 (c) Flame sheet and dividing stream line locations as affected by hydrogen bleed rate (d) on the flow rate of hydrogen when burning in a wake (H = 12.7 mm, M = 1.98) [Davis (1968)]:

1--3, 6--Experiment; 4,5,7,8--Calculation; 1--Injection in burning; 2--Burning; 3--Injection; 7--Front of flame; 8--Separation stream line.

$$J_\eta = \left(\frac{Gi}{p_{t_\infty} H}\right)\left\{T_{t_\infty} R \frac{\gamma-1}{2\gamma}\right\}^{\frac{1}{2}}$$

Gi - injected gas flow rate
H - height of base section
R - gas constant

kinetics of chemical reactions, equations of motion and energy. At present, the problem of the stabilization of the flames with bluff bodies in the gas flow of the combustion mixture is being investigated. But, in spite of numerous studies, up to now, there is no single all-inclusive theory which explains the mechanism of stabilization of the flame by a blunt body.

Zakkay and Fox (1966), analyzed the effect of chemical reactions due to an injection on the base pressure downstream of a flat surface. The results of numerical calculations are presented for a gas (oxygen type) with varying amount of injection, base height and base section temperature.

4. Base Flow Fluctuation Affected by Injection of Gas

The flow fluctuation in the base region is affected by the fluid injection. Lewis and Behrens (1969), measured a fluctuation behind a wedge of 6° helf-angle, injecting nitrogen into the base region at the flow rate $G/\rho_e u_\infty S = 0.034$ and helium at 0.005 for $Re_H = 8.7 \cdot 10^4$ where H is the base height. These mass flow rates correspond to an equal volume flow rate which effects the mean flow. For both cases of injections of nitrogen and helium, the transition to turbulent flow is delayed, locating it downstream of $x/H = 8$. Injection of nitrogen increased fluctuation, reaching a sharp peak at frequency of f = 11 KC (kilo cycles/sec) in the developing wake. At $x/H = 7$ along the wake axis, the frequency becomes maximum if the basic frequency is doubled to f = 22 KC and wake width grows rapidly indicating that the break

down of the laminar wake is non-linear. Fluctuations in the shear layer close to the rear part of the body are at first larger than those in a wake of no injected gas but grow sufficiently slowly delaying the wake transition.

The amplification of fluctuations in the near wake is considerably smaller than at the same station with no injection. Futhermore, there is a pronounced peak in the amplification curve near the frequency where a peak in the spectrum was observed.

Fluctuations increase if helium is injected, reaching a maximum of frequency, but prior to x/H = 8, the fluctuation signal on the wake axis is small and no higher harmonic is observed. Although the volumetric flow rates of nitrogen and helium were close to each other, the nitrogen increased the fluctuation more rapidly. The lower density of the helium which at least initially occupies the interior of the wake apparently had an additional stabilizing effect beyond the alteration of the pressure gradient and the wake thickness.

Surveys made at a fixed station (x/H = 1.5) are shown in Fig.VII.26, in a parameter of a helium flow rate. As the injection rate is increased, the laminar steady region about the wake axis, which is associated with the injectant flow is widened, but the inner shear layers merge with the turbulent remnant of the boundary layer and their fluctuation intensities are increased. Thus Lewis and Behrens (1969), postulates, that a minimum flow fluctuation level in the near wake may be attained by an optimum amount of injection.

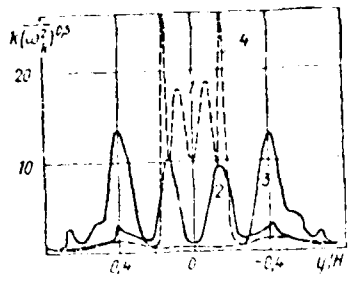

Fig. III.16. Profiles of change of intensity of fluctuations with different flow rates of helium (M = 4);

1--J = 0; 2--J = 0.0017; 3--J = 0.0093; 4--trailing-edge discontinuity. [Lewis and Behrens (1969)].

Later Shvets (1974), confirmed that in the range of M = 0.6 - 3, for each Mach number of free stream, there exists an optimum flow rate of injected gas for minimum fluctuation. It was also found that for supersonic flow, this same amount of injection is optimum to achieve the maximum base pressure.

References

Abramovich, G. N. (1963). The Theory of Turbulent Jets, ed. L. H. Shindel. MIT Press.

Bauer, A. B. (1967). "Some Experiments in the Near Wake of Cones," AIAA J. vol. 5, No. 7.

Bauer, A. B. (1968). "Near Wake Injection Experiments," AIAA J. vol. 6, No. 8.

Baum, E, King, H. H. and M. R. Denison (1964). "Recent Studies of the Laminar Base Region," AIAA J. vol. 2, No. 9.

Bearman, P. (1969). "On Vortex Shedding from a Circular Cylinder in the Critical Reynolds Number Regimes," J. Fluid Mech. 37/3.

Berger, S. A. and H. Viviand (1965). "Effect of Base Bleeding on the Near Wake for Very Low Reynolds Numbers," AIAA J. vol. 3, No. 11.

Bowman, J. E. and W. A. Clayden (1967). "Cylindrical Afterbodies in Supersonic Flows with Gas Ejection," AIAA J. vol. 5, No. 8.

Bowman, J. E. and W. A. Clayden (1968). "Boat-Tailed Afterbodies at $M_\infty = 2$ with Gas Ejection," AIAA J. vol. 6, No. 10.

Bowyer, J. M. and W. V. Carter (1965). "Separated Flow behind Rearward-Facing Step with and without Combustion," AIAA J. vol. 3, No. 1.

Bulmer, ɔ. M. (1972). "Effect of Low Heat Shield Ablation Rates on Flight Test Turbulent Base Pressure," AIAA J. vol. 10, No. 12.

Cassanto, J. M. and R. S. Mendelson (1968). "Local Flow Effects on Base Pressure," AIAA J. vol. 6, No. 6.

Cassanto, J. M. and E. M. Storer (1968). "A Revised Technique for Predicting the Base Pressure of Sphere Cone Configurations in Turbulent Flow Including Mass Addition Effect," ALFM 68-41 General Electric Co. Recntry and Environmental Systems Div. Philadelphia Oct.

Cassanto, J. M. and T. L. Hoyt (1970). "Flight Results Showing the Effect of Mass Addition on Base Pressure," AIAA Paper 70-109.

Cassanto, J. M. (1972). Flight Test Base Pressure Results at Hypersonic Mach Numbers in Turbulent Flow," AIAA J. vol. 10, No. 3.

Chapman, D. R. (1951). "An Analysis of Base Pressure at Supersonic Velocities and Comparisons with Experiment," NACA Report 1051.

Chapman, D. R. (1956). "Theoretical Analysis of Heat Transfer in Separated Flows, NASA TN - 3792.

Chow, W. L. (1959). "On the Base Pressure Resulting from the Interaction of a Supersonic External Stream with a Sonic or Subsonic Jet," J. Aerospace Sci. vol. 26, No 3.

Clayden, W. A. and J. E. Bowman (1968). "Cylindrical After bodies at M_∞ = 2 with Hot Gas Ejection," AIAA J. vol. 6, No. 12.

Collins, D. J. Lees, L. and A. Roshko (1970). "Near Wake of a Hypersonic Blunt Body with Mass Addition," AIAA J. vol. 8, No. 5.

Cortright, E. M. and A. H. Schroeder (1951). "Investigation at Mach Number 1.91 of Side and Base Pressure Distributions over Conical Boat - Tails without and with Jet Flow Issuing from Base," NACA RM E 51, F 26.

Craven, A. (1960). "Base Pressure at Subsonic Speeds in Presence of a Supersonic Jet," Rept. N. 129 The College Aeronautics.

Davis, L. R. (1968). "Experimental and Theoretical Dete mination of Flow Properties in a Reacting Near Wake," AIAA J. vol. 6, No 5.

Emmons, H. W. and D. Leigh (1953). "Tabulation of the Blasius Function with Blowing and Suction," Intermin Tech Rept 9. Combustion Aerodynamic Lab. Div of Applied Sci., Harvard University.

Fuller, L. and J. Reid (1958). "Experiments on Two-dimensional Base Flow at M = 2.4," ARC RM 3064.

Golik, P. J. (1962). "On the Dissipative Mechanism Within Separated Flow Regions ; with Special Consideration to Shear Transfer Across Turbulent Compressible, Pr = 1, Mixing Regions," Ph. D. Thesis, Univ. Illinois.

Herzog, H. T. (1964). "Nitrogen Injection into the Base Region of a Hypersonic Body," GALCIT Hypersonic Res. Proj. Memo. 71, Calif. Inst. Techn. Aug.

Kakuowski, A. K. and C. H. Lewis (1973). "Experimental Study of Supersonic Laminar Base Flow with and without Suction," AIAA J. vol. 11, No. 12.

Korst, H. H. Page, R. H. and M. E. Childs (1956). Theory of Base Pressure in Transonic and Supersonic Flow," Univ. Illinois, Exp. Station. also ASME Paper 56 - APM 30.

Korst, H. H. Chow, W. L. and G. W. Zumwalt (1959). "Research on Transonic and Supersonic Flow of a Real Fluid at Abrupt Increases in Cross-Section," ME - TR - 392 - 5, Univ. Illinois.

Lewis, J. E. and K. L. Chapkis (1969). "Mean Properties of the Turbulent Near Wake of a Slender Body with and without Base Injection, AIAA J. vol. 7, No 5

Lewis, J. E. and W. Lehrens (1969)." Fluctuation Measurements in the Near Wake of a Wedge with and without Base Ejection", AIAA J Vol. 7, No 4.

Libbi, P. A. (1962). " Theoretical Study of Turbulent Mixing of Jet Gases with Application to Supersonic Combustion of Gases" J. Aerospace Sci., No. 3.

Love, E. S. (1957). "Base Pressure at Supersonic Speeds on Two-Dimensional Airfoils and on Bodies of Revolution with and without Fins Having Turbulent Boundary Layers," NACA TN 3819.

Nash, J. F. (1962). "An Analysis of Two-Dimensional Turbulent Base Flow Including the Effect of the Approaching Boundary Layer," Aero. Dept. 1036, National Physical Laboratory.

Page, R. H. and J. E. Horst (1958). "Nonisoenergetic Turbulent Compressible Jet Mixing with Consideration of its Influence on the Base Pressure," Ph.D. Dissertation, Dept Mech. Eng. Univ. of Illinois.

Reid, J. and R. C. Hastings (1959). "Experiments on the Axisymmetric Flow over Afterbodies and Bases at M=2.0," Rept. 21,707, Aero Res Council.

Reid, J. and R. Hastings (1961). "The Effect of a Central Jet on the Base Pressure of a Cylindrical Afterbody in a Supersonic Stream," ARC RM 3224.

Scott, C. J. and E. R. G. Eckert (1966). "Heat and Mass Exchange in the Supersonic Base Region," AGARD Conference Proceedings 4, Separated Flows. Part 1.

Shvets, A. I. (1974). "Flow in the Base Region with Injection," AN USSR MZhG 5.

Shvets, A. I. and I. T. Shvets (1976). Gas Dynamics of Near Wake, Naukova Dumka Press, Kiev.

Sykes, D. M. (1970). "Cylindrical and Boat-Tailed Afterbodies in Transonic Flow with Gas Ejection," AIAA J. vol. 8, No. 3.

Tang, H. H. and J. W. Barnes (1967). "A Combining Parameter for Base Pressure Evaluation," AIAA J. vol. 5, No. 9.

Townend, L. H. and J. Reid (1963). "Experimental Results on the Effect of Combustion on Base Flows at Supersonic Speeds," (abstract) NATO AGARD Combustion and Propulsion Panel Meeting on Supersonic Flow Chemical Processes and Radiative Transfer, Whitehall, London. April.

Yurchenok, K. Ye. (1971). "Pressure and Temperature behind Bodies with Shear in a Supersonic Flow with Supply of Inert and Jet Gases into the Base Region," AN SSSR MZhG 2.

Zakkay, V. and H. Fox (1966). "Experimental and Analytical Consideration of Turbulent Heterogeneous Mixing in the Wake," Rept. New York University AA - 66 - 54 April.


N
DATE
ILME